Wavelet-based Segmentation Techniques in the Detection of Microarousals in the Sleep EEG

Alexei Glavinovitch

A Thesis

in

The Department

of

Electrical and Computer Engineering

Presented in Partial Fulfillment of the Requirements

for the Degree of Master of Applied Science at

Concordia University

Montréal, Québec, Canada

April 2004

Your file Votre référence
ISBN: 0-612-91034-2
Our file Notre référence
ISBN: 0-612-91034-2

ABSTRACT

Wavelet-based Segmentation Techniques in the Detection of Microarousals in the Sleep EEG

Alexei Glavinovitch

This thesis proposes an automatic detection procedure to detect the presence of undesirable frequency bursts, called microarousals (MA), within any of the various stages of sleep. Sleep is examined through the acquisition of the electroencephalogram (EEG). Traditionally, a sleep technologist manually inspects the EEG signal to correctly detect the occurrence of MAs. The presence of these MAs causes a medical condition known as excessive daytime sleepiness (EDS).

Since the EEG is a non-stationary signal, the proposed procedure analyzes it in three stages. The first stage involves spectral decomposition using the discrete wavelet transform (DWT). The DWT is efficient and possesses excellent time-frequency resolution that makes it well suited to exploit the characteristics of a non-stationary signal.

The second stage of the proposed procedure partitions the decomposed signal into stationary segments. Both parametric and nonparametric segmentation techniques are applied. The nonparametric autocorrelation function (ACF) and the nonlinear energy operator

(NLEO) methods as well as the parametric generalized likelihood ratio (GLR) method are each applied to the component waveforms of the EEG signal produced by the DWT.

The third stage of the proposed procedure involves evaluating information about each stationary segment's power and spectral content. Once this information is determined, segments satisfying the definition of a MA are detected and scored.

To examine the effectiveness of the overall procedure, long-term EEG records containing MAs that have been marked by a sleep technologist are compared against the proposed procedure's detected MAs. The successful results obtained demonstrate the effectiveness of the proposed procedure.

Tempus Fugit

ACKNOWLEDGEMENTS

I would like to express my most profound appreciation to my thesis supervisors Drs. E.I. Plotkin and M.N.S. Swamy, whose steadfast support and valuable guidance made this work and its completion possible. I am truly grateful for the insightful advice and the constructive criticism that they gave me and especially for their inspiration and confidence during the course of this work. I feel very fortunate and, quite frankly, priviledged to have had the opportunity to work with two such outstanding scholars. This important collaboration has been, assuredly, one of the most enriching experiences of my life.

I would also like to express my sincere gratitude to Dr. Rajeev Agarwal, whose expertise in both signal processing and sleep technology provided me with a knowledgeable introduction towards understanding and pursuing the task of automated microarousal detection. His patience and discriminating suggestions were of inestimable value.

It is with satisfaction that I extend my genuine thankfulness to Dr. Jean Gotman and Stellate Systems for providing me with both the necessary EEG data and the financial support, which made this work possible.

I gratefully acknowledge Micronet, a national network of centers of excellence, for the valuable financial funding, to my supervisors, that has supported the pursuit and completion of this work.

I would also like to express my heartfelt appreciation to my father, my mothers and my sister for their love and motivation.

A special thanks goes to my friends, Marco, Alina, Zhong, Jimmy and Jessica for their help and advice.

TABLE OF CONTENTS

LIST OF FIGURES

LIST OF TABLES

LIST OF ABBREVIATIONS

ACF	Autocorrelation Function
ANN	Artificial Neural Network
AR	Autoregressive
ARMA	Autoregressive Moving Average
AWGN	Additive White Gaussian Noise
BT	Blackman-Tukey
C3	Centripetal 3 Electrode
CE	Centripetal Electrode
CWT	Continuous Wavelet Transform
DFT	Discrete Fourier Transform
DMW	Discrete Meyer Wavelet
DWT	Discrete Wavelet Transform
EDS	Excessive Daytime Sleepiness
EEG	Electroencephalogram
EKG	Electrocardiogram
EOG	Electrooculogram
EMG	Electromyogram
ERP	Evoked Related Potential
FFT	Fast Fourier Transform
FT	Fourier Transform
FThr	Frequency Threshold
GLR	Generalized Likelihood Ratio
HUP	Heisenberg Uncertainty Principle

IThr	Intersection Threshold
LR	Likelihood Ratio
MA	Microarousal
MA	Moving Average
ME	Electromyogram Electrode
NLEO	Nonlinear Energy Operator
NREM	Non-Rapid Eye Movement
O1	Occipital 1 Electrode
PSD	Power Spectral Density
R&K	Rechtschaffen and Kales Scoring Rules
REM	Rapid Eye Movement
SSW	Spike and Slow Wave
SSS	Strict Sense Stationary
STFT	Short Time Fourier Transform
WL	Window Length
WSS	Wide Sense Stationary
WT	Wavelet Transform

Chapter 1

Introduction

1.1 General

The focus of this thesis is on the automatic detection of events emerging in the electroencephalogram (EEG) of patients suffering from excessive daytime sleepiness (EDS). These events, called microarousals (MA), are uncharacteristic frequency changes, satisfying specifically defined criteria. They occur in the different stages of sleep and their presence in any of these stages deteriorates the overall quality and the necessary restitutive function of sleep for the patient, thereby resulting in EDS. Traditionally, the detection of MAs is a role relegated to sleep technologists who must go through the unenviable task of manually reading an aggregate of different biomedical signals, recorded during a patient's sleep. These various signals, all together called polysomnograms, provide real-time data about the patient's heart rate, muscle tension, brain waves etc. Since a normal period of sleep spans eight to ten hours, a sleep technologist must therefore accurately mark each occurance of an MA, out of, quite literally, miles of data, to correctly establish a reliable account of all relevant elements, in order to enable a credible diagnosis to be justified. Aside from the enormous time demands required for this task, visually marking a microarousal suffers from further problems, involving individual scorer consistency in rescoring the *same* recording, as well as from unsatisfactory interscorer reliability [1]. Clearly, this repetitive

and exhausting task, requires a great deal of time and concentration and, in the end, unavoidably leads to relatively poor or incomplete marking of microarousals; as a result, this situation lends itself readily to some form of automation. The form of automation will be implemented with an appropriately designed detection algorithm, using modern signal processing techniques.

Before discussing the particular type of automatic detection, the nature of the signal under study must be described. The procedure proposed in this thesis attempts to systematize the detection of specific transient events in a biomedical signal. Generally, biomedical signals, whether they be cardiac rhythms, blood flow rate, eye movements or varying brain potientials, exhibit highly non-stationary characteristics, whose understanding is most keenly sought but whose very nature, which is being sought, is most elusive. In fact, the varying nature of biomedical signals, in general, effectively resists most attempts at codification. Without precise guidelines, general automated procedures of information extraction cannot be reliably built and if they are reliably built they cannot be applied generally. To overcome these obstacles, approximations are made. Since our focus in this thesis involves the EEG, a specific type of biomedical signal, we proceed, in the next section, to describe it in greater detail. Following its description, we then describe its role in quantifying sleep. The quantification of sleep is achieved by dividing it into a number of recognizable stages. The recognition of each stage of sleep is made possible largely through the acceptance of certain characteristics, such as specific ranges of EEG frequency and amplitude, as being uniquely representative of a specific stage of sleep. These artificial boundaries, although largely accepted, are clearly assumptions made to facilitate the desired systematization. Once the objective description of sleep is understood, the rules used to define the marking of MAs

are introduced. The physiological motivation for such rules will not be elaborated upon, since that would clearly exceed the scope of this thesis. However, the rules themselves, along with visual examples illustrating their application in identifying the MAs, will be given explicitly. Finally, after describing the overall physical nature of the problem that this thesis addresses, we end this chapter with an outline of the thesis, giving a brief synopsis of each of the following chapters.

1.2 EEG Signal

The EEG is a biomedical signal, which records the electrical activity of the outer layer of the cerebral cortex [2]. Originating from the pioneering work of the German psychiatrist Hans Berger in 1928, who measured the electrical activity of the human brain for the first time, the invention of the EEG sparked a sudden and genuine scientific interest. The reason for this enthusiasm lay in the new possibilty that the EEG offered the researchers. Through the application of the EEG, sleep could now be, for the first time, continuously monitored and quantitatively measured, *without* waking or disturbing the sleeper [3]. The EEG opened the door to a whole new world of objective sleep analysis. Although many improvements were made in the years following its invention to reduce the time required to analyze an EEG record, it was not until the fast Fourier transform (FFT) [4] first made its appearance in the 1960s, that real time gains were made.

1.2.1 EEG Acquisition

The EEG is an electrical signal which records the electro-magnetic reactions produced by the underlying mechanisms of the cerebral cortex or the outer layer of the human brain [5]. Since the brain is not a fixed point but an object that occupies space, a cluster of descriptive EEGs are obtained by uniformly sampling the surface of the scalp, in order to acquire a representative picture of the global electrical activity. Through the application of carefully positioned electrodes, following a standard spatial distribution called a montage, a large number of EEG signals, representing the designated areas of the brain, is produced. Of the different montages adopted for EEG acquisition, the International 10-20 system [6] is commonly used and shown in Figure 1.1.

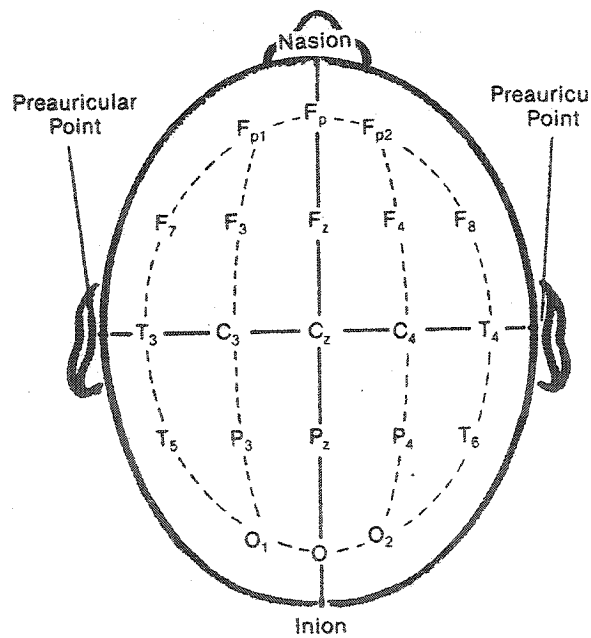

Figure 1.1: International 10-20 montage

This system of electrode placement provides for a uniform *spatial* coverage of the entire scalp. Therefore, the EEG signal charts the dynamic electrical behaviour of the brain as it changes through both time and space. The distance, which separates one electrode from the other, is determined by first measuring the total distance separating bony landmarks of the head. For example, the distance between the nose and a bony mass at the back of the head is one such distance. These measured distances generate a system of lines which run across the head and intersect at intervals of 10 or 20% of their total length, at whose intersections electrodes are placed. The use of the 10-20 system assures symmetrical, reproducible electrode placements and allows comparison of the EEGs from the same patient as well as from different patients, recorded in the same or different laboratories [7].

1.2.2 Description of EEG signal

In order to analyze the content of an EEG signal, it is important that its characteristic components be well understood. This pursuit motivates the description of a 'normal' EEG signal, which necessitates the identification of descriptors important for analysis. Three important descriptors are: one, the naturally occurring *waveform patterns*, which regularly appear within specific sleep stages and therefore must be noted in order to distinguish them from the presence of abnormal patterns, such as MAs, which they may remotely resemble; two, the value of the *frequency* content of the EEG signal as it evolves in time; and three, the value of the *amplitude* of the EEG signal as it evolves in time. These descriptors, especially the last two, provide essential descriptive tools needed to distinctly characterize both normal and abnormal phenomena appearing in the EEG signal. Although there are other

types of descriptors that could be considered, such as wave repetition, spatial distribution, timing etc., these do not help in detecting MAs and therefore are ignored.

1.2.2.1 Normal EEG

Before a descriptive component break down of an EEG signal can be proposed, it must be recognized that a wide variety of normal EEG patterns can be seen in different persons of the same age, and an even greater variety of normal patterns can occur in different age groups. Therefore, the description of a normal EEG is not a trivial task; actually, an EEG is often called normal not because it contains normal patterns but because it lacks abnormal patterns [7]. By this approach, instead of listing all the possible forms of normal patterns and their variations, a non-practical task, the EEG is interpreted by the number of distinct abnormal waveforms it contains. In contrast to the great variety of normal patterns, there are only a few EEG components, such as spikes and sharp waves, certain slow wave and amplitude changes, which are known to be definitely abnormal in each age group.

1.2.2.2 Characteristic EEG Waveforms

However, barring the presence of such abnormal patterns, there also exists various characteristic waveforms that are present during normal sleep, which regularly accompany various stages of sleep. They act as indicators, whose presence participates in defining specific sleep stages. Such characteristic waveforms are shown in Figure 1.2.

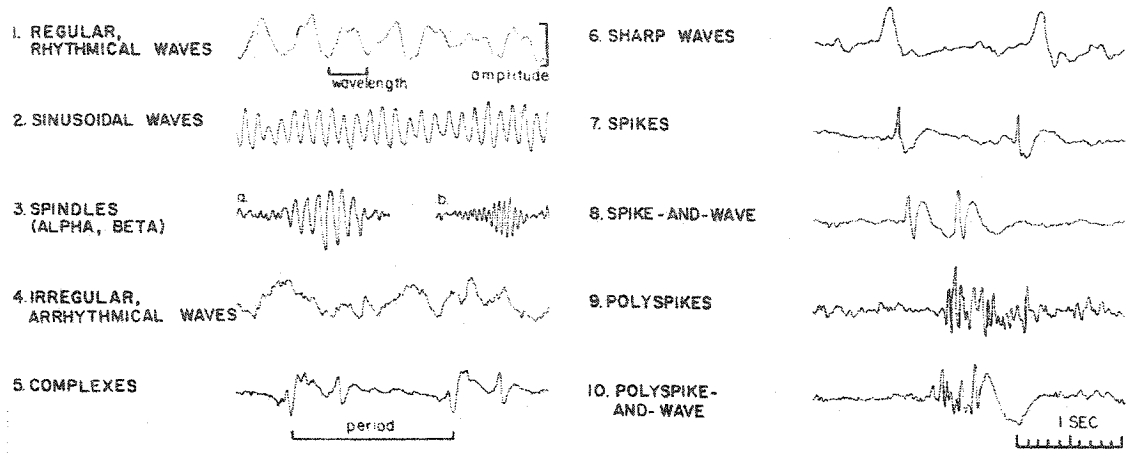

Figure 1.2: Characteristic EEG waveforms

The motivation for describing the normal EEG record arises naturally from the need to identify the presence of an abnormal waveform pattern like the MA, from the rest of the regularly occurring waveform patterns. The benefits offered by a reliable description consequently assists in maximizing the correct detection, while, simultaneously, minimizing false alarms. Again, this goal can only be achieved if the background waveforms can be clearly distinguished from the MA.

1.2.2.3 EEG Frequencies

Throughout the analysis of EEG records, one of the most important criteria for assessing abnormality, and assisting the diagnosis, is the study of the frequency. In the detection of MAs, it plays a major defining role. The total possible frequency range, encountered in EEG records, spans from an ultra-low frequency value of 0.1 Hz, indicative of life threatening coma state, to the ultra-high frequency value of 100 Hz. In normal circumstances,

these extreme values play no significant role in clinical EEG evaluation because it is often unclear that frequencies, at these values, are actually of cerebral origin. [7]. Instead, focus is placed on the clinically relevant frequency bands. By almost universal consent [8], the EEG record is divided into four frequency bands: *beta*, *alpha*, *theta* and *delta*, which are defined in Fig, 1.3. To provide a more intuitive time interpretation of these frequencies, their corresponding wavelength is also included in Figure 1.3

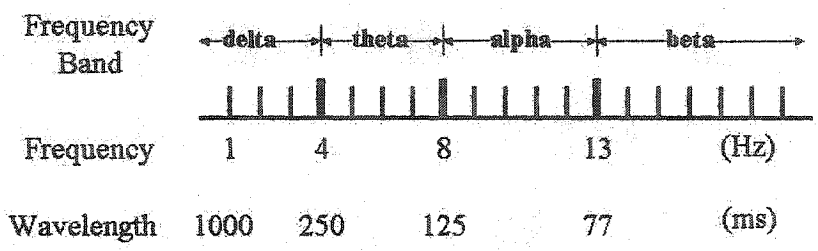

Figure 1.3: Frequency and wavelength of delta, theta, alpha and beta bands.

These frequency bands are somewhat arbitrary, since many EEGs contain waves of frequencies that extend across their boundaries. Nevertheless, these bands help to distinguish normal from abnormal waves in the EEG. The beta and alpha bands were introduced first by Berger [9], while the delta and theta waves were first recorded by Walter [10].

1.2.2.4 EEG Amplitudes

The voltage amplitudes, obtained from measurements taken at the surface of the cerebral cortex (i.e. outer surface of the brain), generally fall in the range of 500 - 1500 μV. In comparison, these measurements are largely attenuated, when taken from the surface of the

scalp, the method most commonly encouraged in practice. The amplitudes recorded from scalp EEG are nearly two orders of magnitude smaller, ranging from 10 - 100 μV or more commonly from 10 - 50 μV, in most adults. This marked reduction is attributable directly to the attenuation caused by the intervening medium, composed of leptomeninges, spinal fluid, bone and scalp, separating the two measurements.

The importance of the waveform amplitudes lies squarely upon their consistent regularity when following the changes in sleep stage. That is, high frequency waves, such as beta or alpha waves, indicative of the drowsiness incurred during sleep onset, regularly have low amplitudes. Likewise, as sleep progresses towards deeper sleep, the dominant waveform frequency decreases to the theta and delta bands and, in the process, these dominant waveforms record a corresponding increase in amplitude. Therefore, the amplitude is inversely related to the frequency of the dominant EEG waveform patterns. This relationship is clearly seen in Figure 1.5 below. Moreover, this relationship contributes directly to the detection of MAs, since the two parameters may now be monitored and used in the detection procedure. Table 1.1 gives a detailed breakdown of this frequency and amplitude relationship.

Table 1.1: Frequency and amplitude properties of the dominant EEG frequency bands.

Dominant Frequency	Frequency Range	Amplitude Range
Beta (β)	HIGH > 13 Hz	LOW < 20 μV
Alpha (α)	HIGH 8 - 13 Hz	LOW < 20 μV
Theta (θ)	MEDIUM 4 - 8 Hz	MEDIUM 20 - 50μV

Dominant Frequency	Frequency Range	Amplitude Range
High Delta (δ_h)	LOW 2 - 4 Hz	HIGH > 50 μV
Low Delta (δ_l)	LOW 0.5 - 2 Hz	HIGH > 50 μV

Having described the major relevant components of the EEG signal, we continue with a description of the tools used to monitor sleep, known as polysomnograms.

1.2.3 Polysomnograms

The International 10-20 system uses 21 electrodes and one ground electrode to record the overall electrical activity of the brain, as shown in Figure 1.1. These signals, generated during the monitoring period, are then fed through wire cables to a computer where they are displayed on a monitor, recorded on magnetic or optical storage devices and preserved for future analysis. These 21 signals constitute the EEG data used for studying sleep.

However, EEG signals alone are often not sufficient to clearly identify some events and trends. In practice, a combination of both EEG and other types of biomedical signals is used to define sleep stages and MAs.

It is the consistent correlation of events, that exists between different types of biomedical signals, that reinforces the decision to score sleep as being in a specific state and scoring an MA as being present. There are many polygraphic variables, which measure the time evolving functions of the body. Some measure the heart rate, such as the electrocardiogram (EKG), others measure the upper airway exchange, some measure temperature while others monitor chest or abdominal respiratory movement and so on. The numerous signals, which

provide a holistic description of the body's overall evolution, during sleep, are called polysomnograms. A sample of a polysomnographic record is shown in Figure 1.4. Of the signals that make up the polysomnogram, the following two signals, in conjunction with the EEG, contribute directly to the detection of MAs:

- Electrooculogram (EOG)
- Electrormyogram (EMG)

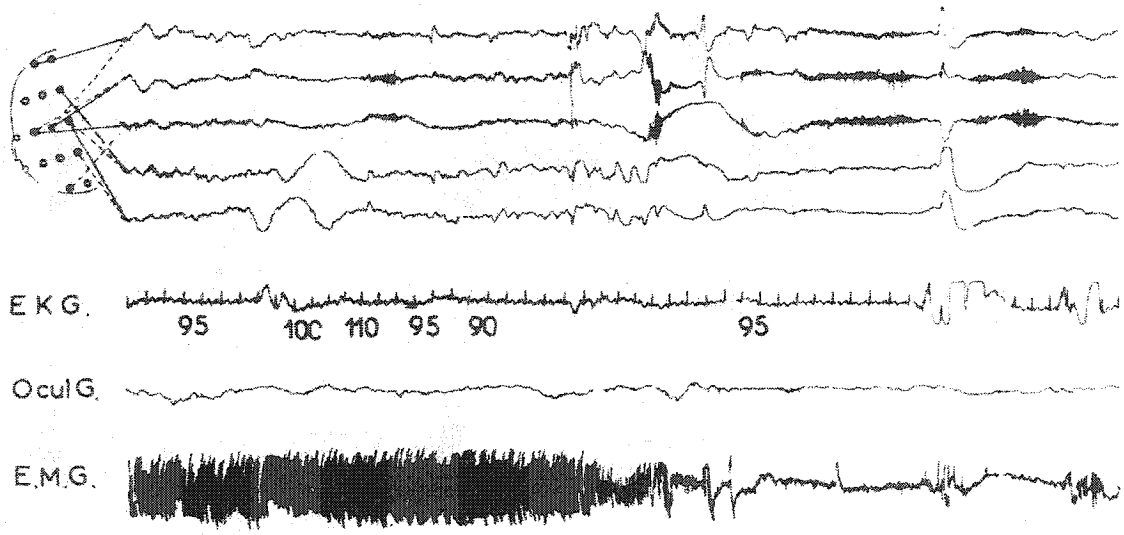

Figure 1.4: Partial sample of a polysomnogram: shown here are five EEG signals taken from the 10-20 montage accompanied by non-EEG signals: Electrocardiagram (EKG), electrooculogram (EOG) and electromyogram (EMG) (taken from [7]).

1.2.3.1 Electrooculogram (EOG)

Because the cornea is slightly positive with respect to the retina, there is a small electropotential or electric field that exists between the front of the eye and the back. By placing electrodes on the side of the eye, variations in potential, resulting from eye movement, can

be detected. The measurement of eye movement in relation to sleep is important for two reasons. The first reason stems from the fact that one particular stage of sleep, called rapid eye movement (REM) sleep or desynchronized sleep can only be detected with the EOG. The second reason is similar. The EOG contributes significantly to the detection of stage 1 sleep [3]. Therefore, the EOG plays a fundamental role in sleep staging.

1.2.3.2 Electromyogram

The electromyogram (EMG), like the EOG, is used as a criterion for staging the REM sleep. The EMG is an electrical signal that records the changes of muscle tension. The muscle traditionally used to represent general muscle tension is the mylohoid, or chin muscle. The reason for this choice is essentially the convenience of electrode placement, although most other muscles are equally suited for this task [8]. The real value of the EMG lies not only in its contribution to staging but especially in its direct contribution to the detection of MAs. As outlined in the rules set forth by Rechtschaffen and Kales (R&K) [11], described later on in this chapter, recognizable concomitant changes in frequency and amplitude, shown in the EMG, compared with similar EEG changes, act as indicators exposing the presence of MAs. Since the EMG gauges the state of wakefulness, exhibited by muscle relaxation, the EMG amplitude level gradually decreases as the transition progresses, from the highly active wakeful state, through the subsequent sleep stages of the non-REM sleep (to be discussed later in this chapter) until it completely disappears during the REM sleep. According to the R&K rules, a sudden frequency burst observed from an EEG channel is, by itself, not exclusively a sufficient indicator necessary to mark such a disturbance as an MA. In certain situations it must also be accompanied by a similar sudden muscle activation, occurring

simultaneously on the EMG channel. Therefore, the EMG is a vital element in the process of MA detection.

To summarize, the measurements needed for the detection of MAs are those provided from the EEG, the EMG and the EOG. Furthermore, regarding the EEG signal itself, and the 10-20 montage, clinical experience has determined that observation of the C_3 electrode alone, shown in Figure 1.1, is sufficient for marking purposes. Because of the limited resources available, in the past, the selection of C_3 for sleep staging became the rule, as established by [11]. However, depending on the purpose of the recording, other selected electrodes, like the O_1 (also shown in Figure 1.1) can be used for analysis, to supply the necessary degree of supporting redundancy in which decisions can be made. In this thesis, only the C_3 electrode is considered.

1.3 The Classification of Sleep Stages

Interest in sleep and dreams has existed since the beginning of recorded history. It was not until the 20th century that the study of sleep acquired the necessary tools to make it objectively worthwhile [3]. As mentioned in Section 1.2, the development of the EEG by Berger [9] opened the door to scientific research into the brain, with sleep as one of the many branches of specific concentration. Through the application of the EEG, valuable insights into the waveform patterns of the brain, during sleep, were revealed in the 1930s in seminal papers [3]. These insights changed the notion that the brain was a passive blob, during sleep, into an understanding that it was actually quite active and functional. A major development in the understanding and objective description of sleep was made in 1951, by Kle-

itman and Aserinsky [12], when they discovered the manifestation of rapid eye movement (REM), during sleep. This discovery, due to the distinctly different nature of the REM from the traditionally recognized patterns, led them to classify REM as a separate stage of sleep and thus, allowed them to 'partition' sleep.

Now, with universal consent, sleep is considered to be divided into two separate and distinct states. One state is called the 'non-rapid eye movement' state (NREM) while the second state is called the 'rapid eye movement' state (REM). The regular cycle of sleep begins first with wakefulness and then proceeds into the NREM state until it finally arrives at the REM state of sleep before the cycle returns to the beginning of the NREM state and then repeats itself for the normal eight to ten hour duration of a person's total sleep time.

1.3.1 NREM Sleep

When a person's sleep is monitored and displayed through an EEG, the NREM state of sleep is, in a normal person, recognized as being synchronous, exhibiting regularities, dominant frequencies and other recognizable wave features such as sleep spindles, K-complexes and high voltage slow waves (see Figure 1.2). Moreover, to facilitate the analysis of a person's sleep cycle, the NREM is subdivided further into four distinct and generally accepted sleep stages, based on the presence of characteristic waveforms which are used to classify each stage. These subdivisions of the NREM sleep aid at recognizing the gradual transition that a person goes through from wakefulness to deep sleep. Typical waveforms occurring during the four different stages of the NREM sleep are shown in Figure 1.5.

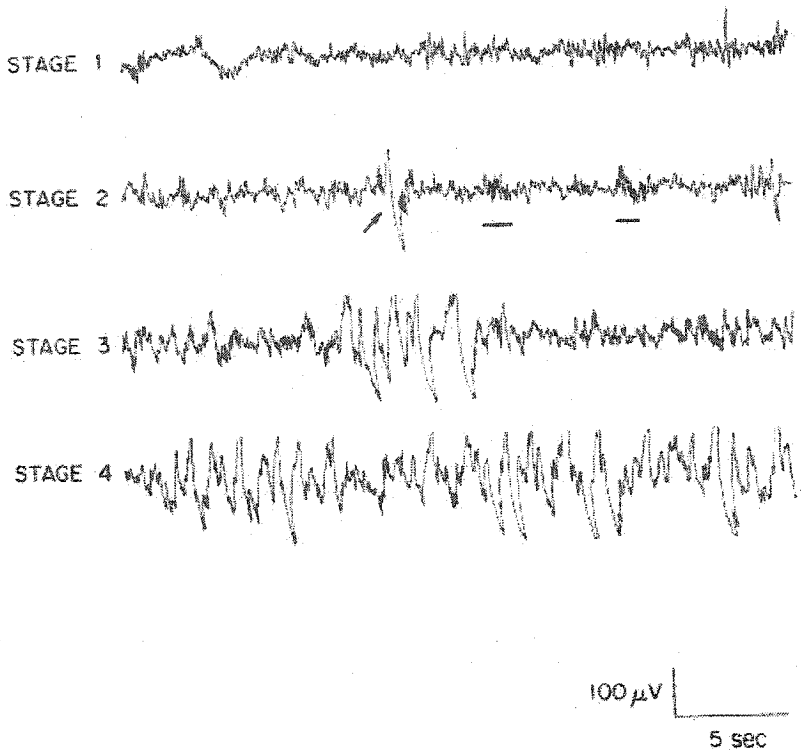

Figure 1.5: The stages of NREM sleep taken from a 19-year-old female. The arrow in the stage 2 waveform indicates a K-complex while the underlining indicates two sleep spindles (taken from [3]).

In the following sections, we briefly discuss each sleep stage as described in [3] and [8].

1.3.1.1 Stage 1: Drowsiness

The first stage of the NREM sleep is commonly referred to as the sleep onset, when a person is still awake but is demonstrating the initial signs of ensuing sleep. Typical frequencies associated with wakefulness are low amplitude high frequency waves. The transition from wakefulness to Stage 1 of sleep is shown in Figure 1.6.

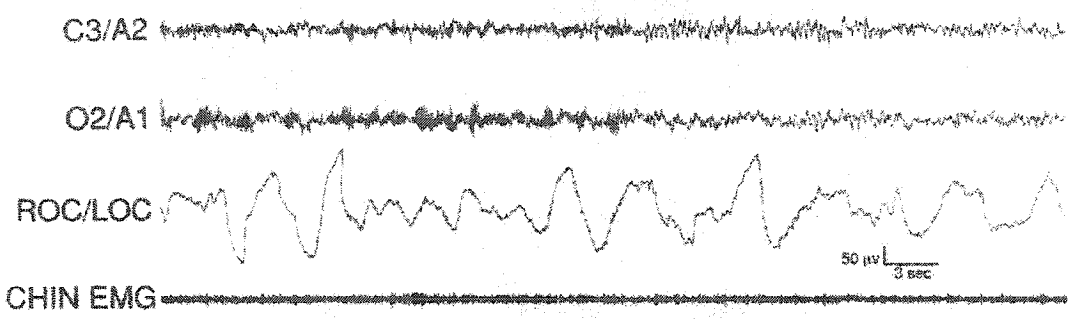

Figure 1.6: This waveform shows the transition from wakefulness to stage 1 sleep. Notice the high frequency portion of the wave followed by a decrease in frequency (taken from [8]).

In the EEG literature, the dominant frequencies and the characteristic waveforms that are present, and serve, by their presence, to define the various sleep stages of the signal, are generally accepted to occur simultaneously, in the defining patterns, shown in Table 1.2.

Table 1.2: Description of the dominant frequencies and waveforms encountered during the different stages of sleep of an adult male.

Sleep Stages	Sleep Type	Dominant Frequencies & Char. Waveforms
Stage 1	drowsiness	α , disappearing α sharp waves
Stage 2	light sleep	mostly θ, some α sharp waves, K-complexes
Stage 3	deep sleep	mix θ and δ, K-complexes, spindles
Stage 4	very deep sleep	very slow δ, some K-complexes
REM	desynchronized	α waves reappear but desynchronized

Therefore, in wakefulness, the presence of high frequency beta waves tends to dominate the EEG waveform. When the onset of sleep begins, alpha waves become more prevalent until

they themselves dominate the majority of the waveform. The amplitude, however, remains relatively unchanged.

1.3.1.2 Stage 2: Light Sleep

As seen in Table 1.2, a typical waveform of Stage 2 activity is composed of mostly theta waves with some residual alpha waves still present. Compared to Stage 1, which is entirely dominated by energetic alpha waves, Stage 2 demonstrates the gradual deepening of sleep by the increased presence of the lower frequency theta waves, replacing the alpha waves of Stage 1. Moreover, in addition to the change in dominant frequencies, there are further differences which distinguish these two sleep stages. In Stage 2, there is an ever increasing presence of unique waveforms such as the K-complexes and sleep spindles (see Figure 1.2). K-complexes are sharp sawtooth like biphasic components of high amplitude usually greater than 100μV; sleep spindles are short frequency bursts of 11.5 - 15 Hz lasting longer than half a second, with a typical amplitude greater than 25μV [3]. Both of these particular waveforms appear exclusively in large numbers during Stage 2.

1.3.1.3 Stage 3: Deep Sleep

The mixed presence of both the high amplitude low frequency theta waves and the higher amplitude lower frequency delta waves as seen in Figure 1.5 typically serve as the representative wave structure of Stage 3. Although both particular waves predominate during this stage it is the changing dynamic of their presence that allows us to classify this stage with a certain degree of confidence. The noticeable traits are the total absence of alpha

waves and the gradual appearance of theta waves. Although in the previous section it was suggested that sleep spindles occurred frequently in Stage 2, they are still present in this stage but considerably less, in comparison.

1.3.1.4 Stage 4: Very Deep Sleep

The predominant waveforms in Stage 4 are a mixture of theta, high delta and low delta waves. Sleep spindles are rarely present. This stage of sleep is commonly referred to as deep sleep and often it is lumped together with Stage 3 because the boundary separating these two stages is not so sharply defined in practice [3].

1.3.2 REM Sleep Stage

The second state of sleep, as mentioned in Section 1.3, is called the REM sleep. This stage of sleep, in a normal person, follows Stage 4 of the NREM sleep and is the stage of sleep when dreaming usually occurs. The waveform structure differs greatly from the NREM sleep because, contrary to that state of sleep, REM sleep is usually asynchronous, where all types of frequencies fast and slow tend to make their appearance in frequent bursts. In sleep monitoring, the EEG is usually accompanied by reading from other physiological sources, in order to help in detecting patterns. As described in Section 1.2.3, along with the EEG readings, we also have EOG and EMG readings. A person is considered to be in REM sleep when the EEG includes a confused assortment of varying frequencies and the EOG simultaneously shows rapid eye movement, as well as an almost total muscle relaxation indicated

by an almost flat EMG reading. A sample polysomnogram, demonstrating a typical example of REM stage sleep, is shown in Figure 1.7.

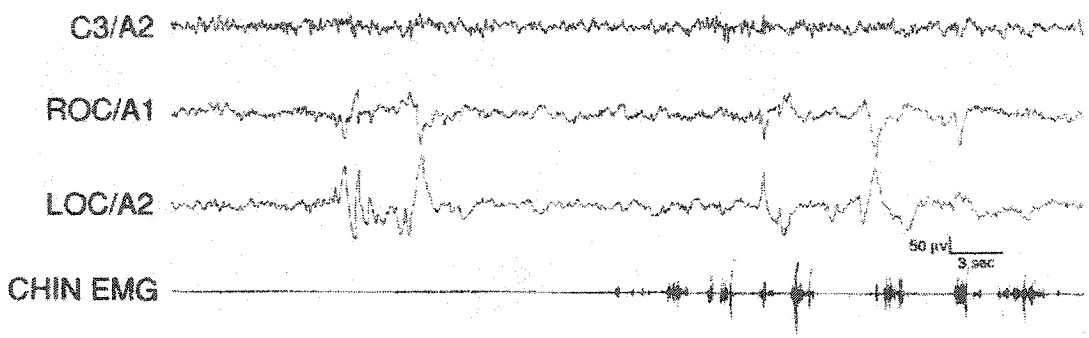

Figure 1.7: Polysomnogram of REM sleep (taken from [3]).

The different stages and the overall sleep cycle that an adult follows during the night is shown in the histogram in Figure 1.8.

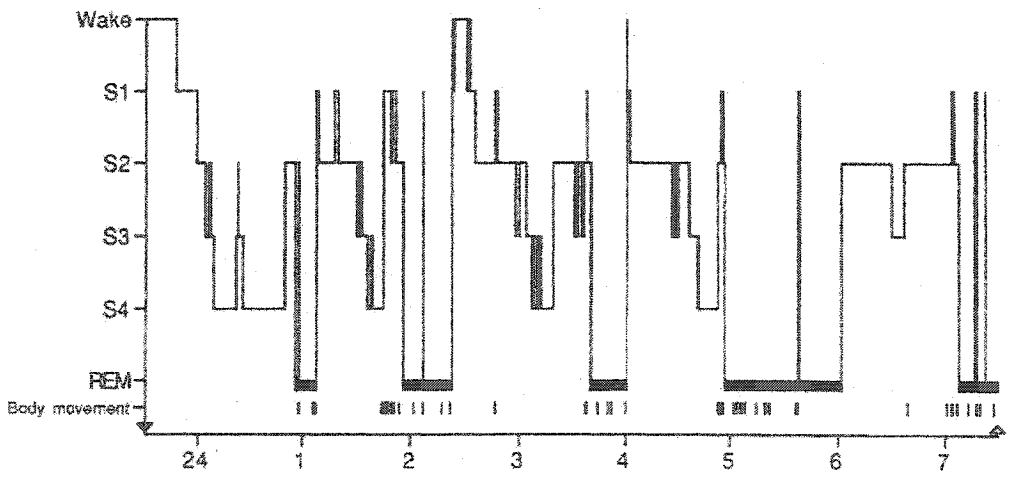

Figure 1.8: The sleep cycle of a young adult (taken from [3]).

1.4 Microarousals

The staging of sleep provides us with a template with which to compare and consequently detect microarousals. Within a certain stage of sleep, if a frequency, different from the characteristic waveforms for that stage, suddenly appears and satisfies the Rechtschaffen and Kales (R&K) criteria, then we can score that frequency burst as an arousal [11]. An EEG arousal is defined as a sudden uncharacteristic burst of EEG frequency. By uncharacteristic, it is meant that, compared with the dominant frequencies occurring during a specific stage of sleep, any sudden change in frequency, excluding stage specific waveforms, such as the K-complexes or spindles, such a frequency may be scored as an arousal. These arousals may include theta, alpha and/or frequencies greater than 12 Hz. More specifically a stricter guideline in order to interpret arousals is provided by the R&K scoring rules [13], which will be outlined below to provide a clearer understanding of the specific waveform we aim to detect in this thesis.

1. A person must be within a certain sleep stage as defined in Section 1.3 for a minimum of at least ten continuous seconds before an EEG arousal can be scored.
2. For a second arousal to be scored, another preceding period of ten continuous seconds of stage specific sleep must have been observed, between the first arousal and the second arousal, as well as any other future arousals.
3. An uncharacteristic burst of frequency must have a duration of at least 3 seconds or greater to be scored as an arousal.
4. In NREM sleep, EEG frequency bursts of greater than 3 seconds can be scored without an accompanying increase in amplitude in the EMG signal.

5. In REM sleep, an EEG frequency burst MUST be accompanied by a concurrent increase in EMG amplitude to be scored.

6. Arousals cannot be scored when the only change observed is an increase in only the EMG amplitude.

7. Artifacts (i.e., waveform disturbances caused by extracerebral sources such as the patient movement or operational errors etc.), K-complexes or delta waves are not scored as arousals unless accompanied by an EEG frequency burst. If these specific waveforms appear before the EEG burst, then that EEG burst is not scored. If they occur during the EEG burst, then they are used to meet the 3 second duration criteria in order to score that EEG burst as an arousal.

8. EEG and EMG bursts having an individual duration of less than 3 seconds, but when observed contiguously have a duration greater than 3 seconds, are not scored as an arousal.

9. A sudden alpha burst of at least 3 seconds, in NREM sleep, following a 10 second segment of alpha free sleep is scored as an arousal.

10. Transitions from one sleep stage to another by themselves cannot be scored as arousals unless the above criteria are satisfied.

In the following, Figure 1.9 through to Figure 1.14, taken from [13], are presented in order to clarify the above rules with examples that illustrate the polysomnographic environment, which the detection algorithm will operate upon.

1.4.1 Examples of True Microarousals

The polysomnograms presented in Figure 1.9 to Figure 1.11 are all examples showing *scored* MAs, based on the above R&K rules [11]

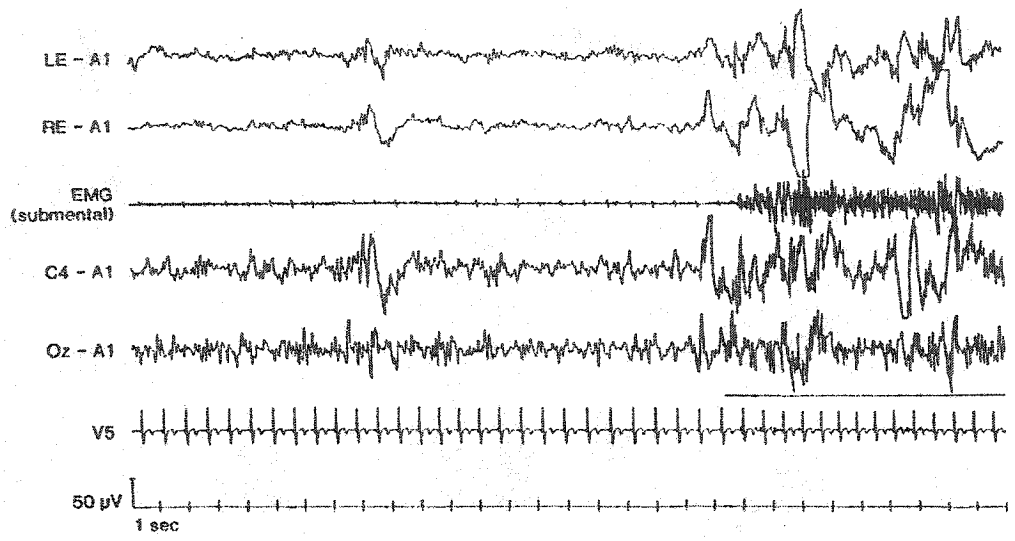

Figure 1.9: This is greater than a 3-second EEG change with frequencies greater than 16 Hz and alpha activity. This EEG arousal also has increased EMG amplitude. There are greater than 10 seconds of sleep preceding this event, and it is scored as an arousal.

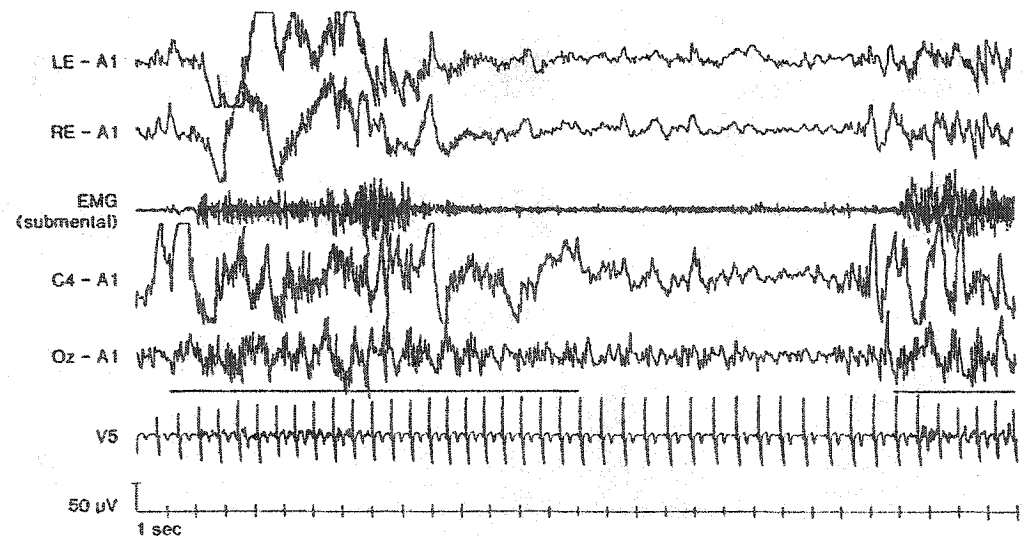

Figure 1.10: Two arousals are scored on this epoch as there are 10 seconds of sleep between the arousals.

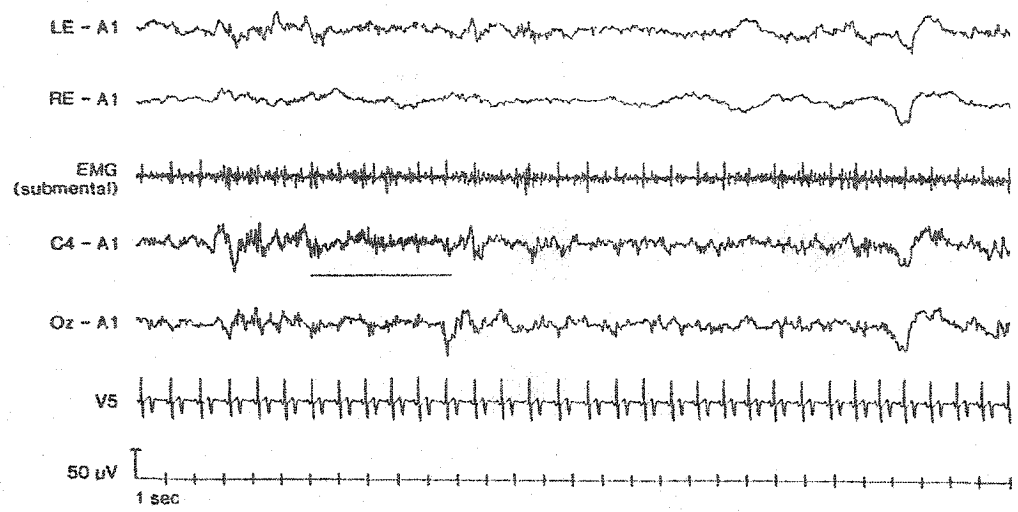

Figure 1.11: The EEG frequency change in this epoch of NREM is scored as an arousal despite the absence of an EMG amplitude increase.

1.4.2 Examples of False Microarousals

Based on the R&K scoring rules, the polysomnograms in Figure 1.12 to Figure 1.14 are presented to highlight the situations where a disturbance, possibly mistaken for a microarousal, is not scored as one.

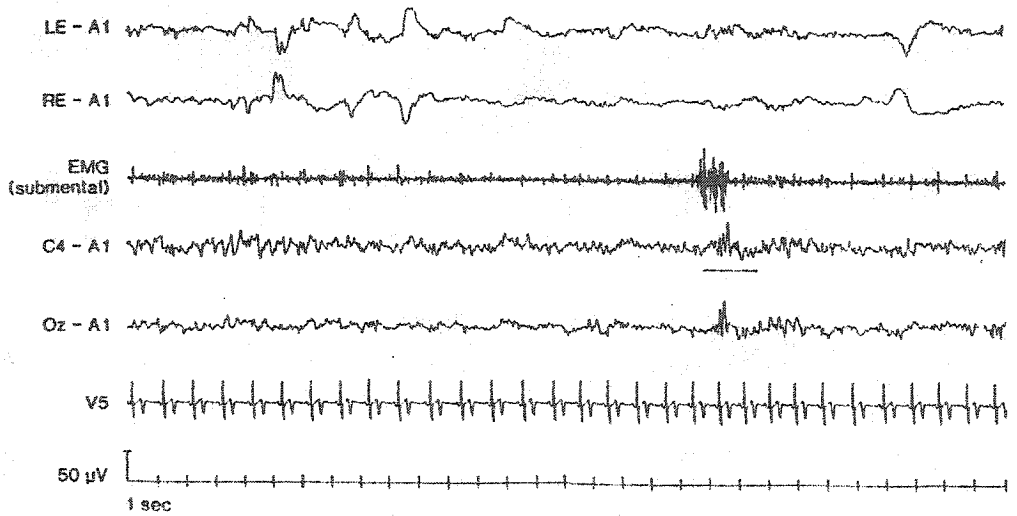

Figure 1.12: The instance of EEG frequency change and EMG amplitude increase in this REM epoch is not long enough in duration to be scored as an arousal.

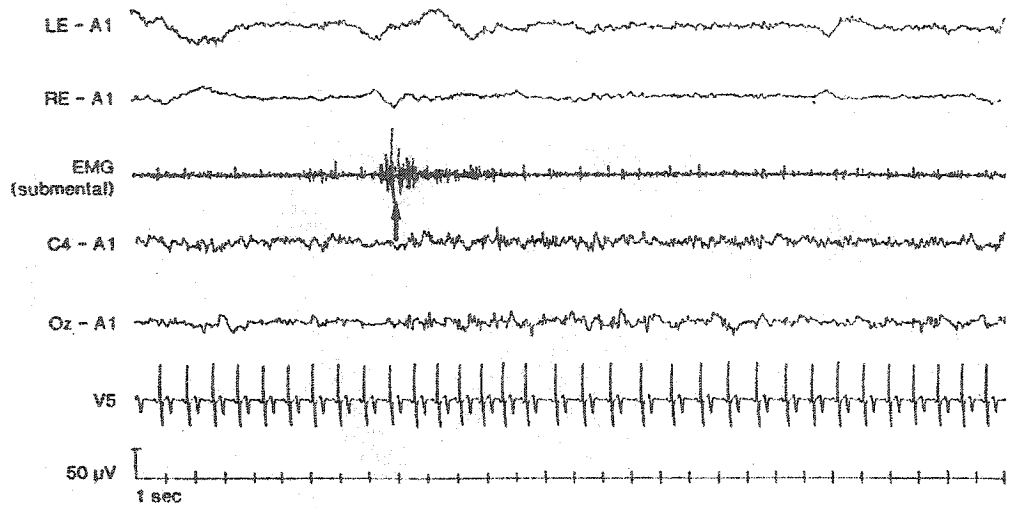

Figure 1.13: While the EMG amplitude is briefly elevated, there is no EEG frequency change and this event is not scored as an arousal.

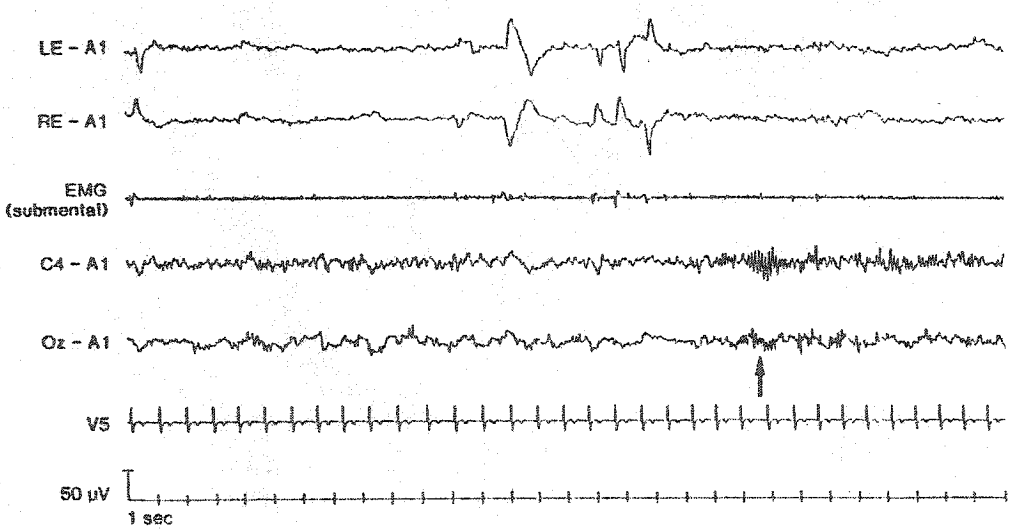

Figure 1.14: The EEG frequency change on this epoch of REM sleep is not accompanied by an increase in EMG amplitude and thus is not scored as an arousal.

1.5 Outline of the Thesis

The objective of this thesis is to correctly determine the presence and exact location of MAs within an EEG record. This problem is in itself new and therefore, no reseach specifically focussing on this particular issue has been found. Based on research conducted on similar topics revealed in the literature and the emergence of the relatively new wavelet transform (WT), whose application is particularly well suited for this problem, a novel, multistage detection algorithm including signal segmentation is proposed in this thesis. This thesis is the first approach to automatic MA detection using the WT. It must be made clear that in the literature, the analysis techniques applied to other EEG detection problems use either the WT or some form of segmentation, but never the two together. Therefore, the proposed procedure is novel in the fact that it uses a combination of these signal processing techniques in contributing to the detection of MAs. It must also be emphasized that apart from combining the WT with a segmentation scheme, the proposed procedure also includes a novel method to identify and extract the MA segments. In other words, the proposed procedure is novel in two ways: first, in applying a combination of both the WT and a segmentation scheme to the EEG signal and second, in its overall design, which uses this combination in conjunction with a novel method of identifying and extracting the MAs from the EEG signal. Comparisons of the results of the proposed procedure with real clinical results are made.

In Chapter 2, the spectral decomposition techniques adopted in practice to investigate neurological signals are described. A comparison is drawn between these and the WT to justify the adoption of the WT as an improved decomposition transform and a novel means of

extracting the MAs. The decomposition of the EEG signal is the first stage of the multistage algorithm.

In Chapter 3, the theory and a detailed description of the different detection techniques employed to isolate the MA is presented. The important statistical concept of stationarity is formally described. The segmentation of the non-stationary EEG signal into its various constituent stationary segments is an essential step in the overall procedure because the MA itself is assumed to be a stationary segment. Separating all of the stationary segments within the EEG allows further tests to be performed in order to uncover the content of each segment and finally leads to the identification of MAs. The application of these detection techniques to the WT of the EEG signal is a novel approach that constitutes the second stage of our multistage algorithm.

In Chapter 4, the experimental results obtained after applying the proposed detection algorithm to a series of artificial signals are presented and discussed in detail. The artificial signals used are designed to represent non-stationary characteristic waveform patterns, resembling MAs, as encountered in an EEG signal.

In Chapter 5, the last stage of the algorithm, which involves feature extraction, is described and the overall procedure is applied to an actual EEG signal. Results are then presented and discussed where a comparison is made against the clinical 'gold standard' detection results obtained from a sleep technologist.

Finally, Chapter 6 concludes the thesis by pointing out the contribution of the proposed investigation and suggesting some related problems and potential avenues for future investigation.

Chapter 2

Comparison of the Wavelet Transform with Traditional Transforms

2.1 General

In Chapter 1, we outlined the goal of this thesis, which is the reliable and automatic detection of microarousals. There, a detailed description of the biological background of the problem was presented. The proposed method of automation is a multistage process. The first stage involves the decompostion of the signal into a more compact form freed of extraneous signal features. To obtain this form, an effective spectral decomposition method or transform operator needs to be selected. Amid the various transforms available, we chose the wavelet transform (WT). However, we must first outline the reasons motivating its selection. Therefore, this chapter proceeds, first, with a comparative analysis of the WT and other transformations traditionally applied to non-stationary signals. This literature survey highlights the WT's superior performance and this result consequently serves as the necessary support behind its selection and use. Secondly, having thus justified its use, the wavelet transform is then described in detail.

2.2 Motivation behind use of Wavelet: Literature Survey

Before we begin to describe some of the techniques used to analyze EEG signals, it must be noted that most of the research being done in this EEG-related field generally applies to detecting evoked potentials, event related potentials, epileptic discharges [14],[15],[16] or some other form of feature extraction related to experiments performed on either humans or animals. There, the specific cause and effect relationships sought are based on the resulting EEG patterns emerging from an applied controlled action.

In trying to justify the use of the WT as a superior spectral analysis technique of non-stationary signals, our search through the literature led us to biomedical experiments mostly involving the EEG. Yet, since the EEG is a particular case of a broader band of similar non-stationary biomedical signals, experiments dealing with other types of similar signals, such as the muscular tremor signals [17] or blood flow sound signals [18],[19] were also included. These, of course, are not EEG signals but they exhibit identical non-stationary properties and since their spectral properties are analyzed with techniques that we are comparing the WT to, their inclusion is warranted.

In humans, research was focussed on the EEG response to specific stimuli in order to establish consistent correlations between the source of the stimulus and the corresponding pattern of the EEG waveforms emerging as a result of this stimulus, the detection of specific types of epileptic spikes in the EEG or the detection of tremors arising from particular diseases such as Parkinson's disease, multiple sclerosis etc. Although the specific area of investigation is different from ours, there is clearly a common ground, which links their research with ours. This common link is based on detecting and isolating specific patterns.

Since we are also looking for specific patterns (i.e., frequency bursts that follow the R&K criteria) involving frequency, then the spectral techniques used in the previous research need only be selected based on those that most closely resemble our particular problem. There exists many types of spectral estimation techniques. These are outlined in Figure 2.1.

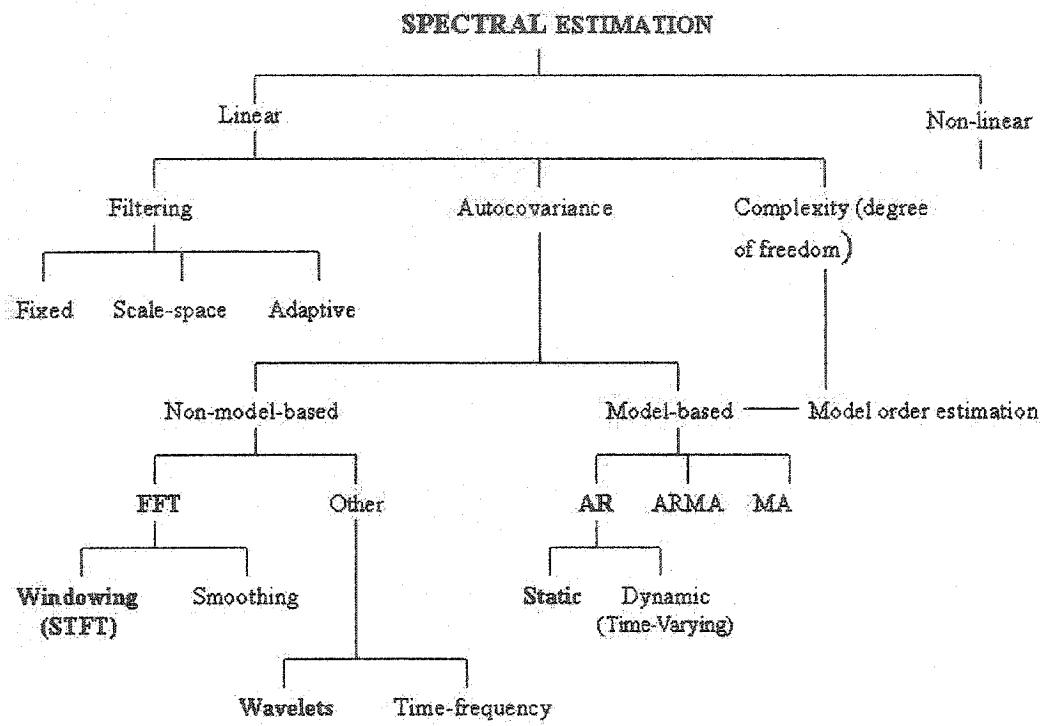

Figure 2.1: Partial break-down of the various spectral estimation techniques available (taken from [17]).

By the nature of the particular problem we are addressing, namely, the detection of uncharacteristic frequency bursts within a specific sleep stage, we are obliged to obtain the clearest possible spectral representation of the signal. Therefore, it seems necessary to look for current spectral analysis techniques applied generally to biomedical signals and specifically to neurological signals, which will enable us to achieve this objective. The current techniques used for spectral analysis are:

1. Discrete Fourier Transform (DFT)
2. Short Time Fourier Transform (STFT)
3. Autoregressive Filtering (AR)
4. Wavelet Transform (WT)

2.2.1 Discrete Fourier Transform

Spectral analysis is an operation whose purpose is to decompose a signal into its frequency or sinusoidal components. In other words, spectral analysis transforms a time-domain signal into the frequency domain. Among the available spectral analysis techniques, the Fourier transform (FT) is considered to be a good transformation between time and frequency domains because of it being time-shift invariant. Moreover, it possesses an inverse which allows the original signal to be recovered from its transform. Its discrete representation, the discrete Fourier tranform (DFT), is expressed as [20]:

$$\text{Transform: } X(k) = \begin{cases} \sum_{n=0}^{N-1} x(n) W_N^{kn} & 0 \le k \le N-1 \\ 0 & \text{otherwise} \end{cases} \tag{2.1}$$

$$\text{Inverse: } x(n) = \begin{cases} \frac{1}{N} \sum_{k=0}^{N-1} X(k) W_N^{-kn} & 0 \le n \le N-1 \\ 0 & \text{otherwise} \end{cases} \tag{2.2}$$

where, $W_N = e^{-j(2\pi/N)}$ and N is equal to the length of the signal x(n).

The DFT is implemented, in practice, by the fast Fourier transform (FFT).

2.2.1.1 Stationary Transform

In [21], the FFT and the WT are both applied to EEG signals and their performance, as spectral analysis tools, is compared. The results demonstrate that the FFT, although good at averaging out the spectral content present in a signal, lacked the ability to detect the presence of small transient changes, which are characteristic of non-stationary signals like the EEG and are essential for detecting MAs. Figure 2.2(a) shows a 30-second EEG segment of Stage 2 sleep and Figure 2.2(b) shows its FT. The FFT shows the relative weight, in terms of the spectral amplitude, of each frequency present in the transformed signal. Unfortunately, the moment in time when each frequency component occurs in the signal cannot be shown by the FFT and this is a severe limitation for the problem under consideration.

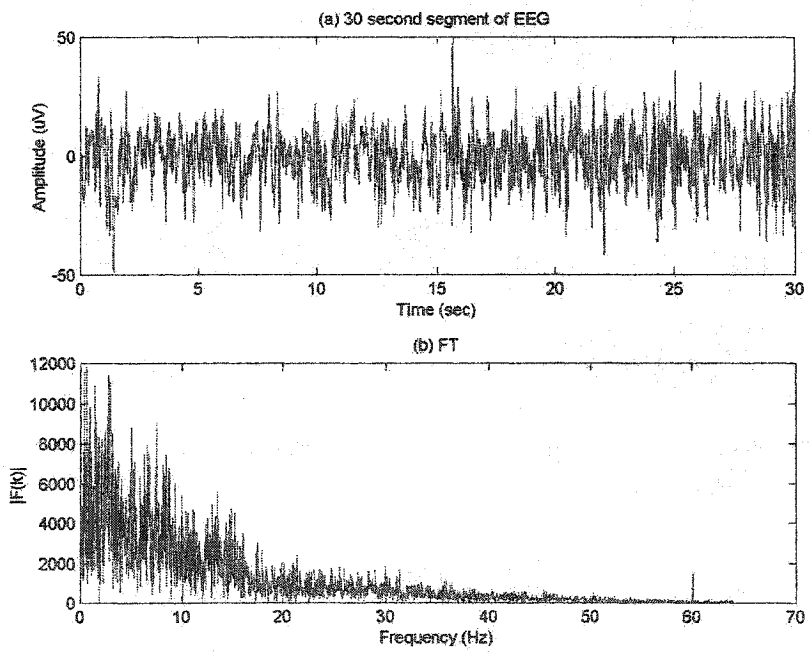

Figure 2.2: (a) 30-second EEG segment of Stage 2 sleep and (b) its FT.

The WT by comparison, due to its ability to resolve frequency and time simultaneously, is clearly more suited to non-stationary signals. It provides clear advantages at capturing transient events such as epileptic discharges, by its ability to represent subspectral components of the EEG in both time and frequency, and as such it is conclusively much more efficient than the FFT.

Therefore, the direct application of the FFT to biological signals, especially when the center of focus is the transient nature of the signal, demonstrates limited analytical use [22]. Although the transient used is an eye saccade or a short-time evoked potential burst, this article clearly demonstrates both the stationarity and time-resolving limitations that result from the application of the FFT to such a waveform. In this paper, various Fourier analyses were applied to a transient, similar to a biological transient, but with a known theoretical FT. The results showed that applying FFT directly to the signal gave erroneous results. To correct these results windowing had to be performed with a cosine window, which led to better results. Therefore, a proposed palliative to this limitation would be to force the signal to be quasi stationary by windowing the signal, a technique called the short time Fourier transform (STFT). The problem one would then be faced with, in order to force the signal to be quasi stationary, would be to decide upon an optimal size and type of window to be used and this is not an obvious question to answer.

2.2.2 Short Time Fourier Transform

In the previous section, it was pointed out that despite providing good spectral quantification of a signal in terms of spectral content present, the FT frequency domain representation

loses all time information regarding the exact time when that content occurred. That is, the spectral analysis based on the classic FT method assumes that the signal is stationary and consequently, it ignores any time-varying spectral content that may appear in the signal [23].

Again, as in [22], [24] describes the FT as being a classic example of a 'stationary transform'. The concept of stationarity will be discussed formally in Chapter 3. As a result, the FT provides a good means of analyzing a signal if that signal is composed of a few stationary components (e.g., sine waves). However, any abrupt change in time (such as an MA) in a non-stationary signal x(t) is spread out over the entire frequency axis making the FT's usefulness in precisely identifying the frequency content acutely limited. The article [24] goes on to suggest that the signal can be made 'quasi stationary' by introducing time dependency, through the use of a windowing function, concentrated at some local frequency. This is the STFT and it is defined as:

$$\mathrm{STFT}(\tau, f) = \int x(t) g^*(t-\tau) e^{-j2\pi f t} dt \qquad (2.3)$$

where g(t) is some window function.

It can be seen that (2.3) maps the signal into a two-dimensional function in the time-frequency plane (τ,f). The parameter f in (2.3) is similar to the Fourier frequency. However, the analysis here, unlike the FT, depends critically on the choice of the window function. Figure 2.3 shows vertical stripes in the time-frequency plane, illustrating the "windowing of the signal" in time perspective of the STFT. Given a version of the signal, windowed around time t, this viewpoint computes "all frequencies" of the STFT. An alternative view is based on a modulated filter bank interpretation of the same process. At a given frequency

f, (2.3) amounts to filtering the signal "at all times" with a bandpass filter having as impulse response the window function modulated to that frequency [24]. This is shown as the horizontal stripes in Figure 2.3.

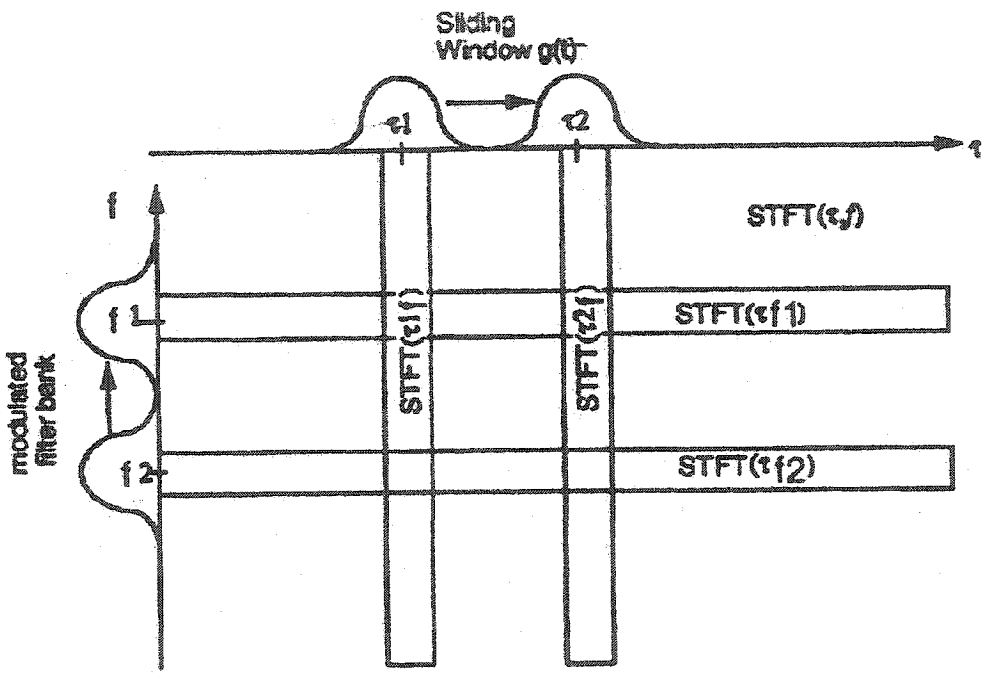

Figure 2.3: Time-frequency plane of the STFT (taken from [24]).

2.2.2.1 Time-Frequency Resolution

The problem with the STFT is the question of the resolution. Because of the Heisenberg uncertainty principle (HUP), we cannot have arbitrarily good frequency (time) resolution without losing time (frequency) resolution [24]. That is, the time-bandwidth product is restricted to a very specific physical bound, imposed by the HUP

$$\Delta t \cdot \Delta f = \frac{1}{4\pi} \tag{2.4}$$

where Δf is defined as:

$$\Delta f^2 = \frac{\int f^2 |G(f)|^2 df}{\int |G(f)|^2 df} \tag{2.5}$$

where the denominator is the energy of the window g(t).

The resolution in frequency of the STFT analysis is given by Δf and indicates that two sinusoids will be distinguishable from one another only if they are more than Δf apart.

Similarly, Δt is defined as:

$$\Delta t^2 = \frac{\int t^2 |g(t)|^2 dt}{\int |g(t)|^2 dt} \tag{2.6}$$

where the denominator is again the energy of the window g(t). Now, two pulses, in time, will only be distinguishable from each other if they are at least Δt apart.

This is called the time resolution of the STFT analysis. It must be noted that Gaussian windows are often used because they meet the time-frequency bound imposed by (2.4). A more important consequence of windowing, in the STFT, is that, *once a window is chosen, its time and frequency resolutions (Δt and Δf) are fixed over the entire time-frequency plane* (since the same window is used at all frequencies) [24], as shown in Figure 2.4, along with the associated basis functions (i.e. windowed Fourier basis functions).

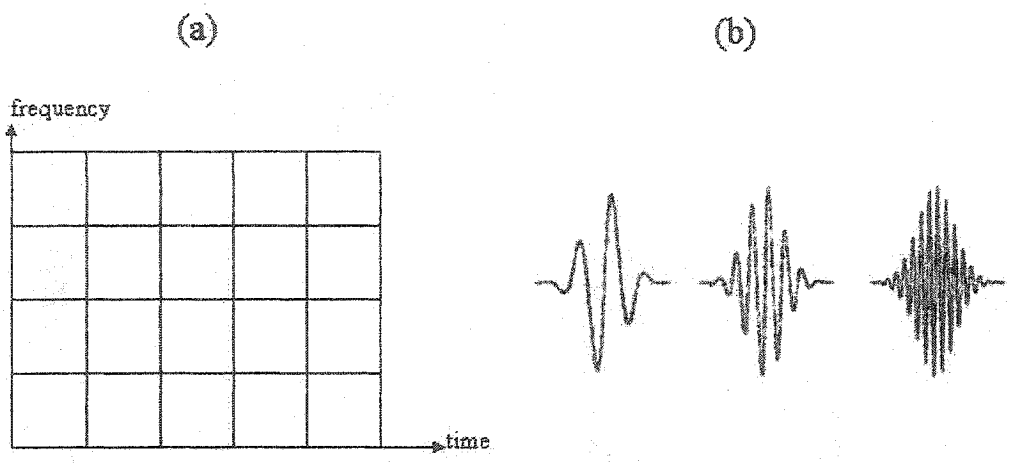

Figure 2.4: a) STFTpartition of the time-frequency plane, b) Basis functions of the STFT. (taken from [24])

Each tile represents the essential concentration in the time-frequency plane of a given basis function. Since the STFT is constrained by a fixed window size, its basis functions have a fixed and therefore a uniform concentration in the time-frequency plane. The direct result of this fixed window size constraint is a uniform partitioning of the time-frequency plane as shown in Figure 2.4(a). In other words, the STFT uses a 'one-size-fits-all' (i.e. one window size) approach to capture all the time-varying signal content that occurs at different regions of the plane. Clearly, this approach is suboptimal for signals exhibiting transients because one size does not optimally fit all types of transients, but once a particular window is chosen its size remains fixed throughout the analysis, which is a major limitation of the STFT. This drawback can be seen in the basis functions, where each function maintains the same length inspite of the changing frequency.

On the other hand, the WT offers a more customized approach, with tiles changing their concentration depending on their position within the time-frequency plane and as a result presents a more effective partition to capture signal transients.

To further demonstrate the STFT's limitations in resolving both time and frequency properties in a signal, let us consider an example taken from [25], with the signal shown in Figure 2.5.

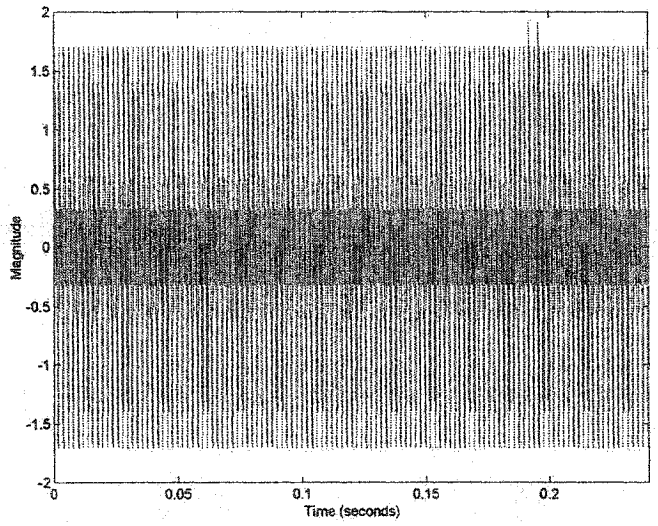

Figure 2.5: STFT analyzed signal containing two sinusoids and two closely spaced delta functions

Here we have a signal, which is composed of two small bursts, associated with two long quasi-stationary components

$$f(t) = \sin(2\pi f_1 t) + \sin(2\pi f_2 t) + K[\delta(t - t_1) + \delta(t - t_2)] \tag{2.7}$$

with $f_1 = 500$ Hz, $f_2 = 1000$ Hz; $t_1 = 192$ ms and $t_2 = 196$ ms; $K = 3$;

When using the STFT, a choice needs to be made, whether the signal should be analyzed with either good time resolution (short window width) or frequency resolution (large window width). Because of its inherent resolution limitations the STFT cannot analyze a

signal with both good time and good frequency resolution using the same window, as shown in Figure 2.6.

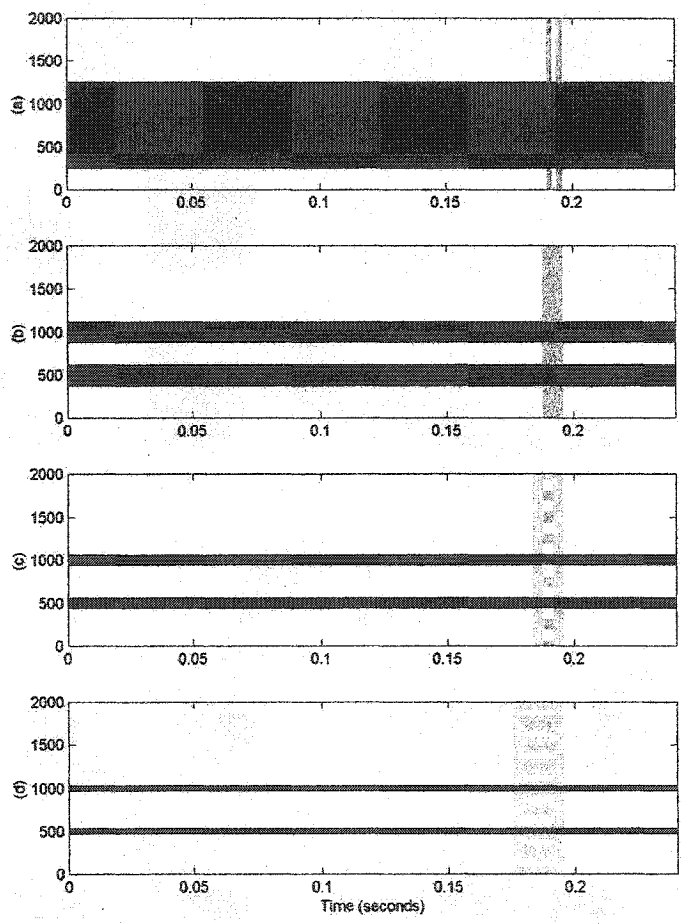

Figure 2.6: The STFT of the signal in Figure 2.5 corresponding to different window widths (W): (a) W=2ms, (b) W=4ms, (c) W=8ms, (d) W=16ms; vertical axis is frequency (Hz) (taken from [25])

Here, the limitations in resolving both time and frequency components present is made quite apparent. Specifically, in Figure 2.6a we see that by using a small window length the two time bursts are well resolved, but at the expense of totally obscuring the frequency content. In fact, the frequency resolution is so poor that we cannot even identify the number of

distinct frequency components that are present, let alone their exact value. Conversely, in Figure 2.6d the window is increased to a value which correctly reveals the two frequency components. Now, the resolution relationship is reversed and the two time bursts are no longer resolvable. To provide some workable compromise between both the time and frequency domains, the window length must be adjusted to some value between the short window used for Figure 2.6a and the long window used for Figure 2.6d. Unfortunately, this compromise, as shown in Figure 2.6b and Figure 2.6c, provides rather poor results in both domains simultaneously.

2.2.2.2 Constant Relative Bandwidth

In Section 2.2.2.1 we showed that the STFT partitioned the time-frequency plane uniformly. Referring back to Figure 2.3 we can consider the STFT as a filter bank. In particular, this filter bank is composed of identical filters of fixed bandwidth spread across the entire frequency range, centered at equally spaced frequency intervals as seen in Figure 2.7a. The fixed time-frequency resolution of the STFT makes it unsuitable in circumstances where analysis requires flexible resolution across the frequency range. To overcome the problem of fixed time-frequency resolution in the STFT, the following constraint is imposed:

$$\frac{\Delta f}{f} = \text{constant} \tag{2.8}$$

where Δf is the filter bandwidth and f is the filter's central frequency.

Implementing constraint (2.8) creates an analysis filter bank which is composed of band-pass filters with constant *relative* bandwidth. Now, instead of having the frequency responses of the analysis filter regularly spaced over the frequency axis, they are now spread logarithmically over the axis, which is shown in Figure 2.7b.

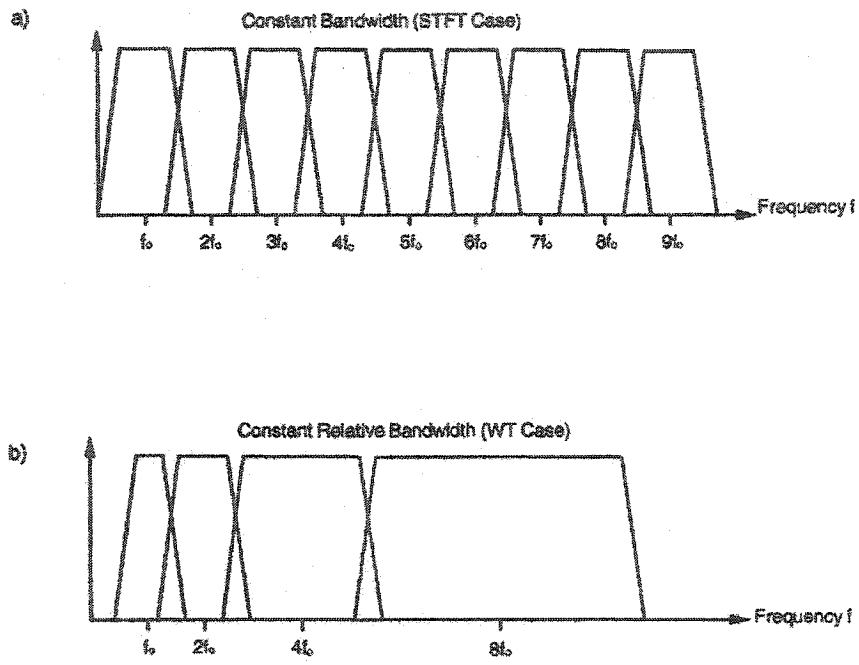

Figure 2.7: Division of the time frequency plane for (a) the STFT (uniform) and (b) the WT (logarithmic) (taken from [24])

With the condition given by (2.8) satisfied, we can change the time and frequency resolution to suit our interests, a property which is explicitly exploited using wavelets.

It is clear that the resolution constraint of the HUP is still satisfied but now the time resolution becomes arbitrarily good at high frequencies, while the frequency resolution becomes arbitrarily good at low frequencies. For example, two very short bursts can always

be eventually separated in the analysis by going up to higher analysis frequencies in order to increase time resolution, as seen in the time-frequency plane partition of Figure 2.9a in Section 2.2.4. This kind of analysis works best if the signal is composed of high frequency components of short duration plus low frequency components of long duration. The new definition in (2.8) provides adjustable frequency and time resolution as opposed to the fixed time and frequency resolution offered in the STFT. This new definition, however, applies to the continous wavelet transform (CWT), which will be explained later. In fact, unlike the STFT, the WT implementation is not frequency-independent, so higher frequencies are studied with analysis filters with wider bandwidths [26] . Before we begin to discuss the relative merits of the CWT, another standard and popular spectral estimation technique called the autoregressive (AR) method is presented.

2.2.3 Autoregressive Method

Unlike the previous spectral analysis methods, the autoregressive (AR) method is parametric. A parametric model of spectral estimation is a mathematical one that approximates the processes underlying the production of the signals using models of data generation governed by a small number of parameters [17]. It involves the selection of a suitable model order (i.e., the total number of parameters involved) and then estimating these parameters based on the available data.

A time series $u(n), u(n-1), u(n-2), \ldots, u(n-p)$ is said to represent a realization of an AR process of order p if it satisfies

$$u(n) + a_1 u(n-1) + a_2 u(n-2) \ldots + a_p u(n-p) = v(n) \qquad (2.9)$$

where $a_1, a_2, a_3, \ldots, a_p$ are constants representing the AR parameters or model coefficients and v(n) is a white noise driving process with zero mean and variance σ^2 [27]. Written more compactly, we have

$$u(n) = -\sum_{m=1}^{p} a_m u(n-m) + v(n) \tag{2.10}$$

The process generating the model given by (2.10) contains p+2 parameters to be estimated from the original time series. These parameters are the coefficients a_m, the mean of the samples and the variance of the noise.

Further analysis, such as spectral estimation, can now be performed directly on the estimated model parameters, a_m, instead of on the original signal.

2.2.3.1 Justifying AR over ARMA and MA

The AR modeling method is one of three fundamental mathematical modeling techniques, the other two being the autoregressive moving average (ARMA) and the moving average (MA). The choice of the model is based on the knowledge about the likely shape of the spectrum. The ARMA model is effective when the spectra to be estimated contain both sharply defined peaks (dominant frequencies) and notches (absence of power at particular frequencies), while the MA model is used when the spectra are well characterized by their notches. The AR model is effective for spectra that are well characterised by their peaks (resonances), making it the most appropriate method for the analysis of stationary time series [17]. AR modeling is often chosen, even when the spectral characteristics are not clearly 'peaky' for the following reasons:

1. Computing the MA and ARMA coefficients involves solving a complicated system of *nonlinear* equations.
2. The computational load to calculate the AR model parameters tends to be less than those for the MA and the ARMA models;
3. The MA and ARMA models can be represented by an AR model if its model order is high enough [27].

Therefore, AR modelling is suitable for time series that exhibit sudden peaks without being accompanied by any sudden deep hollows [18].

2.2.3.2 Comparing AR to FFT Methods

Investigating the sound signals produced by the blood flow in the aortic valves of patients, suffering from heart disease, the authors in [18] and [19] attempt to determine the best spectral analysis method that can resolve both the time and frequency components present in the signal. They compare the FFT, AR and WT.

Applying AR modelling, they first calculate the parameters, a_m, representing a p-ordered AR process as in (2.10), following the Levinson algorithm. With these parameters in hand, the power spectral density of the signal is obtained for a finite set of frequencies, using

$$P(k) = \frac{\sigma_p^2 \Delta t}{\left| 1 + \sum_{m=0}^{p} a_{pm} e^{-j2\pi f m \Delta t} \right|^2} \tag{2.11}$$

where $a_{p0} = 1$ the a_{pm} are the parameters and σ_p^2 is the driving variance.

The results achieved from the AR method demonstrates that although it produces good spectral resolution of the sound signal, it does not yield good results observing the effects of sudden fluctuations (i.e., poor time resolution). Moreover, it also produces misleading frequency components.

By comparison, the paper concludes that the WT is the superior transform in the case of spectral resolution and in the capturing of all frequency components. In addition, where the case of sudden changes is concerned, the WT method gives a better performance for spectral resolution than the FFT and AR methods.

Furthermore, in [17], three techniques are compared when analyzing non-stationary tremor data produced from subjects suffering from multiple sclerosis. The three techniques are:

1. Spectral estimation by FFT-based methods
2. Blackman-Tukey (BT) method of spectral estimation (taking the FFT of the autocorrelation of the signal) Power Spectral Density (PSD) estimator.
3. Autoregressive model of spectral estimation (the PSD is obtained from AR model parameters instead of directly from the original signal).

When the tremor data sequence was analyzed, using these techniques, the following spectral estimates, shown in Figure 2.8, were produced.

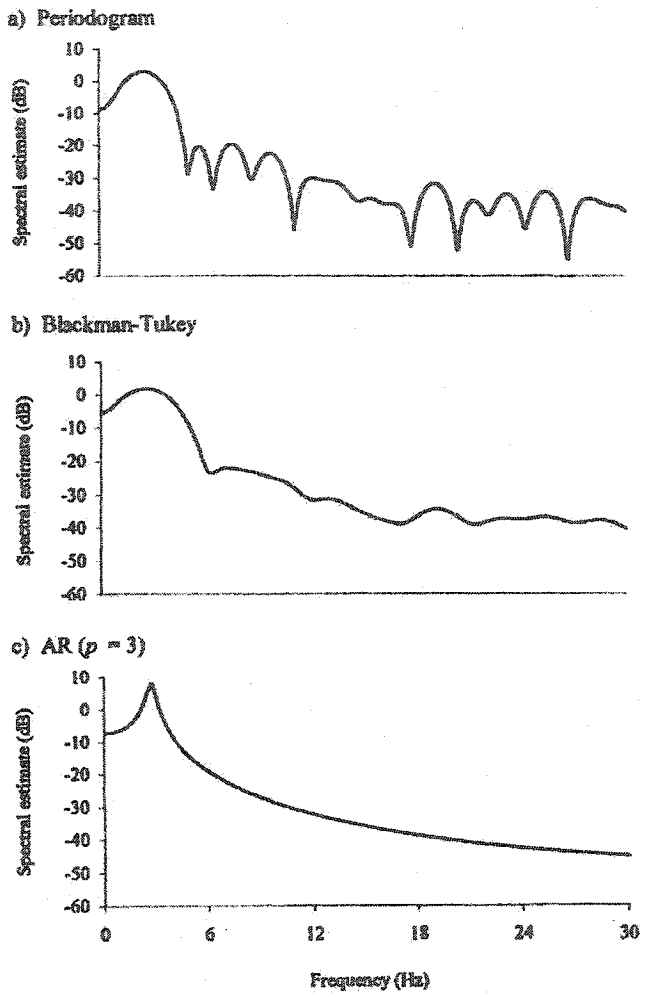

Figure 2.8: A comparison of FFT-based and AR spectral estimates. 60 points of postural tremor data from a patient with multiple sclerosis which has been high-pass filtered, f_{samp}=120 Hz. (a) Periodogram (average PSD obtained from FFT), (b) BT, (c) AR (order=3) (taken from [17]).

For this relatively short time series the AR method produces the clearest spectral estimate with a sharp peak at the tremor frequency of 2.6 Hz. In contrast, the corresponding peaks for the FFT-based estimates are both relatively wide indicating a lower resolution. The periodogram estimate is clearly the most variable while the AR estimate is the smoothest, notwithstanding the sharper peak.

Further testing of AR modeling was performed using simulated signals incorporating different amounts of additive noise. The results produced showed that AR modeling maintains both its smoothness and the sharp peak characterized in Figure 2.8c. However this smoothness comes at the cost of increasing its order. An increase in the model order has the effect of incorporating the additive noise into the AR model. For short data sequences, where the FFT-based methods produce poor results, careful adjustment of the model order can produce reliable AR spectral estimates, although the dangers of setting the order too high should be remembered. Therefore, [17] concludes that the inherent performance limitations of FFT based spectral estimation when analyzing short data segments can often be eliminated by the appropriate use of AR techniques.

The motivation for using AR modeling over the FFT based spectral estimation techniques is further emphasized in [28]. In this paper a comparison is made among the following:

1. FFT method
2. Autoregressive modeling
3. Wavelet based time-frequency

The results in [28] describe the FFT based spectral estimation to be a useful technique when used in analyzing stationary signals whereas the AR model improves the resolution of the spectra in the case of short duration signals, compared to the FFT approach. However, the paper goes on to describe how these two methods are inadequate in capturing the transients appearing in non-stationary signals because of their underlying stationary nature. In contrast, through their experiments on neurological non-stationary signals they conclude that

the WT provides the best means of describing the time-frequency distribution of the signal's spectrum. In other words, it is most useful in capturing and representing the temporal changes (particularly, the transients) in the spectrum of the EEG signal under investigation.

2.2.3.3 Shortcomings of AR

In closing, the major disadvantages of the AR method are:

1. *Stationarity*: The underlying assumption of the AR modeling process is that the signal it is modeling must be assumed to be stationary. This assumption makes the AR process unsuitable in a non-stationary environment. The stationarity requirement is a very restrictive limitation needed to obtain a statistically consistent spectral estimation [29]. With regard to biomedical signals, stationarity is not generally a biological condition, since many physiological changes may take place in short time with a fast adaptation [30].
2. *Model order*: The estimation of the model order poses a problem in a non-stationary environment. Once the model order is fixed, it may be insufficient to reliably track the changes in a non-stationary signal, where it could be too low sometimes or too high at other times.

The shortcomings of the AR process, when faced with a non-stationary signal, may be overcome using time-varying AR models [30], but this method will not be further discussed in this thesis.

2.2.4 Wavelet Transform

In Section 2.2.2, we presented the STFT and defined the frequency and time resolution that was achievable using that technique. It was explained, in that section, that the HUP provided a physical limitation to the amount of resolution one could expect to achieve in resolving a signal in either the frequency or the time domain. In the STFT case, once a window was selected the resolution in both frequency and time was fixed for the remainder of the analysis. However, by scaling the filters logarithmically, we saw that a greater flexibility could be achieved in terms of resolution. It is precisely this adjustability in time/frequency resolution that is used by the continuous wavelet transform (CWT) and consequently makes it a powerful tool in estimating the spectral content of a non-stationary signal.

In general the CWT is defined as:

$$\mathrm{CWT}(\tau, a) = \frac{1}{\sqrt{|a|}} \int x(t) h^*\left(\frac{t-\tau}{a}\right) dt \tag{2.12}$$

where $h^*((t-\tau)/a)$ represents a scaled time shifted version of a particular filter, τ represents the time shift variable and a represents the scale variable. Both variables a and τ are continuous in the CWT [24].

On the other hand, its inverse, which exists, recovers the original signal without loss and is given as:

$$x(t) = \frac{c}{\sqrt{a}} \int\int \mathrm{CWT}(\tau, a) h\left(\frac{t-\tau}{a}\right) \frac{da d\tau}{a^2} \quad , \quad a > 0 \tag{2.13}$$

where c is a constant of integration dependent on h(t) while all the other variables are the same as in (2.12). It must be mentioned that for reconstruction, as described in (2.13), to be possible, h(t) must be band pass and have finite energy. With these conditions satisfied, the time domain representation of h(t) resembles a 'small wave' from which comes the name wavelet [24].

In particular, the filter h(t) as it is used in (2.12) possesses the property of constant relative bandwidth described in Section 2.2.2.2. In other words, the CWT can be viewed as a filter bank of constant relative bandwidth filters which partitions the frequency domain logarithmically, as shown in Figure 2.7b. Moreover, the CWT partitions the time-frequency plane in a similar manner as shown in Figure 2.9a.

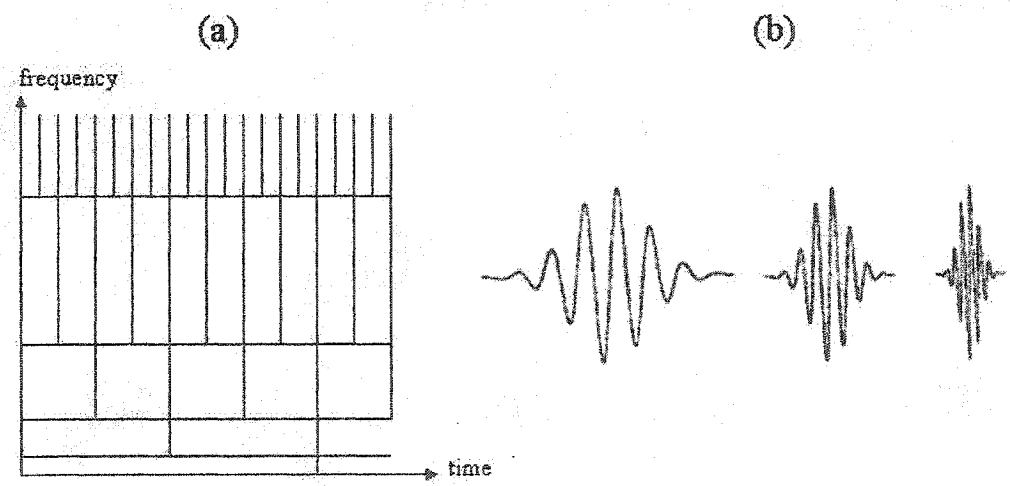

Figure 2.9: (a) CWT partition of the time-frequency plane, (b) CWT basis functions (taken from [24]).

Compared to the uniform time-frequency partition of the STFT of Figure 2.4a, Figure 2.9a shows that the CWT partitions the time-frequency plane into variably-shaped tiles ideally suited to capture the variable time and frequency content (transients) in a non-stationary signal. For example, in Figure 2.9a we see that the tiles with long time and short frequency

dimensions represent areas in the time-frequency plane where the CWT optimally captures the low frequency content of long time duration. Similarly, the tiles with short time and long frequency dimensions represent areas where the CWT optimally captures the high frequency content of short time duration. Therefore, the CWT offers a substantial improvement compared to the STFT because it is able to capture both the low frequency content and the high frequency bursts of short duration *optimally* and *simultaneously*. As a result, the CWT can be used to unambiguously represent a signal and, contrary to the STFT, can provide a clearer signal representation, which would allow more involved operations such as parameter estimation and pattern recognition to be performed on the "transform side" [24], as we shall see in the following sections.

Although function h(t), in the CWT, has been viewed as a filter it can also be viewed from another perspective as a basis function, referred to as a wavelet. Three examples of the CWT basis functions or wavelets, equivalent to scaled versions of h(t), are shown in Figure 2.9b. Viewed from this standpoint, the CWT is the result of taking the inner product between the signal and all of the wavelets forming its basis. For example, one particular wavelet of a given scale can be viewed as sliding over the entire signal producing continuous values or CWT coefficients. These coefficients represent the degree of correlation between the signal content and that particular wavelet. Repeating this action for all values of scale will produce the entire CWT. It is therefore important that the type (shape) of the wavelet used in the CWT resemble the type (shape) of the waveform content within the signal that it is analyzing. It must be mentioned that there are an infinite number of possible wavelets to choose from.

In [31] we see various applications for wavelets in neuroelectric waveforms. Initial evidence demonstrates that wavelet analysis offers real advantages in signal detection, component separation and computation speed over the traditional time-frequency analysis techniques like the STFT [32]. Moreover, wavelet analysis can provide improved methods of extracting and displaying meaningful information contained within neuroelectric waveforms. Clearly, traditional mathematical wavelets like the Haar and Daubechies wavelets shown in Figure 2.10 are not representative of typical biological wave shapes, however, more representative wavelets such as the Coifman and symlet wavelets, also shown in Figure 2.10, are better suited to represent neurological events such as microarousals[31].

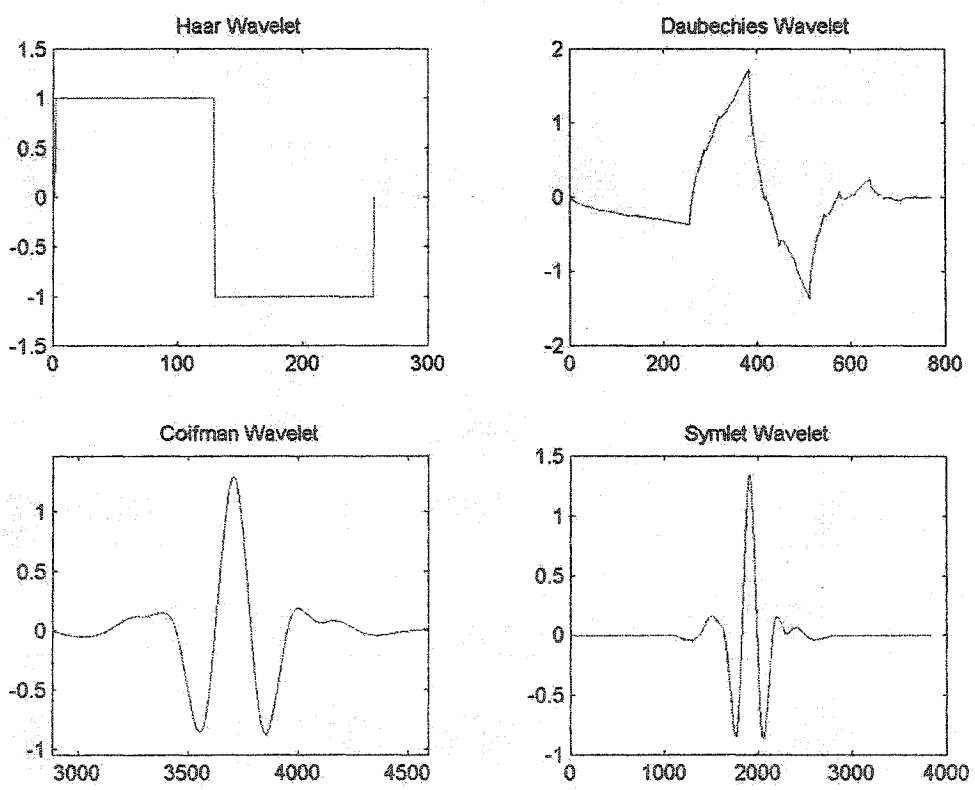

Figure 2.10: Sample of various wavelets.

In general, properly chosen wavelets will closely model the temporal and spectral properties of certain components of neuroelectric waveforms, thereby providing optimum resolution of those specific neuroelectric events. Recent work on designing members of a class of wavelets known as Meyer wavelets ([33] and [34]) to match specific signals now makes it possible to design wavelets that are close matches to the shapes of many of the specific waveforms whose analysis is desired. Wavelet representations provide precise measurements of when and to what degree transient and component events occur in a neuroelectric waveform and of when and how the frequency content of a neuroelectric waveform changes over time. In what follows we show the different ways that the WT transforms a signal and some of the applications in which they are used.

2.2.4.1 Continuous Time-Scale Decomposition (CWT)

The CWT provides a continuous decomposition of the signal in both time and scale. Its ability to resolve a signal over the whole range of scale magnification is a powerful tool for exploring the waveform structure of a non-stationary signal such as the EEG. The CWT is a useful transform, especially for applications where the small scale structure is important. An example of a CWT decomposition of a non-stationary sample of an EEG signal composed of many different small scale waveforms is shown in Figure 2.11.

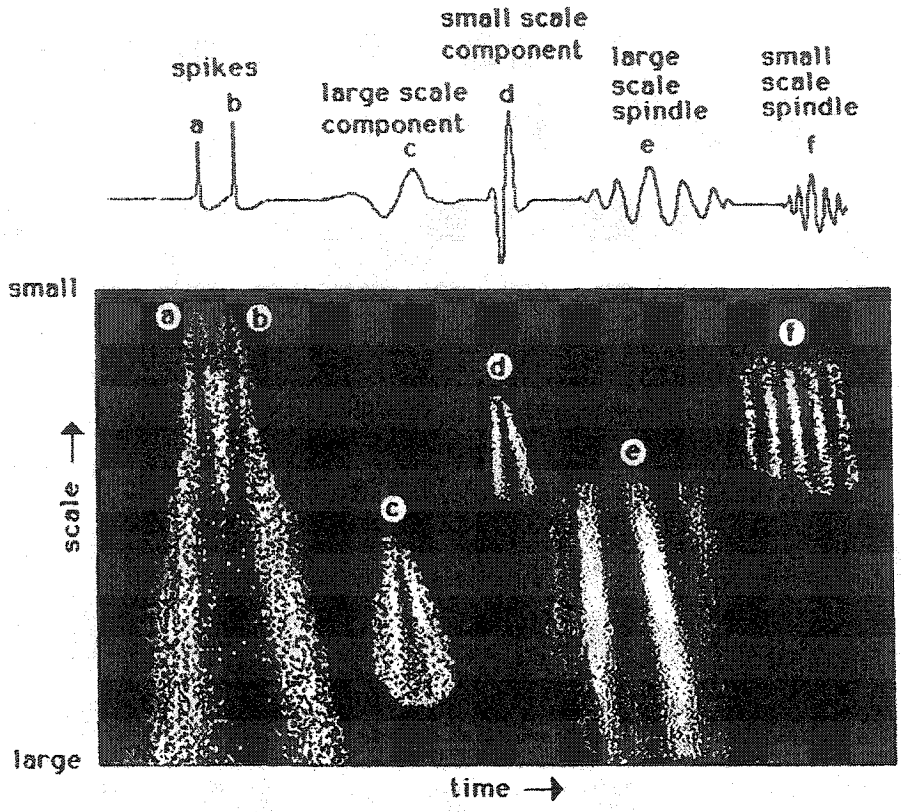

Figure 2.11: Time-scale plot of a sample of an EEG signal based on a CWT (taken from [31])

In Figure 2.11 we note that small scale events such as the spikes are captured compactly in the small scale (high frequency) area of the time-scale plane, where short time bursts are best resolved. Other larger events such as the large scale spindle and large scale component are captured most efficiently in the large scale (low frequency) area of the time-scale plane, where longer time events are best described. Some of the shapes of the waveforms in the signal are similar. As a result, their CWT representations also resemble each other. For example, waveforms c and d are identical in every respect except in scale. Similarly, their CWT representations are identical except that their position in the time-scale plane is different. This difference in position reveals their difference in scale, as well as in latency

(translation in time). The fact that patterns are identical but only their position in the time-scale plane is different can be exploited in pattern-recognition waveform analysis algorithms that search the time-scale plane for energy patterns that correspond to specific components, regardless of their specific width. Therefore, beyond its value as a visualization aid, the time-scale plot provides a good means for developing pattern recognition algorithms to identify meaningful neuroelectric events, especially in the presence of noise [31]. Although the CWT provides a good representation for pattern recognition algorithms, it is highly redundant in describing the signal's time-scale energy patterns. Theoretically, the set of CWT coefficients representing any signal is infinitely large, corresponding to an infinite range of scale and latency values. However, in practice the CWT is represented by a large but finite number of coefficients whose number far exceeds the actual number of samples used in the original signal. Therefore, for applications where a more efficient and concise representation is needed, the discrete wavelet transform (DWT) is used.

2.2.4.2 Discrete Time-Scale Decomposition (DWT)

The DWT removes the redundancy of the CWT by efficiently discretizing both the scale and the time (latency) in the time-scale domain (a detailed description of the DWT is given in Section 2.3). Contrary to the CWT which produces coefficients far in excess of the number of samples in the signal, the DWT produces exactly the same number of coefficients as the number of signal samples. As mentioned in Section 2.2.4, the wavelet slides across the signal at different scales producing the CWT coefficients at each latency with a

value proportional to the degree of correlation it has with the signal. Schematically, the discrete version of this procedure is shown in Figure 2.12.

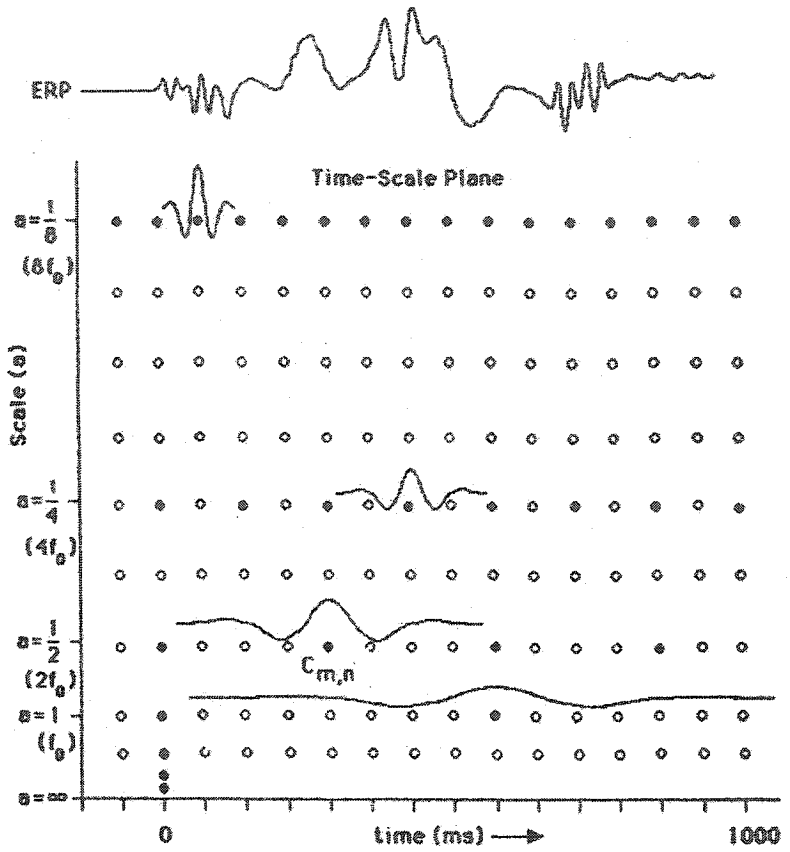

Figure 2.12: DWT coefficients mapping the time-scale contributions at discrete translations at each scale (taken from [31]).

The resulting set of coefficients concisely represents information at each scale separately. The scale in Figure 2.12 is a dyadic scale. We note that scale represents frequency and that scale and frequency are inversely related. Precisely, the term dyadic indicates that the frequency increases by a factor of 2 as you go down in scale to the next lower scale or conversely, that frequency decreases by a factor of 2 as you go up to the next higher scale. To really appreciate the savings in the number of generated coefficients that the DWT makes

compared to the CWT, we compare the black and white dots in Figure 2.12. In the grid of dots, the black and white dots are both included in the CWT coefficients while only the black dots represent the coefficients of the DWT. It is obvious from this small example that the savings offered by the DWT's concise representation is enormous. Furthermore, in this discrete form the signal can be processed by other signal processing tools to further extract the desired signal features. One such application is de-noising a signal of interest. The motivation for de-noising is clear: removing the noise enhances the presence of the signal thereby allowing further reliable analysis to proceed. With WT coefficients, effective de-noising can be achieved by zeroing the small coefficients [31]. Taking the inverse DWT (see Section 2.3) of the remaining coefficients produces a cleaner, de-noised signal.

2.2.4.3 Component Waveforms

With the de-noising example, we saw that a straightforward manipulation of the WT coefficients produces important results. Moreover, from Figure 2.12 we observe that the coefficients can be grouped together by scale. Taking the inverse DWT of these separate scale-grouped coefficients produces the component waveforms, shown in Figure 2.13.

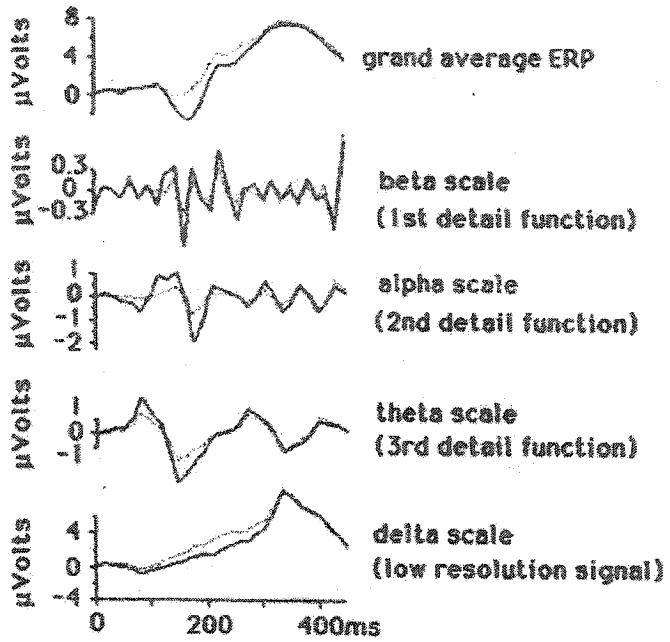

Figure 2.13: Three-level discrete wavelet transform (DWT) showing the component waveforms of the original waveform for each of the classic frequency bands: β, α, θ and δ (taken from [31]).

Seen from a different perspective these component waveforms are similar to the output of a bank of discrete relative frequency bandpass filters. What is especially useful for us is that by separating the different scales from each other the DWT can be used to divide the neurolectric signal into the traditional neurological frequency bands (e.g. delta, theta, alpha, beta) that play a crucial role in sleep staging. Specifically, the component waveforms can provide a moment by moment description of how the sleep activity in each of these frequency bands changes as a function of time [31]. It must be added however, that the unnatural choppiness seen in the component waveforms of Figure 2.13 can be overcome by using a wavelet whose shape is better matched for the general shape of neurolectric signals [38], like the discrete Meyer wavelet for example. With the component waveforms, we can iso-

late the relevant frequency bands in order to efficiently analyze and identify transients of particular interest (i.e., microarousals). Indeed, the component waveforms representing the pertinent frequency bands will provide us with the preliminary foundation on which to conduct further analysis.

2.2.4.4 Examples of some WT applications

The identification of specific types of neurological waveforms such as MAs clearly falls in the category of pattern recognition, a field in which artificial neural networks (ANN) play a key role. Therefore, to further appreciate the representational power of the WT, we include examples of an application where the WT preprocesses the input signal to an ANN. In [35] wavelet representations of the evoke related potentials (ERPs) were used as the input to a neural network algorithm designed to monitor human signal detection performance in a vigilance task. In their experiment a comparison was made with the results produced by using raw ERPs or the principal components (i.e., amplitude, interval) of the ERPs as the inputs to the ANN. Through the WT preprocessed inputs, [35] was able to show significant improvements in the detection of ERPs compared to the other inputs. In another similar experiment [36] the WT was again used to preprocess the input signals to an ANN. In particular, they sought to detect a specific EEG pattern waveform composed of a spike followed by a slow wave (SSW) embedded in a noisy background, as shown in Figure 2.14.

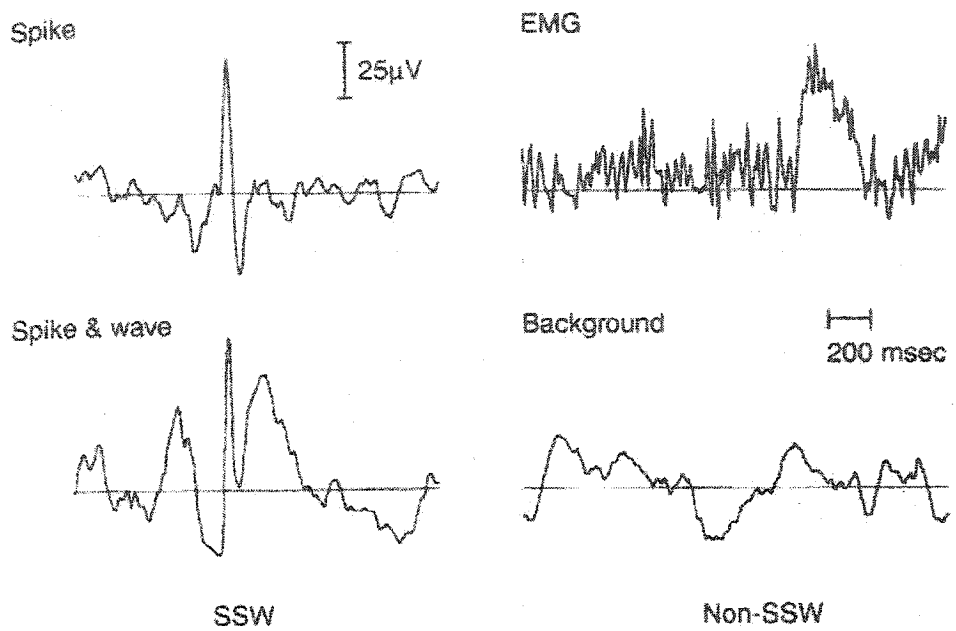

Figure 2.14: Examples of classified EEG events (taken from [36])

They proceeded to test and train the ANN with the WT processed input signal. Due to the concise representation and the fast transformation that the WT offered, [36] shows that the WT sharply decreases the input size of the ANN without much compromise in its performance.

As another example [37] demonstrates that the WT improved the decomposition of ERPs into functionally specific components. The WT offered them a precise means to control the frequency selectivity of the decomposition resulting in precise component identification, even when the components overlapped in time and frequency.

Moreover, due to the infinite variety of wavelet shapes available a great deal of control is made possible in the selection of wavelet shapes to match the shapes of ERPs embedded in

the waveform. Properly selected wavelets such as these are excellent templates to detect and separate those components and events from the background waveform [38]. Once separated, wavelet coefficients provide a direct measure of the feature of those components, including their amplitudes, latencies and duration.

As another example, [39] and [40] demonstrate that wavelet pattern recognition algorithms can be especially useful when the component or event varies in scale from waveform to waveform, as, for example, in the case of a specific (i.e., auditory brainstem) evoked response in different individuals.

2.3 Wavelet Transform Theory

In the previous section, we looked at the results from the literature, comparing the WT with other standard analysis techniques used on various biomedical signals. This survey demonstrated that the WT outperforms them in representing non-stationary signals due to its superior time-frequency resolution. Specifically, the WT, because of its flexible time-frequency resolution, is particularly well suited in describing transients (like MAs) present in non-stationary signals. In this section we will present a brief description of the theory underlying the WT. The classic references to this subject are [41],[42],[43] whereas the texts used to elaborate some of the concepts detailed in these papers and assist in the following theoretical description are [44],[25],[45],[46],[47].

2.3.1 Function Description through Series Expansion

In many situations it is convenient to expand a function by a means of another set of functions expressed as a linear combination

$$f(x) = \sum_k \alpha_k \varphi_k(x) \qquad f(x) \in L^2(\mathbf{R}) \tag{2.14}$$

where k is an integer index of the finite or the infinite sum, α_k are real-valued expansion coefficients and φ_k real-valued expansion functions. One condition that is imposed on f(x), which is a property present in most signals encountered in practice, is that it be of finite energy or an element of the square summable function space denoted as $L^2(\mathbf{R})$.

The individual functions $\varphi_k(x)$ are called basis functions and the expansion set, $\{\varphi_k(x)\}$ form a basis for all functions within the function space, V, expressed as:

$$V = \overline{\operatorname{Span}_k\{\varphi_k(x)\}} \tag{2.15}$$

That is, if f(x) belongs to V then it is capable of being expanded by the closed span $\{\varphi_k(x)\}$ and as a result can be expressed by (2.14).

2.3.2 Multiresolution Approximation of $L^2(\mathbf{R})$

The interest is not to express the function through just one subspace of $L^2(\mathbf{R})$ but to express it completely throughout the $L^2(\mathbf{R})$ space. That is, we would like to express f(x) with the infinite subspaces V_j belonging to $L^2(\mathbf{R})$; we seek a multiresolution approximation.

$$\{0\} \subseteq \dots \subseteq V_{-1} \subseteq V_0 \subseteq V_1 \subseteq \dots \subseteq L^2$$

The function f(x) in one subspace has a piece in all higher subspaces. To put it another way, if f(x) is in the whole space, then a piece of f(x) or $f_j(x)$ is in each V_j, where $V_j \in L^2$. This idea in and of itself is the goal but for it to be possible certain conditions must be imposed.

***Definition**:* the multiresolution analysis: $\ldots \subseteq V_{-1} \subseteq V_0 \subseteq V_1 \subseteq \ldots$, with some function $\varphi(x)$, is an increasing sequence of subspaces of $L^2(\mathbf{R})$ satisfying the following four conditions [45],[46]:

1a.	(density)	$\bigcup_{j \in \mathbf{Z}} V_j$ is dense in $L^2(\mathbf{R})$
1b.	(separation)	$\bigcap_{j \in \mathbf{Z}} V_j = \{0\}$
2.	(scale invariance)	$f(x) \in V_j \Leftrightarrow f(2x) \in V_{j+1}$
3.	(shift invariance)	$f(x) \in V_0 \Leftrightarrow f(x-k) \in V_0$
4.	(orthonormality)	$\{\varphi(x-k)\}_{k \in \mathbf{Z}}$ is an orthonormal basis for V_0

The special function $\varphi(x)$ is called the *scaling function*. It is a real and square-summable function, and as will be seen, in conjunction with the above definitions, plays *the* central role in MRA.

2.3.2.1 Scaling Function

It follows directly from the above definition that the set $\{\varphi_{j,k}(x)\}$ forms an orthonormal basis for V_j.

$$\varphi_{j,k}(x) = 2^{j/2}\varphi(2^j x - k) \tag{2.16}$$

where j, k $\in \mathbb{Z}$. and specifically k denotes translation, 2^j denotes scale and $2^{j/2}$denotes the height or amplitude of the scaling function for the related subspace. Therefore, for a given value of j or scale, the scaling function and all of its integer translations form the necessary basis for that scale.

By the definition of MRA, $V_j \subseteq V_{j+1}$ and from (2.16) it is clear that for higher values of *j* or higher scales, the scaling function becomes narrower or more refined. In other words, as you go up in scale the resolution increases, as does the size of the subspace.

Let us consider two specific subspaces and their scaling functions, where $\varphi_{0,k} \in V_0$ and $\varphi_{1,k} \in V_1$.By condition (4) in the definition, $\varphi_{0,k}$ spans the subspace V_0 and $\varphi_{1,k}$ spans the subspace V_1. However, since $\varphi_{0,k}(x) \in V_0 \subseteq V_1$, we have

$$\varphi_{0,k}(x) = \sum_n g_0(n)\frac{1}{\sqrt{2}}\varphi_{1,n}(x) \tag{2.17}$$

where, substituting values from (2.16) into (2.17), we get

$$\varphi(x) = \sum_n g_0(n)\varphi(2x-n) \tag{2.18}$$

This important recursive relationship is called the *scaling equation* or *dilation equation* and the coefficients $g_0(n)$, are called the scaling *function* coefficients.

2.3.2.2 Wavelet Functions

Now, let us define a subspace W_j that possesses the following properties:

$$W_j \perp V_j \text{ and } W_j \perp W_{j+1}. \tag{2.19}$$

Furthermore, let us also define W_j as the difference between the dependent subspaces V_j and V_{j+1}. Or said differently, using the Hilbertian sum operator of subspaces [46]

$$W_j \oplus V_j = V_{j+1} \tag{2.20}$$

The relationship of (2.20) completes the decomposition description initiated by the MRA. From (2.20) we note that any function $p(x) \in V_{j+1}$ can now be decomposed into any number of different lower scales such that:

$$\begin{aligned} V_{j+1} &= W_j \oplus V_j \\ &= W_j \oplus W_{j-1} \oplus V_{j-1} \\ &= W_j \oplus W_{j-1} \oplus W_{j-2} \oplus \cdots \end{aligned} \tag{2.21}$$

Similar to the development describing the relationship between the scaling function $\varphi(x)$ and subspace V_j, the subspaces $\{W_j\}$ are spanned by a basis function, $\psi(x) \in W_j$, called wavelets

$$\psi_{j,k}(x) = 2^{j/2}\psi(2^j x - k) \tag{2.22}$$

Furthermore, since $\psi(x) = \psi_{0,k}(x) \in W_0$ and from the decomposition sum in (2.20), we clearly have $W_0 \in V_1$, a wavelet in one subspace can be expanded by the scaling functions of the next higher subspace $\psi_{0,k}(x) = \sum_n g_1(n)\frac{1}{\sqrt{2}}\varphi_{1,n}(x)$ leading to

$$\psi(x) = \sum_n g_1(n)\varphi(2x - n) \tag{2.23}$$

which is identical to (2.18), except for constant coefficients, $g_1(n)$, called *wavelet function* coefficients. Similar to (2.18), (2.23) is called the wavelet equation.

2.3.3 Signal Decomposition

Combining (2.18) and (2.23), a function $f(x) \in L^2(\mathbf{R})$ can be expressed for a given $\varphi(x), \psi(x) \in L^2(\mathbf{R})$ as:

$$f(x) = \sum_k a_0(k)\varphi_{0,k}(x) + \sum_{j=0}^{\infty}\sum_k d_j(k)\psi_{j,k}(x) \tag{2.24}$$

where the $a_0(k)$'s and the $d_j(k)$'s are the approximation (scaling) coefficients and detail (wavelets) coefficients respectively. The signal decomposition in (2.24) is referred to as the discrete wavelet transform (DWT). By taking the inner product we get

$$a_0(k) = \langle f(x), \varphi_{0,k}(x)\rangle = \sum_x f(x)\varphi_{0,k}(x) \tag{2.25}$$

and

$$d_j(k) = \langle f(x), \psi_{j,k}(x)\rangle = \sum_x f(x)\psi_{j,k}(x) \tag{2.26}$$

Practically, the calculation of the coefficients $a_j(k)$ and $d_j(k)$ used in the DWT of (2.24) is not performed as descriptively presented in (2.25) and (2.26). Instead, a fast and efficient algorithm using perfect reconstruction filter banks, known as the fast wavelet transform or subband coding, is used.

2.3.4 Fast Wavelet Tranform: Subband Coding

Through an appropriate manipulation of the above material, we can describe a recursive relationship on both the approximation and the detail coefficients.

$$\left.\begin{aligned} a_j(x) &= \sum_m a_{j+1}(x)h_0[2k-m] \\ d_j(x) &= \sum_m a_{j+1}(x)h_1[2k-m] \end{aligned}\right\} \quad j, k, m \in \mathbb{Z} \tag{2.27}$$

where $h_0[k]$ and $h_1[k]$ are appropriate sequences.

In terms of signal analysis this relationship represents a filtering operation followed by a downsampling by 2 of both the detail and approximation coefficients. This operation is shown schematically in Figure 2.15

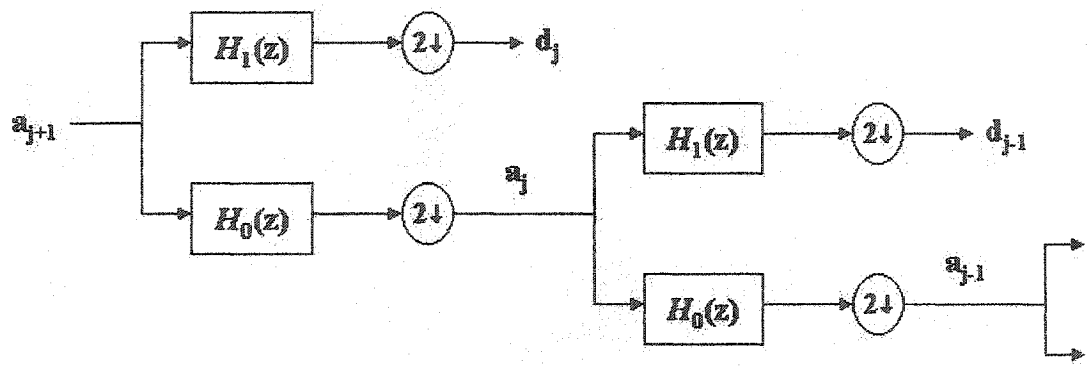

Figure 2.15: Analysis filter bank used in the decomposition of the 2-level DWT.

Similarly, we can reverse the process and reconstruct the next higher level from the previous level, combining (2.18) and (2.23), to obtain the recursive synthesis relationship:

$$a_{j+1,m} = \sum_k \{g_0[m-2k]a_{j,k} + g_1[m-2k]d_{j,k}\} \tag{2.28}$$

Again, looking at (2.28) as a signal processing operation, we note that, compared to (2.27), the operations involved in reconstructing the higher scale coefficients are reversed. Now, interpolation of the lower scale approximation coefficients by a factor of 2 begins the syn-

thesis followed by convolution with either the scaling filter $g_0[n]$ or the wavelet filter, $g_1[n]$. This process is illustrated in Figure 2.16.

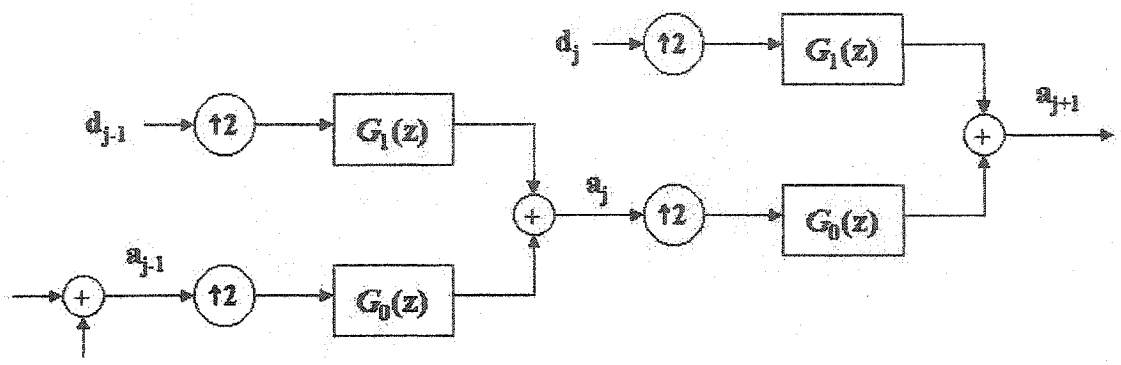

Figure 2.16: Synthesis filter bank used in the reconstruction stage of the 2-level DWT.

2.3.5 Conditions Imposed to achieve Perfect Reconstruction

To obtain perfect reconstruction (PR)[1], certain requirements must be imposed on the analysis filters $h_0[n]$, $h_1[n]$ and the synthesis filters $g_0[n]$, $g_1[n]$. These conditions are clearly explained in [41],[44],[25],[47].

This concludes the description of the discrete implementation of the WT. In closing, it should be added that putting aside the spectral advantages, from the MRA of the WT,[1] its implementation through the FWT offers another desirable property. It is a fast transform. In comparison with the FFT, which executes about $O(n\log n)$ computations, the FWT operates faster by executing roughly $O(n)$ computations, where n is the length of the signal being analyzed, which proves to be advantageous as the value of n increases.[44],[47]

1. PR assumes no intervening destructive process, such as lossy compression, is applied in the processing block between the decomposition stage and the reconstruction stage

2.4 Conclusion

In this chapter, we have described that the first stage or transform stage of the proposed microarousal detection procedure involved the decomposition of the signal into a compact and pertinent form. Since other spectral techniques have been applied to similar types of problems the justification, behind choosing the wavelet transform has been explained.

A comparison between the wavelet transform and various spectral estimation techniques such as the fast Fourier transform, the short time Fourier transform and the autoregressive model, traditionally applied for biomedical signal analysis has been provided. From this literature survey, confident conclusions have been drawn pointing out the wavelet transform's clear advantages over these traditional spectral transforms. In large part the wavelet transform's advantages are due to its excellent ability to resolve both time and frequency simultaneously. Time-frequency resolution is essential in achieving accurate detection. Furthermore, the WT has been shown to be particularly well suited, compared to the other techniques, in the non-stationary environment of biomedical signals. Many different types of biomedical signals, similar to the EEG, in their non-stationary characteristics, have been chosen to compare the wavelet transform against the traditional spectral transforms. The results of the comparisons, based on these biomedical signals, have clearly shown that the wavelet transform is the superior transform in describing and isolating desired small structured wave patterns.

After describing the relative merits of the wavelet transform over the other techniques, a brief yet detailed description of the structure of the wavelet transform has been given. In particular, its orthogonality as was as its ability to perform multiresolution analysis have

been considered. Finally, a procedure outlining its implementation for discrete signals, known as the fast wavelet transform has been given.

Chapter 3

Stationarity Detection Techniques

3.1 General

When using the WT to decompose our signals, we are still left with the task of extracting the relevant patterns from them, to aid us in our goal of establishing a reliable diagnostic tool. The wavelets only provide a new window into the signal that will peel off enough layers of redundancy to allow the analysis tools to more clearly dissect and accurately identify the presence of MAs. The wavelet decomposition is a first step towards detection and identification.

Although the WT simplifies the representation of the EEG signal, by itself, it is not sufficient to isolate the MA. To aid in its detection, the signal's properties must be described in such a way as to take advantage of the various subband frequency information provided by the WT. An effective mathematical procedure which greatly improves the EEG signal's description is the application of statistical modelling. That is, by describing the pseudo random nature of the signal as a stochastic process, the signal's apparantly random nature can be further characterized through its moments (i.e. mean, variance etc.), until the presence of the MAs can be detected by means of a suitable statistical test.

As was pointed out in the previous chapters, the EEG signal, as well as its WT, is a non-stationary signal. That is its statistical properties change with time. In order to establish a

good test, the signal must be broken into piecewise stationary segments, whereupon each segment's statistical properties are made quasi-independent of time. Segmenting the signal into stationary segments allows a comparison to be made between segments. Although each segment may possess different properties, the imposition of stationarity, provides a solid base of characterization, where comparisons can be made to determine the presence of MAs. A formal description of stationarity is needed.

3.2 Stationarity

A random process, $X(t)$, can be given a complete statistical description, for any n and any instant of time $(t_1, t_2, \ldots, t_n)$ if its joint probability density function (pdf), $f_X(x_1, x_2, \ldots, x_n; t_1, t_2, \ldots, t_n)$ always exists. In general, the properties of a random process's joint pdf depends on the specific origin of time. If the joint pdf of a random process is independent of the choice of the time origin, that is, if it is invariant to a shift in time, then that process is said to be a stationary process. There are different types of stationarity assessments, characterizing random processes, two of which are of interest - strictly stationary processess and wide sense stationary processes [48].

Definition: A random (or stochastic) process, $X(t)$, is said to be strict-sense stationary (SSS) if *all* of its statistical properties (i.e. all of its moments) are independent of any shift in origin. In other words a SSS process must be such that it satisifies the following:

$$f_X(x_1, x_2, \ldots, x_n; t_1, t_2, \ldots, t_n) = f_X(x_1, x_2, \ldots, x_n; t_1 + c, t_2 + c, \ldots, t_n + c) \qquad (3.1)$$

for any value of time displacement c.

From this definition, it is clear that the joint pdf characterizing the process depends only on the relative position of the time instants $t_1, t_2, \ldots, t_n$ and not on there specific values. Unfortunately, this definition imposes too severe a constraint to be met realistically in most applications. A loosening of the constraint imposed by 'strict' stationarity is achieved by considering wide sense stationarity (WSS).

Definition: A random process, $X(t)$, is said to be wide-sense stationary if it satisfies the following condition:

i. $E[X(t)] = \mu_X(t) = \text{constant}$

ii. $E[X(t)X(t+\tau)] = R_{XX}(\tau)$

where μ_X is the statistical mean and R_{XX} is the autocorrelation function of the random process.

Specifically, condition (i) states that the mean of the WSS process is independent of time, while condition (ii) states that given time instants $t_1 = t$ and $t_2 = t + \tau$ then, the value of R_{XX} depends only on the time difference $\tau = t_2 - t_1$ and not on t_1 and t_2 individually. Therefore, a WSS process is SSS to the second order and as a result is a subset or particular case of a SSS process. In other words, WSS maintains the requirements of SSS upto the second moment but does not guarantee the same for higher moments, since $\text{WSS} \subset \text{SSS}$.

Describing a random process in order to assess whether or not its statistical properties evolve with time is not trivial. There are two statistical approaches which address this prob-

lem. One of them is called the non-parametric approach and the other is the parametric approach.

3.2.1 Non-Parametric Approach

The non-parametric method is one which makes no assumption with respect to the probability distribution of the random process under investigation. By looking directly at the data representing the process, non-parametric methods try to determine, depending on what feature (i.e. amplitude, autocorrelation, variance etc.) is studied, the stationarity of the process.

3.2.2 Parametric Approach

Parametric methods, on the other hand, *do* make an assumption about the underlying probability distribution generating the random process. With such an assumption, a random process can modelled. Assuming that the assumption is accurate, the model parameters, characterizing the process, are used in determining the stationarity.

The methods used in this thesis to establish piecewise stationarity are as follows:

1. Autocorrelation Method (non-parametric)
2. Nonlinear Energy Operator Method (non-parametric)
3. Generalized Likelihood Ratio Method (parametric)

These methods are described in detail in the following sections.

3.3 The Autocorrelation Function Method

3.3.1 General Procedure

The autocorrelation function (ACF) method [49] functions by first observing the EEG signal through a moving window. This moving window must have not only a window length (WL) that is at least as small as the smallest waveform segment expected, but also long enough to observe the slowest frequency component. A second window is fixed as a reference at the beginning of the observation interval. A comparison is made between the content of both the windows. If the difference between the EEG segments seen through both of these windows is significant enough, then a decision is made to set a boundary line indicating that two different stationary segments exist on either side of this boundary. To set this boundary reliably two steps must be performed.

1.Detection of Non-stationarity

2.Optimal Non-stationarity Positioning.

3.3.2 Detection of Non-stationarity

To establish the occurance of a non-stationarity, we must determine a difference measure between the reference and the moving windows. This difference measure must possess certain properties that minimize ambiguity and further support the claim that a non-stationarity has been observed. Therefore the difference measure must:

1.be zero when the EEG content of both the windows is the same,

2.be indifferent to direction of the window sliding over the non-stationarity. Whether the window slides from left-to-right or from right-to-left over the non-stationarity, it should be detected equally,

3.ensure that the degree of change in an occurring non-stationarity, like an increase in amplitude/frequency should record the same magnitude difference measure as a similar decrease in amplitude/frequency, and

4.allow that, if two or more parameters (the two parameters we use are frequency and amplitude) are used to detect non-stationarities, their combined contribution towards detection is relevently weighted to reflect each parameter's proportional contribution.

The ACF method proposed in [49] addresses the points above, as well as the critical factors just mentioned. By incorporating the above points, the ACF method establishes stationarity as a linear sum of relative amplitude change plus relative frequency change, referred to as the *energy distance* and the *spectral distance*, respectively. Specifically, the combination of the approximated ACFs, obtained from both the reference and sliding window, shown in Figure 3.1, assists in computing the energy and spectral distance. Furthermore, with suitably chosen thresholds, the spectral and energy distances are normalized and combined into a final distance measure, which serves to detect non-stationarities in the signal.

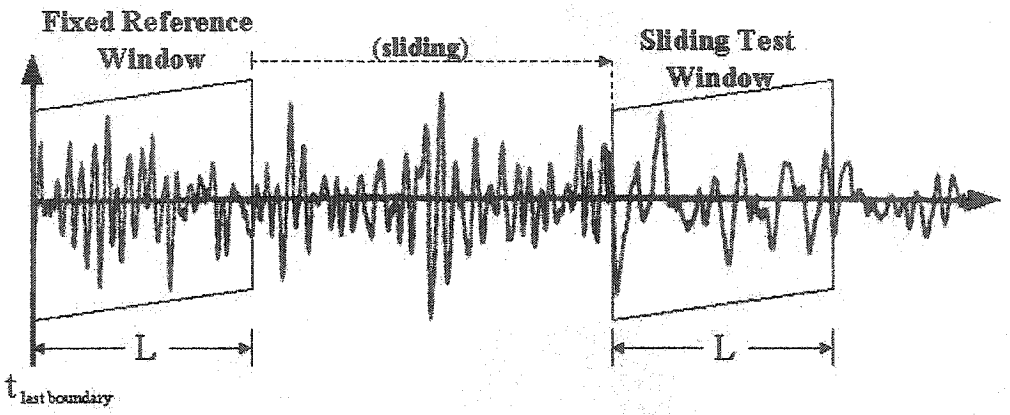

Figure 3.1: Difference measure obtained using a fixed reference window and a sliding test window.

3.3.2.1 Energy Distance

The energy distance, or percentage change in amplitude $d_a(t)$, is obtained directly from the ACFs of the reference and the test windows. This percentage change in amplitude is given by the absolute value of the difference between the standard deviations (i.e. the square root of the power given in the ACFs) divided by their minimum. Precisely, let us assume that

$R_r = [r_r(0), r_r(1), \ldots, r_r(L\text{-}1)]$ is the ACF of the reference window and that

$R_t = [r_t(0,t), r_t(1,t), \ldots, r_t(L\text{-}1,t)]$ is the ACF of the test window, where L denotes the window length.

Now, the energy distance is calculated using signal's power or in terms of the ACF as the ACF at zero lag:

$$d_a(t) = \frac{\left|\sqrt{r_t(0,t)} - \sqrt{r_r(0)}\right|}{\min\{\sqrt{r_t(0,t)}, \sqrt{r_r(0)}\}} \qquad (3.2)$$

The two superimposed ACFs are shown in Figure 3.2, as are the parameters used to determine $d_a(t)$, in (3.2), where the A is the difference between the two ACFs and P_a and P_b represent the ACF at zero lag for the reference and test window respectively.

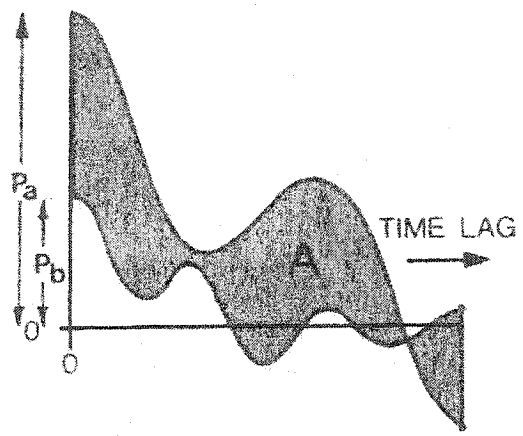

Figure 3.2: The superimposed reference and test ACFs used to estimate the energy distance (taken from[49]).

3.3.2.2 Spectral Distance

Contrary to the energy distance, which relies directly on the ACFs obtained from both the reference and the test windows, the spectral distance or percentage change in frequency is obtained through the *normalized* ACFs of the two windows. These normalized ACFs are shown in Figure 3.3.

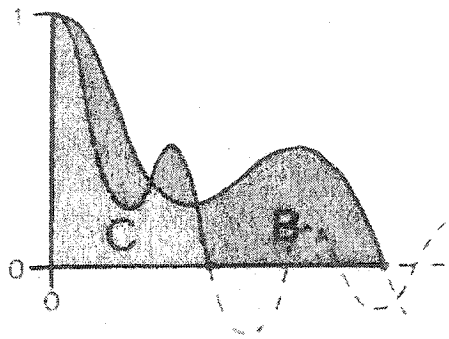

Figure 3.3: The superimposed normalized reference and test ACFs used to estimate the spectral distance (taken from[49]).

As noted in [49], the overall spectral distance of a signal is always directly coupled to the changes in the signal's normalized ACF. That is, the information about the spectral content is obtained through a comparison of the normalized ACFs from both the reference and the test windows. Specifically, the spectral distance is given by dividing the spectral difference between the two windows, indicated by region B in Figure 3.3 by the spectral region common to both windows, indicated by region C. In other words, considering Figure 3.3, $d_f(t) = \frac{B}{C}$. Furthermore, following the procedure outlined in [49] each ACF must be truncated to its first positive section to obtain a reliable frequency measure so as to provide an overall estimate of the frequency change between the two windows. Consequently, truncation of the normalized ACFs, R_{nr} and R_{nt}, reduces their overall length, L, to M, where $M < L$. The new truncated ACFs are now denoted as $\overline{R}_{nr}$ and $\overline{R}_{nt}$, while the *spectral distance* is given as [54]:

$$d_f(t) = \frac{2\sum_{k=1}^{M} |\bar{r}_t(k,t) - \bar{r}_r(k)|}{1 + 2\sum_{k=1}^{M} \min\{\bar{r}_t((k,t), \bar{r}_r(k))\}} \tag{3.3}$$

3.3.2.3 Detection Thresholds

Since the threshold is the critical measure used to identify non-stationarities, deciding its value requires careful consideration. We denote these critical values for amplitude and frequency changes as T_a and T_f. They can both be set independently from each other but they are usually made equal for best results. For this reason, any change in the amplitude per-

centage will be equivalent to the same percentage change in the frequency. Bearing this in mind, the overall autocorrelation distance measure is given by:

$$d(t) = \frac{d_a(t)}{T_a} + \frac{d_f(t)}{T_f} \tag{3.4}$$

A threshold point is declared whenever the overall threshold $d(t)$ crosses the normalized global threshold, T_g, of unity. When a threshold point is declared, then, a non-stationarity is said to have been detected. However, the detection of the non-stationarity is only half of the problem solved; we still do not know accurately *where* the non-stationarity is. Therefore, the other half of the problem, requires optimizing the real position in time of the non-stationarity.

3.3.3 Optimal Non-stationarity Positioning

In the previous section we determined, by the overall threshold, if the test window *detected* the presence of a nonstationarity. Now, our goal is to determine *where*, in time, it occurred within the signal. In other words, we must now *estimate* its exact position.

The point in time (t), when detection is confirmed is only nominal. This point is not precise. When the difference measure crosses the threshold, indicating the presence of a non-stationarity, this event can only guarantee that a non-stationarity has occurred somewhere within the test window. The reason for this ambiguity lies in the varying nature of the changes between the signal content in the test window compared to the content in the reference window. Because the difference in content takes the form of an abrupt change, the distance offset, $d_{off}(t)$, between the detection time, t, and the actual position of the change,

varies directly according to the size, type (frequency/amplitude) and direction (increase/ decrease) of the change and as such can vary accordingly from zero to the entire window length. In Figure 3.4, a general description of the problem is illustrated.

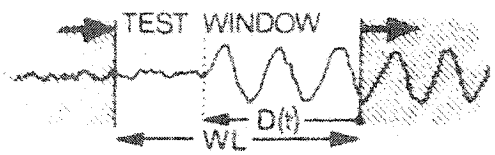

Figure 3.4: Estimating the optimal position of the non-stationarity (taken from[49]).

To estimate $d_{off}(t)$ (i.e. shown as D(t) in Figure 3.4) we take advantage of the fact that the test window's non-normalized ACF is a sum of linear products. Keeping this in mind, we note that after the point t, as the test window continues to slide past this threshold point, the value of A, shown in Figure 3.2 continues to increase linearly until the full window length is reached. Recording this maximum value of A, we determine the value of $d_{off}(t)$ by multiplying the ratio of the value of A at time t when detection was declared, and the maximum value of A with the length of the window. The offset distance is then given by:

$$d_{off}(t) = L \frac{\sum_{k=0}^{L-1} |r_t(k,t) - r_r(k)|}{\max \sum_{k=0}^{L-1} |r_t(k,t_o) - r_r(k)|}, \qquad t_o \in [t, t+L] \tag{3.5}$$

Once the exact non-stationary position is obtained, the reference window is moved to this new location and the procedure repeated again throughout the entire signal.

3.3.4 Parameter Adjustment

Although the procedure just outlined is quite straightforward, serious attention must be focussed on the main parameters. Both the window length and the thresholds are working parameters whose values fundamentally impact the operation of the ACF method. Due to the varying nature of the signal, which consistently defies systematization, selection of their values must rely on empirical estimates determined ad hoc. Following the argument that each person and as such each EEG is unique, we cannot propose a global value for these parameters to optimize performance to work for every different EEG. However, for a specific EEG (realization), we can estimate realization-specific parameters after preliminary testing of a small sample of the overall signal.

3.4 Nonlinear Energy Operator Method

3.4.1 Introduction

Another non-parametric method that we will use to partition the EEG signal into stationary segments is the nonlinear energy operator (NLEO) method. Proposed as a means of automatically analyzing EEG during long term monitoring [50], this method develops a four step algorithm, which can reduce a 24h recording to a two page summary that contains an efficient breakdown of the salient waveforms present in the signal. The obvious real-time advantage, when such a concise summary is transmitted by fax or email to an experienced physician from an hospital emergency room or an intensive care unit (ICU), requiring rapid and accurate diagnosis, cannot be overstated.

3.4.2 Method

The overall algorithm involves four steps:

1.segmentation

2.feature extraction

3.classification

4.presentation

The focus of our attention will only concentrate on the first two steps. In this chapter, we discuss segmentation and postpone the discussion of feature extraction to chapter 5. The procedure used in the segmentation of the EEG signal into stationary segments and the feature extraction applied to each segment, will allow us to compare with the R&K rules and decide whether a microarousal is scored.

3.4.3 Segmentation

Part of the problem in determining the presence of a non-stationary boundary is in developing a reliable measure of statistical properties and especially in quantifying the changes that occur with these on both sides of this boundary. In the previous section, we dealt with the ACF method and saw that in that case the adequate difference measure was established by comparing the autocorrelation produced by signal content in the reference window with the autocorrelation produced by the signal content in the test window and then deciding if this difference exceeded a predetermined threshold. In the present case, we apply a proce-

dure that operates on a similar principle but with different characteristics. As outlined below, this segmentation procedure, contrary to the ACF method, applies:

1. the *NLEO* as the difference measure;
2. *one window,* instead of two windows to compare the difference measure with the threshold;
3. an *adaptive threshold,* instead of a fixed threshold;

A further advantage offered by the NLEO method, which makes it more attractive for segmentation is its reliance on minimal parameter adjustment. Remember that the ACF method critically relied on the choices made on both the window length and the values for the frequency and amplitude thresholds, which for convenience were made equal.

3.4.3.1 Nonlinear Energy Operator

The NLEO, as a measurement of a signal's properties, possesses the advantage of simple description. Proposed by Teager, while conducting research on nonlinear speech modeling, his simple NLEO was then expressed in discrete form by Kaiser [51], which is the form used in this theses and is shown in (3.6).

$$\Psi_{\mathrm{NLEO}}[x(n)] = x^2(n) - x(n-1)x(n-2) \tag{3.6}$$

The particular relevance of the description provided by the NLEO, especially with regards to EEG, is nicely emphasized by one of its key properties, illustrated in (3.7).

$$\Psi_{\text{NLEO}}[A\cos(\omega_o n+\theta)] = \frac{1}{2}A^2\omega_o^2 \tag{3.7}$$

Here, we see, in its effect on a pure sine wave, that it extracts both of that sine wave's amplitude and frequency components, which is important since they are the most important parameters used for evaluating changes in the signal. The proportional relation given in (3.7) has been termed frequency-weight energy.

Because of the square term in (3.6), this expression does not properly ignore the presence of white noise. We first note that the expression proposed by [51] is a particular case of the more generalized form of the NLEO presented by [52]

$$\Psi_{\text{general}}[x(n)] = x(n-r)x(n-p)-x(n-q)x(n-s) \qquad r+p = q+s \tag{3.8}$$

This generalized form of the NLEO, offers a more flexible means of combating the presence of noise. For instance, if we set $r \neq p$ and $q \neq s$ it can be easily shown that Ψ_{general} is more robust to the presence of white noise. Again, because of this condition, the presence of the square term and consequently the white noise is no longer present. Furthermore, in [50] a proposed set of values for r,p,q and s is presented, where $r = 1$, $p = 2$, $q = 0$ and $s = 3$

By selecting these values, the presence of white noise is reduced and the properties of the NLEO discussed above remain intact, thus allowing the detection of changes in the stationarity of the signal to proceed.

3.4.3.2 Single Window Difference Measure

In order to use the NLEO to detect changes in the signal's stationarity, a comparison is made between different segments of the signal. The mechanism that performs this comparison employs a sliding temporal window [53]. As illustrated in Figure 3.5, a single window of size $2N$ samples slides over a signal, which demonstrates time varying ampitude and frequency portions.

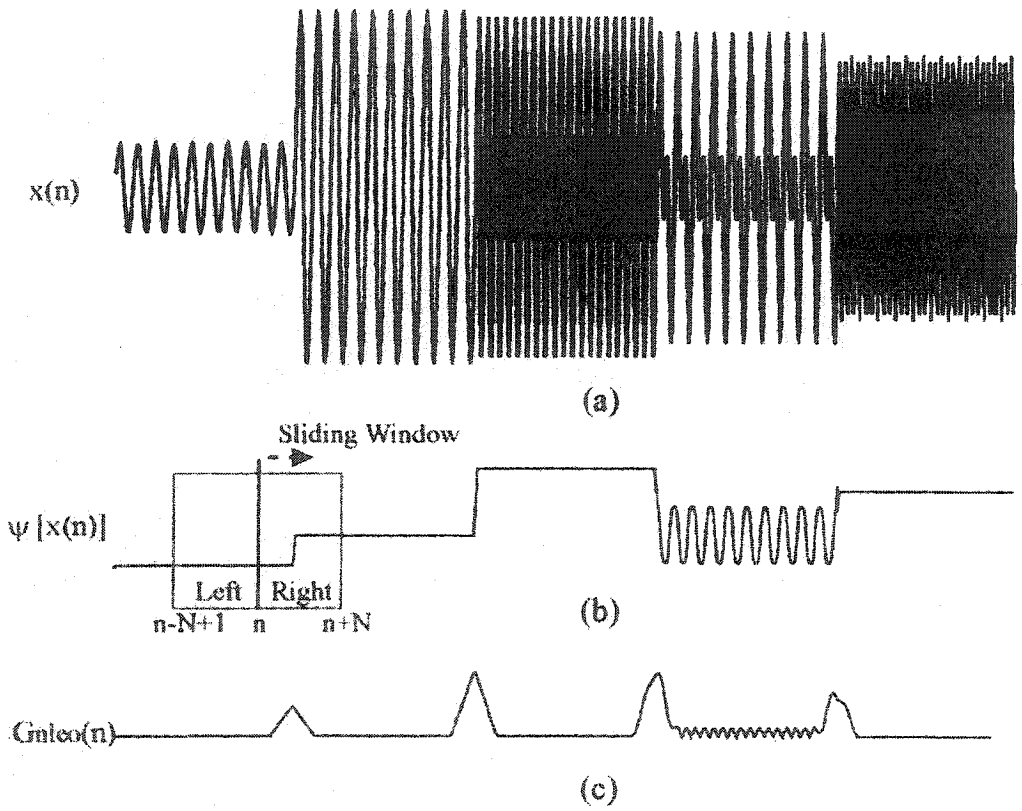

Figure 3.5: General outline of NLEO method. (a) Synthetic signal. (b) NLEO output. (c) Resulting boundaries used for segmentation (taken form[50]).

The comparison is made between the two halves of the window. When the window is centered at some time instant n over the signal, the NLEO, or frequency-weighted energy, produced in the left half of the window, is subtracted from the NLEO produced in the right half. Explicitly, this difference measure, $G_{nleo}(n)$ is expressed as

$$G_{nleo}(n) = \sum_{m=n-N+1}^{n} \Psi(m) - \sum_{m=n+1}^{n+N} \Psi(m) \tag{3.9}$$

This window comparison scheme produces results that are intuitively satisfying. As the window slides across the signal, if it slides over a stationary portion, that is, if the entire content within the window is stationary, then the energy produced from both halves of the window must be equal and consequently the difference measure, $G_{nleo}(n)$ will be zero. However, whenever the window slides over the boundary of two different stationary segments then the maximum difference will occur, unless one of the stationary segments is smaller than half of the window, when the window's center is positioned directly over the non-stationary boundary (i.e., the point separating the two *different* stationary segments), as shown in Figure 3.5. Therefore, once a maximum $G_{nleo}(n)$ occurs, say at time instant n, we can mark the beginning of a new stationary segment as the center of the window and place the segment boundary at time instant n.

3.4.3.3 Adaptive Thresholding

Unfortunately, the $G_{nleo}(n)$ is plagued with its own inherent fluctuations that may produce spurious redundant segment boundaries. This effect, however, can be considerably mini-

mized by thresholding $G_{nleo}(n)$. Unlike the ACF method, where a fixed value is chosen throughout the entire signal, the NLEO method *adapts* the threshold locally

$$T(n) = \begin{cases} \max\left[G_{nleo}\left(n-\frac{N}{2} : n+\frac{N}{2}\right)\right] & \text{for } n = \frac{N}{2}, \left(\frac{N}{2}+1\right), \ldots \\ 0 & \text{for } n = 0, 1, \ldots, \left(\frac{N}{2}-1\right) \end{cases} \tag{3.10}$$

With this adaptive threshold, we now reformulate the difference measure as

$$G(n) = \begin{cases} G_{nleo}(n) & G_{nleo}(n) \geq T(n) \\ 0 & G_{nleo}(n) \leq T(n) \end{cases} \tag{3.11}$$

Applying this adaptively thresholded version of $G_{nleo}(n)$, all of the necessary criteria are established to allow the detection of non-stationarities to be made.

3.5 Generalized Likelihood Ratio Method

3.5.1 Introduction

In the previous sections we discussed at length the operation of the ACF method and the NLEO method of segmenting the EEG signal into stationary parts. Both of these methods are examples of non-parametric methods of segmentation; we now turn our attention to one example of a parametric method: the generalized likelihood ratio (GLR) method [54].

As with the other two methods, the GLR applies an overall general procedure that is essentially the same. The procedural breakdown involves the use of:

1. the likelihood ratio (LR) as a difference measure,

2.•two sliding windows to establish segmentation boundaries using the LR,

3.•optimizing the boundary position.

It is clear that all the three methods share a common methodology in segmenting the signal; however, the real difference between the GLR and the other methods lies squarely on the use of the parametric modelling of the signal in conjunction with the LR (a parametric measure of stationarity) as the central stationarity measure. Other differences include its use of two growing windows as well as the distinct procedure it uses to optimize the boundary postions.

3.5.2 Likelihood Estimation

The nucleus of the GLR method lies in its ability to distinguish two statistically varying portions of the EEG signal from one another. To achieve this objective the algorithm makes use of the LR. The ratio is obtained by comparing the likelihood estimate produced by the two segments of the signal. To understand the way the likelihood estimate works, we assume a stationary random time series $x(t)$ of length N, which we model using the typical autoregressive process model of order p [27]:

$$\sum_{i=0}^{p} a_i x(t-i) = e(t) \qquad (3.12)$$

where a_i are the constant AR parameters, with $a_0=1$ and $e(t)$ is the white noise, innovation process, that is composed of uncorrelated, independent and identically distributed Gaussian samples with zero mean and variance $\sigma^2=1$.

By considering N samples of the noise process, we obtain its likelihood function l [55]:

$$l = (2\pi\sigma^2)^{\frac{(N-p)}{2}} \exp\left[-\frac{1}{2\sigma^2}\sum_{t=p+1}^{N} e(t)^2\right] \tag{3.13}$$

In (3.13) we see that l corresponds to the joint probability density function of the set $\mathbf{e}=\{e(1), e(2), ..., e(N)\}$. We can also consider (3.13) in matrix form and rewrite it as:

$$l = (2\pi\sigma^2)^{\frac{(N-p)}{2}} \exp\left[-\frac{1}{2\sigma^2}(N-p)\mathbf{a}\mathbf{C}\mathbf{a}^T\right] \tag{3.14}$$

where the set $\mathbf{a}^T = \{1, a_1, a_2, ..., a_p\}$ is the (p+1)-dimensional AR parameter vector of the time series x(t) and C is the (p+1) x (p+1) covariance matrix, which is given by:

$$c(i,j) = \frac{1}{N-p}\sum_{t=p+1}^{N} x(t-i)x(t-j) \qquad i = 1, 2, \ldots, p \tag{3.15}$$

To obtain the maximum likelihood estimate $\mathbf{a}$, which we denote by $\bar{\mathbf{a}}$, we must solve the following set of normal equations:

$$\sum_{j=1}^{p} c(i,j)\bar{a}_j = c(i,0) \qquad i = 1, 2, \ldots, p \tag{3.16}$$

Once the estimate of $\mathbf{a}$ has been determined, the estimate of the time series' variance σ, denoted as $\bar{\sigma}$ can now be obtained by:

$$\bar{\sigma}^2 = \bar{a}C\bar{a}^T \tag{3.17}$$

Now that we have described the likelihood estimate, we will shift our attention to the development of the likelihood ratio.

3.5.3 Likelihood Ratio

In order to obtain the likelihood ratio, let us consider two finite duration random time series, $x_R(t)$, of length N_R, which will be used to denote the *reference* sequence and $x_T(t)$ of length N_T, which will represent the *test* sequence. Furthermore, let us assume that these two series can be modeled by a stationary, normally distributed AR process of order p. That is, both series satisfy an AR equation:

$$\sum_{i=0}^{p} a_{R,i} x_R(t-i) = e_R(t) \tag{3.18}$$

$$\sum_{i=0}^{p} a_{T,i} x_T(t-i) = e_T(t) \tag{3.19}$$

As defined above, the sets $\mathbf{a}_R = [1, a_{R,1}, a_{R,2}, ..., a_{R,p}]$ and $\mathbf{a}_T = [1, a_{T,1}, a_{T,2}, ..., a_{T,p}]$ are the $(p+1)$-dimensional constant AR coefficient vectors, for the reference and the test sequences, respectively. Similarly, the white noise processes, $e_R(t)$ and $e_T(t)$, have variances σ^2_R and σ^2_T respectively. Again, we define the covariance matrices, corresponding to both the reference and test sequences, $\mathbf{C}_R$ and $\mathbf{C}_T$, shown above for the general case, as [54]:

$$c_R(i,j) = \frac{1}{N'_R} \sum_{t=p+1}^{N_R} x_R(t-i) x_R(t-j) \qquad i,j = 0, 1, ..., p \tag{3.20}$$

and

$$c_T(i,j) = \frac{1}{N'_T} \sum_{t=p+1}^{N_T} x_T(t-i) x_T(t-j) \qquad i,j = 0, 1, ..., p \tag{3.21}$$

where, $N'_R = N_R - p$ and $N'_T = N_T - p$.

Having thus established the covariance matrices for the two sequences, we are now in a position to use them in conjunction with the likelihood estimate of (3.14) and to calculate their joint likelihood, conditioned to the first p observations of each sequence [55]:

$$l = (\sigma_R\sqrt{2\pi})^{-N'_R}(\sigma_T\sqrt{2\pi})^{-N'_T}\exp\left[-\frac{N'_R}{2\sigma_R^2}\mathbf{a}_R^T\mathbf{C}_R\mathbf{a}_R-\frac{N'_S}{2\sigma_S^2}\mathbf{a}_T^T\mathbf{C}_T\mathbf{a}_T\right] \tag{3.22}$$

With (3.22), a test can now be performed on the two sequences to determine statistical similarity. This comparison is achieved by comparing the maximum likelihood, l_1, given arbitrary settings, with the maximum likelihood, l_0, under the null hypothesis. These two choices are given as:

$$H_0 \; : \; a_R = a_T \qquad \sigma_R^2 = \sigma_T^2$$
$$H_1 \; : \; a_R \neq a_T$$

The absolute maximum likelihood, l_1, under hypothesis H_1 can be determined by:

$$l_1 = (\bar{\sigma}_R\sqrt{2\pi})^{-N'_R}(\bar{\sigma}_T\sqrt{2\pi})^{-N'_T}\exp\left[-\frac{1}{2}(N'_R+N'_T)\right] \tag{3.23}$$

while the conditional maximum likelihood, under the null hypothesis, H_0, is given by:

$$l_0 = (\bar{\sigma}_p\sqrt{2\pi})^{-(N'_R+N'_T)}\exp\left[-\frac{1}{2}(N'_R+N'_T)\right] \tag{3.24}$$

with,

$$\bar{\sigma}_p^2 = \bar{\mathbf{a}}_p\mathbf{C}_p\bar{\mathbf{a}}_p^T \tag{3.25}$$

Comparing (3.25) and (3.17), we can see that these equations are almost identical. However there is a difference which exists between the two that arises directly from the manner in which the $\bar{\mathbf{a}}_p$ or estimates of the constant AR coefficients $\mathbf{a}$, are derived. The $\bar{\mathbf{a}}_p$ are esti-

mated from **a**, by 'pooling' or combining the reference and test sequences together, under the null hypothesis. The effect of this pooling results in the covariance matrix, $\mathbf{C_p}$, used in (3.25), which is given as:

$$\mathbf{C}_p = \frac{N'_R \mathbf{C}_R + N'_T \mathbf{C}_T}{N'_R + N'_T} \tag{3.26}$$

Having thus derived the necessary likelihood estimates, we can now formulate the desired likelihood ratio:

$$\lambda = \frac{l_0}{l_1} = \bar{\sigma}_p^{-(N'_R + N'_T)} \bar{\sigma}_R^{N'_R} \bar{\sigma}_T^{N'_T} \tag{3.27}$$

The range for this likelihood ratio is $0 < \lambda < 1$. Now that we have the likelihood ratio, we can now define the distance measure, which will enable us to distinguish statistically dissimilar segments.

3.5.4 Distance Measure

To convert the likelihood ratio to a suitable distance measure *d*, we apply the logarithm to it and obtain the generalized likelihood ratio (GLR):

$$d = -2\ln\lambda = (N'_R + N'_T)\ln\bar{\sigma}_p^2 - (N'_R \ln\bar{\sigma}_R^2 + N'_T \ln\bar{\sigma}_T^2) \tag{3.28}$$

The non-stationarity detection is achieved by comparing *d* to a reasonably chosen threshold, used as means of detecting whether both the sequences are statistically similar or not. In addition to its statistical meaning, the distance *d* can be shown to represent the information loss caused by the assumption that the null hypothesis is true [54].

3.5.5 Detection of Non-stationarity

In order to detect the presence of a non-stationarity, two windows are used. One window, called the reference window, is positioned at the start of the last detected segment boundary and grows continuously, from an initial length of L, as new samples are made available. The second window, called the test window, of fixed length L, slides contiguously with the reference windows as shown in Figure 3.6

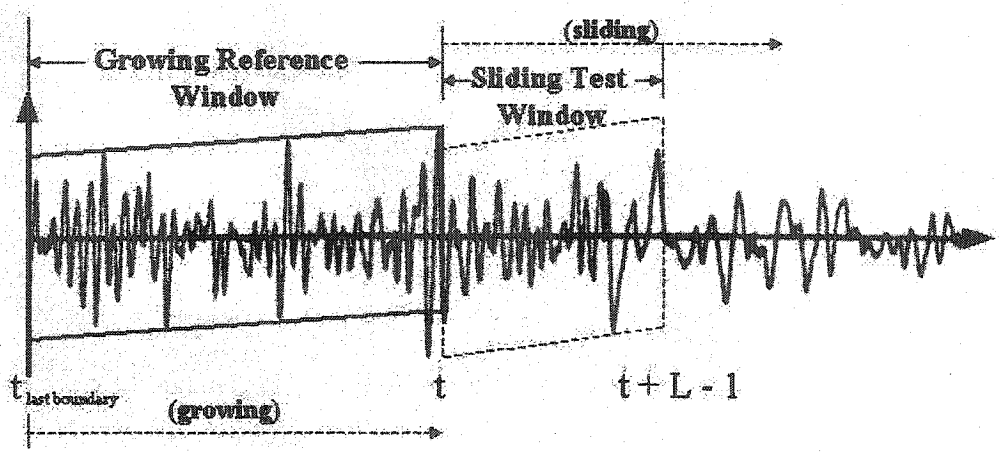

Figure 3.6: Detection of non-stationarity using a growing reference and sliding test window.

With the reference window positioned at the start of a new stationary segment, it begins growing at time $t = t_{last\ boundary} + L$. The fixed sized test window is adjoined to the reference window and slides along with the growing reference window in the manner shown in Figure 3.6. The decision that a non-stationarity occurs is made by applying the GLR to both of the sequences, within the two windows, x_R and x_T. Therefore, we have $N'_R = t\text{-}1$, $N'_T = L$ and the pooled length of both sequences as: $N_p = N'_R + N'_T = t + L\text{-}1$. Substituting these values into (3.28), the GLR distance becomes:

$$d(t, t+L-1) = (t+L-1)\ln\bar{\sigma}_p^2 - [(t-1)\ln\bar{\sigma}_R^2 + L\ln\bar{\sigma}_T^2] \qquad (3.29)$$

where $\bar{\sigma}_R^2$ and $\bar{\sigma}_T^2$ are the error variance computed respectively on the reference window and on the test window, and $\bar{\sigma}_p^2$ is the error variance calculated on the pooled window formed by the concatenation of both the reference and test windows. A decision on a new segment boundary is made whenever the GLR distance for a potential boundary position t, denoted by d(t, t + L - 1), in (3.29), exceeds a predetermined threshold *T*:

$$d(t, t+L-1) > T \tag{3.30}$$

The moment in time, (t+L-1), when the threshold T is crossed, is recorded and labelled as the *detection time* t_d.

3.5.6 Optimal Non-stationarity positioning

After a non-stationarity is detected, its precise location must then be found. It is assumed that the optimal position lies somewhere in the range (t_d - L + 1, ... , t_d) or one window length prior to the detection position t_d. The optimization procedure searches this optimal position through a sequence of GLR tests, as shown in Figure 3.7.

Initialization

The first GLR test involves two windows: a fixed reference window of constant length, L and a growing test window, which initially, before it starts growing is also of length L. These windows are positioned as shown in Figure 3.7a. They are positioned with respect to t_d. Explicitly, the reference window is positioned $2L$ samples before t_d and the test window is positioned L samples before t_d. In other words, at the beginning $t_{initial} = t_d - 2L + 1$,

$t_o = t_d - L + 1$ and $t = t_o$ where for clarity $t + L - 1 = t_d$. The window distance measure for Figure 3.7a is $d(t_o, t + L - 1)$ and is used to compare with the window distance measure from the second GLR test of Figure 3.7b.

In Figure 3.7b, initially the growing reference window is of length L and the fixed length sliding test window is also of length L. Before the procedure begins, the growing reference window is positioned $2L$ samples before t_d, while the sliding test window is positioned L samples before t_d. Explicitly, the initial values of the variables are defined as

$t_{initial} = t_d - 2L + 2$, $t = t_d - L + 2$, and $t + L - 1 = t_d + 1$.

We note that the value t in Figure 3.7b is initially one sample greater than the value of t_o in Figure 3.7a. That is, $t = t_o + 1$. The window distance measure is $d(t, t + L - 1)$ for Figure 3.7b.

Iteration and Update

The procedure begins by incrementing the value of t in both Figure 3.7a and Figure 3.7b by one sample with the constraint that $t_d - L + 2 \leq t \leq t_d$. For each value of t, the distance measures of Figure 3.7a and Figure 3.7b are compared to each other. If

$$d(t, t + L - 1) > d(t_o, t + L - 1) \tag{3.31}$$

then the optimal postion is updated to the new value $t_o = t$. This procedure is repeated for each time increment, until $t = t_d$. Finally, the best possible position of the non-stationarity corresponds to the last value of t_o.

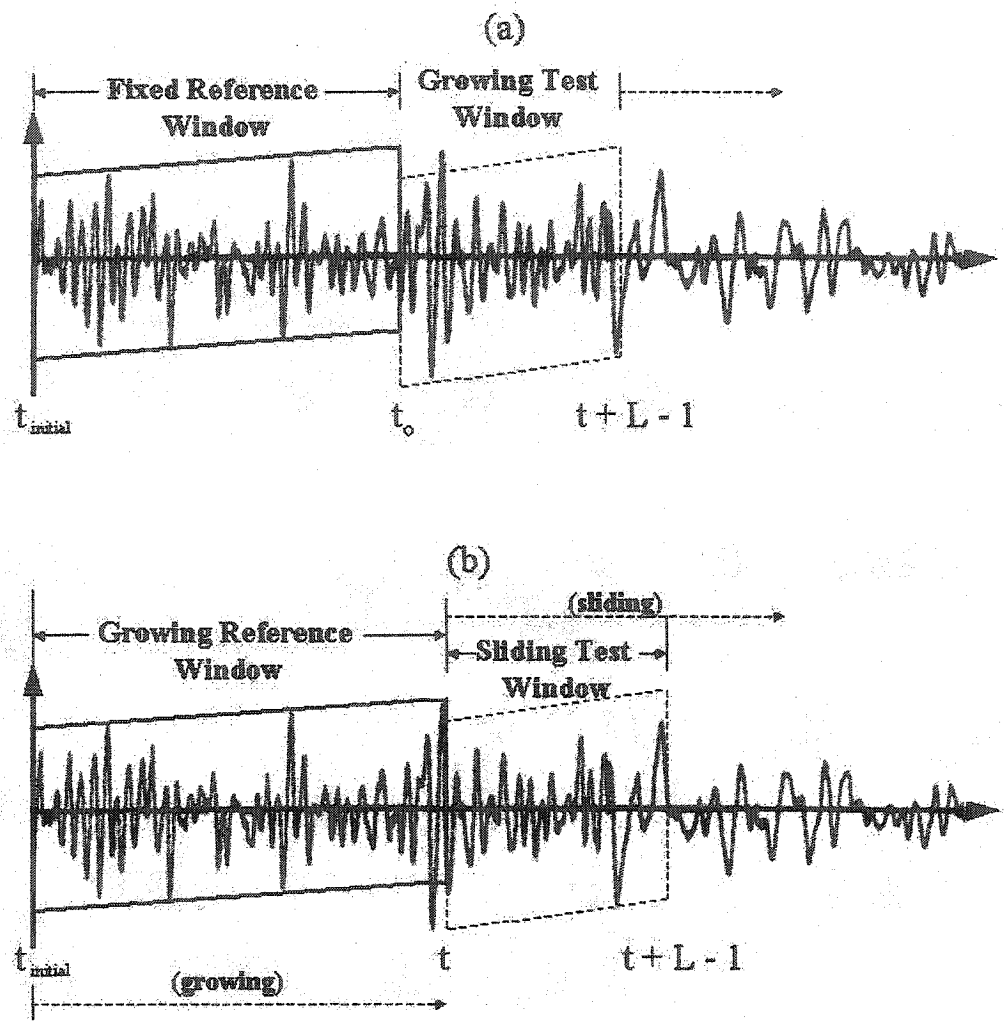

Figure 3.7: Optimization of the boundary position by comparing the distance measure produced by two different window schemes (a) Fixed Reference/ Growing Test scheme (b) Growing Reference/Sliding Test scheme.

3.5.7 Parameter Adjustment

Now that we have described the inner workings of the GLR method for detecting a non-stationarity, our attention focusses on the particular values and limits that the involved parameters are permitted to take, in order to ensure that the method achieves its maximum

performance. As described above, the three critical parameters that impact the performance are:

1.The AR-model order p

2.The test window length, L

3.The detection threshold T

Although parameter adjustment requires some degree of experience to select the best compromise for a given signal, some objective rules can be applied to a wide range of practical applications.

3.5.7.1 AR Model Order

For AR signals there exists two traditional methods commonly employed to determine the suitable model order, given a specific signal. These classic methods are the Akaike's information-theoretic criterion (AIC) [56] or Rissanen's minimum description length (MDL) [57]. It must be pointed out however, that the AIC criterion often overestimates the model order, while the MDL provides a more consistent model order estimator [27].

3.5.7.2 Test Window Length

Deciding on the length of the test window, *L*, depends upon a compromise between choosing a long window, which would ensure stable statistical results, and a short window, which would guarantee that short stationary segments are also detected. In [54], given a signal

segment of length N to be detected, a suitable tradeoff between these conflicting goals can be achieved, if L is chosen such that:

$$\left(\frac{p}{3}\right)^2 \leq L \leq 0.7N_{min} \tag{3.32}$$

where N_{min} is the shortest stationary segment that can be detected. Moreover, the lower bound $(p/3)^2$ allows for obtaining small error rates, whereas the 70% threshold is chosen to guarantee that the addition of the test window length L and the detection delay $t_d - t_o$ is always smaller than N_{min}.

3.5.7.3 Detection Threshold

The adjustment of the detection threshold T depends on the application for which the stationarity test has been implemented. Based on information theory, some general results can be derived [54]. The selection of an appropriate threshold can result in a very economical partition of the segment into stationary segments. If N_0 is the number of bits required to encode a new set of AR parameters, then the optimum coding is obtained by minimizing the sum of bits necessary to describe the prediction error signal added to N_0 bits times the number of stationary segments. Let us assume that the prediction error signal is optimally encoded. In this case, the number of bits required to describe it is provided by its information content:

$$I = -\log_2 l \tag{3.33}$$

where l is the likelihood of the prediction error signal. Since the latter is equal to the likelihood of the original time series, the maximum prediction error data reduction that can be

obtained by modifying the AR parameters at a boundary is given with respect to the GLR distance d by

$$\mathrm{I} = -\log_2 l_0 + \log_2 l_1 = \frac{\mathrm{d}}{2\ln 2} \tag{3.34}$$

where l_0 and l_1 represent the maximum likelihoods with invariant and changing AR parameters, respectively. So the GLR distance providing an optimal description of the time series is

$$T = (2\ln 2)N_0 \tag{3.35}$$

As [54] points out, this threshold value does not apply to all applications of the GLR and therefore should be adjusted according to the requirements of the application under study.

3.6 Conclusion

In this section, three window based methods were proposed to partition a non-stationary signal into segment-wise stationary pieces in order to detect MAs. Two of these methods, the ACF and the NLEO, represented non-parametric means of assessing the stationarity of the signal. The third method, the GLR, was the only parametric method used, which modeled or parametrized the signal, as an AR process.

Each method uses its own particular window scheme to detect and estimate the location of the non-stationary boundary. The ACF uses two constant-length windows with one window fixed while the other was allowed to slide; the NLEO uses only one window split

into two halves; the GLR used two windows with one constant length window immediately adjoined by a second window, which is allowed to grow.

The content of the windows, used in each of the schemes, are measured against an established threshold or difference measure, whose determination was specific to each method. For the ACF method this threshold is used to compare against the combined contributions given by both the normalized and non-normalized ACFs of each window; the NLEO method compares the nonlinear energies of each half window against its difference measure; the GLR measures the differences in likelihood ratios in the fixed and growing windows and compares against its threshold. Once the thresholds of the different methods are exceeded, a sufficient difference is judged to exist between segments of the signal. The position in the signal where this sufficient difference exists is marked as a non-stationary boundary. Once a non-stationary boundary is marked, further refinement is required to optimize the location of that position within the windows, where detection was first scored. The NLEO method localizes the non-stationary occurance simultaneously with its detection, whereas both the ACF and the GLR methods employ a second test to optimize the non-stationary position.

Chapter 4

Simulation Results

4.1 General

In the previous chapters, we discussed the individual stages, whose combination will ultimately lead to reliable automation in microarousal detection. These stages are

1. Wavelet Decomposition

2. Stationary Segmentation

The main components of the proposed procedure employed for the purpose of detection are shown in Figure 4.1. In this chapter, we test these components with a variety of signals. Through the application of relevant simulated signals, the performance of each component as well as the performance of the overall combination of these components making up the proposed procedure, will be examined.

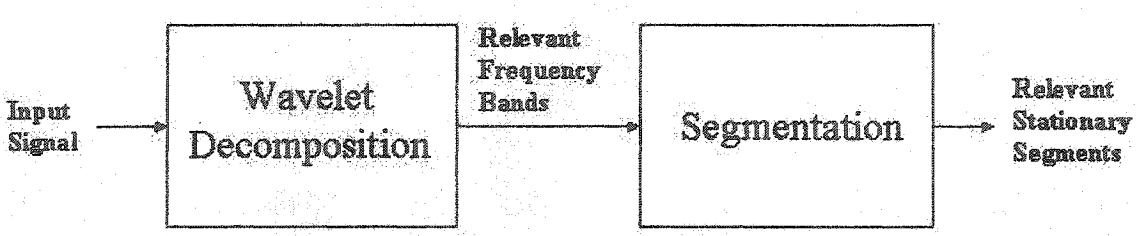

Figure 4.1: General outline of the proposed procedure

The chapter is broken up in the following manner. In Section 4.2, the wavelet decomposition is tested with various types of sinusoidal signals with and without the presence of noise to determine its effectiveness in highlighting relevant signal properties. In Section 4.3, the segmentation algorithms, ACF, GLR and NLEO, are tested. First, they are tested with sinusoids exhibiting various amplitude and frequency non-stationarities, then with similar non-stationarities but in the presence of noise, in order to uncover the statistical reliability of each algorithm, and finally with a second order autoregressive signal, to gain further statistical reliability insights. Section 4.4 demonstrates the effectiveness of combining the segmentation with wavelet decomposition. The same test signals as those used in Section 4.3 are applied to allow comparisons to be made. Finally, in Section 4.5, we summarize the results and observations made based on these experiments.

4.2 Wavelet Decomposition

The first step in the detection procedure involves the decomposition of the EEG signal into relevant frequency bands, using the WT. The main motivation behind this step lies in the WT's ability to unclutter the signal from the extraneous frequency content accompanying the EEG. It reveals a clearer picture of the desired signal and thereby allows the segmentation algorithms, discussed in Chapter 3, to track significant frequency changes more efficiently. As a result, the detection rate of MAs improves. Moreover, the WT possesses two important characteristics that lend themselves vitally to this application. These two characteristics are the WT's ability to resolve the decomposed signal in both frequency and time. Because the goal of the detection procedure is to detect uncharacteristic frequency changes

constituting the MAs, as well as the precise location of their occurance within the overall EEG signal, this criteria naturally leads to the involvement of the WT, as discussed in Chapter 2.

4.2.1 Selection of Wavelet Used

The type of wavelet chosen for the decomposition is clearly important. For the reasons explained in Chapter 2, the wavelet chosen should, as closely as possible, represent the signal that is being decomposed, which in this case is a biological signal. A good candidate, shown in Figure 4.2, is the discrete Meyer wavelet (DMW) [31], which is an approximation of the Meyer wavelet.

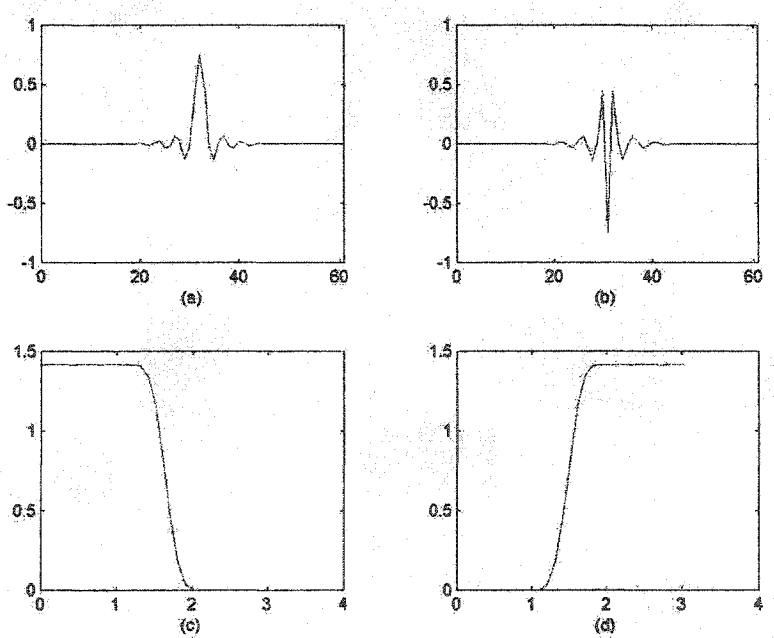

Figure 4.2: Discrete Meyer wavelet; (a) Low pass decomposition filter of DMW in the time domain; (b)High pass decomposition filter of DMW in the time domain; (c) Frequency domain version of (a); (d) Frequency domain version of (b).

Reasons motivating the use of the DMW is that it provides an orthogonal basis and therefore can represent a signal with a concise number of coefficients. Its structure allows it to be used in the fast wavelet transform (FWT) described in Section 2.3.4. It is a finite impulse response (FIR) digital filter and therefore assures us that it is a stable filter. Although there are many other filters available which satisfy theses conditions, what is important for us about the DMW, as [31] points out, is that it is especially well suited to pursue and capture frequently encountered neurolectric signals like sleep spindles for example. Finally, having selected the DMW as the wavelet for the decomposition, it will remain the only wavelet used throughout the following experiments.

4.2.2 Simulation Signals Used

The following deterministic signals have been chosen to illustrate the WT's ability to decompose a signal, and resolve it both in time and frequency.

1. Concatenated Sinusoids
2. Superimposed Sinusoids
3. Concatenated Sinusoids in the presence of AWGN
4. Superimposed Sinusoids in the presence of AWGN

Although simple in nature, these signals clearly demonstrate the WT's desired properties. Furthermore, the level of decomposition chosen throughout the remainder of this section is selected as 5. That is, this decomposition will produce five detail functions (d1,d2,d3,d4

and d5), and one approximation function (a5). The frequency content represented by each function is shown in Table 4.1

Table 4.1: Level - 5 wavelet decomposition detail and approximation functions with their related frequency bands

Approximation and Detail Functions	d1	d2	d3	d4	d5	a5
Related Frequency Bands (Hz)	[32-64]	[16-32]	[8-16]	[4-8]	[2-4]	[0-2]

4.2.3 Concatenated Sinusoids

With the application of the WT decomposition, we see that the frequency bands associated with the different outputs of the filter bank provide a viewpoint into the frequency makeup constituting the whole of the original signal. The concatenated sine wave signal, shown in Figure 4.3a is composed of same length sine waves, of gradually increasing frequency, which are adjoined to one another. The frequency of each distinct sinusoidal segment is chosen specifically so that at least one falls into the different scales or frequency bands represented by the various detail functions Figure 4.3c-4.3g and the approximation function Figure 4.3b.

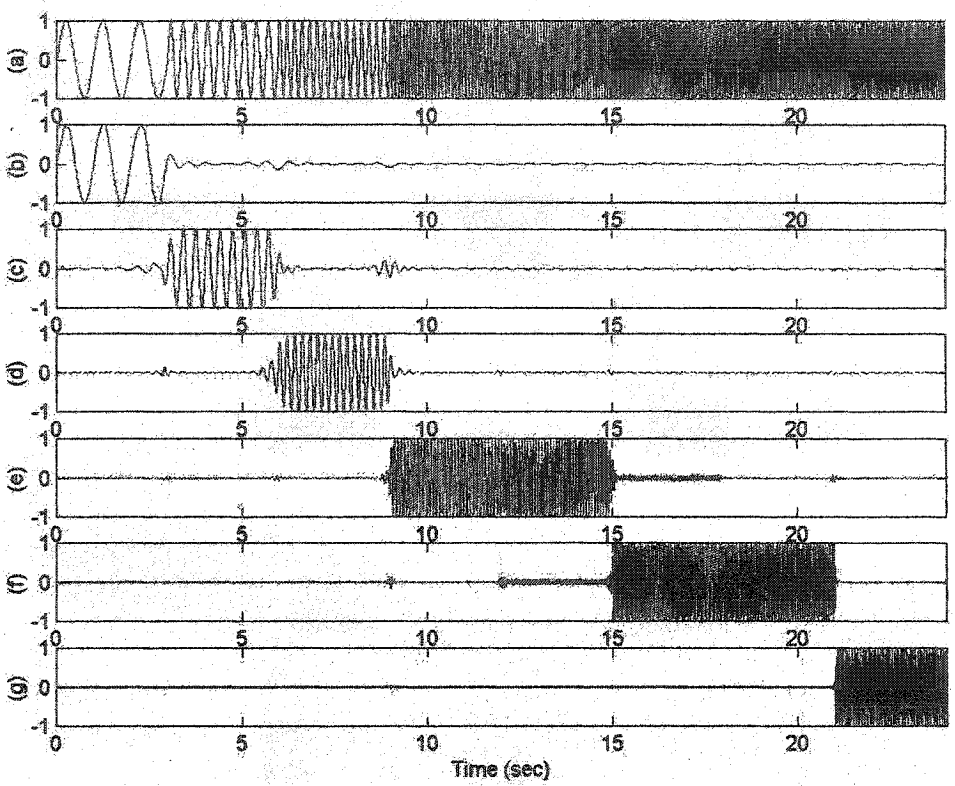

Figure 4.3: Concatenated sinusoidal signal (a) Complete signal constructed by adjoining same length sine waves of gradually increasing frequency. each sine wave segment is 3 seconds long and their respective frequencies, in order, from left to right are [1 ; 3 ; 5 ; 11 ; 13 ; 19 ; 23 ; 47] Hz. (b) Approximation function a5 representing the frequency range [0-2] Hz. (c) Detail function d5 representing frequency range [2-4] Hz, (d) Detail function d4 with range [4-8] Hz, (e) Detail function d3 with range [8-16] Hz. (f) Detail function d2 with range [16-32] Hz, and (g) Detail function d1 with range [32-64].

First, the presence of the component sine waves, whose frequencies occur within a specific frequency band appear displayed in the detail or approximation function corresponding to that frequency band. Second, the *location* and *duration* in time of a component sine wave, displayed in its respective frequency band is seen to coincide exactly to its location and duration in the original concatenated signal. Moreover, if only one component sine wave

has a frequency which falls into a particular frequency band then that sine wave should be displayed in the detail or approximation function representing that frequency band.

In particular, the analyzed signal is constructed with sine waves of length N = 384 samples, or 3 seconds, (i.e. the sampling frequency is 128samples/second, corresponding to the sampling frequency of the EEG signals to be seen later on). Therefore, according to the above discussion, each sine wave should be present in the frequency band corresponding to its frequency. In the [0 – 2] Hz. frequency band, in Figure 4.3b, we see that only the 1 Hz. signal is indeed shown and its duration is equal to its actual length in the original signal, 3 seconds, while the rest of the band is zero. Similarly, the frequency bands [2 – 4] Hz, [4 – 8] Hz. and [32 – 64] Hz. only display the sine wave segments that each *should* display, which are the 3 Hz., the 5 Hz. and the 47 Hz. segments respectively, as seen in Figure 4.3c, Figure 4.3d and Figure 4.3g. In the [8 – 16] Hz. frequency band, two sine wave segments, namely 11 Hz and 13 Hz. frequencies appear as indicated in Figure 4.3e. Due to the compact form of the plots, we do not clearly distinguish the two distinct adjacent bursts. Since they are adjacent to one another in the original they will also be adjacent in the corresponding detail function. Now, to show that those sine wave bursts present in each frequency band, do indeed correspond to the frequencies of the sine waves, we take the Fourier transform of the signal, the approximation function and the detail functions, shown in Figure 4.4.

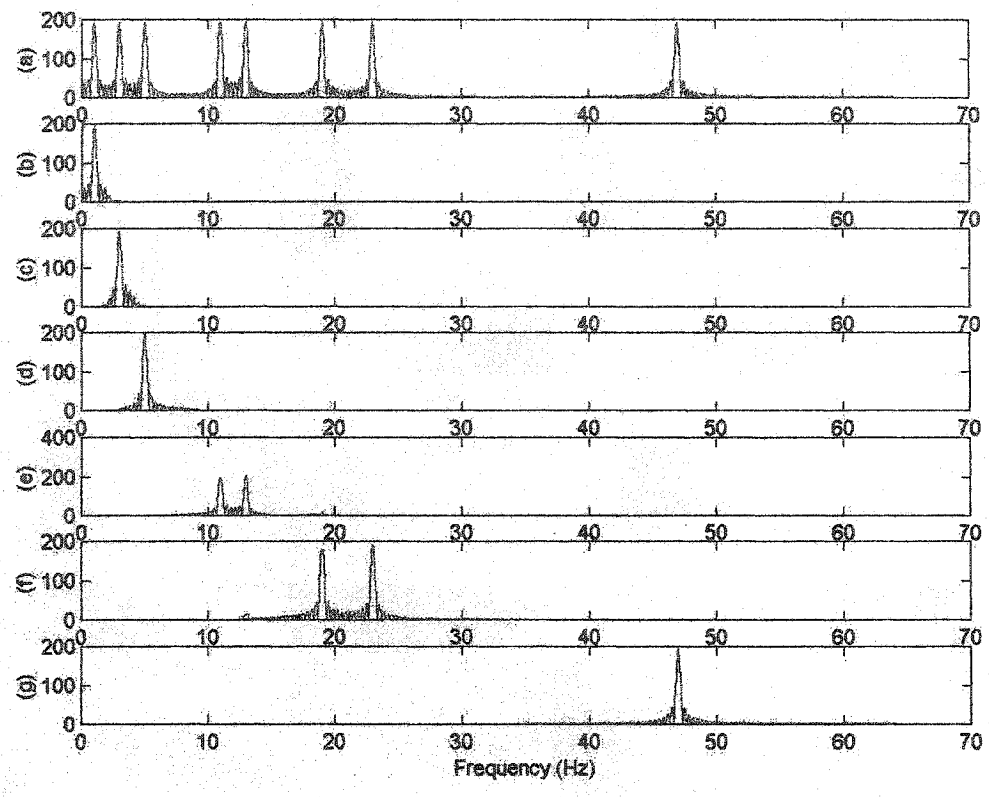

Figure 4.4: Fourier transform of the wavelet decomposition of the concatenated sinusoidal signal: (a) Original signal; (b) Approximation function; (c)-(g) Detail functions

From Figure 4.4 we can see that the FT of the different decomposition levels reveals the presence of specific frequency content in the form of a frequency spike. The spikes correspond exactly to the frequencies of the sine wave segments which, as the previous discussion suggests, are expected to occur in their respective detail function. For example, we mentioned that the two sine wave segments of 11Hz and 13Hz, seen in Figure 4.3e, were not clearly identified as such. Now, by observing the FT of Figure 4.3e, which is displayed in Figure 4.4e, we see that the only two frequency spikes that are observed occur exactly at

11 Hz and 13 Hz, which confirms the presence of the expected sine wave segments. Likewise, the other channels reveal the same information. Although Figure 4.4 reveals the frequency content of each detail function, it does not reveal the location in time that the particular frequency burst occurs, which the WT clearly does.

4.2.4 Concatenated Sinusoids in the Presence of AWGN

Before we proceed to the results of the WT decomposition of the concatenated sinusoid signal, we must first describe the signal-to-noise ratio (SNR). The SNR is a means of describing the relationship between the noise and the signal. Specifically, it describes the degree of the noise added to the signal. For sinusoidal signals in the presence of zero mean AWGN the SNR in decibels is given by (4.1)

$$\text{SNR} = 10 \log\left(\frac{A^2}{2\sigma^2}\right) \tag{4.1}$$

where A is the amplitude of the sine wave (note: $A^2/2$ is the sinusoidal signal power) and σ^2 is the variance of the noise or noise power.

It is apparent from both Figure 4.3 and Figure 4.4 that the WT decomposition provides a good breakdown of a 'clean' deteministic signal both in the time domain as well as the frequency domain. However, this signal is not representative of a realistic signal. In order to make it more realistic and further highlight the WT's consistent reliability in extracting pertinent information from different types of signals, including realistically degraded ones, we contaminate the concatenated sinusoidal signal with representative AWGN. The values

chosen for the amplitude of the signal and the zero mean AWGN produced a SNR = -3 dB. This new signal, along with its decomposition is shown in Figure 4.5

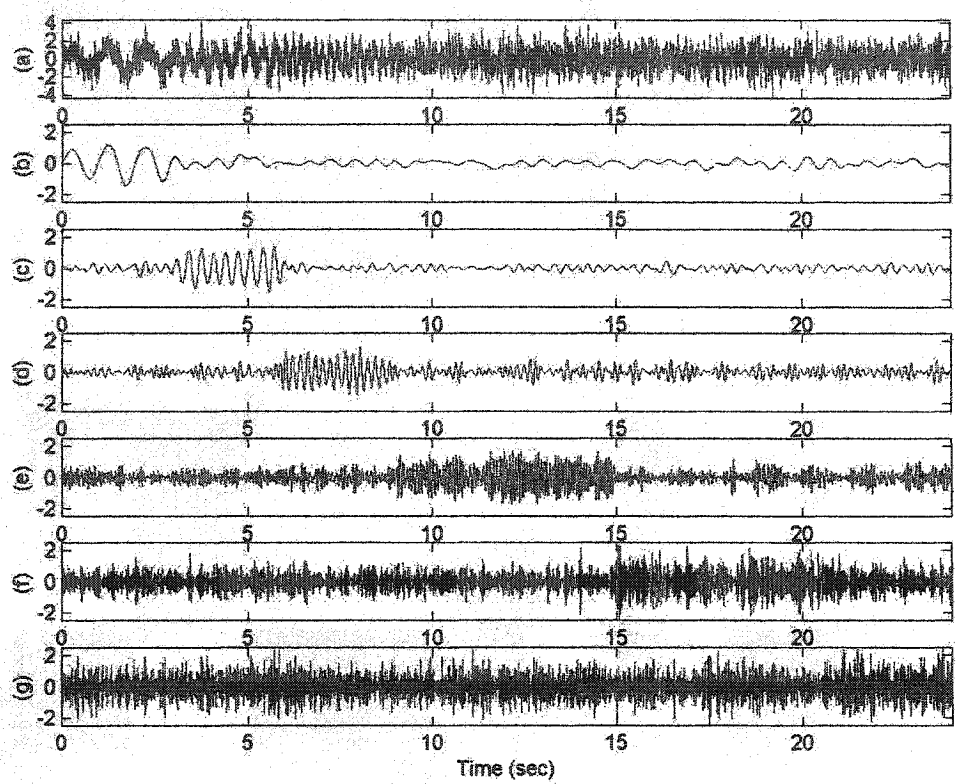

Figure 4.5: Concatenated sinusoidal signal with AWGN, SNR = -3 dB; (a) Complete signal constructed by adjoining same length sine waves of gradually increasing frequency. Each sine wave segment is 3 seconds long and their respective frequencies, in order, from left to right are [1 ; 3 ; 5 ; 11 ; 13 ; 19 ; 23 ; 47] Hz. (b) Approximation function a5 representing the frequency range [0-2] Hz. (c) Detail function d5 representing frequency range [2-4] Hz, (d) Detail Function d4 with range [4-8] Hz, (e) Detail function d3 with range [8-16] Hz. (f) Detail Function d2 with range [16-32] Hz, and (g) Detail function d1 with range [32-64].

Although somewhat distorted, compared to Figure 4.3, the WT decomposition shown in Figure 4.5 clearly identifies the presence of the appropriate sine wave segments in the four lowest frequency bands, Figure 4.5b to Figure 4.5e. The heightened amplitude of the segments, set against the noisy background in each of the subbands, is unambiguously evident.

Even in the higher frequency bands, Figure 4.5f and Figure 4.5g, there is a noticeable increase in height although relatively not as large as the lower bands, where the segments occur, which also sets them apart from their background. Nevertheless, any question regarding the presence of the segments, is quickly answered if we look at the FT of the noisy signal's decomposition, shown in Figure 4.6.

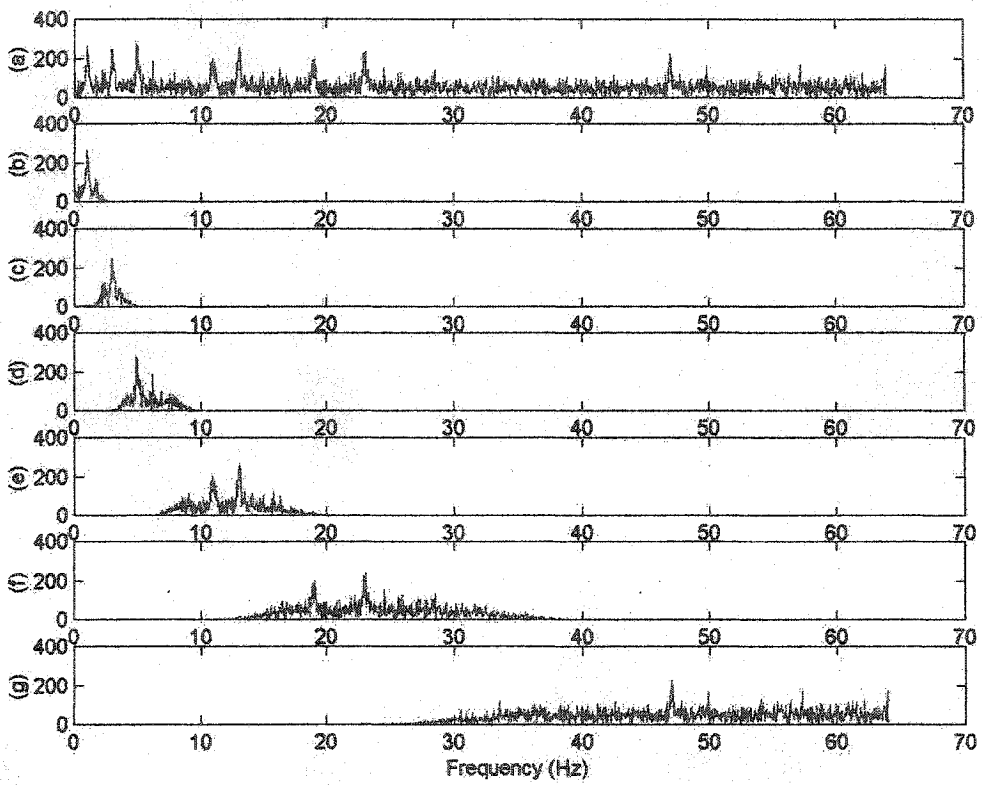

Figure 4.6: Fourier transform of the concatenated sinusoidal signal in the presence of AWGN, SNR=-3dB; (a) Original signal; (b) Approximation function; (c)-(g) Detail functions.

Here, we can see that the frequencies associated with all the sine wave segments are clearly displayed. By comparing Figure 4.6 with Figure 4.4, we observe that the same spikes occur at the same frequencies, as they should. Moreover, despite the presence of noise, the fre-

quency spikes in Figure 4.6 easily stand out, against the noise, as the dominant peaks in each of the subbands.

4.2.5 Superimposed Sinusoidal Signal

To look at the decompositional power of the WT from another perspective, we construct a signal using sinusoids of varying frequencies and superimposing them together. To maintain consistency with the previous sections, the sinusoids, which are superimposed have the same frequencies as those used for the concatenated signal. Each component sinusoid in this case, instead of being 3 seconds long, is equal to the length of the whole concatenated signal, that is, 24 seconds long (see Figure 4.3). The resulting superimposed signal is *not* normalized, so that the component sinusoids could maintain the same amplitude as the amplitude of the sine components used in the concatenated case.

As in the concatenated case, we expect to find each frequency band indicating the presence of the sine wave, whose frequency falls within the range of its corresponding band to be displayed for the duration of its presence within the superimposed signal. In this case, since each sine wave has the same length as the superimposed signal, as does the length of each detail function (i.e. frequency band), we expect to see the presence of each of these sine waves appearing throughout the entire length of the detail function. The WT decomposition of the superimposed sinusoidal signal is shown in Figure 4.7.

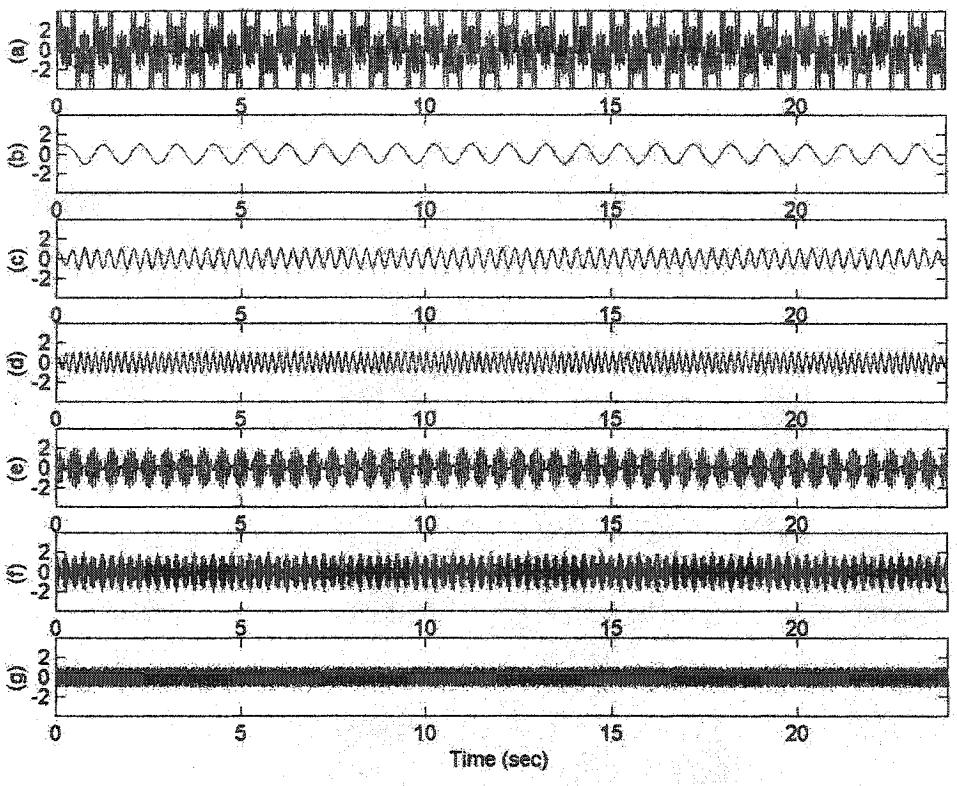

Figure 4.7: Wavelet decomposition of superimposed sinusoidal signal: (a) Complete signal constructed by superimposing sine waves of gradually increasing frequency. Each sine wave segment is 24 seconds long and their respective frequencies are [1 ; 3 ; 5 ; 11 ; 13 ; 19 ; 23 ; 47] Hz. (b) Approximation function a5 representing the frequency range [0-2] Hz. (c) Detail function d5 representing frequency range [2-4] Hz, (d) Detail function d4 with range [4-8] Hz, (e) Detail function d3 with range [8-16] Hz. (f) Detail function d2 with range [16-32] Hz, and (g) detail function d1 with range [32-64].

As expected, we can see that the component sine waves are each displayed within the frequency band which corresponds to their frequency. For example, looking at the [4 – 8] Hz frequency band corresponding to detail function d4 in Figure 4.7d, we see that only one sine wave appears, which should be true, since only one component sine wave falls within this range, namely the 5 Hz frequency sine wave. Furthermore, the 11Hz and 13Hz sine waves

should appear together in the [8 – 16] Hz frequency band or detail function d3, shown in Figure 4.7e. The "beats" that we see in this band certainly indicate the presence of two similar (i.e. close in frequency but not equal) frequency sine waves. However, the time domain decomposition offered by d4 does not reveal the exact frequencies of the sine waves present. Therefore, to further clarify the picture, the FT of each level of the decomposition in Figure 4.7 is shown in Figure 4.8.

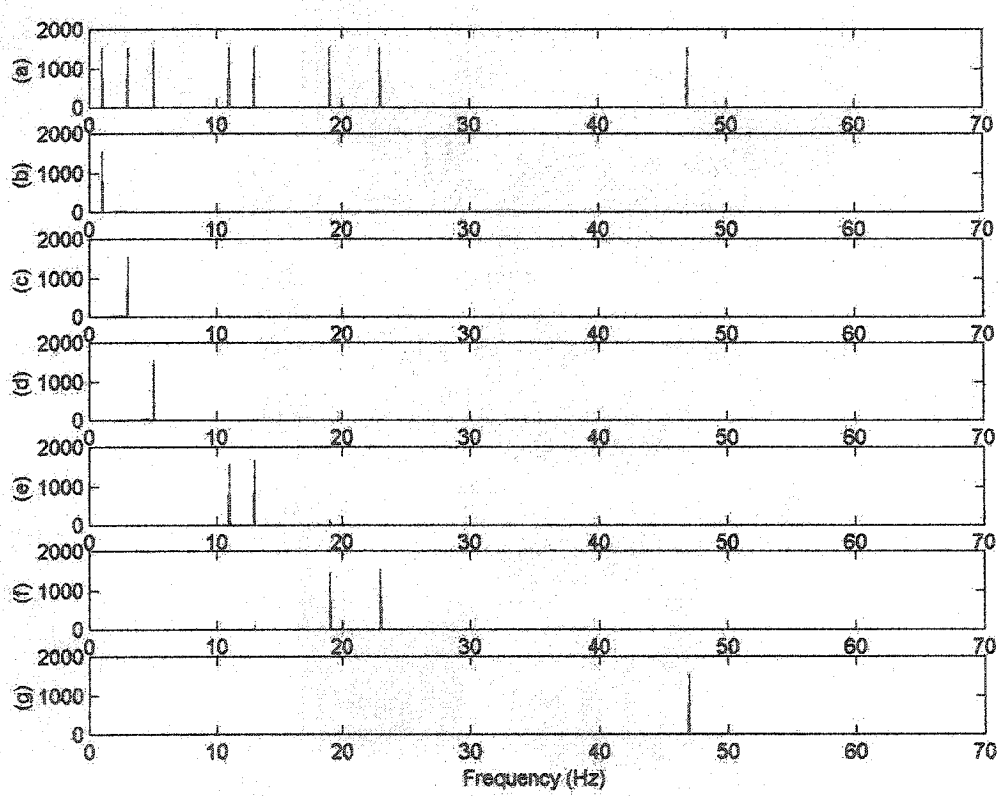

Figure 4.8: Fourier transform of the wavelet decomposition of the superimposed sinusoidal signal: (a) Original signal; (b) Approximation function; (c)-(g) Detail functions

The dominant peaks present in each frequency band correspond exactly to the frequencies of the sine waves displayed in each of the detail funtions. In the case of the sine wave dis-

played in the [4 – 8] Hz frequency band (or detail function d4) of Figure 4.8d, we see a peak present exactly at 5Hz. Similarly, the earlier confusion relating to the exact frequency sinusoids present in the detail function of Figure 4.7e is resolved with the two sharp peaks centered exactly at 11Hz and 13Hz, within the spectrum of the [8 – 16] Hz band of Figure 4.8e.

Comparing the peaks displayed in the spectrum for the superimposed sinusoids of Figure 4.8 with those displayed in the spectrum for the concatenated sinusoids of Figure 4.4, we must make one observation. The proportion of the component sine waves present in the overall superimposed signal is equal to the length of the overall signal as opposed to the fractional presence of each component sine wave in the concatenated case. For this reason and due to the nature of the FT, the frequency peaks in Figure 4.8 are much sharper than the 'fatter' peaks of Figure 4.4. The sharpness of the peaks, therefore has nothing to do with the WT but is a direct result of the FT itself.

4.2.6 Superimposed Sinusoidal Signal in the Presence of AWGN

We now perform the same decomposition to the superimposed signal but this time, to make the signal more realistic, we add AWGN. A SNR = -3dB is used, as was the case with the concatenated sinusoidal signal. The noisy superimposed signal along with corresponding

approximation and details functions resulting from the wavelet decomposition are shown in Figure 4.9.

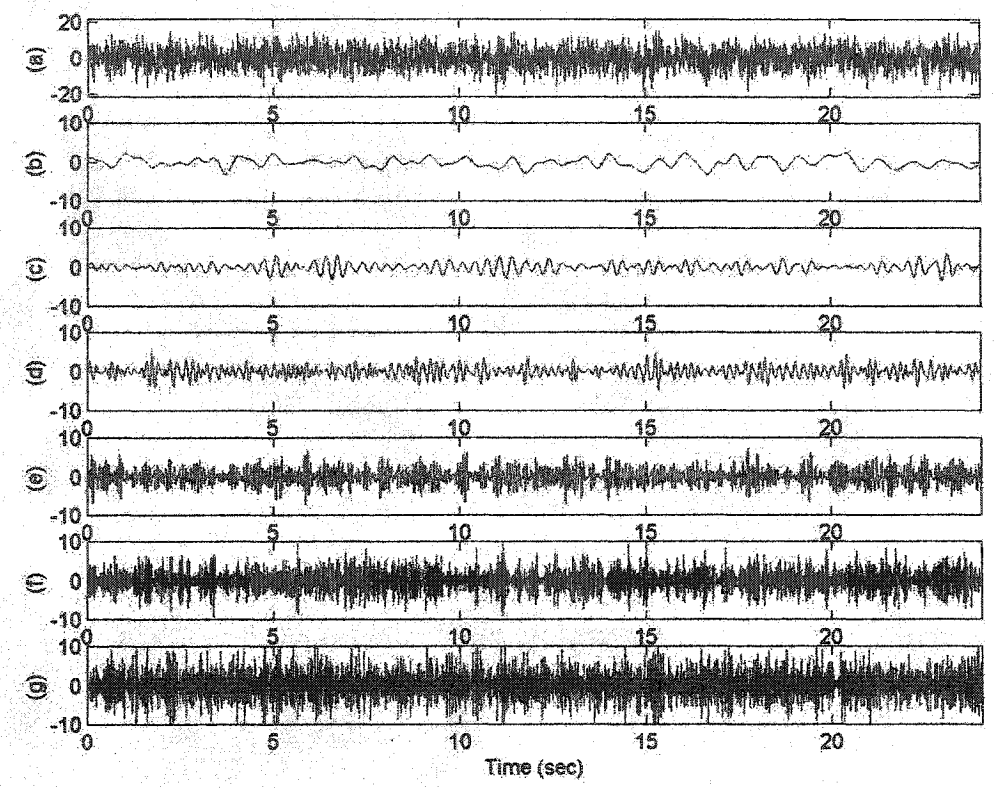

Figure 4.9: Wavelet decomposition of noisy superimposed sinusoidal signal in AWGN, SNR=-3dB; (a) Complete signal constructed by superimposing sine waves of gradually increasing frequency. Each sine wave segment is 24 seconds long and their respective frequencies are [1 ; 3 ; 5 ; 11 ; 13 ; 19 ; 23 ; 47] Hz. (b) Approximation function a5 representing the frequency range [0-2] Hz. (c) Detail function d5 representing frequency range [2-4] Hz, (d) Detail function d4 with range [4-8] Hz, (e) Detail function d3 with range [8-16] Hz. (f) Detail function d2 with range [16-32] Hz, and (g) Detail function d1 with range [32-64].

By comparing Figure 4.9 with Figure 4.7, we can see that the noisy signal's component waveforms are visually degraded to a varying degree. In the lower frequency bands, this degradation is apparently not that severe, but as we go up in frequency the detail functions tend to lose their original shape. For example, the "beat" like pattern, indicating the pres-

ence of two sine waves of different but close frequencies, seen in detail function d3, Figure 4.9e, is not at all apparent compared to the same detail function in Figure 4.7e. The same thing can be said for detail function d2 (cf. Figure 4.9f and Figure 4.7f). However, to clear up any ambiguity, concerning which waveform is actually present in each frequency band, we take the FT of these approximation and detail functions, shown in Figure 4.10.

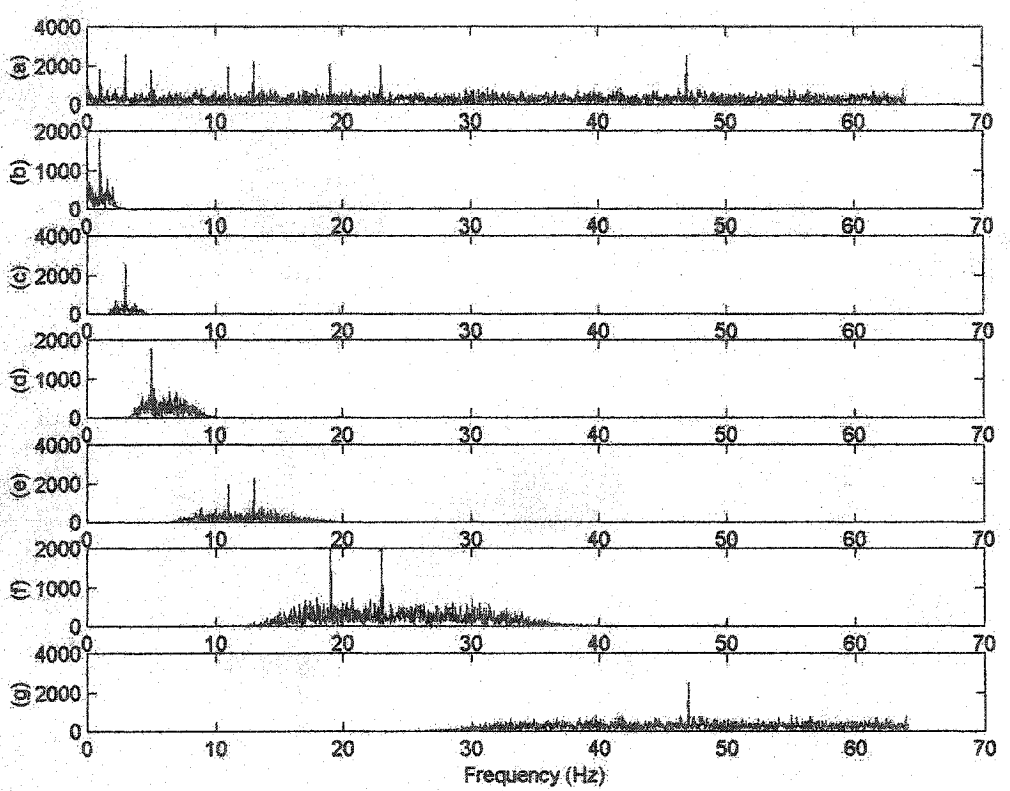

Figure 4.10: Fourier transform of the wavelet decomposition of superimposed sinusoidal signal, in AWGN with SNR=-3dB; (a) Original signal; (b) Approximation function; (c)-(g) Detail functions

The spectrum shown in Figure 4.10 reassures us, by the presence of peaks at the appropriate frequencies, that the wavelet decomposition of the signal, despite the presence of significant AWGN, still manages to retain the presence of the original component sine waves.

Thus, by these examples, it is apparent that the WT possesses a good ability to resolve a signal into its time and frequency components, with or without noise present. The confidence that we inherit from these results justifies our selection of the WT as a suitable means of decomposing a sinusoidal signal in general (with the EEG signal as a particular case) in order to reduce it to a form that will facilitate the task of segmentation.

4.3 Segmentation: Detecting Various Types of Non-Stationary Boundaries

4.3.1 Introduction

In the previous section we demonstrated the usefulness of the WT for decomposing a sinusoidal signal with or without noise and revealing the underlying sinusoidal components that are present. We observed that, in the concatenated signal case, the various frequency sinusoidal segments fell within their respective frequency band as revealed in the detail function of the decomposition. In the detail functions, noticeable amplitude differences between the sinusoidal segment and the surrounding noisy background are observed. Since each detail function represents a range of frequencies, the identification of different frequency segments within a particular detail function requires the introduction of a segmentation procedure. The sudden appearance of a stationary segment (i.e. the 3 second 5Hz sinusoid in Figure 4.5d) within another different stationary segment (i.e. the $[4-8]$ Hz background noise of Figure 4.5d) makes the combination of the two (i.e. the entire detail function d4 or all of Figure 4.5d) non-stationary. Therefore, to identify the presence of sinusoidal seg-

ments within a signal, which may suddenly appear, showing either heightened amplitude or heightened frequency in a specific detail function, a segmentation function needs to be introduced. This section analyzes the performance of the segmentation algorithms presented in Chapter 3, namely the autocorrelation function (ACF), the generalized likelihood ratio (GLR) and the non-linear energy operator (NLEO) algorithms. To study the performance of each algorithm three categories of test signals have been considered:

1. Sinusoidal non-stationarities without AWGN noise
2. Sinusoidal non-stationarities with AWGN noise
3. Second order autoregressive non-stationarity.

At the end of each signal category a comparison is drawn between the algorithms.

4.3.2 Sinusoidal Non-stationarities WITHOUT Noise

In this section, the signals used contain no noise and therefore segmentation of these signals, based on the same operational parameters, will either occur or not. Therefore the parameters, which govern the performance of each algorithm, are adjusted so as to ensure the segmentation of the non-stationary signal. In other words, in this section, all non-stationary boundaries, separating different stationary sections, present in the signal *will* be detected. The motivation behind this process is to illustrate the functioning of the segmentation, whereby each algorithm's distinct difference measure, used to detect the presence of boundaries between non-stationary segments, will be illustrated. Along with the difference

measure function, detected boundaries as well as the final boundary position resulting from the optimization procedure are shown. In particular, the signals used in this experiment are chosen to test the segmentations' performance in the face of varying kinds of possible non-stationarities that may be encountered in the EEG. These are:

1. Increasing and decreasing amplitude sinusoids with constant frequency
2. Increasing and decreasing frequency sinusoids with constant amplitude
3. Amplitude and frequency increasing and decreasing together
4. Amplitude and frequency increasing and decreasing opposite to one another
5. Randomly positioned segments of amplitude and frequency changing together
6. Randomly positioned segments of amplitude and frequency changing opposite to each other.

These signals, shown in Figure 4.11, are designed to maintain a certain degree of consistency. That is, all the values of amplitude and frequency used in the signals of Figure 4.11 belong to the same amplitude and frequency set. Specifically, the overall set of amplitude values used are {10, 20, 40, 80, 160} while the overall set of frequency values used are {2, 4, 8, 16, 32}. Therefore, the amplitude and frequency values available are the same for all signals. It is the difference in the distribution of these values which produce the various test signals of Figure 4.11. Likewise, the length of each segment and consequently the overall signal length are also equal across the board. Specifically, there are n=10 individual stationary signals concatenated together to make up the overall signal. Each of the n segments is N=128 or t=1 second long and accordingly, the overall signal is 10 seconds long. Although these signal parameters may be chosen arbitrarily, their values are selected to correspond

to those of the actual EEG signal sampling frequency, which is fs=128. These measures are established in order to maintain the greatest degree of comparison between the results.

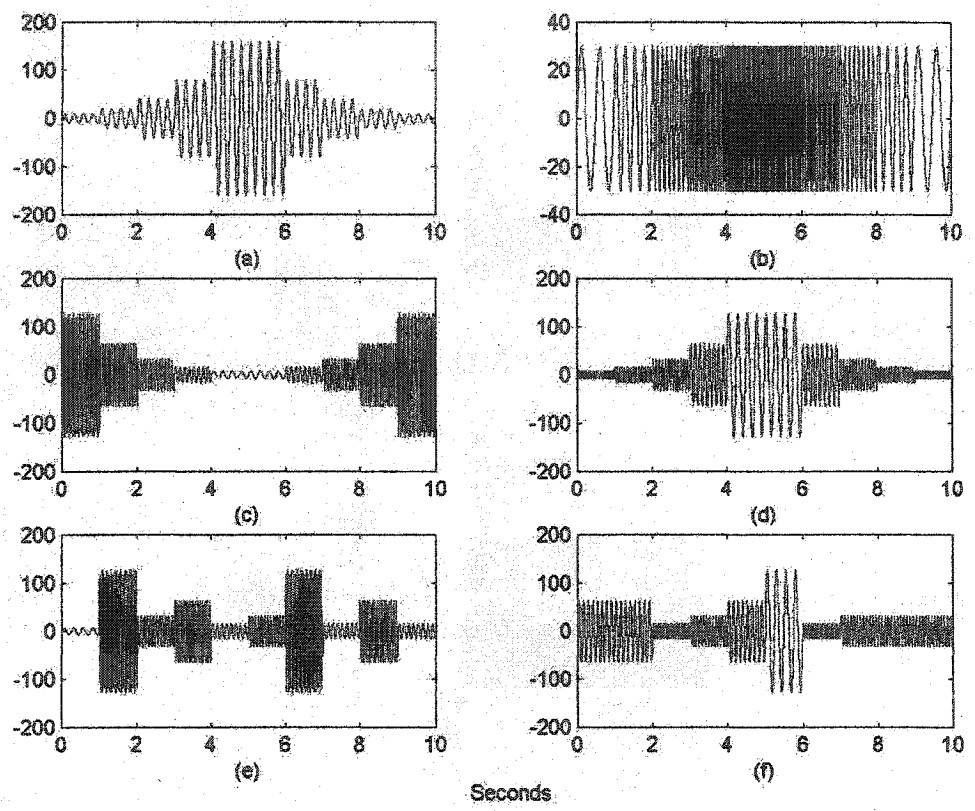

Figure 4.11: Various noise free non-stationary signals (a)Varying amplitude (A=[10 20 40 80 160]) with constant frequency (f = 8Hz); (b) Varying frequency (f=[2 4 8 16 32]) with constant amplitude (A=30); (c) Amplitude and frequency (f=[2 4 6 8 10]) changing together (i.e. high amplitude with high frequency or low amplitude with low frequency) (d) Amplitude and frequency changing in opposite directions (i.e. high amplitude with low frequency or low amplitude with high frequency); (e) Randomly distributed segments of part (c); (f) Randomly distributed segments of part (d).

4.3.2.1 ACF

Following the procedure described in Chapter 3, in this subsection, the autocorrelation function segmentation algorithm is applied to the signals mentioned in the previous section. The operational parameters that critically affect the performance of the ACF, namely the

- window length
- thresholds (amplitude, frequency and global)

are chosen, to illustrate the ability of the ACF to detect boundaries between two different but stationary segments. It must be mentioned that, from now on, the use of the word 'boundary' will refer exclusively to the non-stationary boundary, separating two different stationary segments. Due to the simple, but illustrative, nature of these noise free signals, these operational parameters can be chosen in a straight forward manner based on the values provided in [49]. Nominally, these values are chosen as:

- $T_a = T_f = 1$
- $T_g = 1$
- WL $\geq$ 64 samples

where T_a, T_f, and T_g are the amplitude, frequency and global thresholds, respectively, and WL is the window length.

The reason for equating T_a to T_f stems from the desire to make a change in amplitude equal to a change in frequency when deciding if their combined presence is sufficient to record a detected non-stationarity. Furthermore, the WL must be at least as long as the smallest stationary segment sought after. Because we are dealing with sine wave segments that are 128 samples long (i.e 1 second), some having a frequency of 2 Hz., the minimum WL allowing

for one full cycle of the smallest frequency sine would have to be half of the sine segment size, or 64 samples (i.e. 1/2 second) long; we chose WL = 70 samples. The results of the ACF on the forementioned signals are shown in Figure 4.12 to Figure 4.17. The various values, for both the amplitude and frequency, are chosen to represent the realistic range of values present in an EEG signal, to see if the segmentation operates correctly in the appropriate ranges.

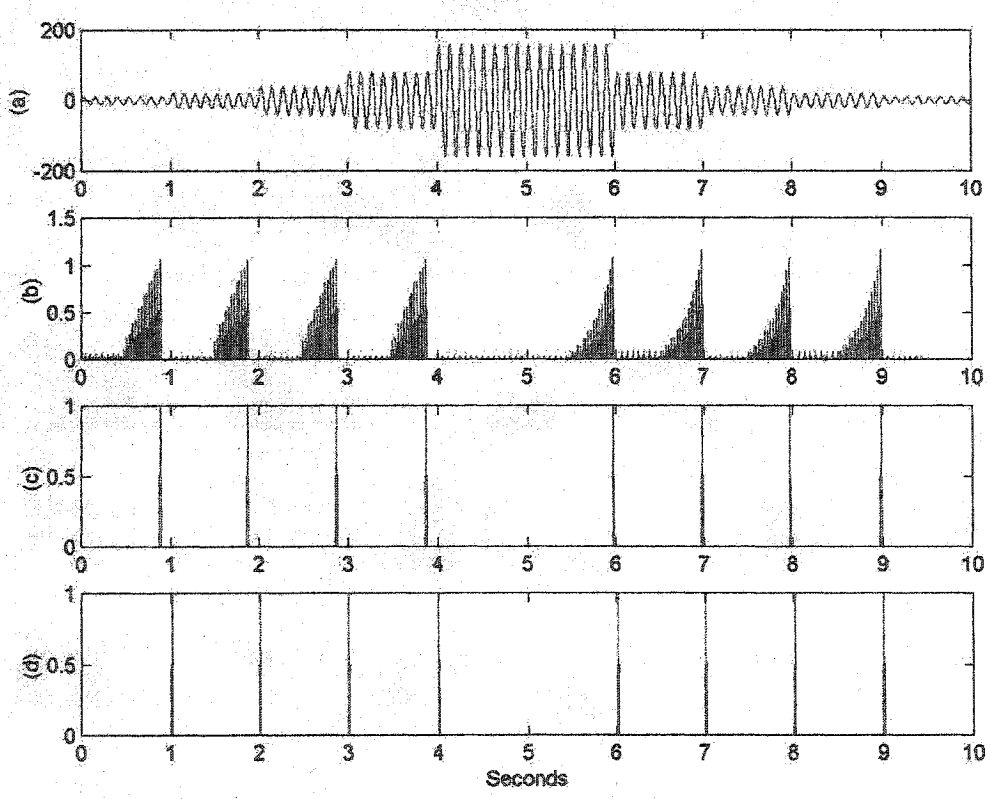

Figure 4.12: ACF segmentation for sinusoidal signal with varying amplitude and constant frequency. (a) Signal: A = [10 20 40 80 160 160 80 40 20 10], and f = 8Hz; (b) Difference measure with WL = 70, T_a=T_f=1 and T_g = 1; (c) Non-stationary boundary detection; (d) Optimized positioning of detected boundaries.

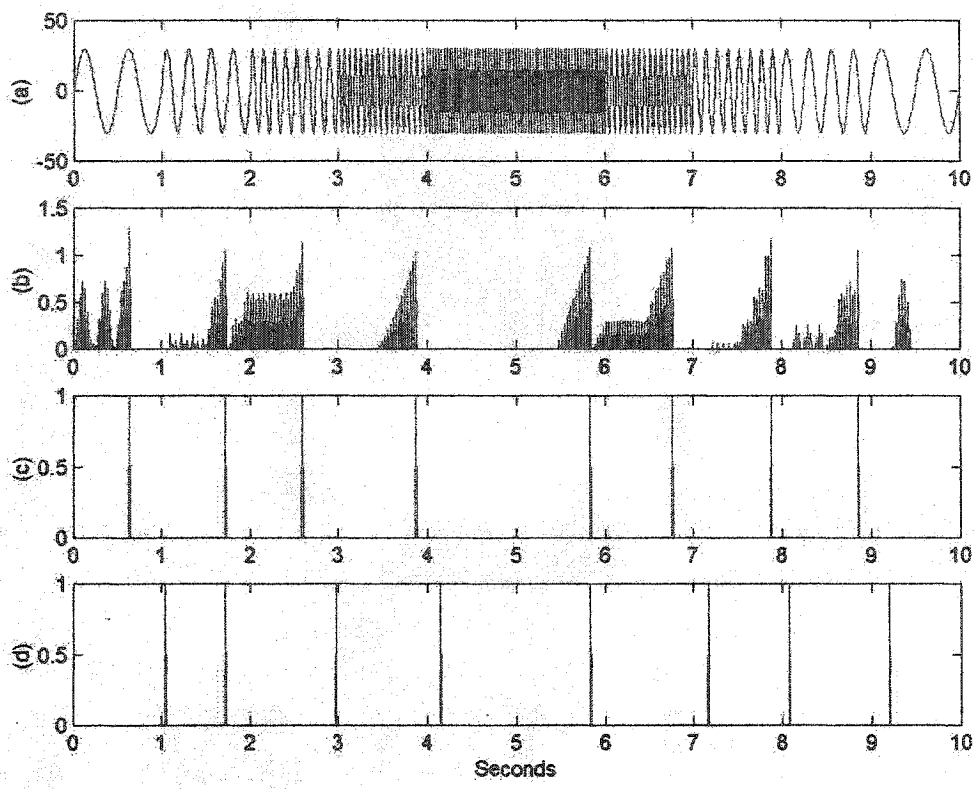

Figure 4.13: ACF segmentation for sinusoidal signal with varying frequency and constant amplitude. (a) Signal: A = 30, and f = [2 4 8 16 32 32 16 8 4 2] Hz; (b) Difference measure with WL = 70, T_a=T_f=0.45 and T_g = 1, and ; (c) Non-stationary boundary detection; (d) Optimized positioning of detected boundaries.

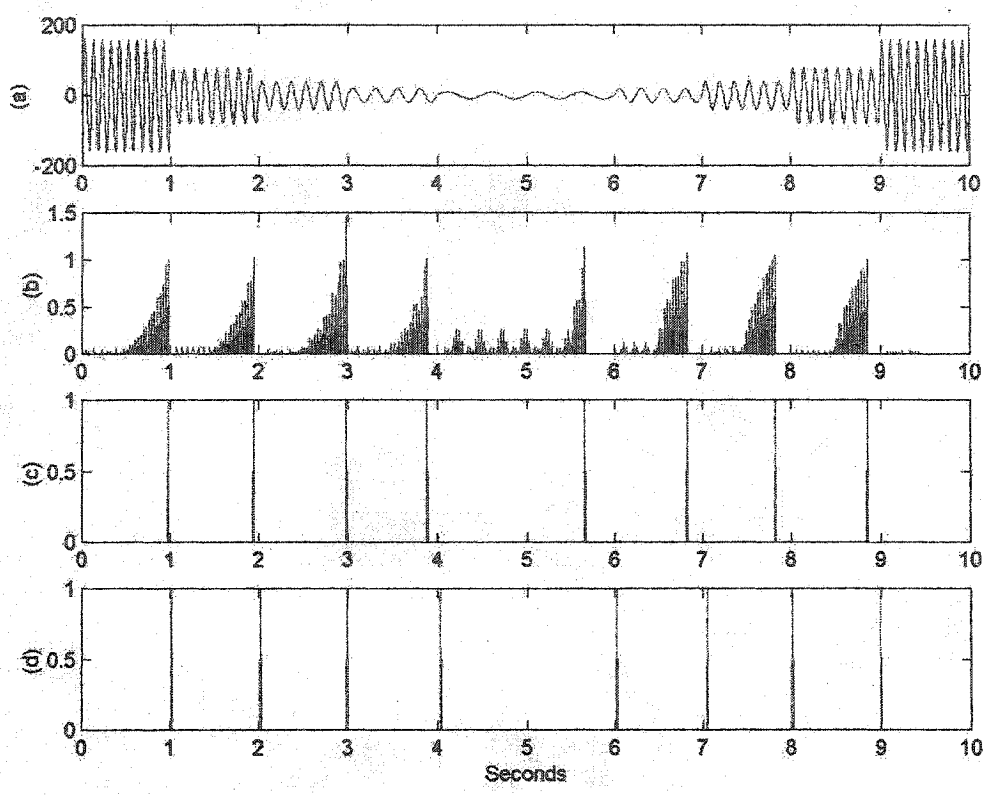

Figure 4.14: ACF segmentation for sinusoidal signal with amplitude and frequency changing together in the same direction. (a) Signal: A = [160 80 40 20 10 10 20 40 80 160] and f = [10 8 6 4 2 2 4 6 8 10] Hz; (b) Difference measure with WL = 70, $T_a = T_f = 1$ and $T_g = 1$; (c) Non-stationary boundary detection; (d) Optimized positioning of detected boundaries.

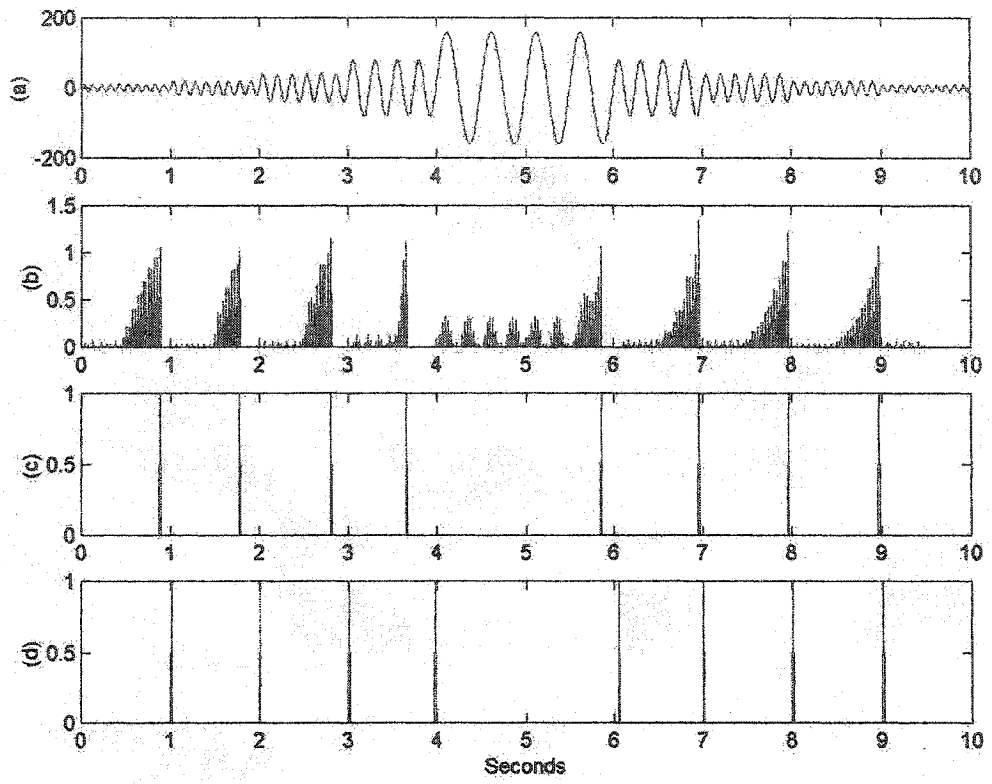

Figure 4.15: ACF segmentation for sinusoidal signal with amplitude and frequency changing in opposite directions to one another. (a) Signal: A = [10 20 40 80 160 160 80 40 20 10] and f = [10 8 6 4 2 2 4 6 8 10] Hz and ; (b) Difference measure with WL = 70, $T_a = T_f = 1$ and $T_g = 1$; (c) Non-stationary boundary detection; (d) Optimized positioning of detected boundaries.

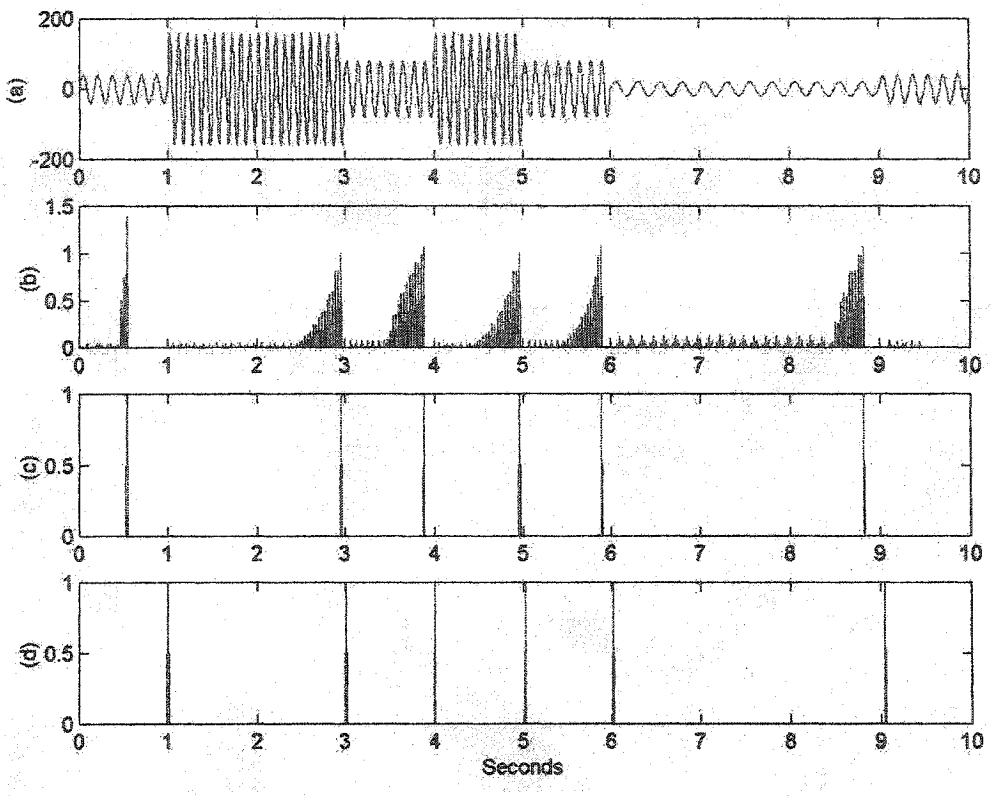

Figure 4.16: ACF segmentation for sinusoidal signal with randomly distributed segments of Figure 4.14 where amplitude and frequency change together in the same direction. (a) Signal; (b) Difference measure with WL = 70, $T_a = T_f = 1$ and $T_g = 1$; (c) Non-stationary boundary detection; (d) Optimized positioning of detected boundaries.

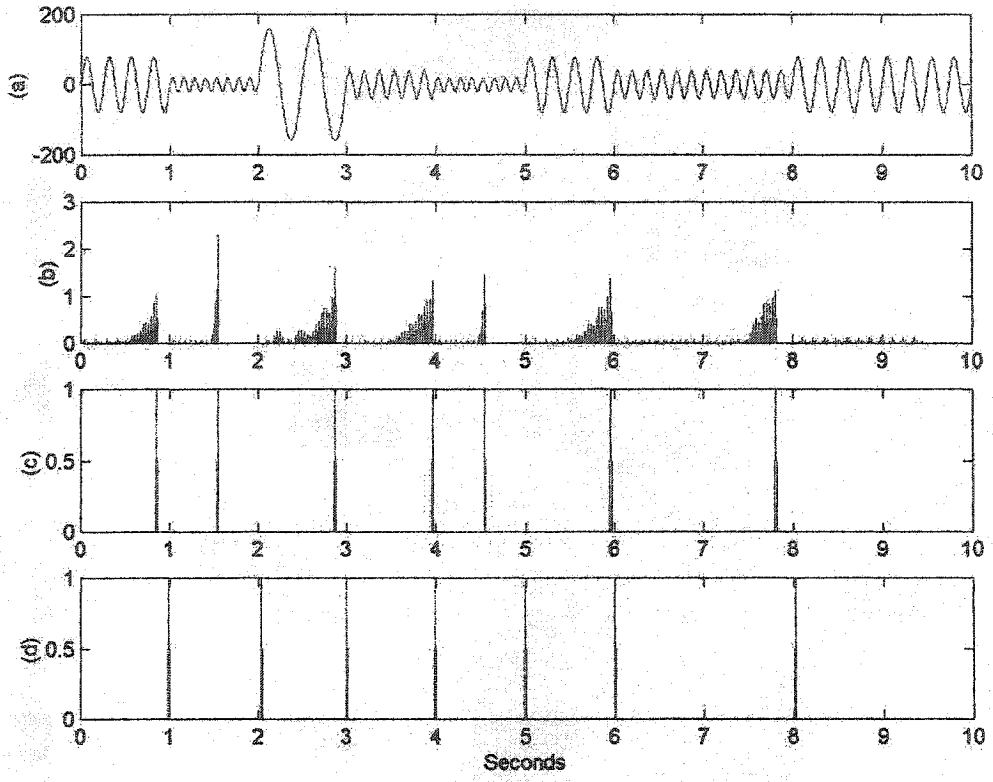

Figure 4.17: ACF segmentation for sinusoidal signal with randomly distributed segments of Figure 4.15 where, amplitude and frequency change in opposite directions. (a) Signal; (b) Difference measure with WL = 70, $T_a = T_f = 1$ and $T_g = 1$; (c) Non-stationary boundary detection; (d) Optimized positioning of detected boundaries.

The results shown in Figure 4.12 to Figure 4.17, segment the signals as expected. Each distinct segment of the signal, whether it is distinguished by amplitude, frequency or some combination of the two, in order or randomly distributed are all extracted appropriately. The same thresholds are applied to each, which does not affect the performance. This outcome is not surprising, considering that no noise is present. However, there are two notable exceptions that require some adjustment, so as to properly segment the signal. These excep-

tions involved the varying amplitude constant frequency (VACF) and the varying frequency constant amplitude (VFCA) signals, seen in Figure 4.12 and Figure 4.13, respectively. In the first case, involving the VACF the thresholds T_a and T_f are reduced to 0.8, while T_a and T_f are reduced to 0.45 for the VFCA signal. These values are used to ensure detection and optimization. The reason for their lower value appears to stem from the combined role both the frequency and the amplitude play in the ACF algorithm. Although artificial in nature, these signals provide insight into the working of the algorithm. Because the changes in both the amplitude and the frequency are doubled at each higher value, their relative change is the same, a power of two. Therefore, the difference in thresholds ensuring detection indicates that the algorithm is more sensitive to the amplitude change than to the frequency change. Moreover, Figure 4.13d shows that determining the precise position for the signal where only the frequency changes, is more difficult to optimize accurately, as the difference between the position of the optimized boundary and the position of the actual non-stationary boundary shows. Despite these observations, the ACF algorithm works effectively for the cases where *both* the amplitude and the frequency change, Figure 4.14d to Figure 4.17d, which is the case encountered in practice, since the EEG signals register changes in the amplitude when changes in the frequency occur, as mentioned in Chapter 1.

4.3.2.2 GLR

In this section, we apply the GLR to the same signals as those used in the previous section, shown in Figure 4.11. As discussed in Chapter 3, its performance in segmentation is controlled by a similar set of parameters, which are:

- Window length (WL)
- Threshold (T)
- Order (p)

It is similar to the ACF because it relies on the window length as well as the threshold, but different because it uses autogregressive modelling and therefore needs a model order. These parameters are set nominally as WL = 70 samples or approximately 0.5 seconds to be consistent with the ACF; T = $2\ln(2)N_0$, where N_0 represents the least number of bits necessary to encode the signal information, as explained in Chapter 3. N_0 is chosen as 32 bits, which corresponds to a threshold of T = 44. The order is chosen as $p = 2$. With these values, the GLR is applied to the forementioned signals and the results, displayed in Figure 4.18 to Figure 4.23, show clearly that the non-stationary segments are partitioned correctly

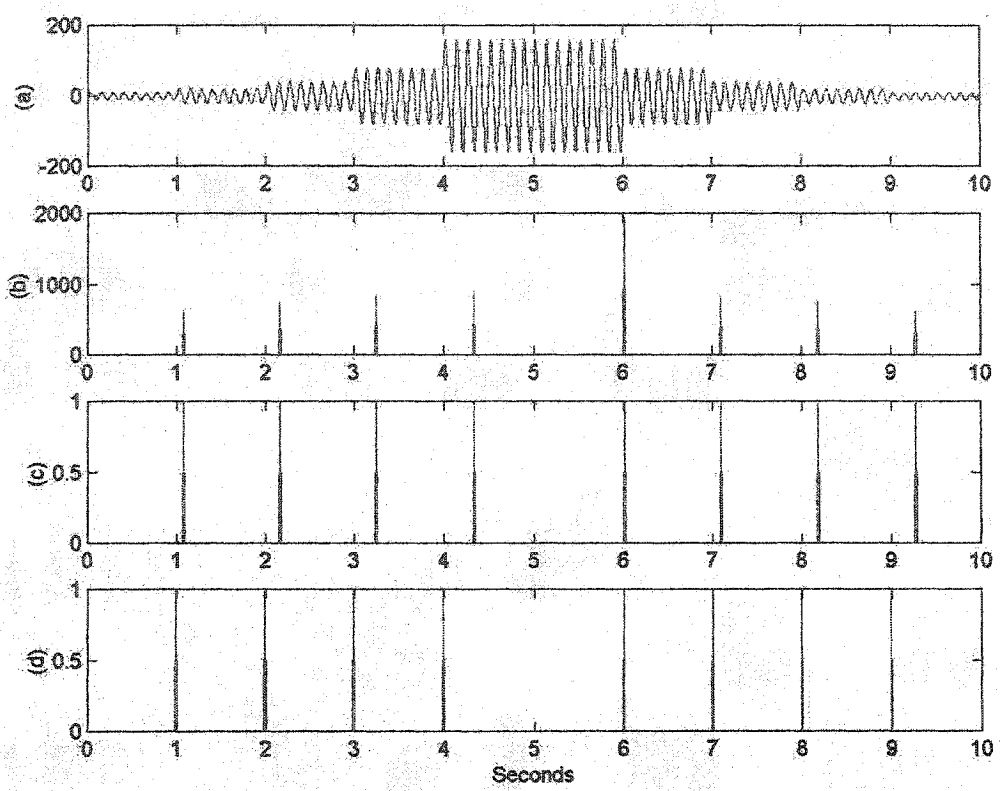

Figure 4.18: GLR segmentation for sinusoidal signal with varying amplitude and constant frequency. (a) Signal: A = [10 20 40 80 160 160 80 40 20 10], and f = 8Hz; (b) Difference measure with WL = 70 and T=44; (c) Non-stationary boundary detection; (d) Optimized positioning of detected boundaries.

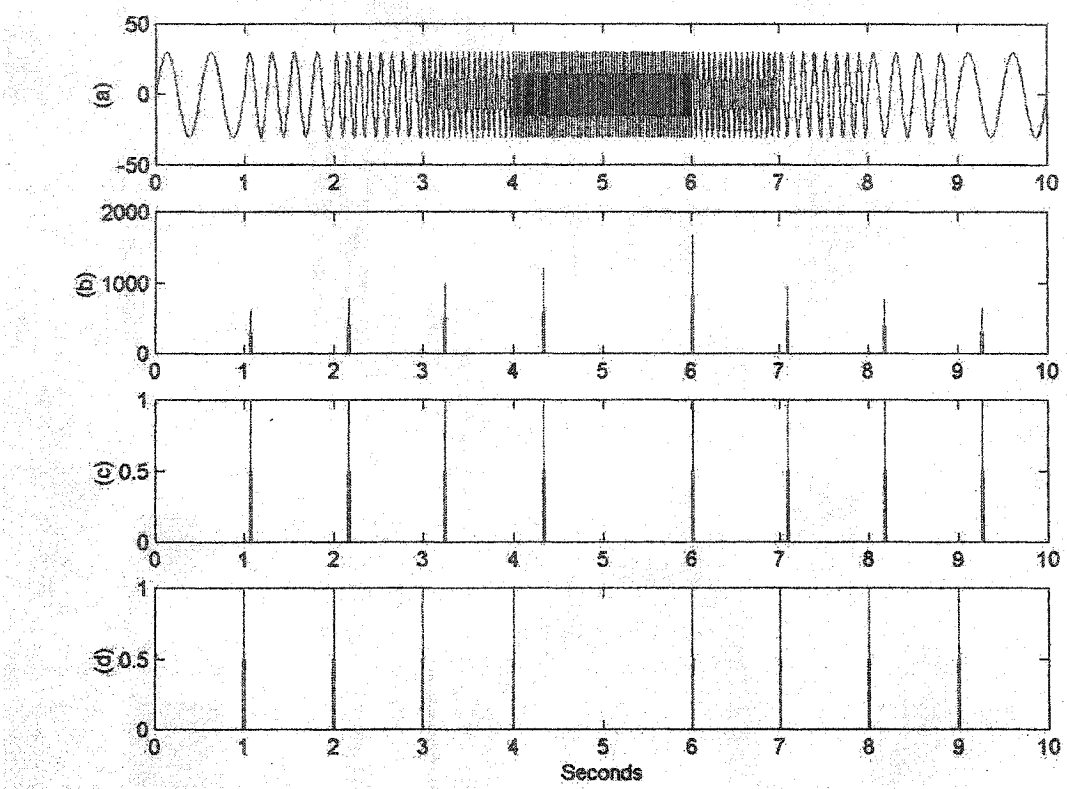

Figure 4.19: GLR segmentation for sinusoidal signal with varying frequency and constant amplitude. (a) Signal: A = 30, and f = [2 4 8 16 32 32 16 8 4 2] Hz; (b) Difference measure with WL = 70 and T = 44; (c) Non-stationary boundary detection; (d) Optimized positioning of detected boundaries.

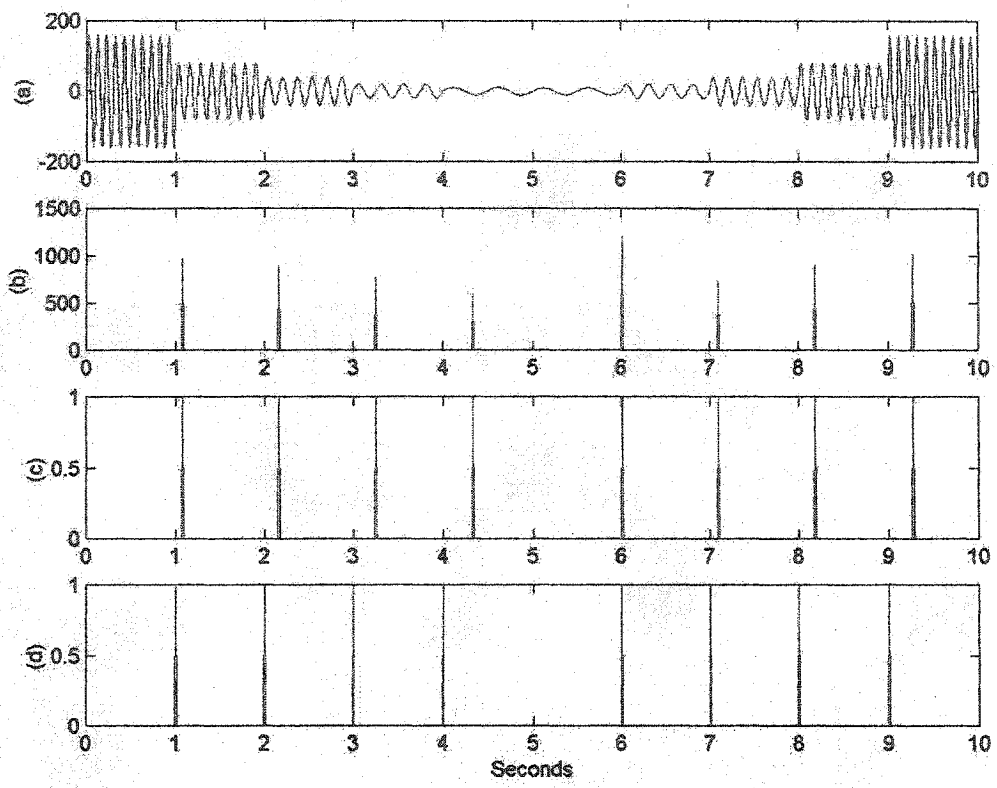

Figure 4.20: GLR segmentation for sinusoidal signal with amplitude and frequency changing together in the same direction. (a) Signal: A = [160 80 40 20 10 10 20 40 80 160] and f = [10 8 6 4 2 2 4 6 8 10] Hz; (b) Difference measure with WL = 70 and T = 44;; (c) Non-stationary boundary detection; (d) Optimized positioning of detected boundaries.

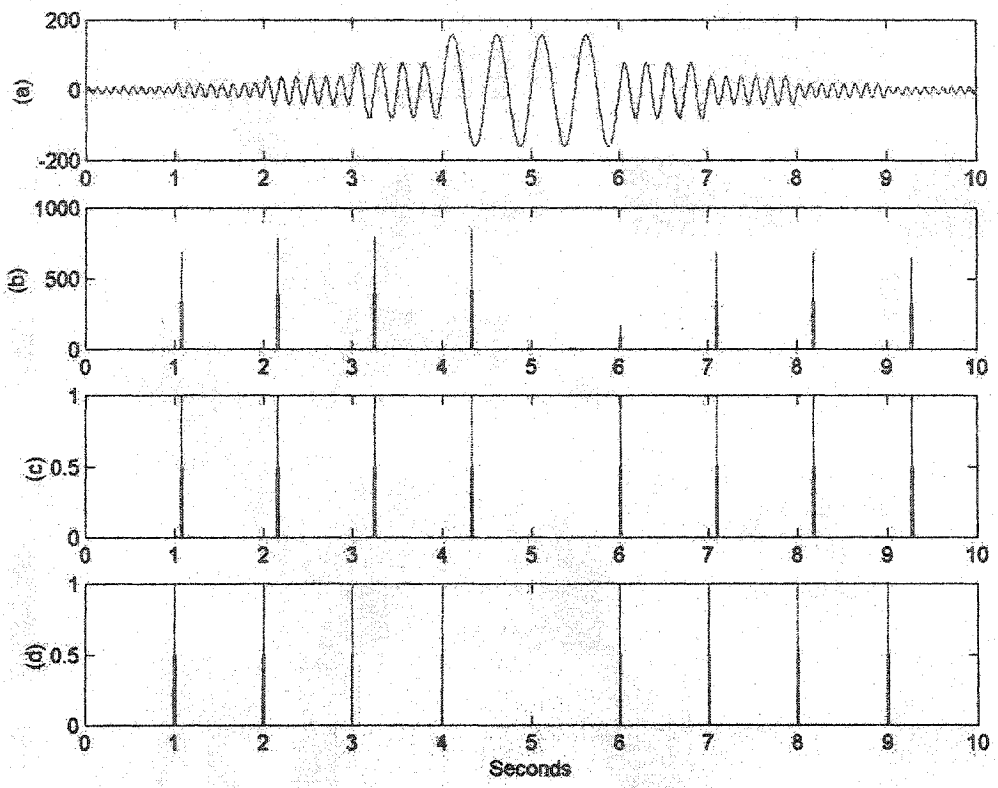

Figure 4.21: GLR segmentation for sinusoidal signal with amplitude and frequency changing in opposite directions to one another. (a) Signal: A = [10 20 40 80 160 160 80 40 20 10] and f = [10 8 6 4 2 2 4 6 8 10] Hz; (b) Difference measure with WL = 70 and T = 44; (c) Non-stationary boundary detection; (d) Optimized positioning of detected boundaries.

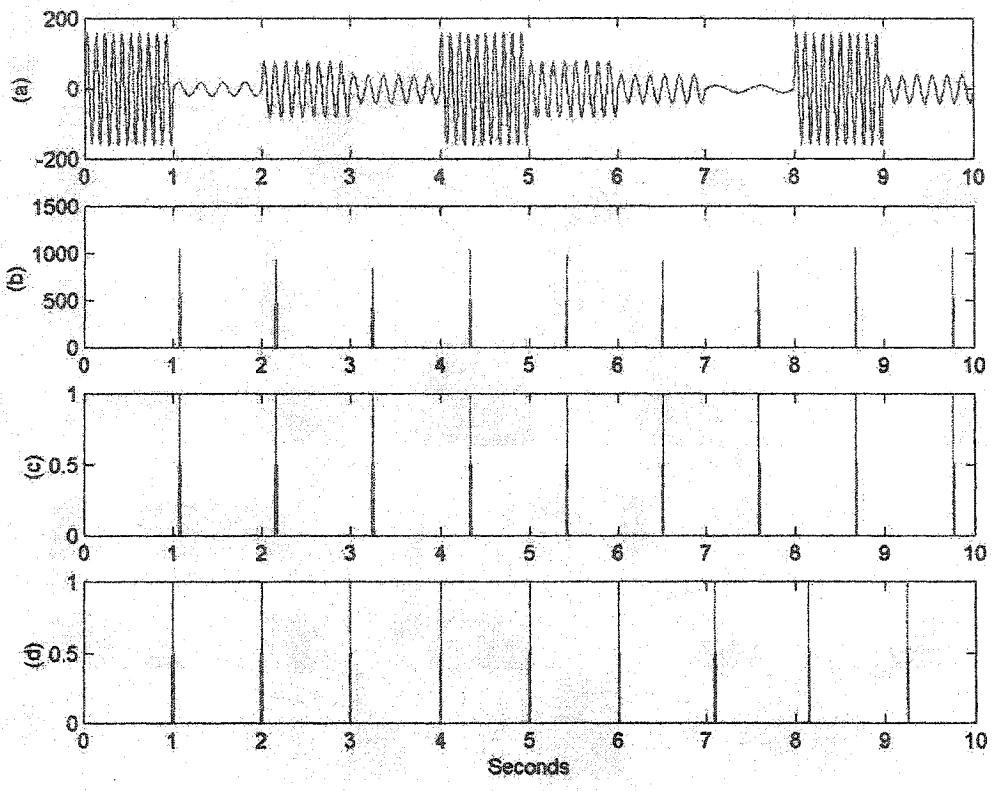

Figure 4.22: GLR segmentation for sinusoidal signal with randomly distributed segments of Figure 4.20 where amplitude and frequency change together in the same direction. (a) Signal; (b) Difference measure with WL = 70 and T = 44;; (c) Non-stationary boundary detection; (d) Optimized positioning of detected boundaries.

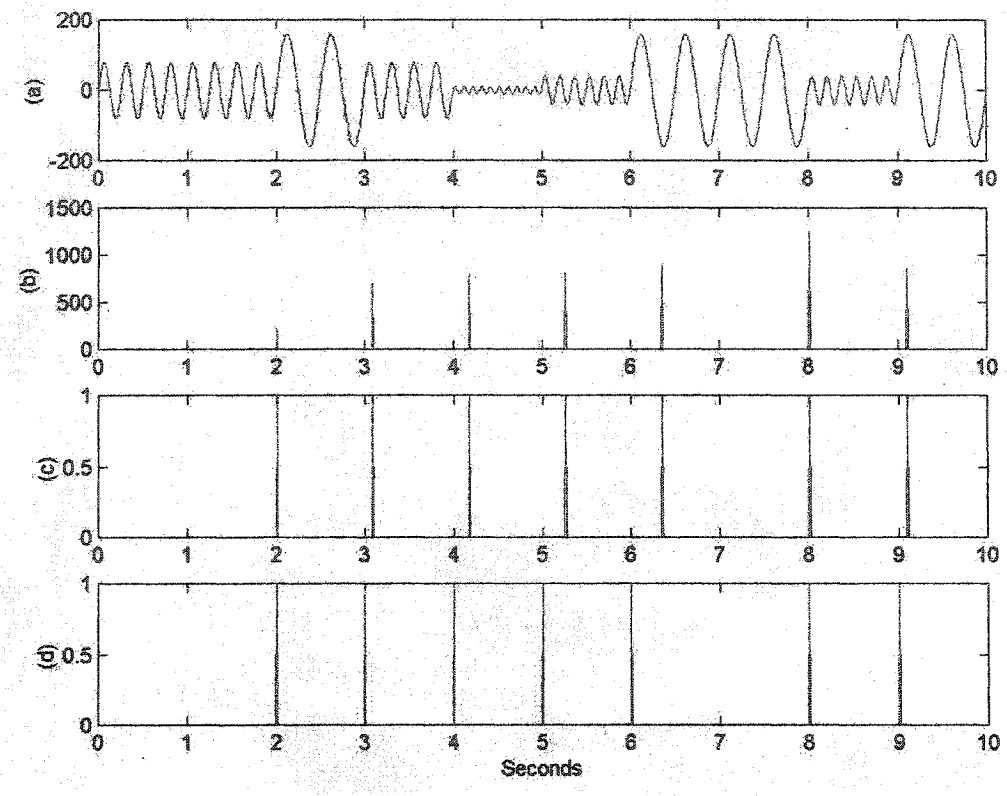

Figure 4.23: GLR segmentation for sinusoidal signal with randomly distributed segments of Figure 4.21 where, amplitude and frequency change in opposite directions. (a) Signal; (b) Difference measure with WL=70 and T=44; (c) Non-stationary boundary detection; (d) Optimized positioning of detected boundaries.

These results show, by the optimized position boundaries, that the GLR can successfully segment a noise-free non-stationary signal. However, it must be noted that, by virtue of the likelihood ratio, which depends on the calculation of the different variances (Chapter 3), we were obliged to add a very small amount of noise to the signal. Because the matrices involved in calculating the variances were close to being singular, they contributed directly to erroneous detections. To remedy this problem, a standard deviation (σ) of $\sigma = 0.001$,

was added to the signal. Adding such a negligable amount of noise to the signal leaves the signal, for our purposes virtually noise-free. Comparing these results with those of the ACF, we can see that despite a small but significant displacement seen in the detection stage of the procedure, the optimization stage effectively compensates for it and places the boundary exactly where it belongs. Compare the results for the VFCA signal in Figure 4.13, for the ACF with those produced by the GLR, in Figure 4.19, for example.

4.3.2.3 NLEO

Here, we apply the NLEO to the signals shown in Figure 4.11. Like the other two methods it depends on the window length and threshold values.

However, the threshold, in this case, unlike the other two methods is *not fixed* but *adaptive.* Its value is readjusted constantly, based on the current local values of the signal present, within the window. In other words it is set and reset 'on the fly' as the window slides through the entire signal, based on the scheme discussed in Chapter 3. To conform with the parameter values set in the other algorithms, WL is set to 70. The segmentation results are shown in Figure 4.24 to Figure 4.29.

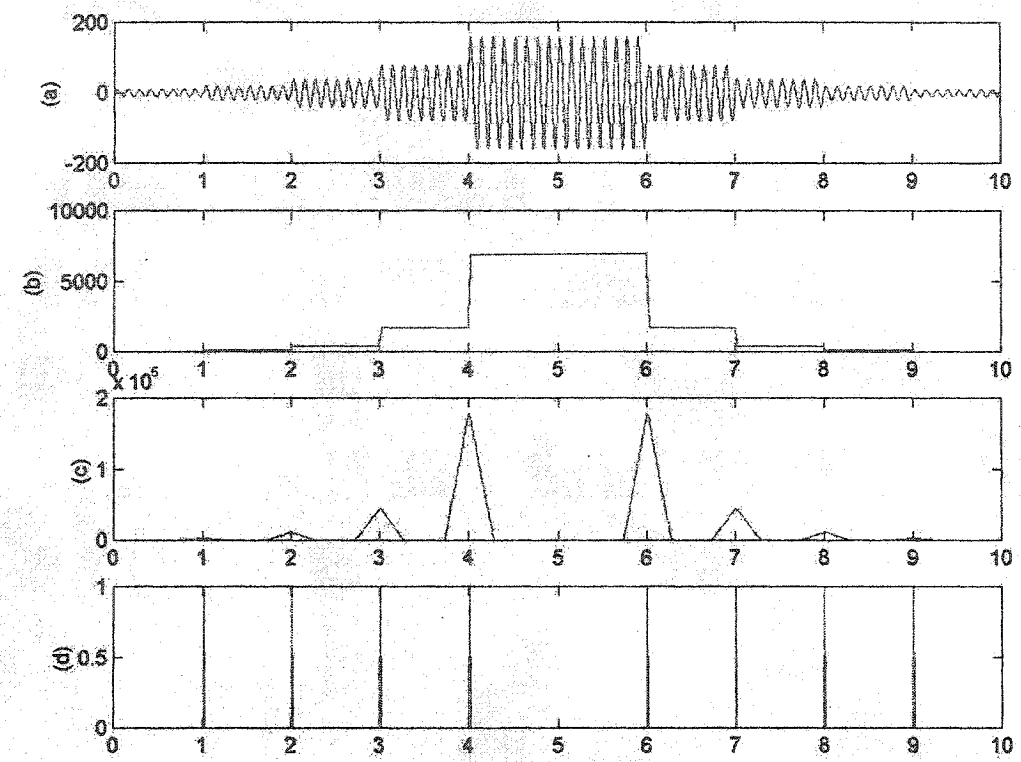

Figure 4.24: NLEO segmentation for sinusoidal signal with varying amplitude and constant frequency. (a) Signal: A = [10 20 40 80 160 160 80 40 20 10] and f = 8Hz; (b) Result of energy operator, Ψ_{NLEO}, to the signal; (c) Difference measure, G_{NLEO}, using WL = 70; (d) Final position of detected boundaries.

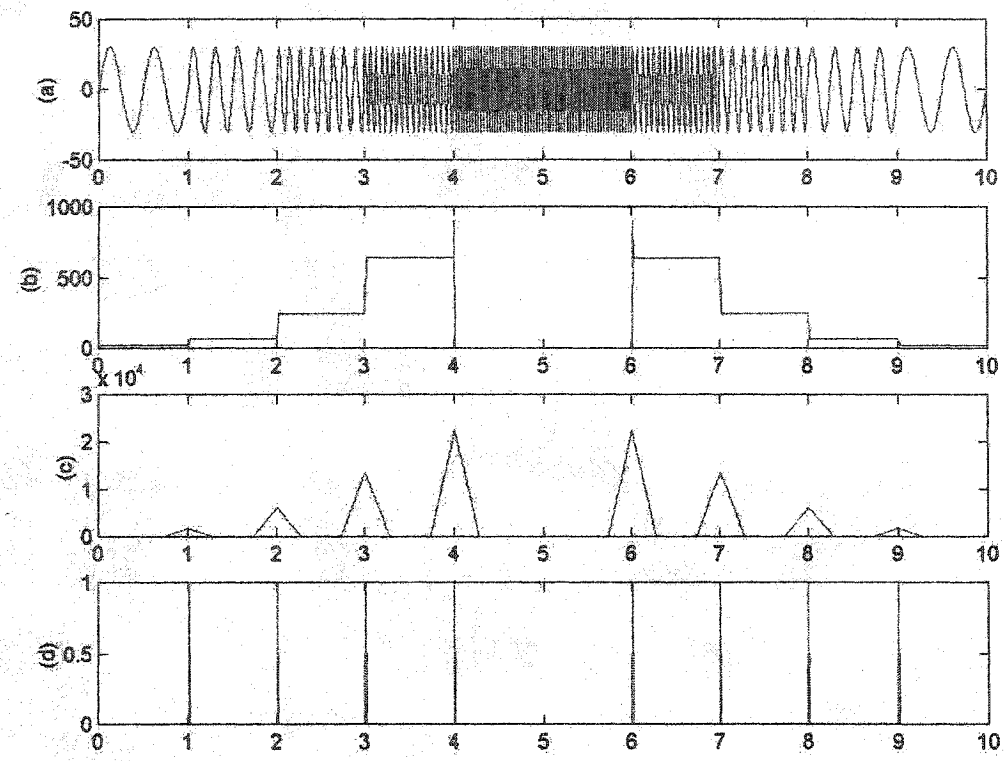

Figure 4.25: NLEO segmentation for sinusoidal signal with varying frequency and constant amplitude. (a) Signal: A = 30, and f = [2 4 8 16 32 32 16 8 4 2] Hz; (b) Result of energy operator, Ψ_{NLEO}, to the signal; (c) Difference measure, G_{NLEO}, using WL = 70; (d) Final position of detected boundaries.

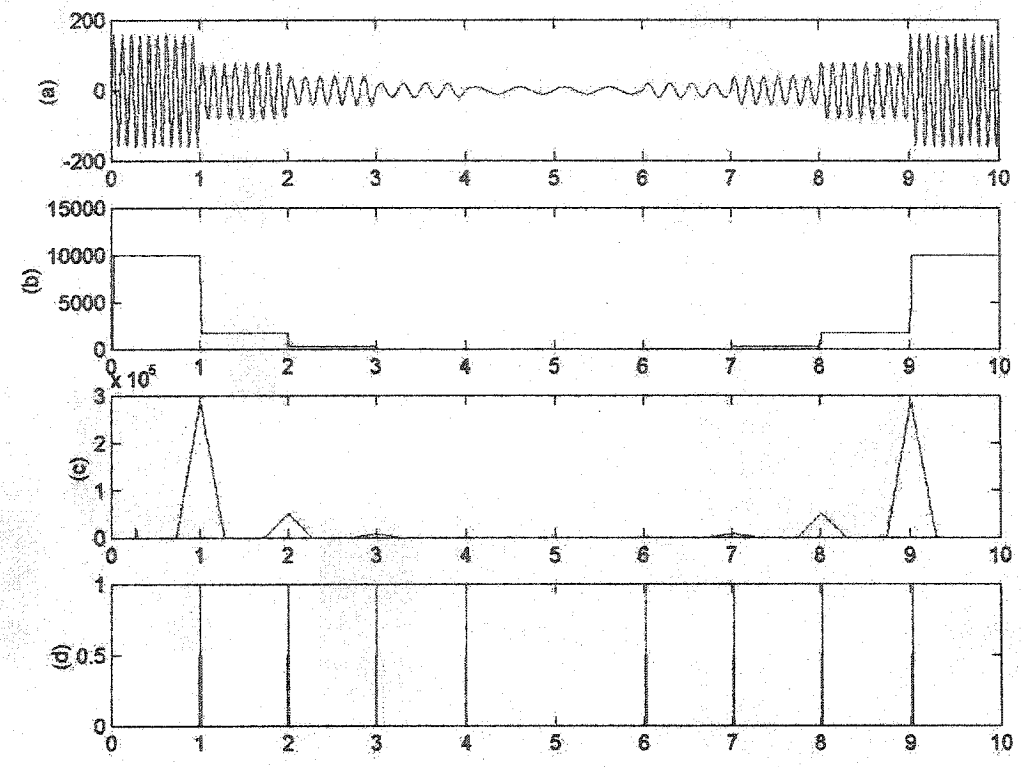

Figure 4.26: NLEO segmentation for sinusoidal signal with amplitude and frequency changing together in the same direction. (a) Signal: A = [160 80 40 20 10 10 20 40 80 160] and f = [10 8 6 4 2 2 4 6 8 10] Hz; (b) Result of energy operator, Ψ_{NLEO}, to the signal; (c) Difference measure, G_{NLEO}, using WL = 70; (d) Final position of detected boundaries.

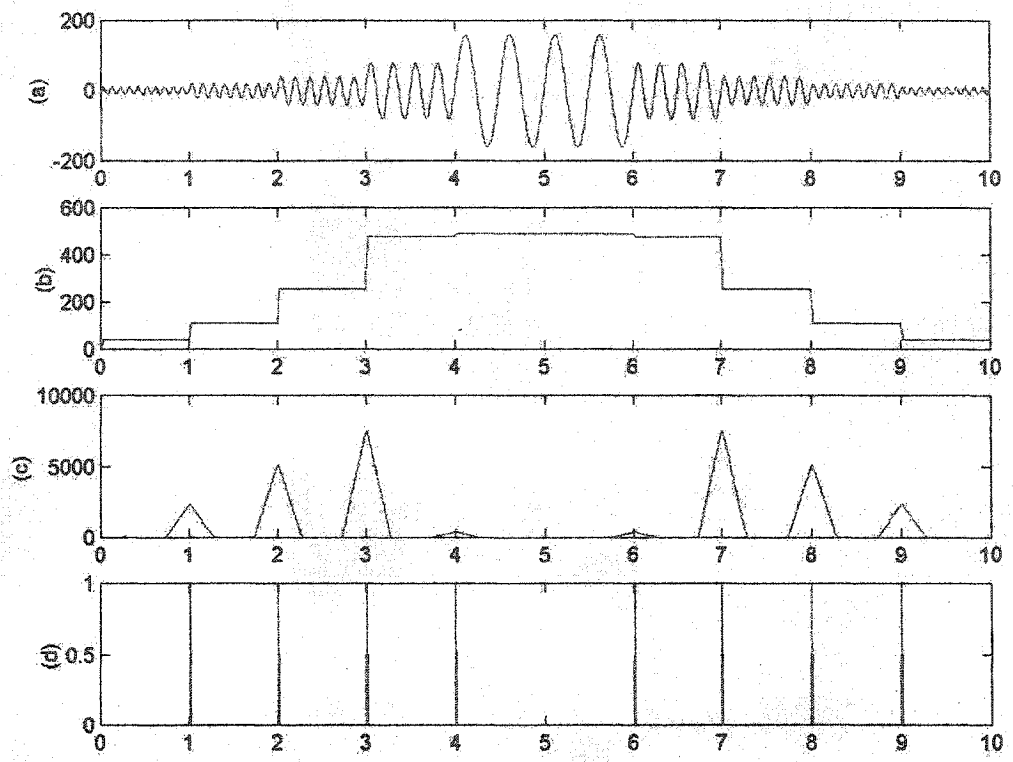

Figure 4.27: NLEO segmentation for sinusoidal signal with amplitude and frequency changing in opposite directions to one another. (a) Signal: A = [10 20 40 80 160 160 80 40 20 10] and f = [10 8 6 4 2 2 4 8 10] Hz; (b) Result of energy operator, Ψ_{NLEO}, to the signal; (c) Difference measure, G_{NLEO}, using WL = 70; (d) Final position of detected boundaries.

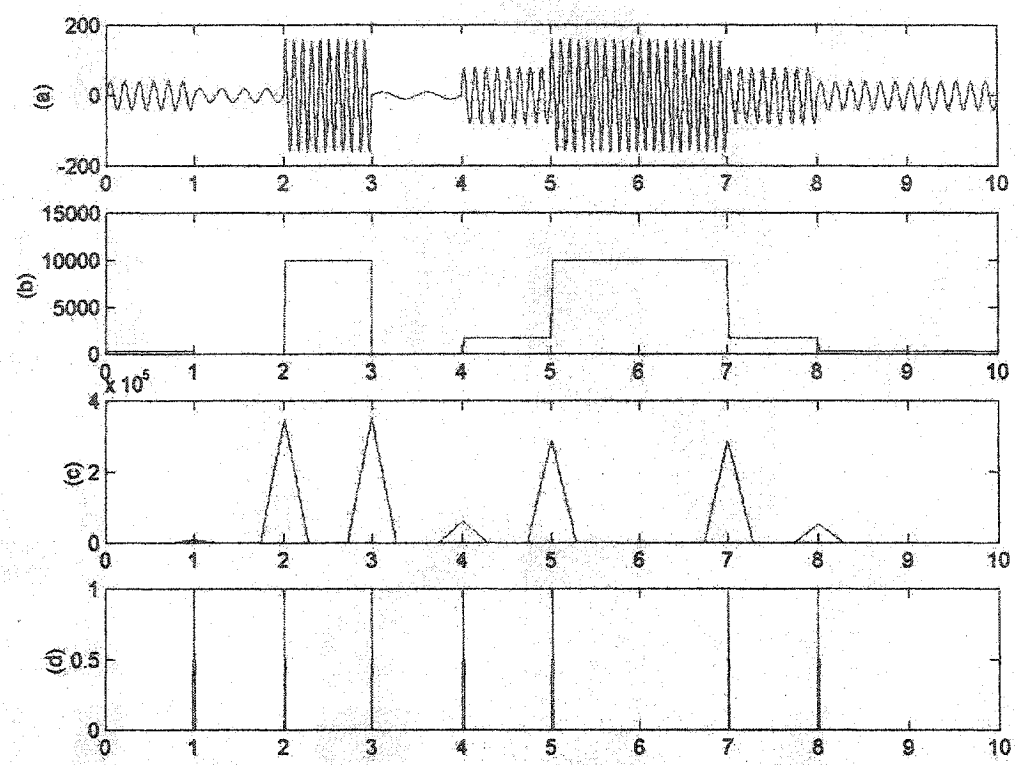

Figure 4.28: NLEO segmentation for sinusoidal signal with randomly distributed segments of Figure 4.26 where amplitude and frequency change together in the same direction. (a) Signal; (b) Result of energy operator, Ψ_{NLEO}, to the signal; (c) Difference Measure, G_{NLEO}, using WL = 70; (d) Final position of detected boundaries.

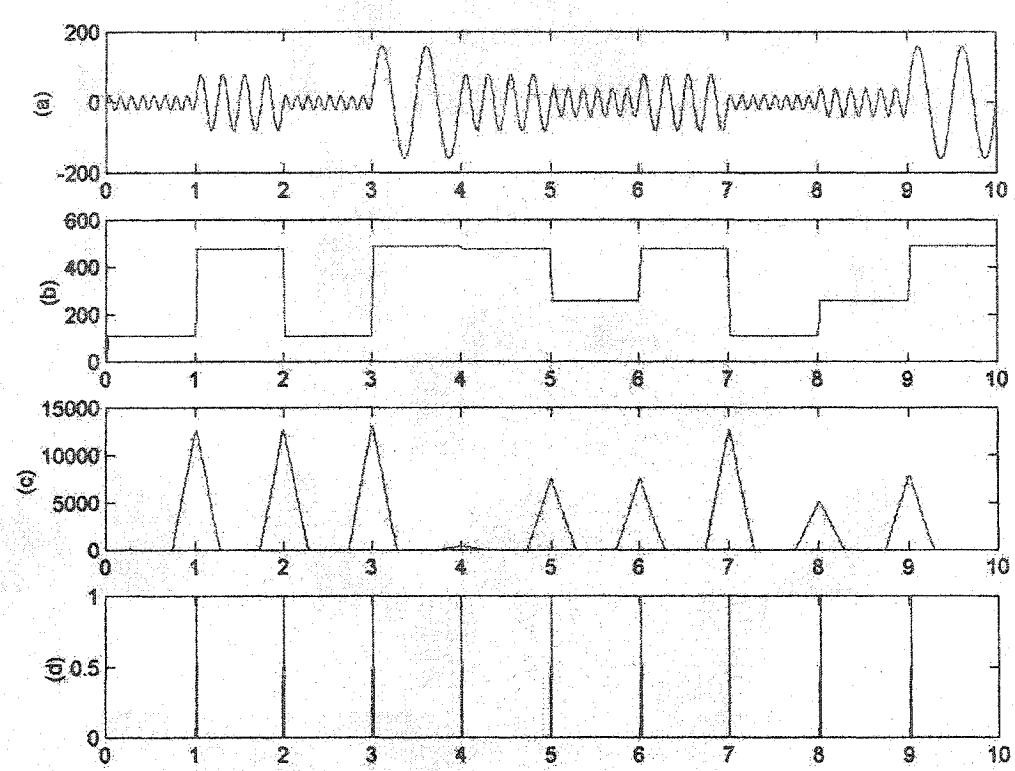

Figure 4.29: NLEO segmentation for sinusoidal signal with randomly distributed segments of Figure 4.27 where, amplitude and frequency change in opposite directions. (a) Signal; (b) Result of energy operator Ψ_{NLEO} to the signal; (c) Difference measure, G_{NLEO}, using WL = 70; (d) Final position of detected boundaries.

In view of the results of Figure 4.24 to Figure 4.29, we see that the NLEO algorithm correctly segments the various signals, but also precisely identifies their position. Again, with no noise present, this result is to be expected. By its very nature, there is no optimization scheme used by the NLEO method to determine the optimal boundary position, as is the case for both the ACF and GLR methods. Instead, the peaks produced in the G_{NLEO} difference measure are taken directly to be the boundary's final position. The relative heights of

the Ψ_{NLEO} plateaus show the proportional energy relationship between the Ψ_{NLEO} and the signal's amplitude and frequency. For example, the plateaus increase in height as the amplitude increases, as shown in Figure 4.24, as is the case for the frequency increase in Figure 4.25. In Figure 4.25, the zero plateau produced for the highest frequency (i.e., 32 Hz) although inconsistent with the present argument, is simply a result of accidental values chosen for this experiment. With a sampling frequency of fs = 128 and the given frequency of 32 Hz, this combination produces a function $f(n) = A\sin\left(\frac{\pi}{4}n\right)$, where n is the sample number. The application of Ψ_{NLEO} to this function, in particular, results in a zero plateau. However, the peaks occurring at the borders of the 32Hz section, outline the true position where that section's plateau should be. The other signals, otherwise, reveal the energy proportionality clearly.

4.3.2.4 Comparison between the three Segmentation Schemes

Comparing the performance of the three algorithms on the noise-free signals, we can make the following observations.

The ACF requires that the thresholds T_a and T_f be lowered in order to detect the non-stationary boundaries for the two cases, where only the amplitude changes in one case and only frequency changes in the other. The GLR does not need to change its threshold for any of the signals, but on the other hand it does need to insert a negligible amount of noise into the signal. It inserts noise to overcome the inherent computational instability, which produces erratic false detections. Comparing the detected boundaries, the GLR optimizes the final position of the boundaries visibly better than the ACF.

Since the NLEO does not have any adjustable parameters, apart from the window length, which remains constant, it does not need any adjustment to detect the boundaries. Also its detected boundaries are visibly better positioned than those produced by the ACF while, at the same time, comparable to the those of the GLR.

4.3.3 Sinusoidal Non-stationarities WITH Noise

In the previous section it was shown that with very little adjustment all three algorithms segment the signal properly without any undue degree of parameter adjustment. The notable exception was, without question, the signal involving only frequency change. Now, the emphasis is placed on evaluating the segmentation capabilities of the ACF, GLR and NLEO with signals exhibiting the same various forms of non-stationary events adopted before, but this time with noise added. The addition of noise further complicates the segmentation and demands a systematic evaluation of a key parameter shared by all schemes; that is, the window length (WL).

In the previous section, it was also possible to adjust by inspection, quickly and effectively, the most efficient WL suitable to detect all non-stationarities for all three schemes, which was WL = 70 samples. On the other hand, with noisy signals, this situation no longer applies. Although this parameter does not singlehandedly define the algorithms, it does critically impact their performance. With the introduction of noise into the signal, a uniform range of WLs is applied for each algorithm, to each different non-stationary signal. The goal behind this uniform WL sweep is to uncover the reliable operational WL values that work in detecting non-stationarities over a general span of real possibilities.

4.3.3.1 Description of the Signals Used

One typical realization of the non-stationary signals used to evaluate the performance of the segmentation schemes is shown in Figure 4.30.

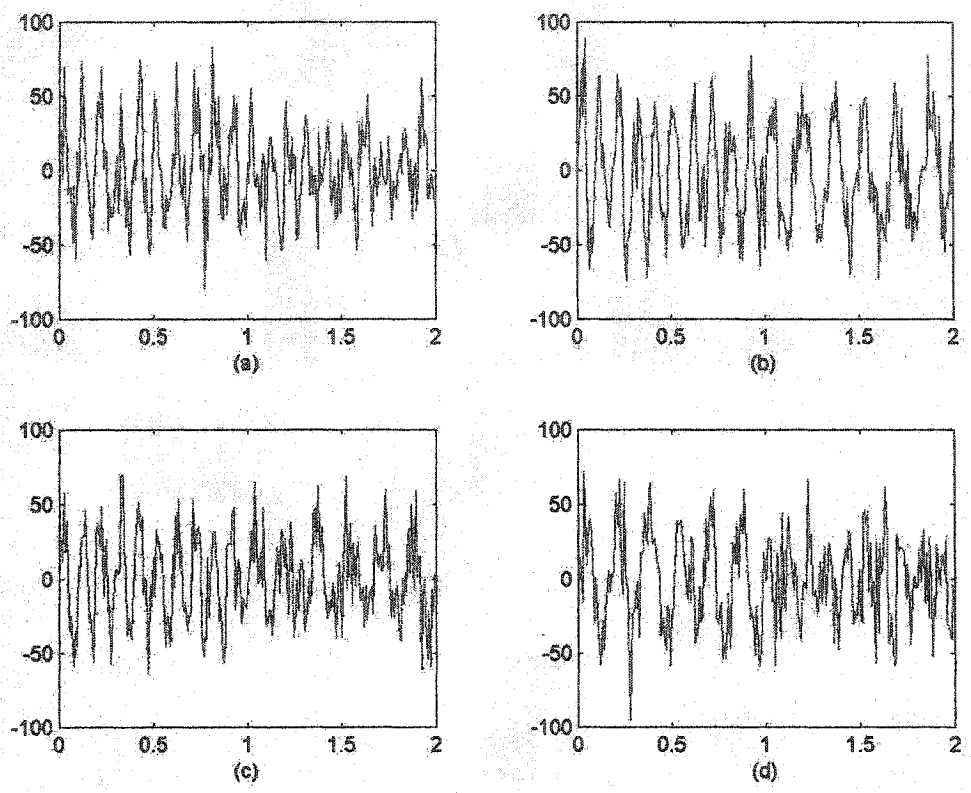

Figure 4.30: Various non-stationary segments (a) Decreasing amplitude with constant frequency (b) Decreasing frequency with constant amplitude (c) Amplitude decreasing with frequency (d) Amplitude decreasing while frequency increasing

At this point, a description of these signals must be given so as to allow a suitable discussion of their relevance with regard to the overall objective, involving the EEG. To begin with, all of the signals in Figure 4.30 consist of a combination of two values for the amplitude and two values for the frequency. These values are:

- Low amplitude = 20
- High amplitude = 40
- Low frequency = 6 Hz
- High frequency = 10 Hz

Following the tables presented in Chapter 1, the underlying assumption in the selection of these values is that by choosing closely spaced yet representative values, the segmentation performance can be readily identified in a more difficult environment rather than in one where largely-spaced values are used. In such a purposely hostile but realistic scenario, each algorithm's effective capacity to properly segment the signals is studied, in order to observe its performance, while recognizing that ample room for adjustment is still available, since these signals are but a narrow slice of the overall range of possible EEG variability encountered in practice.

In addition to the non-stationarities illustrated in Figure 4.30, there exists 'reciprocal' signals. For example, Figure 4.30a shows a decreasing amplitude constant frequency signal. Its reciprocal would be an increasing amplitude constant frequency signal. Similarly, the other three signals also possess a reciprocal. Although there is some difference between the same algorithm's response to these reciprocal signals, this difference sheds no more meaningful light on the algorithms' performance and therefore are not considered any further.

4.3.3.2 Description of the Noise Added to the Signals

The noise used in the signal is based on the SNR. A reasonably strong presence of noise is represented by AWGN with standard deviation of $\sigma = 20$, which corresponds to a

SNR = 3 dB for the half of the signal with the amplitude of 40, while at the same time it corresponds to a SNR = -3 dB for the half of the signal with the amplitude of 20.

4.3.3.3 Performance Measuring Parameters

To obtain exploitable statistical results, we generate 100 realizations of the noisy signals shown in Figure 4.30. To measure the performance of each algorithm, as the WL changes, we need to define three parameters. These parameters are:

1. Probability of a correct detection (P_c)
2. Probability of multiple false detections (P_f)
3. Standard deviation of correct detection from actual position (σ_c)

Probability of Correct Detection

Because all of the signals are designed to possess only one non-stationary boundary, which occurs, in all of the signals in Figure 4.30, at sample position n = 128, then only one detection can be made. However, the detection of only one boundary is not sufficient to score that detection as a correct one. To score for a correct detection, the boundary detected must be within a certain proximity of the actual non-stationarity. We define the necessary proximity that a detection needs to fall into, in order to be counted as a successful detection, arbitrarily as distance equal to 5% of the total signal length or 13 samples on either side of the actual boundary. Since the total length of the signal is 256 samples, then a detection is considered correct if it falls anywhere within the range [115 - 141] samples. Therefore, the criteria used in establishing whether a correct detection is made is:

- only one detection is made,
- detection made occurs within 5% range of actual boundary.

If these two criteria are satisfied, then the realization, where they occur, is counted towards correct detection. In other words, P_c is defined as the number of realizations with correct detections divided by the overall number of realizations.

Probability of Multiple False Detections

This key parameter is crucial in revealing an algorithm's propensity to produce misleading results. Whenever more than one detection is made, regardless of whether one of them is correct, the realization in which this situation emerges is judged as a false detection. Therefore, P_f is defined as the number of realizations where a false detection occurs divided by the overall number of realizations.

Standard Deviation of Correct Detection from Actual Position

During any realization, if a correct detection is made, then its position, in samples, away from the true position where the actual non-stationary boundary lies, is counted. Consequently, the final value for σ_c is calculated as the average value of all of the standard deviations produced in the realizations, where correct detections are made. It is clear that σ_c will never be greater than the imposed range limit, which in this case is equal to 13 samples.

4.3.3.4 ACF

In the previous section we set the operational values of the ACF's parameters. In this section, we test the ACF with these values. Since our objective here is to discover the dynamic reaction the ACF has with regards to a changing WL, we select the values for the various thresholds in a straightforward manner so as not obfuscate the results. First of all, we impose the condition that $T_a = T_f$ to ensure that relative changes in the amplitude and the frequency are balanced. Secondly, following the cues provided for, by the results of the ACF when applied to noise-free signals, the threshold values are chosen as: $T_a = T_f = T_g = 1$ for every signal except the case where only the frequency changes, in which case the thresholds are chosen as: $T_a = T_f = 0.45$, while the global threshold is maintained as: $T_g = 1$.

4.3.3.5 GLR

In the application of the GLR to the noisy sine signals of Figure 4.30, we select the following fixed values for two of the operational parameters: the model order number $p = 2$ and the number of bits used in threshold $N_0 = 2$. The model order number is chosen as 2 since higher values result in completely missed detections, which is directly attributable to the large degree of noise added to the signal.

4.3.3.6 NLEO

In this section we follow the same procedure as that used in the noise-free section, with one exception. Due to the presence of noise, we will impose, following the procedure proposed

in [50], a constraint limiting the minimum distance between any subsequent detections. Without this restriction, in the presence of noise, the NLEO tends to produce significantly higher false detection rates. Although the value chosen in [50] corresponds to another situation, we choose the minimum distance to be 35% of the overall signal size, that is MD = 90 samples = 0.7 seconds. The two segments, making up the overall signal, are each 128 samples or 1 second long. The value chosen for MD is selected to reduce the number of false detections.

4.3.3.7 Comparisons between the Results Generated by the ACF, GLR and NLEO

To begin this section, we present the results that each of the segmentation algorithms, as defined in the three previous sections, produced when applied to the signals of Figure 4.30. These results are superimposed upon each other, in graphic form, in Figure 4.31 through to Figure 4.34 to emphasize the differences between the methods. Here, we mention that throughout each of the following graphs the solid curve corresponds to the ACF results, the dashed curve to the GLR results and the dotted curve to the NLEO results, as explicitly depicted in subsection (b) of each graph.

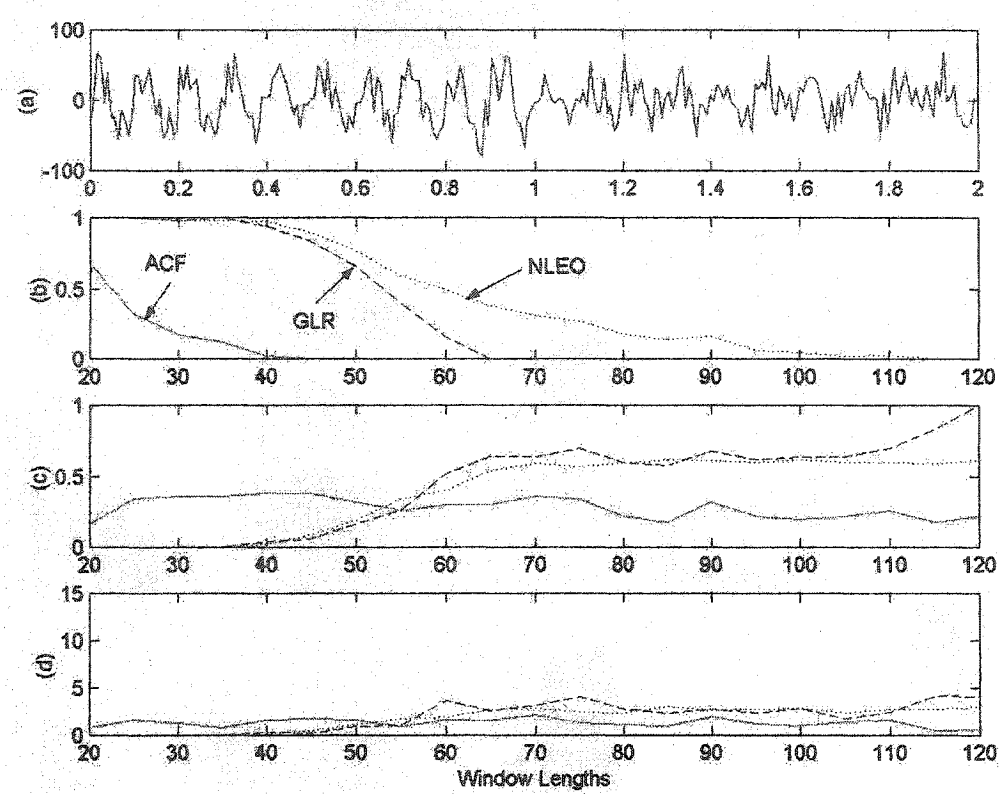

Figure 4.31: ACF (solid line), GLR (dashed line) and NLEO (dotted line) segmentation of noisy signal with amplitude decreasing and constant frequency (a) Signal; (b) P_f; (c) P_c; (d) Average σ_c.

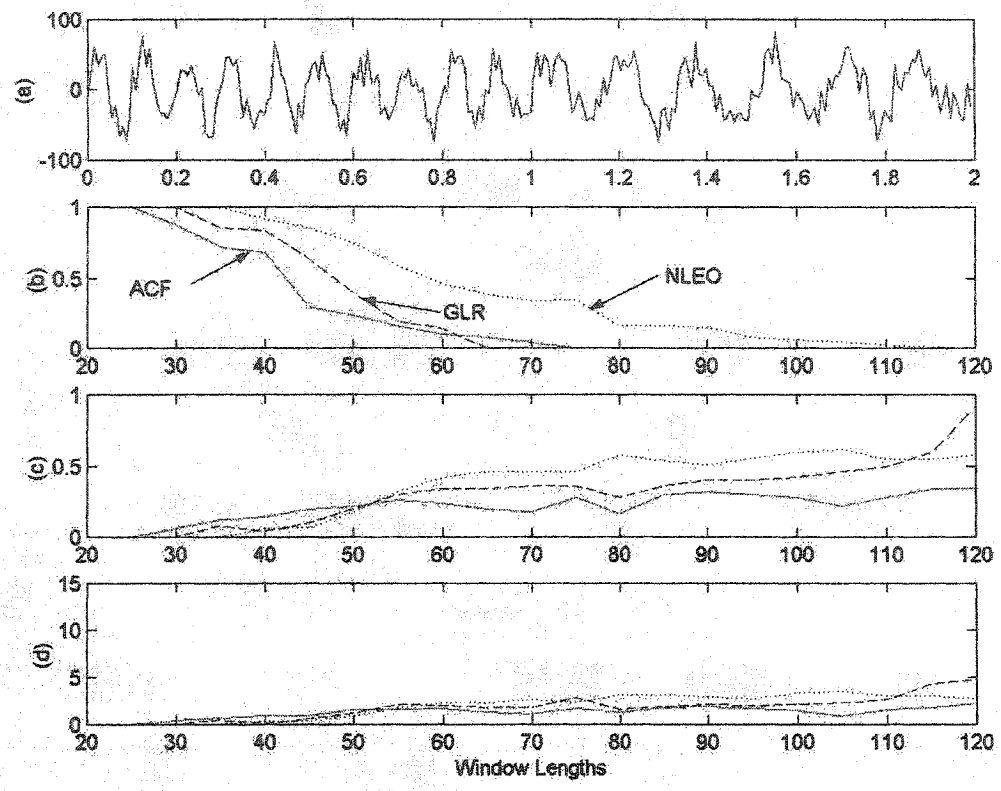

Figure 4.32: ACF (solid line), GLR (dashed line) and NLEO (dotted line) segmentation of noisy signal with frequency decreasing and constant amplitude (a) Signal; (b) P_f; (c) P_c; (d) Average σ_c.

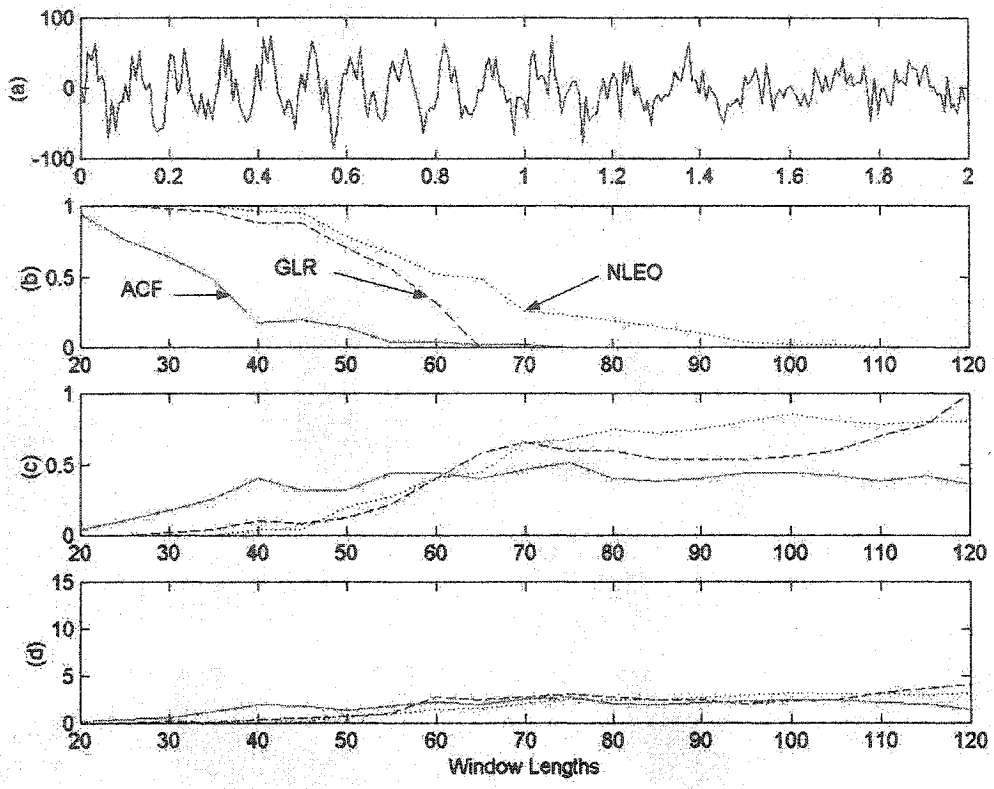

Figure 4.33: ACF (solid line), GLR (dashed line) and NLEO (dotted line) segmentation of noisy signal with amplitude decreasing and frequency decreasing (a) Signal; (b) P_f; (c) P_c; (d) Average σ_c.

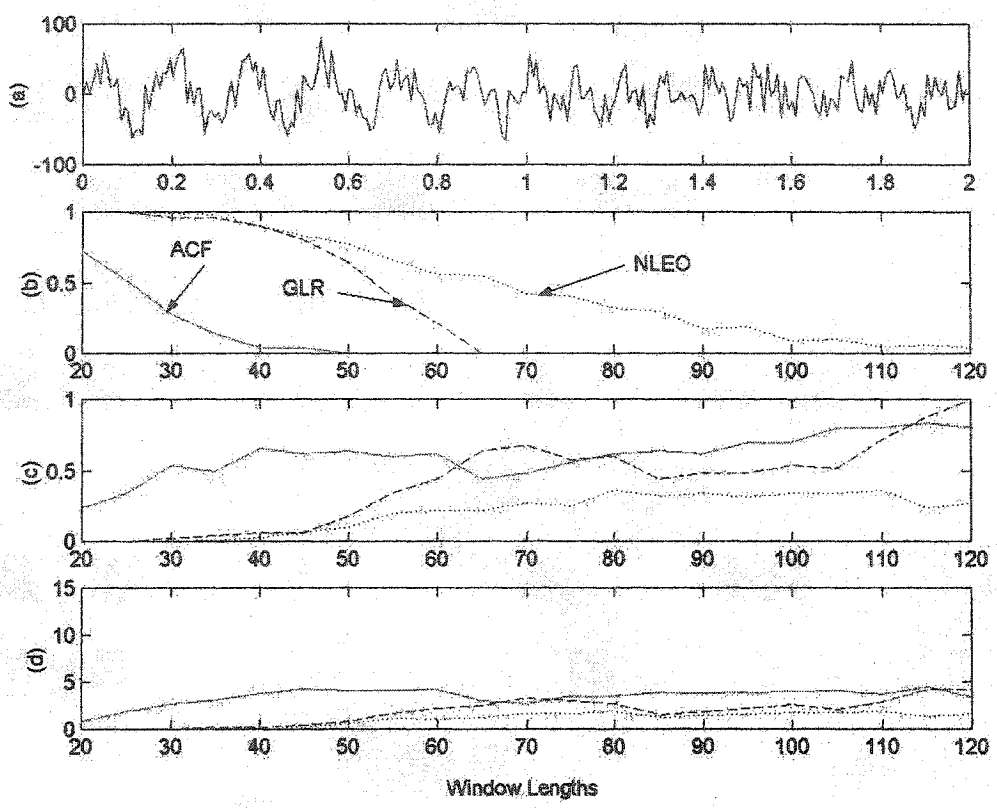

Figure 4.34: ACF (solid line), GLR (dashed line) and NLEO (dotted line) segmentation of noisy signal with amplitude decreasing and frequency increasing (a) Signal; (b) P_f; (c) P_c; (d) Average σ_c.

General Observations

Comparing the graphs, it is clear that the size of the WL, in all segmentation schemes, critically impacts the correct detection of the non-stationarities in a signal. We see that for smaller WLs, that is, for WLs smaller than 30 samples long, every method demonstrates near zero correct detection and conversely near total multiple false detection. The GLR and NLEO are especially noteworthy in this regard. The reason for such poor performance at these values of the WL lies possibly due to the fact that the sinusoidal signals all have one

half of their content possessing a frequency of 6 Hz.. Being a relatively low frequency, it is consequently longer in time. Since one second is 128 samples and dividing this by 6, we see that one entire cycle is represented concisely by 22 samples. Therefore, values of WL close to this value, although containing all of one cycle, do not reveal *enough* distinct information about the signal, due to the heavy presence of noise. This is why there is so much false detection.As the WL grows and more signal content is captured, better means of distinguishing the signal content is achieved.

For all of the realizations, the value of the standard deviation in the detected position from the actual position, σ_c, is well within the 5% range imposed, for all of the algorithms. In addition, because of its unvarying nature, the resulting σ_c appears to be independent of WL, apart from the WLs where no correct detection is possible.

All of the segmentation schemes appear to produce a relatively constant P_c in the range starting from WL = 65 samples all the way to the end of the range. The reason why noticeable stability is reached at WL = 65 samples is because this value is exactly one quarter of the overall signal length and consequently when two windows are positioned concurrently, as is the case for the ACF and GLR methods, their overall length reaches the midpoint of the signal, where the non-stationarity occurs. As a result, right from the start, potential false detections are avoided because the first non-stationarity detected, happens to be the actual non-stationariy. However, that is not to say that this circumstance will necessarily produce correct detection, as is evidenced in the imperfect P_c values, shown in Table 4.2 but it does assist somewhat in avoiding some false detections.

ACF

The ACF outperformed all of the other schemes in terms of producing the lowest P_f. This result is due to its reliance on a combination of both the amplitude and frequency measures. Having two independent measures of the signal gives a better means of distinguishing significant changes. Whereas only the amplitude changes in Figure 4.31 and only the frequency changes in Figure 4.32, the values for P_c is 0.28 and 0.21 for these two cases. These values are averages of the respective probability over the entire WL range and are taken from Table 4.2 in Section 4.4.2, where the algorithms' performance is compared when WT is applied. One possible reason for this result is because not enough significant change is present.

By significant change, we imply significant change in either the amplitude or the frequency of the signal or both. Remember that the ACF method reveals the combined difference for *both* the amplitude and the frequency. Since Figure 4.31 shows only the amplitude changing while the value of the frequency remains constant, only one of the two parameters (amplitude and frequency), which the ACF uses in measuring significant difference in the signal, actually contributes to making a difference. Therefore, since only one parameter is changing, the significance of the change present is only half as strong as it would be if both parameters were changing (i.e. which is normally the case). Moreover, the considerable amount of noise present further diminishes the significance of the actual change in the amplitude from a value of 40 to a value of 20. Both of these factors taken to together contribute in explaining the low value of P_c for Figure 4.31. A similar argument holds for the results of Figure 4.32.

To further understand the importance of having both the amplitude and the frequency changing for the ACF, we consider Figure 4.33 where we have the amplitude decreasing from 40 to 20 and at the same time the frequency decreasing from 10 Hz to 6 Hz. Here, the amplitude and the frequency change together, that is, they are both decreasing. The P_c value produced is 0.36 which is modestly higher than Figure 4.31 and significantly higher than that of Figure 4.32. The P_c value resulting from Figure 4.34 where both the amplitude and the frequency change in opposition to each other (i.e., amplitude decreases while frequency increases) is 0.61. This value is clearly superior to the P_c values of either Figure 4.31 or Figure 4.32.

Another reason for the low P_c values may come from the definition of the P_c parameter itself. A detection is considered to be correct only if it falls within a 5% range on either side of the actual position of the non-stationary boundary. Perhaps this value is too strict. In Section 4.3.4 we will define the probability of a detection falling outside of this range. Although a 2nd order AR signal is used in that section, we will see that a considerable number of detections do indeed fall outside of the range. Furthermore, we will see that detections are in fact made but that they fall ouside of our arbitrarily defined range. Assuredly the same situation applies in this case with the sinusoidal signals. Therefore, we can improve the low P_c values by simply increasing the 5% range, which may possibly be too strict a value, but this gain nevertheless comes at the cost of reducing the precision of detection. However, such a compromise may be worthwhile if it means higher detections are made.

GLR

The GLR performed well, having the intermediate value for P_f while maintaining a relatively high value of P_c. We note that the GLR P_c value reaches 100% correct detection at WL = 120 samples, for every signal, which is a misleading result. This value of WL is equivalent to the entire signal length when two such windows are positioned side by side. Thus, the two distinct signal halves each fall squarely, one, into the reference window and, the other, into the test window. This accounts for the gradual P_c increase, seen at the larger WLs. However, this result shows, when compared with that of the ACF, which also uses two windows, that GLR has a much better ability, at least as far as these test signals are concerned, to detect and isolate the correct boundary position. The ACF, on the other hand, despite having two windows positioned exactly above the two distinct portions of the signal, does make a correct detection but is not able to resolve the correct location of the boundary as precisely as the GLR within the larger window length.

NLEO

The NLEO achieves good P_c for all signals except for the signal in Figure 4.34. Since most detections could very likely be falling outside of the imposed range, this result, as discussed in the general observations section, does not considerably detract from the overall effectiveness of this method. However, the most prevalent feature that strikes one's attention is its poor ability to avoid false detections. For all signals it is the NLEO method which performs the poorest in this regard, with high values of P_f, extending over a large range of WLs. The main reason for this result stems directly from its adaptive threshold or, said differently, from its lack of a fixed threshold. Due to the sporadic effects caused by the added

noise, false detections are inevitable. Nevertheless, P_f does show an improved performance as the WL increases. Unlike the previous methods, only one window is used. Therefore, for WLs approaching half the signal length, the NLEO demonstrates that stable P_c can be maintained as well as reducing the P_f, so long as the WL is close to the size of the segment being sought and that a minimum distance between consecutive detections is imposed.

4.3.4 Second Order AR Non-stationarity

We now turn our attention to non-stationary signals generated by a second order AR model. The signal used in this section is generated by concatenating two stationary, but dissimilar second order AR signals. Adjoining two such signals together produces the desired non-stationary signal. The two component signals used are defined by the following AR relationships:

$$x(t) = -x(t-1) - 0.2 \cdot x(t-2) + e(t) \qquad t = 1, 2, \ldots, 128 \tag{4.2}$$

$$x(t) = x(t-1) - 0.4 \cdot x(t-2) + e(t) \qquad t = 129, 130, \ldots, 256 \tag{4.3}$$

where $x(t)$ is the signal and $e(t)$ is white Gaussian noise with zero mean and unit variance. We chose the length of each signal, as in the previous section, to be 128 samples (or 1 second) long. The overall signal created by combining these two signals is shown in Figure 4.35.

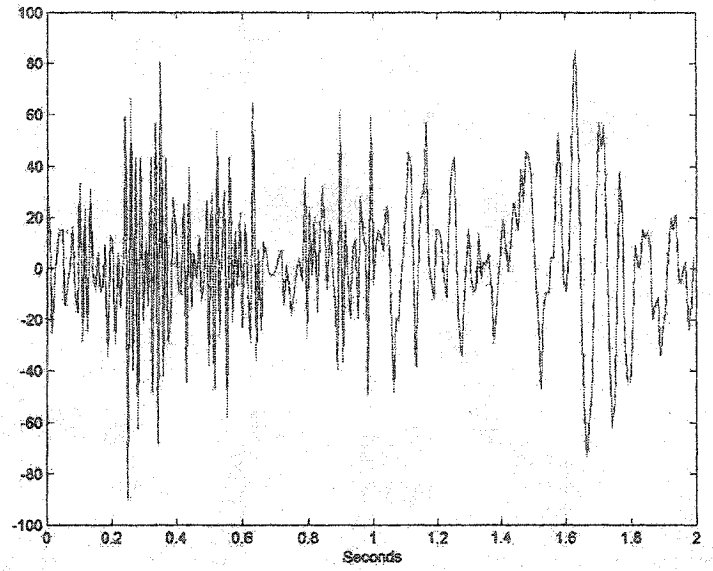

Figure 4.35: One realization of the non-stationary signal generated by 2nd order AR process used as the test signal.

In this section, we apply the three algorithms to this second order autoregressive non-stationary signal to study their performance under a different light. The performance measures used throughout Section 4.3, namely, P_c, P_f and σ_c, are again used here. Similarly, 100 realizations of the AR non-stationary signal are generated to obtain reliable results. Moreover, two additional measures are included and these are:

- Probability of a missed detection (P_m)
- Probability of out of range detection (P_o)

These new measures are included to reveal a clearer picture of the segmentations' performance, some of which remained hidden, when only P_c, P_f and σ_c were used.

Probability of a Missed Detection

Simply put, P_m counts the number of realizations where no detection is made. Remember that the signal under study possesses only one non-stationary boundary and therefore only one detection should be made. To calculate P_m, all the realizations where no detection is made are counted and divided by the total number of realizations used. This performance measure is important in determining the situations where the segmentation scheme is unable to make a detection.

Probability of Out of Range Detection

Recall that the non-stationary boundary of the test signal occurs in the middle of the signal or 128 samples (i.e. 1 second). Moreover, in determining σ_c we had to decide upon an acceptable range, away from this boundary, which we chose reasonably to be 5% of the overall signal length. Realizations where only one detection appeared and that detection occurred within this range, were counted towards calculating P_c. Now, the number of realizations, where only one detection occurs but falls outside the given range, is counted towards calculating P_o. This measure sheds light on the precision of a segmentation method in localizing a detection.

4.3.4.1 Varying WL

As in the previous sections, we vary the WL, for all three methods using the same WL range. The same values for the threshold used before for the ACF and the GLR are again applied. In addition, the same imposed minimum distance is applied again to the NLEO to

mimimze the overall number of false detections. The results are shown in Figure 4.36 and they include the two additional performance measures.

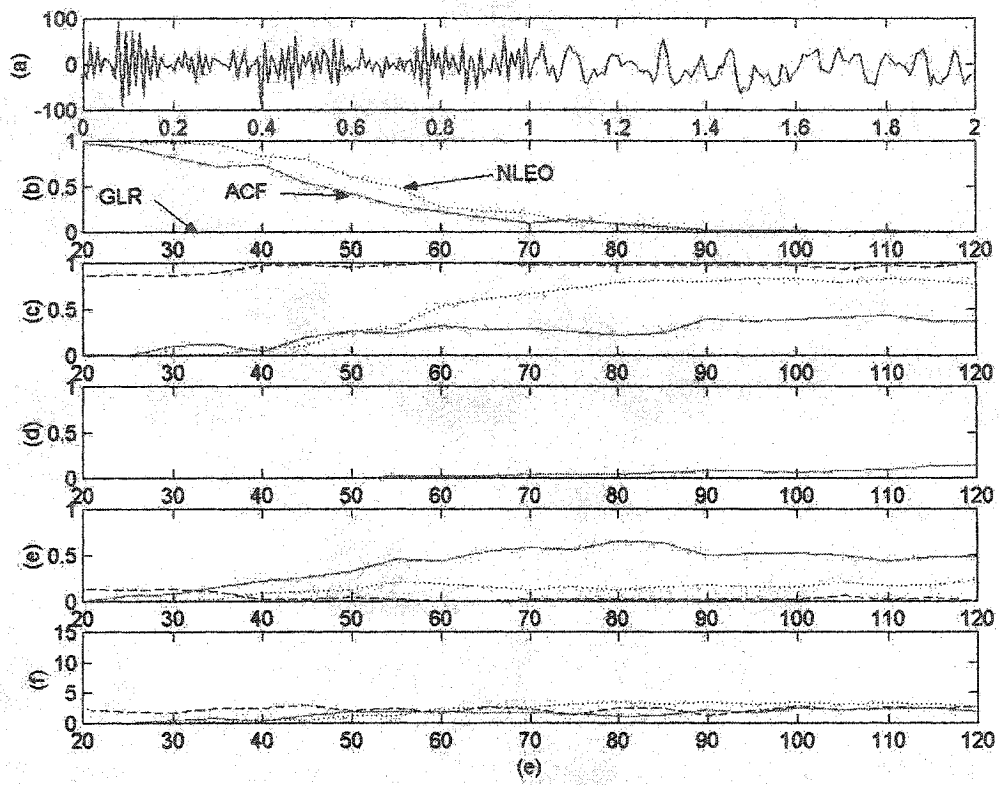

Figure 4.36: ACF (solid line), GLR (dash-dot line) and NLEO (dashed line) segmentation of 2nd order AR modelled non-stationary signal for various windows, with $T_a = T_f = T_g = 1$, for the ACF, $N_{bits} = 32$, for the GLR. (a) Non-stationary signal; (b) P_f; (c) P_c; (d) P_m; (e) P_o; (f) σ_c.

ACF

Comparing the P_f values of Figure 4.36 with those produced for the sinusoidal signals, we observe that the ACF has more difficulty in suppressing false detections, as evidenced by the longer WLs needed to bring this value to zero. In addition, it produces P_c values that

are quite low, similar to those emerging from the segmentation of the only-frequency changing signal, in Figure 4.32.

Yet, by looking only at the P_c values produced by the ACF, we get a somewhat discouraging picture. However, this is only part of the picture. Taking P_o into consideration, we see that the larger part of the other detections made by the ACF fall outside of the 5% range. This result is encouraging because it reveals that the ACF does make detections overwhelmingly, but most fall out of an artificially imposed range. So the question, concerning its performance involves precision in location rather than ability of detection, although its ability to detect is slightly affected, since it is the only segmentation scheme that produces non-zero value of P_m for this signal.

GLR

The most noticeable feature of Figure 4.36 is, without question, the near perfect P_c values produced by the GLR over the entire WL span. This result demonstrates the GLR's exceptional ability to both detect and optimize the position of the non-stationary boundaries. However, it must be noted that due to the nature of the signal, a second order AR process, such a result is to be expected because the GLR is also an AR process. Moreover, since the GLR is also second order, it is therefore optimally suited for this kind of signal. This event is no fortuitous accident, but on the contrary was deliberately chosen to demonstrate the excellent capabilities of the GLR segmentation scheme, when its order corresponds precisely to the signal under study. However, the selection of the order, a critical parameter in its performance, is no trivial issue, and its solution can be approached by either of the model order estimation methods discussed in Section 3.5.7.1.

NLEO

The NLEO shows the same high P_f as was witnessed with the noisy sinusoidal signals, although it appears to be slightly better in comparison. It does produce a higher P_c than in the other signals. Its average P_c, taken from Table 4.3 of Section 4.4 below, is 0.50 and is higher than the P_c produced by the previous signals. Furthermore, it is clear from the probability breakdown in Figure 4.36 that it either correctly detects a boundary or it makes multiple false detection. It makes some detections out of range but unlike the ACF it never misses a boundary.

4.3.4.2 Varying Thresholds

In this section, we attempt to ascertain the optimal threshold value for the ACF and the GLR, by applying a relevant threshold sweep to each, exactly as we did when sweeping through the WLs.

ACF

Along with testing the effect of changing the WL on the ACF's performance, a test wherein both the amplitude and the frequency thresholds T_a and T_f are varied, is also applied. This second test is used to determine as to which threshold produces the best detection. However, two constraints are applied. They are:

- $T_g = 1$
- $T_a = T_f$

where, T_a, T_f and T_g are the amplitude, frequency and global thresholds respectively, as before. The first constraint is chosen to conform with the values of Section 4.3, while the second constraint enforces a relative change of amplitude to have the same weight as a relative change in frequency. The variable test range applied for the threshold is [0.2 - 2.0]. While the threshold is varied, the WL is fixed at WL = 70 samples. We choose this value because throughout most of the results generated in the previous section, where WL is varied, it is observed that P_f falls to zero at around WL = 65 samples for the GLR, while for the ACF it does in most cases well before this value and in others a little after. Therefore, the present choice is made to enable a good and consistent comparison to be made between the two methods. The results of varying threshold are shown in Figure 4.37

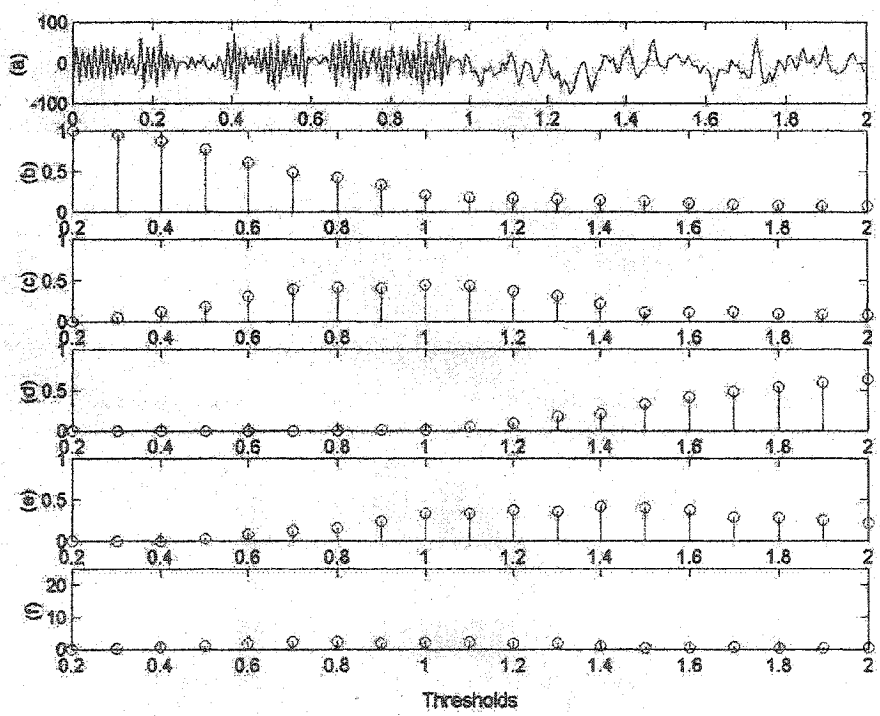

Figure 4.37: ACF segmentation of 2nd order AR modelled non-stationary signal for various thresholds, with WL = 70. (a) Non-stationary signal; (b) P_f; (c) P_c; (d) P_m; (e) P_o; (f) σ_c.

We observe from these results a number of important features. Firstly, low threshold values produce high P_f values which gradually taper off as the threshold increases. These low threshold values tend to overemphasize the changes in frequency and amplitude, which consequently lead to greater false detections, as shown in Figure 4.37b. Secondly, as the threshold increases, we notice that the number of missed detections, as seen in Figure 4.37d, begins to steadily increase. Here, instead of overestimating the combined weight of frequency and amplitude signal content, the increasing threshold values tend to underestimate their presence, thereby leading the ACF to miss them althogether. Fortunately, our third point reveals when considering Figure 4.37c, that between these two worlds of overestimation and underestimation their does exist an optimal threshold range. We can see that for values of the threshold in the range of [0.7 - 1.2], the values of P_c reach their peak values. In particular, the optimum threshold value is unity, because at this value P_c is highest and both P_f and P_m are very low. However, the one drawback to this value is that it also corresponds to a near peak value in P_o. Nevertheless, as was discussed in the varying WL section, the imprecision in the P_o value does not critically damage the overall effectiveness of the ACF algorithm. This higher P_o value, to a certain degree, can be tolerated, so long as false detections are minimized and missed detections are avoided.

GLR

The application of the GLR to the signal in Figure 4.43 necessitates further investigation of its performance, and more specifically its optimal performance with regards to threshold. In particular, in this section, the number of bits used in determining the GLR's detection threshold is varied. The number of bits varies from a value of 2 to a value of 32, in steps of

2 to conform with the values used in the previous sections. The model order is maintained, for consistency with Section 4.3.3.5, at $p = 2$. The results of varying threshold and WL are shown in Figure 4.38.

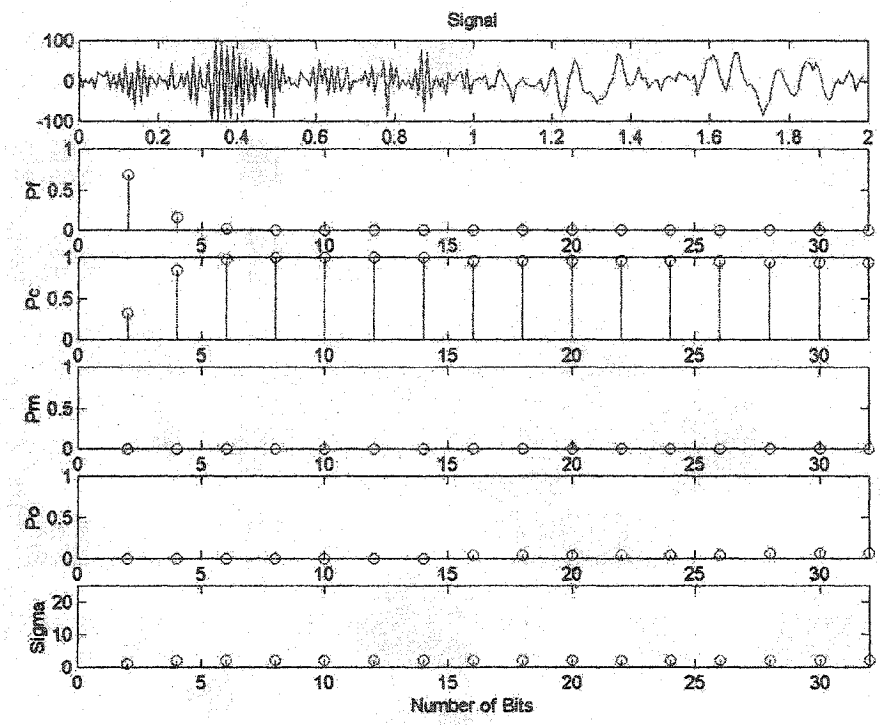

Figure 4.38: GLR segmentation of 2nd order AR modelled non-stationary signal for various thresholds, with WL = 70. (a) Non-stationary signal; (b) P_f; (c) P_c; (d) P_m; (e) P_o; (f) σ_c.

The results of Figure 4.38 show a much simpler situation than that for the ACF. We see that there is a sharp transition threshold, which occurs at $N_{bits} = 6$, whereby P_f falls to zero, in Figure 4.38b and maintains this value for every higher threshold value, while the P_c rises to nearly 100% detection, in Figure 4.38c. Apart from the slight increase in P_o starting at 16, the GLR demonstrates superior overall performance compared to the ACF.

4.4 Segmentation of Wavelet Decomposed Signal

In this section, we demonstrate the validity and effectiveness of the combined procedure shown in Figure 4.1, involving both the segmentation algorithms and the wavelet decomposition. Applying the same signals that were used in Section 4.3 to this section, we now demonstrate the improvement that such a combination yields over the results produced in those sections, where no wavelet decomposition was used. The comparison drawn between the two sets of algorithms (i.e., those with WT and those without) is, again, accomplished by means of varying WLs, as was done in the previous sections, for the simple reason that WL is common to all the three algorithms and therefore provides a good basis for judging quantitatively the similarities and dissimilarities amongst the three.

4.4.1 Comparison of Segmentation with Wavelet Decomposition

The results presented in this section are broken into two parts. One part shows the comparative results, both graphical and in tablular form, of the various sinusoidal signals used previously and described completely in Figure 4.30. The comparative results produced from the second order AR signal are presented in the second part.

The wavelet decomposition used to generate all of the subsequent results involves a 4-level discrete Meyer decomposition, where the sum of the detail functions, d_3 representing the [4 - 8] Hz. frequency band and d_4 representing [8 -16] Hz. frequency band, is substituted for the original signal to perform the segmentation. Apart from this substituion, the parameters for the ACF, GLR and NLEO are left exactly the same as in Section 4.3.

This time, only P_c and P_f are displayed graphically, while all of the probabilities are given in the tables.. The values shown in Table 4.2 and Table 4.3 are those that are obtained by taking the average value of a specific probability over the entire WL sweep range. The values produced in this way provide a means of assessing the overall improvement, provided by all the methods and their performance measures in a consistent manner.

4.4.2 Results of Varying Sinusoids

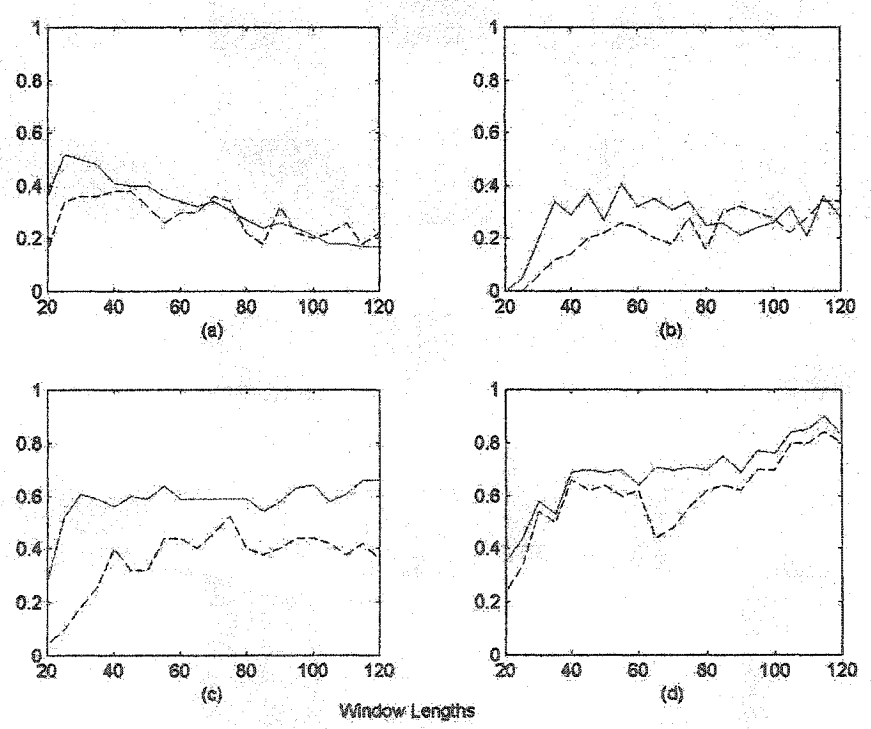

Figure 4.39: P_c for ACF segmentation of various sinusoidal signals without WT (dashed line) and with WT (solid line) over WL range. The sinusoidal signals are (a) Only amplitude changing; (b) Only frequency changing; (c) Amplitude and frequency changing together; (d) Amplitude and frequency changing opposite to one another.

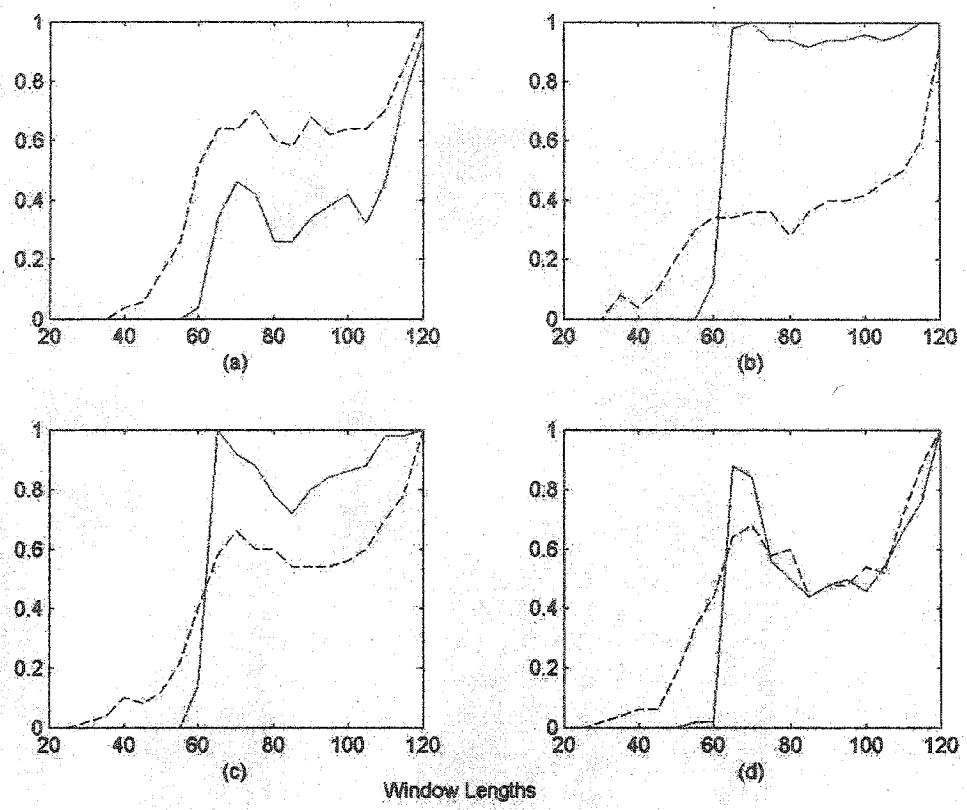

Figure 4.40: P_c for GLR segmentation of various sinusoidal signals without WT (dashed line) and with WT (solid line) over WL range. The sinusoidal signals are (a) Only amplitude changing; (b) Only frequency changing; (c) Amplitude and frequency changing together; (d) Amplitude and frequency changing opposite to one another.

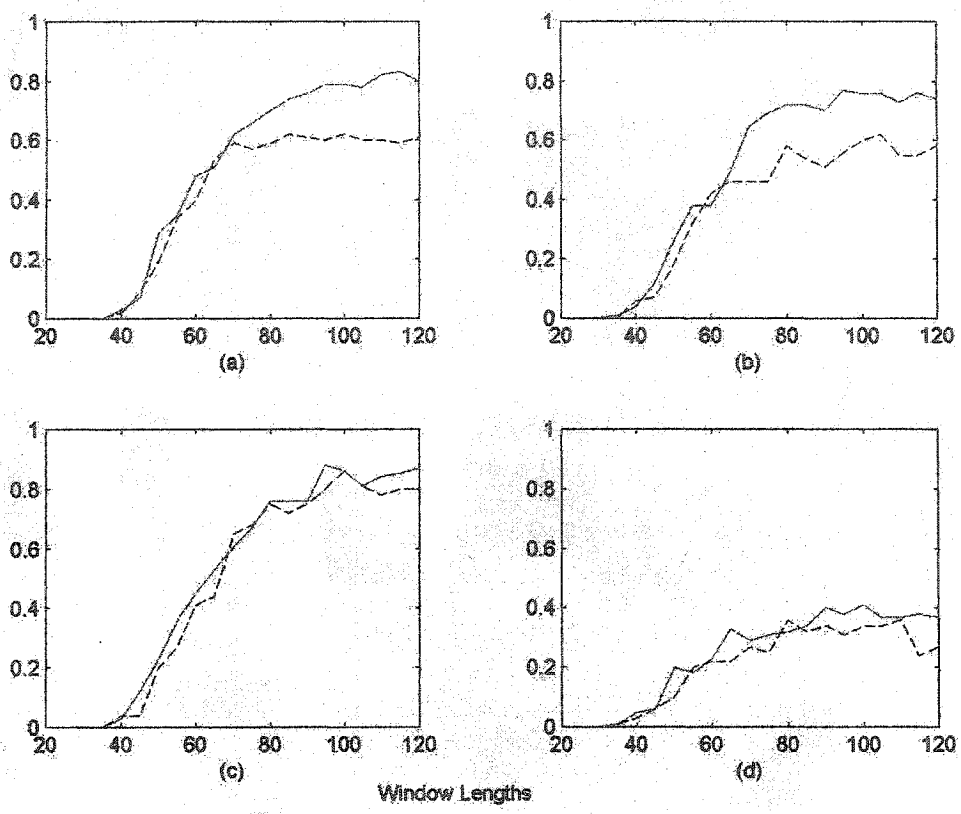

Figure 4.41: P_c for NLEO segmentation of various sinusoidal signals without WT (dashed line) and with WT (solid line) over WL range. The sinusoidal signals are (a) Only amplitude changing; (b) Only frequency changing; (c) Amplitude and frequency changing together; (d) Amplitude and frequency changing opposite to one another.

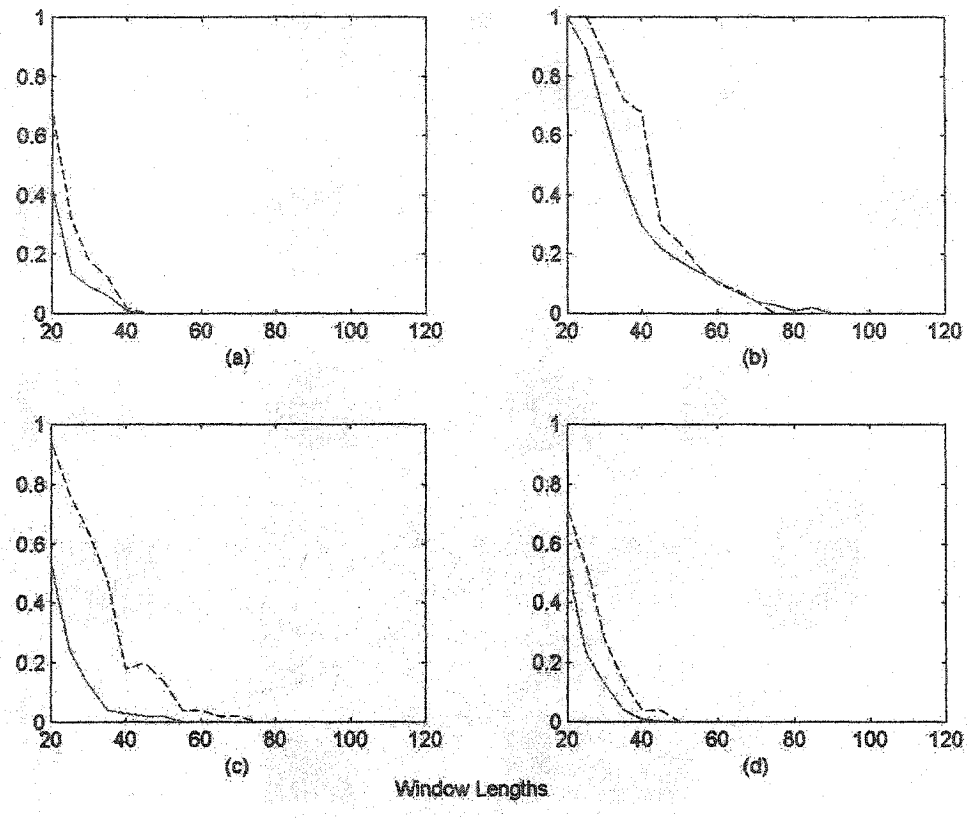

Figure 4.42: P_f for ACF segmentation of various sinusoidal signals without WT (dashed line) and with WT (solid line) over WL range. The sinusoidal signals are (a) Only amplitude changing; (b) Only frequency changing; (c) Amplitude and frequency changing together; (d) Amplitude and frequency changing opposite to one another.

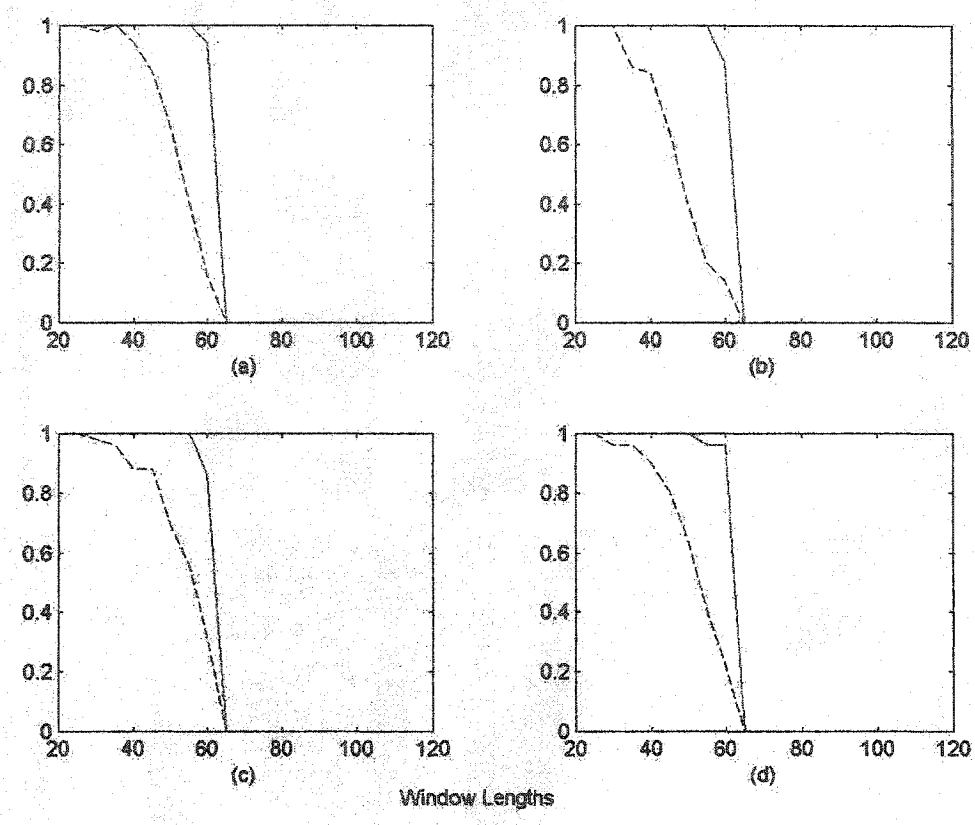

Figure 4.43: P_f for GLR segmentation of various sinusoidal signals without WT (dashed line) and with WT (solid line) over WL range. The sinusoidal signals are (a) Only amplitude changing; (b) Only frequency changing; (c) Amplitude and frequency changing together; (d) Amplitude and frequency changing opposite to one another.

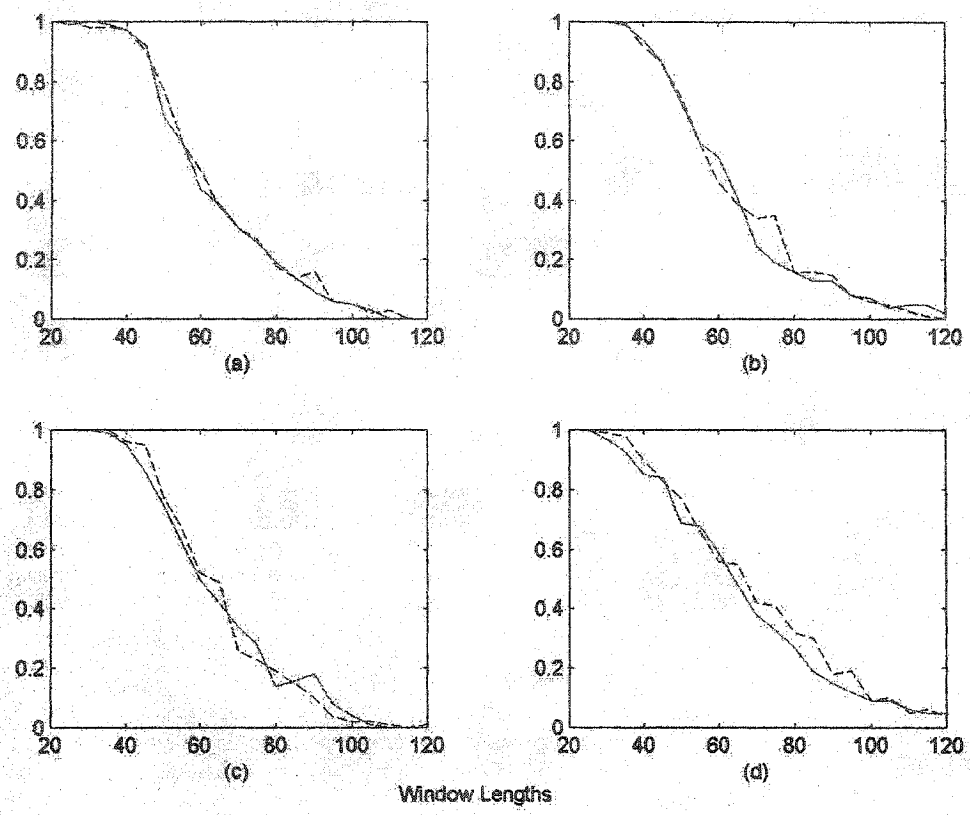

Figure 4.44: P_f for NLEO segmentation of various sinusoidal signals without WT (dashed line) and with WT (solid line) over WL range. The sinusoidal signals are (a) Only amplitude changing; (b) Only frequency changing; (c) Amplitude and frequency changing together; (d) Amplitude and frequency changing opposite to one another.

Table 4.2: Comparison of P_c, P_f and P_m for the three segmentation schemes applied to varying sinusoidal signals without the WT and with the WT. Note: Amp refers to only amplitude changing signal; Frq refers to only frequency changing signal; Tog refers to amplitude and frequency changing together in the same direction; Opp refers to amplitude and frequency changing in opposite directions.

		P_c			P_f			P_m		
		ACF	GLR	NLEO	ACF	GLR	NLEO	ACF	GLR	NLEO
Amp	NoWT	0.2800	0.4438	0.3895	0.0629	0.3324	0.4424	0.4543	0	0
	WT	0.3171	0.2562	0.4771	0.0343	0.4257	0.4333	0.4648	0.0067	0
	% Chg	13.3	-42.3	22.5	-45.6	28.1	-2.0	2.3	0	0
Frq	NoWT	0.2114	0.3076	0.3581	0.2476	0.2895	0.4457	0.0419	0.0248	0
	WT	0.2681	0.5543	0.4610	0.1967	0.4229	0.4400	0.0090	0	0
	% Chg	26.8	80.2	28.7	-20.6	46.1	-1.3	-78.4	0	0
Tog	NoWT	0.3581	0.4133	0.4667	0.1648	0.3467	0.4476	0.2762	0	0
	WT	0.5829	0.5133	0.4948	0.0481	0.4219	0.4438	0.1429	0	0
	% Chg	62.8	24.2	6.0	-70.8	21.7	-0.85	-48.3	0	0
Opp	NoWT	0.6076	0.4143	0.2019	0.0829	0.3276	0.4952	0.0171	0	0
	WT	0.6919	0.3648	0.2381	0.0448	0.4248	0.4671	0.0600	0	0
	% Chg	13.9	-11.9	17.9	-46.0	29.6	-5.7	250.0	0	0
Note:		Comparing the results of WT to non-WT segmentation, we mention that: • a *positive* % change, in P_c, indicates improvement. • a *negative* % change, in P_f and P_m, indicates an improvement.								

General Observations

The results in Table 4.2 show that the segmentation involving the WT of sinusoidal signals provides a definite overall improvement for the ACF and the NLEO, compared to the segmentation of the same signals without the WT. The GLR presents mixed results where on

the one hand there are some improvements in P_c but on the other hand, there is a general decrease in the value of P_f when the WT is added.

ACF

The ACF shows improvement in correct detection in all of the four cases, when the WT is included. In addition, it also shows an improvement in the reduction of false detections for all the four signals. This improvement is shown by the negative percent change indicating lower P_f values obtained with the WT. The number of missed detections is also lowered, with the exception of the sinusoid where the amplitude and frequency change in opposite directions. Although the percent change, in this case, is 250 %, this value is misleading because it represents a change in small values.

GLR

With the inclusion of the WT, the GLR performs better in terms of P_c for signals, where either the amplitude and frequency change together or where only the frequency changes. However, its performance deteriorates for signals, where only the amplitude changes or where the amplitude and frequency change in opposite directions. The biggest improvement occurs for the case of a signal where only the frequency changes. This signal's P_c value improves by 80%. The presence of the WT deteriorates the value of P_c significantly for signals, where only the amplitude changes. Its value drops by 42%.

The number of false detections, on an average, increased with the WT for all the signals, while the missed detections, which was essentially zero, stayed the same with or without

the WT present. By looking at Figure 4.43, we see that the P_f values with the WT are poorer than those without the WT only at values of the WL smaller than 65 samples. Therefore, with an adequately chosen WL, the values for P_f can be lowered to zero, with the WT present. Furthermore, since the order number is maintained at two throughout all of these experiments to provide consistency, this value may very well be inadequate (i.e., too small) in capturing some of the types of changes represented by the sinusoids involved. That is, a higher order number may be more suitable for some signals, for example, like those which only the amplitude changes, compared to others for which only the frequency changes. The exact value for this order would have to be obtained by the traditional methods used for this purpose, mentioned in Section 3.5.7.1.

NLEO

With the WT, the NLEO segmentation shows an all round improvement. For all the signals, it shows an increased correct detection, a reduction of false detection and no missed detections. Its degree of improvement is at par with the ACF, except for the signal where amplitude and frequency change together, in which case the ACF (62.9% of P_c improvement) considerably outstrips it (6% of P_c improvement). Although it shows a reduction in P_f, this improvement is quite modest with the highest savings of 6% in the case of amplitude and frequency changing in opposite directions and the lowest savings of 1% coming from the case where amplitude and frequency change in the same direction. Since the NLEO does not miss any detections with or without the WT present, there is no real improvement by including the WT, but by the same token there is no deterioration either by its presence. So, in terms of P_m the WT does not affect the NLEO's performance.

4.4.3 Second Order AR

The results produced by the segmentation procedures applied directly to the AR signal and to the wavelet-decomposed AR signal are shown in Figure 4.45 and presented in Table 4.3.

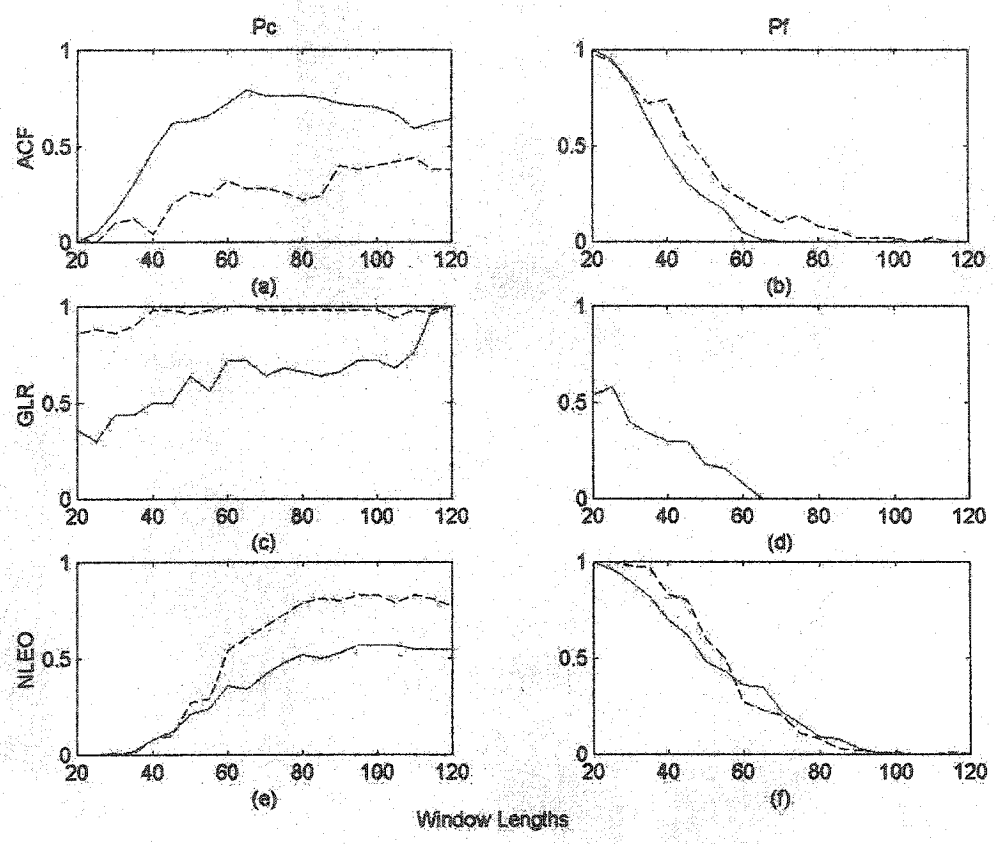

Figure 4.45: ACF, GLR and NLEO segmentation of second order AR signal with WT (solid line) and without WT (dashed line). ACF: (a) P_c; (b) P_f; GLR: (c) P_c; (d) P_f; NLEO: (e) P_c; (f) P_f;

Table 4.3: Comparison of P_c, P_f and P_m for the three segmentation schemes applied to a 2nd Order AR signal without the WT and with the WT

	P_c			P_f			P_m		
	ACF	GLR	NLEO	ACF	GLR	NLEO	ACF	GLR	NLEO
No WT	0.2562	0.9590	0.5033	0.2990	0	0.3643	0.0438	0	0
WT	0.5762	0.6343	0.3419	0.2210	0.1371	0.3433	0	0	0
% Chn	124.9	-33.9	-32.1	-26.1	0	-5.7	0	0	0

ACF

As in the previous section, involving the varying sinusoids, we see that with the second order AR signal, the ACF outperforms all of the other segmentation algorithms in terms of improved P_c, reduced P_f and reduced P_m, with the WT included.

GLR

Not surprisingly, the GLR in conjunction with the WT produces worse P_c results. This result seems inevitable considering that the GLR is an AR based algorithm with order number matching that of the signal and as such is optimally suited for correct detection on just such a signal. Consequently, any modification of the signal, as that produced with the application of the WT, would necessarily detract from the GLR's performance. Moreover, its P_f values also diminish with the WT, demonstrating that at least with respect to the signals used the GLR does not improve with the WT being present.

NLEO

The NLEO shows a deterioration in the correct boundary detection for the AR signal with the WT present. However, it does show a mild improvement in terms of reduced false detections.

4.5 Conclusion

In this chapter, we have studied both the wavelet transform and three different segmentation schemes, the ACF, the GLR and the NLEO. Together, these two functional operations form the core blocks of the proposed detection scheme, to be considered in Chapter 5.

We first established the validity of the WT as a pertinent tool in decomposing a signal in frequency while simultaneously preserving its time domain features. Using both concatenated and superimposed sine waves, with and without the presence of AWGN, we have shown that the WT does indeed partition the frequency bands correctly, while preserving the frequency content as well as the time domain content of the signal within each partitioned frequency band. This result, therefore, establishes the WT as a reliable means of isolating relevant frequency bands from the rest of the signal, without a loss in the time domain content (i.e., sine segment positioning remains unchanged after the WT is applied) thereby allowing the selected bands to be used for further processing.

Next, we tested the ability of the segmentation algorithms to correctly segment concatenated sinusoidal signals exhibiting various types of changes in either amplitude or frequency or some combination of the two. No noise was added to these test signals. Apart from some some minor adjustments to some working parameters, each algorithm is seen to correctly detect all non-stationary boundaries present, as well as correctly position them.

To examine the performance of each algorithm in a more realistic setting, significant AWGN was added to four different types of sinusoidal signals, each representing a different type of non-stationary boundary. They involved signals where only the amplitude was changing, signal, or only the frequency was changing, or both the amplitude and frequency

were changing together (i.e. both increasing or decreasing simultaneously) or the amplitude and frequency changing in opposite directions. Since all of the segmentation schemes critically rely on some form of windowing, performance was determined by sweeping through various WLs and evaluating the probabilities of correct and false detections. None of the schemes achieved 100% correct detection for any of the signals; however, each did show high correct detection for at least one of the signals, although no scheme did so for all of the signals. Apart from the NLEO, the ACF and GLR could, upon choosing an appropriately sized window length, reduce the probability of false detections to near zero values.

As far as the second order AR signal, which was the fifth test signal used to reveal the performance ability, the GLR was clearly superior all round to the other schemes. By sweeping through various possible thresholds for both the ACF and the GLR, it was shown that an optimal threshold exists for the ACF and that a minimum threshold needed to be satisfied in order to maximize correct detections, while keeping false detections to a minimum.

The underlying assumption behind the use of the wavelet-transformed signal is that it provides an improved, better suited version of the signal, with which to apply the segmentation schemes. This assumption is partially validated in Section 4.4. In that section, it was seen that the ACF reacted, in terms of performance, most positively to the inclusion of the WT. Improvements for the ACF appeared in higher probabilities of correct detections and lower probabilities of false detections. Similarly, the NLEO also showed an overall improvement with the signals preprocessed with the WT compared to those that were not. The only notable exception for the NLEO was in its reduced correct detection with regard to the second order AR signal. The biggest surprise came from the GLR, which showed improvement in

only two of the five test signals, while showing reduced performance for all of the signals in terms of false detections, when the WT was included compared to when it was not.

Now, an important point must be made. Of the three segmentation schemes the ACF generally provided the best results in terms of P_c and P_f. The NLEO, on the other hand, provided generally good P_c results, but of all the schemes had the worst performance in terms of the P_f. As mentioned in Section 3.4.3.3, since the NLEO applies an adaptive threshold, it is plagued by inherent fluctuations which generate false boundaries and in turn, large values of P_f. However, to correct this problem, contrary to the development proposed in [50], an outside fixed threshold can be applied. Although deciding on the exact value for this threshold adds more complexity to the NLEO scheme, such an adjustment is certainly warranted when comparing with the improved results produced by the ACF which uses a fixed threshold.

At this point, it must be added that the NLEO was the fastest of the three schemes. In fact, the NLEO was roughly two times faster than the ACF which in turn was approximately two times faster than the GLR in analyzing the signal. In view of the sizeable speed advantage of the NLEO, it is clearly the most attractive candidate of the three schemes to use in a real time EEG processing environment.

Before continuing to the next chapter, it must be noted that the test signals used througout this chapter, represent only a narrow slice of the potential variability, in terms of changing amplitude and frequency, that the procedure is likely to encounter in an actual EEG signal.

Chapter 5

EEG Application

5.1 General

The schematic, of the overall procedure, proposed in this thesis was shown in the previous chapter. Now, in order to adjust to the practical EEG application that model is expanded and amended. A clearer breakdown of the process is shown in Figure 5.1.

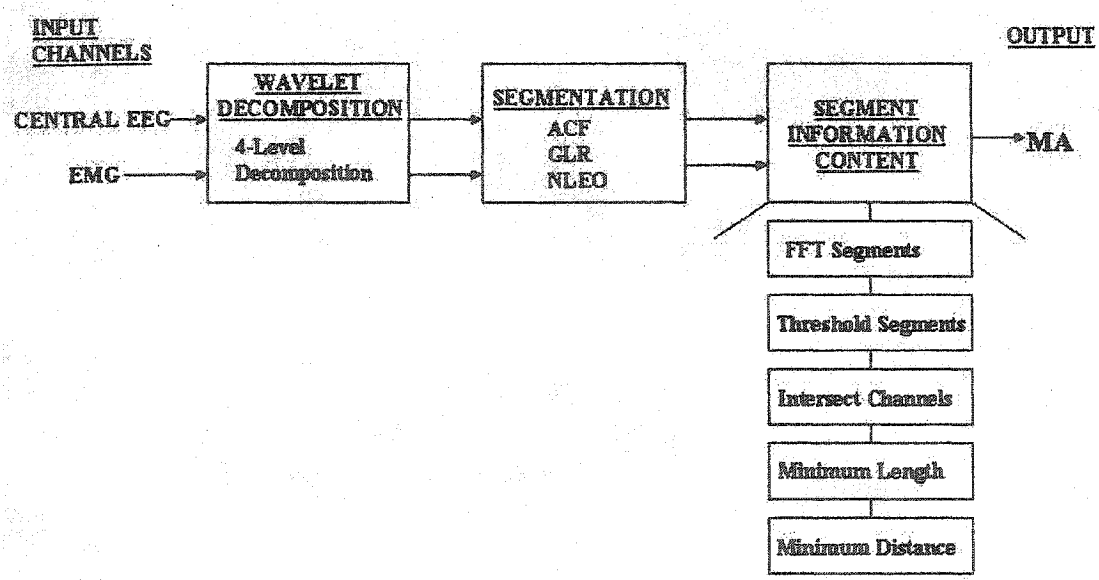

Figure 5.1: General Detection Procedure

Here, by comparing with Figure 4.1 it is seen that another block, decifering the Information Content of the individual segments produced after segmentation, is inserted. This block is

used to determine the amplitude and frequency content of the assumed stationary segment that it represents. After this step is accomplished, a reasonable thresholding criteria is applied in order to establish whether or not the content within any of the segments is sufficient to score that segment, as being a microarousal. In addition, constraints imposed by the R&K criteria, namely, minimum segment lengths, minimum distance lengths between scored segments and minimum time delays between newly entered sleep stages (see Section 1.4), are applied, as is shown in Figure 5.1.

In the block diagram of Figure 5.1, we see that the application of the detection procedure is not only applied to one channel exclusively. In order to score with greater reliability, more than one channel is used. The reasoning behind this added complexity is simple: since the presence of an MA simultaneously appears, in various degrees, across several channels of the polysomnogram, better decisions about its presence can be made if contributing information, available from these other channels is taken into account. For the case of microarousals, occurring during the REM stage of sleep, this requirement is mandatory, since the accompanying increases in the EMG signal amplitude, along with a concurrent increase in the central electrode EEG frequency, define the presence of a microarousal for that stage. The overall breakdown of the steps involved in the MA detection algorithm are as follows:

1. Wavelet decomposition
2. Segmentation
3. Assessment of dominant frequency and power present in each segment.
4. Frequency and power thresholding of segments
5. Intersecting surviving segments with similar segments derived from other channels

6. Imposing minimum segment length (3sec)

7. Imposing minimum inter-segment length (10sec)

The application of this procedure includes two variations. In one case, the procedure, excluding the intersection step, is applied to only one channel; in the second case, the procedure, including the intersection step, is applied to two channels. The only two channels involved in the experiment, are the central EEG electrode (CE) and the EMG electrode (ME) channels. However, it must be noted that any of the other channels available from the montage, such as the occipital, temporal electrodes, for instance, could just as easily have been included.

We describe in section 5.2 the application of the above procedure and the specifics regarding each segmentation algorithm. The results produced by the application of these steps, follow in Section 5.3, where they are presented and discussed in detail. Finally, in Section 5.4, a summary of the overall results obtained are given.

5.2 Description of Proposed MA Detection Scheme

In this section, we present all of the details involved in the application of the proposed detection scheme. Although the first two steps, wavelet decomposition and segmentation, have been extensively discussed in Chapter 4, the particular details governing their specific adaptation to the EEG signal will be addressed here.

5.2.1 Wavelet Decomposition

The first step in the proposed procedure is applying the WT to the EEG channel. As in Chapter 4, we chose the discrete meyer wavelet (DMW), for the reasons discussed there. Furthermore, a level-4 signal decomposition is selected, which produced the detail and approximation function with corresponding frequency bands shown in Table 5.1.

Table 5.1: Level - 4 wavelet decomposition detail and approximation functions with their related frequency bands

Approximation and Detail Functions	d1	d2	d3	d4	a4
Related Frequency Bands (Hz)	[32-64]	[16-32]	[8-16]	[4-8]	[0-4]

Only detail functions d3 and d4 are selected and preserved for further analysis. These functions represent the principal frequency bands involved in the detection of MAs. Combining the two functions provides us with a template signal, which offers a more fruitful signal representation to proceed with segmentation. However, it must be pointed out that no wavelet decomposition is applied to the ME signal, since only its amplitude or power characteristics contribute in MA detection.

5.2.2 Segmentation

The wavelet decomposition of the CE signal, as described in the previous section, serves as the input to all three of the segmentation schemes, without any additional alteration, with respect to either scheme. In the following, we describe the values selected for the key parameters governing the performance of each segmentation algorithm.

5.2.2.1 ACF

Based on the results observed in Chapter 4 the values for the ACF algorithm's operating parameters are chosen as follows:

Thresholds: $T_a = T_f = 1$ and $T_g = 1$

Window Length: WL = 3 · (128 samples) = 3 seconds

The motivation behind the selection of these values stems directly from the results obtained from the AWGN-corrupted sine signals in Section 4.3. The choice of the WL is made because we seek MAs, which are at the least 3 seconds long. The advantage of a long WL is that detection is more reliable, since more signal content lies within the window to allow a better gauging of the frequency and amplitude differences and less false detections are made, which is the case for smaller windows. However, the drawback with this choice, as mentioned in Chapter 4, is the reduced precision in exact boundary position, which results with the use of a longer WL. Nevertheless, the tradeoff, which is reasonable, warrants such a selection.

5.2.2.2 GLR

Similarly, following the results of Section 4.3 and Section 4.4, we chose the parameters as follows.

Order: p = 3

Threshold: N = 8 bits

Window Length: WL = 3 · (128 samples) = 3 seconds

We choose a higher order than the one we used in the simulations of Chapter 4 to allow the algorithm to contend with greater possible variability. Considering the threshold values produced in Section 4.4, we take a middle ground approach to the final value of the threshold. The same reasoning, as the one used for selecting the window length in the ACF algorithm, also applies here.

5.2.2.3 NLEO

The only parameter that requires adjusting for the NLEO algorithm is the window length and its value is chosen as:

Window Length: $WL = 6 \cdot (128 \text{ samples}) = 6 \text{ seconds}$

Since this algorithm only uses one window, where both the halves are compared to each other, to judge if a boundary is present, each half is designed to meet the minimum length of the signal to be detected, namely 3 seconds. Although a smaller window could have been selected, the larger window size is selected so that false detections may be minimized. Because of the larger window size, smaller non-stationary segments are neutralised or averaged out, leaving only non-stationary segments larger than 3 seconds.

5.2.3 Dominant Frequency and Power in Segments

In this section, we seek to identify the dominant frequency and power, present in the segments produced by the segmentation algorithms. We must first mention that all frequency thresholding is applied to the central electrode signal (CE) of the EEG, while all power

thresholding is performed on the EMG electrode signal (ME) because the frequency of the one and power of the other together assist in the detection of MAs as per the discussion of Chapter 1. We now begin with the description of the dominant frequency determination.

5.2.3.1 Dominant Frequency of each Segment of the Central Electrode Signal

In trying to determine the most representative or dominant frequency, we make two assumptions.

Assumption 1: The first assumption, which is the underlying assumption governing each of the segmentation algorithms is that once a signal has been segmented, the information content present in each segment is *stationary*. This assumption is the underpinning of the entire procedure and although expressed explicitly here as an assumption, it is, in fact, a tacitly held measure of each segmentation algorithms' ability to successfully partition the non-stationary signal into stationary segments. Holding this condition to be true, however, we may proceed with traditional stationary techniques, in assessing the frequency content and amplitude content available within each segment.

In Chapter 2, we mentioned that the FFT was not suitable to treat non-stationary segments because it is a stationary algorithm, which is effective only when applied to stationary signals. With the segmented stationary segments provided by the segmentation algorithms, we are now justified in using the FFT to find the frequency content present within each segment. Although more sophisticated means, like AR modelling for instance, of determining the spectral properties present in a given signal are available, these usually add to the com-

plexity of the whole algorithm. Moreover, the FFT, in a stationary environment, does provide a robust and reliable breakdown of frequency content quickly and simply, without any additional parameters, like model order selection, to contend with.

Assumption 2: A further assumption, imposed on each stationary segment, is that the frequency content, which provoked the segmentation, from one segment to the next, is represented by the dominant frequency present in each segment. In other words, from segment to segment, only amplitude or frequency will cause a sufficient change to occur, so as to cause a boundary to be detected. Our assumption is that a change in frequency is represented by the largest peak produced in the FFT of that segment. Although noise is present throughout the signal, its power is weaker than the decomposed signals present in the lower [4-16]Hz frequency bands of the WT decomposition. Consequently, any change in frequency between segments is caused by the change in the dominant frequency between those segments. Therefore, the highest peak produced by the FFT in each segment is assumed to be the most prevalent frequency present in that segment. As a result it is selected to represent that segment when thresholding of frequency content is performed, in order to decide whether the frequency change is sufficient to score a segment as a MA. As an example, a 60 second sample of a WT central EEG signal, along with dominant frequencies associated with each segment are shown in Figure 5.2a and Figure 5.2c, where the NLEO segmentation procedure was used.

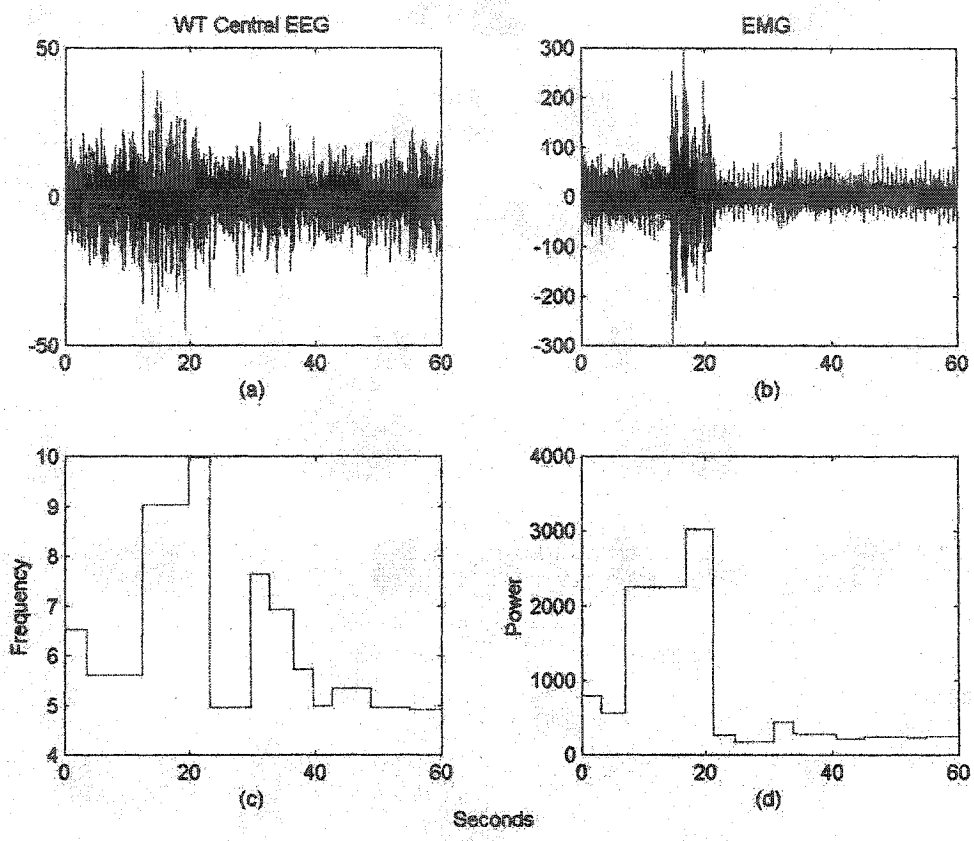

Figure 5.2: (a) 60 second sample of the WT Central EEG Signal; (b) 60 second sample of the EMG corresponding to the same time interval as in the preceding; (c) Dominant frequency in each segment of the signal in (a); (d) The average power of each segment of the signal in (b).

5.2.3.2 EMG Segment Power

In the previous section, we discussed the acquistion of the dominant frequency of each partitioned segment of the CE signal. Now, we turn our attention to the power of the ME signal segments. Segmenting the ME signal produces stationary segments, as discussed in the last section. The power of each segment is chosen as the average variance of the entire segment (i.e., each segment is assumed to be zero mean). Since each segment is assumed to be sta-

tionary, then all of its attributes, including the amplitude, are also stationary and consequently the average variance produces an acceptable measure of the power for each segment. A 20 second sample of EMG along with the power associated with each segment are shown in Figure 5.2, with NLEO being again used for segmentation.

5.2.4 Thresholding Dominant Frequency and Power

The thresholding of the dominant frequency segments does not pose the usual problem that the selection of a threshold usually does. Since we are looking for the sudden appearance of α–waves or waves greater than 8 Hz, as defined in Chapter 1, this value provides a solid choice for the selection of a threshold. However, since 8 Hz. is a boundary separating 'distinct' wave bands the threshold, namely,

Frequency Threshold: $FT = 9$ Hz

is chosen to ensure that indeed the frequency over this value clearly belongs to the α–wave category. Although this choice will necessarily lead to a certain degree of missed detection, the benefits achieved by greater certainty is considered to outweigh such a disadvantage.

The power, on the other hand, does not provide such a clear choice for a threshold value. In order to decide upon a generous but useful value for it, we examined the power produced over several representative stretches. A global value was quickly decided upon:

Power Threshold: $PT = 2000$

Although threshold adaptability could have been introduced with regards to each individual sleep stage since the start and stop times for every stage as they appear throughout the entire record are available, yet, to avoid additional complexity, it is not considered.

5.2.5 Intersecting Different Channels

As mentioned in the introduction of this chapter, the motivation for intersecting two different EEG channels arises from the added certainty that such an action creates. Although optional for sleep stages 1 to 4, it is mandatory to combine the CE and ME when treating the REM sleep stage.

Following the thresholding of the CE and the ME channels, we are now in a position to compare their resulting segments. The intersection of channels is done by determining whether a segment from one channel occurs at the same time as any other segment from the other channel. By segment we mean one that has survived the thresholding process.

Let us define this process more clearly.

Definition: Assume that a segment, say s_c, taken from the CE channel is bounded in time by $[t_{c1},t_{c2}]$ and another segment, say s_m, from the ME channel, itself bounded in time by $[t_{m1},t_{m2}]$, both occur within the same 'vicinity' of time.

Then, the intersection of segments s_c and s_m exists if they satisfy the 3 possible cases shown, in Figure 5.3.

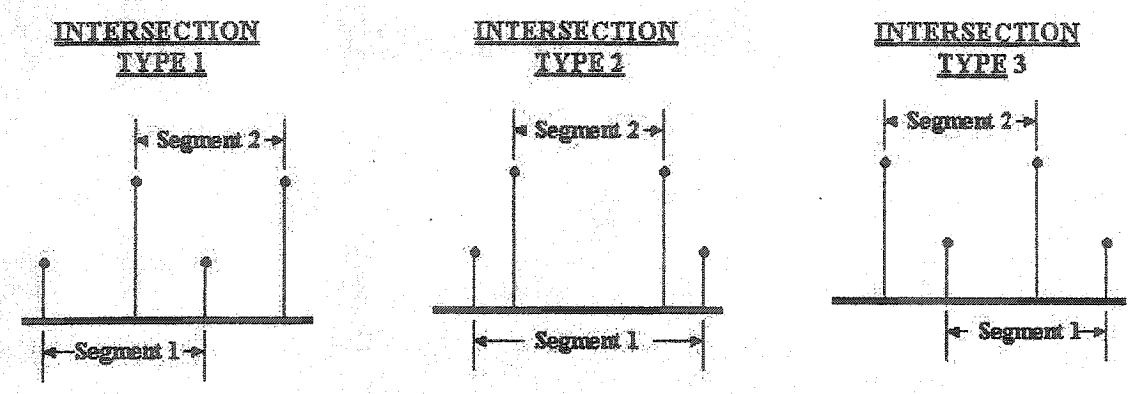

Figure 5.3: Three possible cases of Intersection of thresholded segments originating from two different channels.

In addition, the final intersecting segment, say s_i, is chosen as the largest possible combined segment resulting from s_c and s_m . In other words, s_i is bounded in time by $[\min(t_{c1},t_{m1}), \max(t_{c2},t_{m2})]$. Although it is quite clear that another choice for the final time bounds designating s_i can be chosen, the present choice is based on maximizing the total potential MA that may be present. That is, since both s_c and s_m may individually represent only a partial portion of a detected MA due to inaccurate segmentation, it is assumed that by selecting the largest possible range of each segment, more of the actual MA will be captured.

The obvious disadvantage of such a choice lies in the larger detected MA sizes that result. However, this shortcoming is manageable, especially in view of higher degree of correct detection that it provides.

As a final note, since the intersection of two channels provides a greater certainty of detecting an MA, the rather strict frequency threshold adopted for only one channel is lowered to allow more segments that survive the thresholding process to be compared.

This new threshold is

Intersection Frequency Threshold: IFT = 7 Hz

To repeat, two forms of thresholding are performed. Both apply to the CE channel. However, the result of the stricter FT, produces segments that are considered by themselves as MAs due to the strict nature of the applied threshold, whereas the result for the less strict threshold, IFT, produces more segments but with the further aim of intersecting these with the segments produced from the ME thresholded signal.

5.2.6 Minimum Segment Length

Following the R&K criteria for scoring MAs, a minimum length of any frequency length disturbance must be imposed. R&K establishes this constraint to be 3 seconds. Having thresholded the segments, we now apply this minimum length constraint to filter out the viable segments.

5.2.7 Minimum Distance between Consecutive Segments

Again referring to the R&K criteria, for a MA to be scored, it must occur no less than 10 seconds after another MA has been marked. Therefore, after scanning all the segments that

have survived the previous step, a further elimination is carried out. All segments that remain after this final stage of the procedure are then considered to be MAs.

A point must be made concerning the order of the last two steps. It is important to impose the minimum length constraint *before* the minimum distance. Although the order of these operations seem interchangeable, they are not. If minimum distance is applied first, then viable 3-second segments may be lost, leaving instead smaller segments which will inevitably be eliminated in the minimum length step.

5.2.8 Performance Measures

Before proceeding to the results, we define the performance measures used to gauge the effectiveness of the procedure. In calculating the performance of the algorithms, the following probability measures are used.

5.2.8.1 Probability of Correct Detection

We define the probability of correct detection as:

$$P_c = \frac{\text{Number of correct detections}}{\text{Total number of actual MAs}} \tag{5.1}$$

The 'number of correct detections' correspond to the number of detections outputted from the algorithm that agree with the actual MAs present in the record. By agreement, we mean that in the sense of intersection as described above, a potential MA segment is scored as a real MA segment and thus counted if it intersects with any portion of the actually scored MAs.

The 'total number of actual MAs' refers to all of the MAs scored manually by the sleep technologist and therefore assumed to be the benchmark of comparison.

The parameter P_c corresponds, therefore, to the successful detection of the marked MAs. However, for reasons discussed later in the comparison section, this evaluation parameter leaves some room for interpretation.

5.2.8.2 Probability of False Detection

We define the probability of false detection as:

$$P_f = \frac{\text{Number of false detections}}{\text{Total number of detections}} \tag{5.2}$$

The 'number of false detections' are all the remaining output detections which do not intersect with the marked MAs. The 'total number of detections' correspond to all of the output detections produced by the algorithm. The parameter P_f reveals the percentage of all the detections that do not intersect with any of the marked MAs and consequently are false. This value serves to demonstrate the weakness of the algorithm.

5.2.8.3 Probability of a Missed Detection

Another parameter used to measure the algorithm's weakness is P_m, the probability of missing an MA. It measures the number of MAs present in the record which were not marked by the algorithm because it was not able to detect it. We define it as:

$$P_m = 1 - P_c \tag{5.3}$$

where P_c is the probability of correct detection.

With these measures we are now in position to present our results.

5.3 Results

In this section, we present the results of our proposed algorithm for the three cases involving the ACF, GLR and NLEO segmentation algorithms. The record that we are working with contained MAs only in Stage 1, Stage 2 and the REM stage of sleep. Consequently, these are the only sleep stages for which we can give results. The other stages, although they contain no MAs are implicitly treated when considering the results produced by applying the detection procedure to the overall signal, which includes all the sleep stages. The number of actual MAs that exist in the sleep record, which were marked by the sleep technologist, and that are assumed to be the gold standard to which our detection procedure aspires to reach or duplicate are presented in Table 5.2.

Table 5.2: Distribution of the gold standard MA throughout the sleep stages of the sleep record

Sleep Stages	Entire Record	Stage 1	Stage 2	REM
No. of MAs	136	65	60	11
% of Total No. of MAs	100 %	48 %	44 %	8 %

This table shows how many actual MAs are present in each sleep stage. Explicitly, the times of occurance in the EEG record, for each of these gold standard MAs, are presented in the Appendix, along with the detected MAs generated by the detection procedure, for each of the three segmentation schemes.

5.3.1 Overall Sleep Record

The results generated by the proposed procedure when applied to either the Central EEG alone or applied to the combination of the Central EEG and EMG channels, for the entire EEG record, are presented next.

Results of Solo Channel

Table 5.3: Probability results of the MA detection procedure applied to the central electrode channel

Segmentation Algorithm	Without Wavelet Transform			With Wavelet Transform			% Change		
	P_c	P_f	P_m	P_c	P_f	P_m	P_c	P_f	P_m
ACF	0.2132	0.8129	0.7868	0.3824	0.8102	0.6176	79.4	-0.3	-21.6
GLR	0.1765	0.7526	0.8235	0.3971	0.7866	0.6029	125.0	4.5	-26.8
NLEO	0.2574	0.7348	0.7426	0.4412	0.7952	0.5588	71.4	8.2	-24.8

In general, from Table 5.3, we notice that for every segmentation scheme the probability of correct detection P_c improves significantly when the WT is applied, while the probability of false detection P_f deteriorates slightly or stays the same. Because the probability of a missed detection is directly dependent on P_c, the value for P_m naturally improves as P_c improves, and deteriorates as P_c deteriorates; for this reason, P_m will be discussed no further. It is included in the tables only for the sake of completeness.

In particular, the NLEO produces the highest rate of correct detection, with or without the WT present. The presence of the WT produces the largest relative improvement in the GLR.

Table 5.4: Average start times (S.T.) and length differences between detected MAs and actual MAs. All values are in seconds.

Segmentation Algorithms	Without Wavelet Transform				With Wavelet Transform			
	S.T. Diff.	Absolute S.T. Diff.	Len. Diff	Absolute Len. Diff	S.T. Diff.	Absolute S.T. Diff.	Len. Diff	Absolute Len. Diff
ACF	+3.3922	3.7885	-6.1401	6.3406	+1.0832	2.7290	-3.2759	3.8573
GLR	+1.5006	3.5244	-2.4909	4.1653	+1.1092	3.3419	-2.3690	3.3131
NLEO	+0.9882	2.9065	-4.0975	4.2775	+1.9497	3.4932	-3.6930	4.2471

1. Actual MA S.T. is defined as starting at time $= 0$.
2. Detected MA S.T. occurring before is defined as negative value.
3. Detected MA S.T. occurring after is defined as positive value.
4. Negative Len. Diff indicates Det. MA is smaller than the corresponding Actual MA.
5. Positive Len. Diff indicates Det. MA is larger than the corresponding Actual MA.

Table 5.4 shows the start time (ST) difference and the absolute start time difference between the detected MAs and the actual MAs. The ST difference gives the average difference between the two MA sets, while the absolute ST difference gives the average of the absolute value of the ST difference, for each detected MA. The positive sign of the ST difference indicates that, on average, MAs are detected later than the actual MAs occur. The reason for the difference in magnitude between the ST difference and the absolute ST difference arises from the inclusion of negative and positive values of difference in the calculation, where cancellation necessarily occurs, thereby reducing the overall value, when it does. A value approaching zero for the ST difference shows either nearly identical MA ST values or a balanced distribution of ST detections occurring before and after the actual MA ST. The absolute ST difference gives the average ST difference, in magnitude, regardless of whether the detected MA's position occurs before or after the actual MA's ST position. Similarly, length difference (LD) gives the average difference between the detected MA's length with that of the actual MA's length. A negative value for LD means that the detected

MA's length is shorter than the actual MA's length. The absolute LD provides a measure of the overall magnitude difference in length between the two MA sets, regardless of whether the detected MA is shorter or longer than the actual MA.

The results in Table 5.4 show that without the WT, the ACF procedure detects MAs, on average, 3.79 seconds away from the ST of the actual MAs. Moreover, its ST difference value, +3.39 seconds, reveals that *most* of the detections are made *later* than the actual MA, as indicated by the positive sign. The ACF's absolute LD difference shows that, on average, the difference in length between the detected MAs and the actual MAs is 6.34 seconds long and that the majority of these are shorter than the actual MA, as the negative sign reveals.

With the inclusion of the WT, the ACF shows a definite improvement with the absolute ST difference diminishing from 3.79 seconds to 2.72 seconds; the absolute LD also improves with a reduction from 6.34 seconds to 3.85 seconds. Although the ACF shows improvement, the NLEO shows increases in both the absolute ST (from 2.91 seconds to 3.49 seconds) and the absolute LD (from 4.28 seconds to 4.25 seconds) with the involvement of the WT. However, this slight deterioration is reasonably offset by the near doubling of its P_c value.

Combined Channels

The results of combining the central EEG channel with the EMG channel are presented in Table 5.5 and Table 5.6.

Table 5.5: Probability results of the MA detection procedure applied to both the central electrode and the EMG electrode channels

Segmentation Algorithm	Without Wavelet Transform			With Wavelet Transform			% Change		
	P_c	P_f	P_m	P_c	P_f	P_m	P_c	P_f	P_m
ACF	0.2059	0.3778	0.7941	0.6691	0.3592	0.3309	225.0	-4.9	-58.3
GLR	0.0882	0.4286	0.9118	0.5588	0.3559	0.4412	533.6	-17.0	-51.6
NLEO	0.1324	0.4375	0.8676	0.6250	0.3885	0.3750	372.1	-11.2	-56.8

In Table 5.5, we see that there is improvement for all probability values and for all segmentation schemes by comparing the results of those which include the WT with those that do not. The increase in P_c values reveals the greatest degree of improvement. For example, the ACF value for P_c increased by 225% with the WT. On the other hand, the values of false detections, although improved for all schemes, are only modest in comparison.

Of the three schemes, the ACF produced the highest P_c value, followed closely by the NLEO and finally by the GLR. This order of segmentation algorithm performance is nearly a reversal of the sequence which emerged when the solo channel was used. The reason for this change may be due to the included segmentation of the EMG channel.

What is noteworthy about the improvements shown in these P_c values is that the MAs, which were detected using the procedure described above, but without the WT, could only correctly detect roughly between 1 out of 10 MAs in the worst case (GLR) and 1 out of 5 MAs in the best case (ACF). With the inclusion of the WT, everything else remaining the same, the proposed procedure could detect more than 1 out of 2 MAs in the worst case (GLR) and 2 out 3 MAs in the best case (ACF). Therefore, we can see, by comparing the

results for the solo channel and the combined channels, that the proposed procedure involving the WT performs significantly better than the same procedure using only the segmentation algorithms, a result which validates the proposed procedure in a practical setting.

When comparing the P_c values produced for the solo channel and the combined channels, we notice that the overall values without the WT were lower for the combined channels. One reason for the lower value of P_c in the combined channel may come from the likely possibility that thresholded ME segments did not always overlap with their thresholded CE segment counterparts. In other words, if a CE segment survived the frequency thresholding imposed and, at the same time, a segment of EMG survived the power thresholding but, due to imprecisions in correct positioning, these segments did not overlap, then the same MA, which they were separately recognizing, would be missed.

Consequently, the combined channels, without WT present, produces values of P_c lower than when only the solo channel is considered. The fact that the frequency threshold for the solo channel is higher than that used for the combined channels confirms this result, since the solo channel P_c value would most certainly have been even higher if a lower frequency threshold had been applied, but so too would the number of false detections.

We have already noted that with the introduction of the WT there is an improvement in P_c values compared to the case when it is absent. In addition, we have also noticed that it improves the performance of P_c values in both the solo channel case and the combined channel case. Now, in light of what we have just discussed regarding the procedure's performance without the WT, in the cases of the solo and the combined channels, we see that the WT provides an efficiently processed signal more suitable for segmentation. In turn,

this better-suited signal reduces the imprecision in segment positioning, which leads to a reduction in missed segment intersections, and consequently higher P_c values.

Table 5.6: Average start times (S.T.) and length differences between detected MAs and actual MAs. All values are in seconds.

Segmentation Algorithms	Without Wavelet Transform				With Wavelet Transform			
	S.T. Diff.	Absolute S.T. Diff.	Len. Diff	Absolute Len. Diff	S.T. Diff.	Absolute S.T. Diff.	Len. Diff	Absolute Len. Diff
ACF	+2.3800	2.6953	-0.8800	7.7478	-0.2621	2.0051	-0.9648	4.1322
GLR	-2.4225	4.0801	-0.1875	4.9909	-1.1306	3.0981	0.5829	3.9175
NLEO	+1.2144	3.3750	-3.1675	5.2813	-0.8932	3.4684	-0.5674	4.3072

1. Actual MA S.T. is defined as starting at time = 0.
2. Detected MA S.T. occurring before is defined as negative value.
3. Detected MA S.T. occurring after is defined as positive value.
4. Negative Len. Diff indicates Det. MA is smaller than the corresponding Actual MA.
5. Positive Len. Diff indicates Det. MA is larger than the corresponding Actual MA.

Similarly, when considering the start times and lengths of the detected MAs compared to those of the actual MAs, we observe improvements in both, for all the schemes, when the WT was included. Moreover, we notice that the absolute lengths produced by combining the channels are indeed slightly bigger than that in the case of the solo channel. This result was expected, as mentioned above in the section describing the combination of channels; however, what was not expected was that this increase would be so small, which is an encouraging outcome.

In the following sections, we only show the performance probabilities of each of the sleep stages present in the EEG record.

5.3.2 Sleep Stage 1

The results obtained using the proposed procedure to detect MAs in Stage 1 of the sleep are presented in Table 5.7 and Table 5.8.

Solo Channel

Table 5.7: Probability results of the MA detection procedure applied to the central electrode channel

Segmentation Algorithm	Without Wavelet Transform			With Wavelet Transform			% Change		
	P_c	P_f	P_m	P_c	P_f	P_m	P_c	P_f	P_m
ACF	0.2576	0.7385	0.7424	0.4091	0.6966	0.5909	58.8	-5.7	-20.4
GLR	0.2273	0.6512	0.7727	0.4394	0.6506	0.5606	93.3	-0.1	-27.4
NLEO	0.2879	0.6724	0.7121	0.5303	0.6196	0.4697	84.2	-7.9	-34.0

Combined Channels

Table 5.8: Probability results of the MA detection procedure applied to both the central electrode and the EMG electrode channels

Segmentation Algorithm	Without Wavelet Transform			With Wavelet Transform			% Change		
	P_c	P_f	P_m	P_c	P_f	P_m	P_c	P_f	P_m
ACF	0.1818	0.5200	0.8182	0.6970	0.4390	0.3030	283.4	-15.6	-63.0
GLR	0.0758	0.5000	0.9242	0.5455	0.4545	0.4545	619.7	-9.1	-50.8
NLEO	0.1364	0.4000	0.8636	0.5909	0.5125	0.4091	333.2	28.1	-52.6

Comparing the results produced for the solo and the combined channels, we see that the inclusion of the WT in the detection procedure improves the performance in both the cases. The only exception is in the significant increase in P_f involving the NLEO.

5.3.3 Sleep Stage 2

Results using the proposed procedure with regard to the detection of the MAs in Stage 2 of the sleep are presented in Table 5.9 and Table 5.10.

Solo Channel

Table 5.9: Probability results of the MA detection procedure applied to the central electrode channel

Segmentation Algorithm	Without Wavelet Transform			With Wavelet Transform			% Change		
	P_c	P_f	P_m	P_c	P_f	P_m	P_c	P_f	P_m
ACF	0.1500	0.8916	0.8500	0.3000	0.8953	0.7000	100.0	0.4	-17.6
GLR	0.1167	0.8478	0.8833	0.3000	0.8831	0.7000	157.1	4.2	-20.8
NLEO	0.2000	0.8209	0.8000	0.3167	0.8939	0.6833	58.6	8.9	-14.6

Combined Channels

Table 5.10: Probability results of the MA detection procedure applied to both the central electrode and the EMG electrode channels

Segmentation Algorithm	Without Wavelet Transform			With Wavelet Transform			% Change		
	P_c	P_f	P_m	P_c	P_f	P_m	P_c	P_f	P_m
ACF	0.2333	0.4400	0.7667	0.6500	0.4265	0.3500	178.6	-20.5	-54.3
GLR	0.1000	0.5385	0.9000	0.5833	0.4167	0.4167	483.3	-22.6	-53.7
NLEO	0.1333	0.5789	0.8667	0.6500	0.4348	0.3500	387.6	-24.9	-59.6

5.3.4 Sleep Stage REM

Results using the proposed procedure with regard to the detection of the MAs in REM Stage of the sleep are presented in Table 5.11 and Table 5.12.

Solo Channel

Table 5.11: Probability results of the MA detection procedure applied to the central electrode channel

Segmentation Algorithm	Without Wavelet Transform			With Wavelet Transform			% Change		
	P_c	P_f	P_m	P_c	P_f	P_m	P_c	P_f	P_m
ACF	0.1818	0.8182	0.8182	0.5455	0.7273	0.4545	200.1	-11.1	-44.5
GLR	0	1	1	0.6364	0.7200	0.3636	0	-28.0	-63.6
NLEO	0.2727	0.7857	0.7273	0.4545	0.8214	0.5455	66.7	4.5	-25.0

Combined Channels

Table 5.12: Probability results of the MA detection procedure applied to both the central electrode and the EMG electrode channels

Segmentation Algorithm	Without Wavelet Transform			With Wavelet Transform			% Change		
	P_c	P_f	P_m	P_c	P_f	P_m	P_c	P_f	P_m
ACF	0.1818	0	0.8182	0.5455	0.1429	0.4545	200.1	0	-44.5
GLR	0.0909	0	0.9091	0.4545	0.1667	0.5455	400.0	0	-36.4
NLEO	0.0909	0.5000	0.9091	0.5455	0.1429	0.4545	500.1	-71.4	-45.5

5.3.5 Some Reasons for Low Probabilities

Often frequency bursts appear to occur consecutively along sizeable stretches of EEG. Since the R&K criteria impose a 10 second minimum distance between these bursts, some bursts along this series of bursts are scored as MAs, while other bursts, lying in between these marked MAs and which in all other respects satisfy the defining characteristics of an MA, are ignored. To clarify the problem, which may diminish the apparent success of the detection procedure, let us give an example.

Let us assume that n MA potential bursts occur, with each consecutive burst occurring exactly 5 seconds apart from its neighbouring bursts. The sleep technologist, by recogniz-

ing the first burst, would then score bursts 1, 3, 5,... until the end, while ignoring the bursts 2, 4, 6,... for no reason other than the 10 second minimum distance constraint. However, if the detection procedure were to, for some reason, miss the first burst but recognize all the rest, then it would mark bursts 2, 4, 6,... while ignoring bursts 3, 5, 7,...The immediate consequence for this example would be that the detection algorithm, would score 100 % missed detection and 100 % false detections! Although this example is extreme, often such situations appear, which inevitably leads to slightly poorer results.

Although it is assumed that the actual MAs detected by the sleep technologist are the 'gold standard' for the experiment and therefore unquestionable, it is possible, however, that due to possible errors in these values, the results produced by the detection procedure may be slightly better than they appear. The motivation behind this assertion rests primarily on the fact that the sleep technologist marks arousals based on pattern recognition. Consequently, the underlying content of the visual pattern may not, in reality, match the perceived content displayed. For this reason, differences between the sleep technologist's detections and those of the automated detection procedure may appear in the results of this chapter. For example, the sleep technologist may have incorrectly marked one of the MAs, which actually does not have the necessary frequency to satisfy the definition of an MA. Consequently, if the detection procedure correctly rejects this false MA then this correct decision will nevertheless still lead to an increase in the probability of missed detections. Conversely, segments of EEG, which actually contained adequate frequency changes to mark as MAs but did not visually appear as such, could be ignored by the sleep technologist and correctly captured by the program, which would, nevertheless, based on the nature of this experiment, lead to increased false detections.

5.4 Conclusion

In this chapter, we have presented a novel approach to detect microarousals in the EEG signal. This approach involved the combined use of the wavelet transform with some form of stationarity segmentation, as its core functional blocks. In addition to these blocks, a further block was included to complete the overall detection procedure. This new block processed the power and spectral content of the resulting stationary segments, produced by the two previous blocks. By using the Fourier transform and selecting a reasonable frequency value that is based on the R&K criteria, the individual segments were thresholded in frequency, so as to extract frequency-significant segments.

The most positive result in combining both the wavelet transform and the segmentation blocks is that the rate of correct detection increased significantly everywhere the procedure was applied. That is, whether the procedure was applied to just the central EEG channel or to a combination of the central EEG and EMG channels, or whether the entire record was analyzed or separate sleep stages were analyzed, the result remained the same. The presence of the wavelet transform resulted in a significantly higher correct detection, generally lower false detection and definitely lower missed detections, when combined with any of the segmentation schemes than when these detection schemes were applied without the wavelet transform.

The universal improvement achieved with the application of the wavelet transform to the EEG signal compared to the results produced by applying the wavelet transform to the simulated signals in Section 4.4 may be attributable to two factors. First, as mentioned in the conclusion of Chapter 4, the signals used there represent an insightful *but* narrow range of

possible variability present in an actual EEG, which, given the constraints of allowable space, could not be otherwise. Therefore, the proposed combination of wavelet transform and segmentation operates generally well on a larger signal set, which could not be exhaustively represented by the signals used in Chapter 4. Secondly, the severity of the additive white Gaussian noise added to the signals in the previous chapter, may have negatively impacted and perhaps overly distorted the underlying signal present, compared to the noise present in the EEG itself. In other words, the noise applied to the signals in Chapter 4 may have overemphasized the actual noise of the EEG it was intended to mimick, but as mentioned earlier, the goal of that section was to test the segmentation procedures in a harsh environment in order to judge their effectiveness, since a noise free environment had already been examined. Nevertheless, this degree of noise difference may possibly reflect as to why such a notable improvement appeared in the results of this chapter.

Compared to the segmentation algorithms alone, the proposed procedure demonstrated significant improvements in higher correct detections and in modest reductions in false detections when applied to only one channel. However, because the overall value of these results is not high enough, the potential application of the procedure to a single channel is limited. On the other hand, the very real gains made when combining only two channels, does indeed make practical implementation possible. Nevertheless, at this preliminary stage, however encouraging these results may seem, the procedure would have to be further refined if it were to be profitably applied to the computerized long-term monitoring system it was intended to be incorporated into.

Chapter 6

Conclusion

6.1 Contributions and Concluding Remarks

The goal of this thesis has been to detect and clearly identify the presence of microarousals in the sleep electroencephalogram of a patient suspected of suffering from excessive daytime sleepiness. The monitoring of sleep is effectively accomplished by obtaining a polysomnogram, a collection of relevant biometric signals quantifying sleep state of which the electroencephalogram is one such signal. The different stages of sleep are characterized in the electroencephalogram by a variety of recognizable frequency and amplitude features. However, the electroencephalogram signal far from being one which demonstrates enduring regularity, is on the contrary one which exhibits highly non-stationary behaviour over the entire length of its duration. Moreover, interspersed amidst these constantly changing features, the microarousals appear. This problem is not one explicitly encountered in the literature and so no specific algorithm exists for its solution. Nevertheless, being a problem that involves the identification of sudden frequency bursts in time, a specific non-stationary phenomena, the literature involved in similarly-related pursuits led us to adopt techniques specialized in the partitioning of non-stationary signals into contiguous stationary segments.

Moreover, because the detection of microarousals requires an accurate resolution of the signal content of the electroencephalogram in both time and frequency, a necessary form of signal preprocessing is needed to enhance the capabilities of segmentation. The wavelet transform, which possesses the capacity to decompose a signal in both frequency and time, as well as being a fast transform, lends itself readily to the task at hand.

Therefore, to address the detection of microarousals we have proposed combining both the wavelet transform and stationary segmentation to form the basis for extracting microarousals from the electroencephalogram signal. To complete the detection procedure we have proposed a simple method of identifying whether or not the resulting stationary segments satisfy the conditions imposed by Rechtschaffen and Kales, defining the microarousals. This method uses the Fourier transform, in conjunction with thresholding. Furthermore, since the presence of a microarousal extends through much of the polysomnagram, to further refine the capabilities of the proposed procedure in isolating the microarousals, we have combined two relavant channels, namely, the central electroencephalogram and the electromyogram.

The validity of the two components comprising the proposed procedure has been tested with simulations, which have shown that individually each of the components achieves the expected results. That is, the wavelet transform correctly decomposes both the concatenated sinusoids and the superimposed sinusoids, with and without noise, while revealing both the frequency content and the time occurance of such frequency changes.

Similarly, the segmentation procedures correctly segments noise-free sinusoids of varying amplitude and frequency, precisely identifying the position in time of the non-stationary boundaries separating two different segments of the signal. Also, the segmentation algo-

rithm was tested further to determine the optimal values of the operating parameters used in the autocorrelation function method (ACF), the generalized likelihood method (GLR) and the nonlinear energy operator method (NLEO). Various sinusoidal non-stationarities, such as varying only the amplitude, varying only the frequency, increasing the amplitude while decreasing the frequency, and decreasing the amplitude while increasing the frequency, as well as a time varying second order AR signal, have been used for the purpose of testing these methods. Each of the sinusoidal signals was subjected to heavy additive white gaussian noise. The overall results have shown that some segmentation algorithms produced superior segmentation for certain test signals, while others produced superior results with other test signals. Therefore, segmentation was achieved with varying degrees of success depending on the signal and on the algorithm used. Finally, the wavelet transform and the segmentation components were combined and their results compared to the case without the wavelet transform, the former showing mixed but generally improved segmentation results compared to the latter.

Applying the proposed procedure to the electroencephalogram signal, we have demonstrated that the proposed microarousal detection algorithm involving the combination of the wavelet decomposition and stationarity segmentation algorithms provides an improvement on the detection capabilities over those of the stationarity segmentation algorithms alone. Referring to tested and proven techniques [49],[50],[54] concerned with the segmentation of non-stationary signals into stationary segments, we have demonstrated that the combination of these techniques with wavelet decomposition achieves a much higher degree of reliable stationarity segmentation than using the former works alone without the wavelet decomposition. This result applies to non-parametric techniques (ACF, NLEO) and para-

metric techniques (GLR) alike, which further demonstrates the general applicability and benefit of the proposed method.

In closing, we would like to mention that the best results of the three segmentation procedures were those produced by the ACF procedure, where the probability of correct detection was 67% and the probability of false detections was 36%. Although these values do not reflect the degree of certainty that is required in a clinical setting, they are, however, high enough to still play a important role. Specifically, because the proposed procedure is fast, it can be used in real time in conjunction with a sleep technologist. When a detection is made by the procedure, which is still 2 out 3 times correct (in the case involving the ACF), the sleep technologist can then quickly, in vivo, verify whether such a detection is valid. The important indication, provided by the procedure, can consequently alert the sleep technologist to periods when microarousals are actually taking place, which satisfies two important goals. Firstly, it liberates the sleep technologist from the need for absolute concentration in the exhaustive error-prone task of marking the microarousals thereby improving their ability to correctly and efficiently identify the presence of microarousals. Secondly, it alerts the sleep technologist, in real time, to the likely occurance of microarousals, which can provide a trigger for the application of further clinical procedures. Moreover, when considering the operation of the proposed scheme in a real time operating environment we must mention the NLEO. In the conclusion of Chapter 4 it was mentioned that, of the three segmentation schemes, the NLEO was the fastest. Furthermore, the results in Chapter 5, when the two channels were combined showed that the NLEO produced P_c and P_f values comparable to the ACF. Therefore, taking these points into consideration it is a very reasonable compromise to replace the ACF with the NLEO scheme

whenever speed is an important factor, eventhough there might be a slight degradation in terms of P_c and P_f.

6.2 Future Work

Although the results produced in this work demonstrate some potential applicability to the intended task of microarousal detection, there is still a considerable amount of room for improvement. Referring more generally to non-stationary signals as a whole, improvements in the detection and extraction of well-defined features, within this context, necessitates further investigation into the following fields.

6.2.1 Segmentation

Our research through the literature revealed that the topic of stationarity segmentation is one that lacks clear and workable implementation on a broad scale. Apart from segmentation procedures similar to the ones used in this thesis that largely depend upon the establishing of ad hoc thresholds and are acutely application dependent, none of the available research provides a reliable means of partitioning non-stationary signals. In other words, there is no universal segmentation procedure or global theory available that can be modified in order to apply to particular cases. Although the problem of segmentation is not trivial, it is surprising that there is not much research into it, especially when non-stationary signal segmentation is such an important topic with potential applications in so many different fields. Considering the techniques used in this paper, it seems more work needs to be

done in establishing new difference measures, which will enable a higher degree of reliable segmentation.

6.2.2 New Wavelet Based Methods

With the expansion of available wavelet-based techniques, more refined applications exist that may serve to improve signal decomposition and consequently, lead to better diagnostic tools in detecting specifically-defined non-stationary phenomena. One such technique of interest involves matching pursuit, whereby a dictionary of possible signals is constructed and used as reference to compare against the various waveform patterns encountered throughout the signal.

6.2.3 Adaptive Algorithms

The constantly changing nature of the features of a non-stationary signal, whether in frequency or in time, requires the presence of a procedure that has the ability to effectively adapt to these changes. Many time-varying filters such as Kalman filters, recursive least square filters or least mean square filters exist. A further study as to which filter can be most effectively applied to the present context would be an important one to be undertaken.

6.2.4 Neural Networks

Since the sleep technologist relies primarily on visual pattern recognition to detect the occurance of microarousals, a natural attempt at automating the capturing of these desired signal features could involve the application of other pattern recognition methods, such as neural networks.

Since each of these techniques offers a specific perspective on analyzing a non-stationary signal, it is important to determine and then use some optimal combination of the above, with the explicit goal of establishing a more precise means of stationarity segmentation with the further goal of clearly identifying desirable signal content reliably. Therefore, all future investigations should be pursued for a non-stationary signal in the general sense, while maintaining, in particular, the focus on potential applications to electroencephalogram monitoring.

References

[1]] Monroe L.J., 1969, Intra-rater reliability and the role of experience in scoring EEG sleep records: Phase I. Psychophysiol. vol. 5, pp. 376-384, 1969

[2] Pei-Chen Lo, and C. Principle, "Dimensional Analysis of EEG Segments: experimental consideration", *Proceedings of International Joint Conference on Neural Networks*, vol. 1, pp. 693-698, Washington DC, 1989.

[3] M.H.Kryger, T.Roth, W.C. Dement, *Principles and practice of Sleep Medicine*, Philadelphia, Pennsylvania: W.B. Saunders Company, 2000.

[4] J.W.Cooley and J.W. Tukey, "An algorithm for the machine calculation of complex Fourier series". *Math. Comput.* vol.19, pp. 297-301, 1965.

[5] P.L.Nunez, *Electric Fields of the Brain: The Neurophysics of EEG*, New York, Oxford University Press, 1981.

[6] Jasper, H.H., 1958. "The ten-twenty electrode system of the International Federation", *The Electroencephal. Clin. Neurophysiol.*, 10:371-375

[7] B.J.Fisch, *Spehlmann's EEG Primer 2nd Edition*, Amersterdam, Elsevier, 1991.

[8] E.Niedermeyer and F. Lopes da Silva, *Electroencephalography: Basic Principles, Clinical Applications and Related Fields*, Baltimore, Md., 1987.

[9] H.Berger, "Uber das Electroenzephalogramm des Menschen", *Arch. Psychieat. Nervenkr.* vol.87, pp.527-570, 1929.

[10] W.G.Walter, "The location of cerebral tumors by electroencephalography". Lancet. vol.2, pp.305-308, 1936.

[11] A. Rechtschaffen, and A. Kales, "A Manual of Standardized Terminology, Techniques and Scoring System for Sleep Stages in Human Subjects", *US Department of Health, Education and Welfare, Public Health Service*, Washington: US Government Printing Office, 1968.

[12] E. Aserinsky, N. Kleitman, "Regularly occurring periods of eye motility and concomitant phenomena, during sleep", *Science*, vol.118, pp.273-274, 1953.

[13] "EEG Arousals: Scoring Rules and Examples", *Sleep*, vol.15, No.2, pp.174-184, 1992.

[14] J.Gotman, J.R.Ives, and P.Gloor, "Automatic recognition of interictal epileptic activity in prolonged EEG recordings", Electroenceph. clin. Nuerophysiol., vol.46, pp.510-520, 1979.

[15] J.Gotman, "Automatic recognition of epileptic seizures in the EEG. *Electoenceph. clin. Neurophysiol.*, vol.54, pp.530-540, 1982.

[16] J.Gotman, "Seizure Recongition and Analysis", In : J.Gotman, J.R.Ives and P.Gloor (Eds), Long-term Monitoring in Epilepsy, *Electroenceph. clin. Neurophysiol.*, suppl.37, Elsevier, Amsterdam, pp.133-145, 1985.

[17] J.M. Spyers-Ashby, P.G. Bain and S.J. Roberts, "A comparison of fast fourier transform (FFT) and autoregressive (AR) spectral estimation techniques for the analysis of tremor data", *Journal of Neuroscience Methods*, vol.83, pp.35-43,1998.

[18] I.Guler, F.Hardalac and S.Muldur, "Determination of aorta failure with the application of FFT, AR and wavelet methods to Doppler technique", Computers in Biology and Medicine, vol.31, pp.229-238, 2001.

[19] I.Guler, F.Hardalac and F.S.Erol, "Comparison of FFT, AR and Wavelet Methods in Transcranial Doppler signal obtain from intracerebral vessels", 2001 Proceedings of the 23rd Annual EMBS International Conference, October 25-28, Istanbul, Turkey.

[20] A.V.Oppenheim and R.W.Schafer, Discrete-Time Signal Processing, Prentice Hall, Englewood Cliffs, NJ.,1989.

[21] M.Akin, "Comparison of Wavelet Transform and FFT Methods in the Analysis of EEG Signals", Journal of Medical Systems, vol. 26, no.3, pp.241-247, 2002.

[22] C.M.Harris, "The Fourier analysis of biological transients", Journal of Neuroscience Methods, vol.83, pp.15-34, 1998.

[23] M.Akin, M.K.Kiymik, "Application of periodogram and AR spectral analysis to EEG signals", J.Med. Syst., vol.24, no.4, 2000.

[24] O.Rioul and M.Vetterli, "Wavelets and Signal Processing", IEEE SP Magazine, October, pp.14-38,1991.

[25] J.C.Goswami and A.K.Chan, "Fundamentals of Wavelets: Theory, Algorithms, and Applications", New York, NY, John Wiley & Sons Inc.,1999.

[26] N.V.Thakor, D.Sherman, "Wavelet (Time-Scale) Analysis in Biomedical Signal Processing", *Biomedical Signal Analysis*, CRC Press, pp.886-906,1995

[27] S.Haykin, *Adaptive Filter Theory*, Prentice Hall, Upper Saddle River, NJ.,1996.

[28] J.Muthuswamy and N.V.Thakor, "Spectral analysis methods for neurological signals", *Journal of Neuroscience Methods*, vol.83, pp.1-14, 1998.

[29] S.L.Marple, Digital spectral analysis with applications. Englewood Cliff, NJ: Prentice-Hall, 1987.

[30] A.M.Bianchi, L.T.Mainardi and S.Cerutti, "Time-frequency analysis of biomedical signals", *Transactions of the Institute of Measurement and Control*, vol.22, no.3, pp.215-230, 2000.

[31] V.J.Samar, A.Bopardikar, R. Rao and K.Schwartz, "Wavelet Analysis of Neuroelectric Waveforms: a Conceptual Tutorial", *Brain and Language*, vol.66, pp.7-60, 1999.

[32] G.Strang, "Wavelet transforms versus Fourier transforms", *Bulletin (New Series) of the American Mathematical Society*, vol.28, no.2, pp.288-305, 1993.

[33] J.O. Chapa and M.R. Raghuveer, "Optimal matched wavelet construction and its application to image pattern recognition . In H.H. Szu (Ed.), *Wavelet applications:II. Proceedings of the Society for Photo Instrumentation Engineering*, vol. 2491, pp. 518-529, 1995.

[34] M.R. Raghuveer and J.O. Chapa, In *Wavelet applications III. Proceedings of the Society for Photo Instrumentation Engineering*, vol. 2762, 1996.

[35] L.J. Trejo and M.J. Shensa, "Feature extraction of event-related potentials using wavelets: An application to human performance monitoring", *Brain and Language*, vol.66, pp.89-108, 1999.

[36] T. Kalayci, O. Ozdamar and N.Erdol, "The use of wavelet transform as a preprocessor for the neural network detection of EEG spikes. *Proceedings of the IEEE Southeastcon* pp.1-3, 1994.

[37] J.Raz, L.Dickerson and B.Turetsky, "A wavelet packet model of evoked potentials", Brain and Language, vol.66, pp.61-88, 1999.

[38] V.J.Samar, H.Begleiter, J.O. Chapa, M.R.Raghuveer, M.Orlando, D.Chorlian, "Matched Meyer neural wavelets for clinical and experimental analysis of auditory and visual evoked potentials", In G. Ramponi, G.I. Sicuranza, S.Carrato, and S.Marsi (Eds.) *Signal processing: VIII Theories and application, Proceedings of EUSIPCO-96*, pp.387-390, Trieste: Edizioni LINT, 1996.

[39] H.E.Hanrahan, "Extraction of features in auditory brainstem response (ABR) signals", COMSIG 90, *Proceedings of the Third South African Conference on Communications and Signal Processing* (IEEE Catalog No. 90TH0314-5/90), pp. 61-66, 1990.

[40] H.E.Hanrahan, "A family of wavelets which are dilatable by simple IIR filters", *International Conference on Acoustics, Speech and Signal Processing* (pp. IV285-IV288, IEEE Catalog No. 0-7803-0532-9/92, March 23-26, San Francisco),1992.

[41] S.G.Mallat, "A theory of multiresolution signal decomposition: The wavelet representation. *IEEE Transactions on Pattern Analysis and Machine Intelligence*, vol.11, pp.674-693, 1989.

[42] Y.Meyer, *Ondelettes et Operateurs*, Hermann, 1988.

[43] I.Daubechies, *Ten Lectures on Wavelets*, Society for Industrial and Applied Mathematics, Philadelphia, PA, 1992.

[44] M.Vetterli and J.Kovacevic, *Wavelets and Subband Coding*, Prentice-Hall, Englewood Cliffs, NJ, 1995.

[45] G.Strang and T.Nguyen, *Wavelets and Filter Banks*, Wellesley-Cambridge Press, Wellesley, MA, 1996.

[46] R.Strichartz, "How to make wavelets", *American Mathematical Monthly*, vol.100, no.6, pp.539-556, 1993.

[47] R.C.Gonzalez and R.E.Woods, *Digital Image Processing*, Prentice-Hall, Upper Saddle River, NJ., 2002.

[48] A.Papoulis, *Probability, Random Variables, and Stochastic Processes*, McGraw-Hill Inc., New York, NY., 1991.

[49] D.Michael and J.Houchin, "Automatic EEG analysis: a segmentation procedure based on the autocorrelation function", *Electroenceph. clin. Neurophysiol.*, vol.46, pp.232-235, 1979.

[50] R.Agarwal, J.Gotman, D.Flanagan and B.Rosenblatt, "Automatic EEG analysis during long-term monitoring in the ICU", *Electroenceph. clin. Neurophysiol.*, vol.107, pp.44-58, 1998.

[51] J.F.Kaiser, "On a simple algorithm to calculate the 'energy' of a signal", *In: IEEE Int. Conf. Acoust., Speech, and Signal Processing*, Albuquerque,NM, vol.1, pp.381-384, April 1990.

[52] E.I.Plotkin and M.N.S.Swamy, "Nonlinear signal processing bsed on parameter invariant moving average modeling", *In: Proc. CCECE '21*, Toronto, Canada, pp. TM3.11.1 - TM3.11.4, September, 1992.

[53] V.Krajca, S.Petranek, I.Patakova and A.Varri, "Automatic identification of significant graphoelements in multichannel EEG recording by adaptive segmentation and fuzzy clustering", *Int. J. Biomed. Comput.*, vol.28, pp.71-89, 1991.

[54] U.Appel and A.V.Brandt, "Adaptive Sequential Segmentation of Piecewise Stationary Time Series", *Information Sciences*, vol.29, pp.27-56, 1983.

[55] P.V.de Souza, "Statistical Tests and Distance Measures for LPC Coefficients", *IEEE Trans. on Acoust., Speech and Signal Processing*, vol.ASSP-25, no.6, pp.554-559.

[56] H.Akaike, "A new look at the statistical model identification, *IEEE Trans. Automat. Control* AC-vol.19, no.6, pp.716-723, 1974.

[57] J.Rissanen, "Modelling by shortest data description, *Automatica*, vol.14, pp.465-471, 1978.

Appendix

List of the Detected Microarousals obtained from the Different Methods used in the Thesis and the Actual Microarousals scored by the Sleep Technologis

	MA Scored by Sleep Technologist		ACF Detected MA		GLR Detected MA		NLEO Detected MA	
	Start Time	Stop Time	Start Time	Stop Time	Start Time	Stop Time	Start Time	Stop Time
1.	00:41:04	00:41:15					00:41:05	00:41:12
2.	00:43:56	00:44:04	00:43:47	00:43:58	00:43:47	00:43:58	00:43:52	00:44:02
3.	00:44:28	00:44:32	00:44:21	00:44:31	00:44:23	0:44:47		
4.	00:45:12	00:45:18			00:45:07	00:45:15	00:45:07	00:45:16
5.	00:45:48	00:45:53	00:45:47	00:45:50			00:45:50	00:45:57
6.	00:46:53	00:46:57						
7.	00:47:36	00:47:43	00:47:36	00:47:44				
8.	01:36:16	01:36:22						
9.	01:36:48	01:36:52	01:36:47	01:36:53	01:36:47	01:36:52	01:36:47	01:36:56
10.	01:37:02	01:37:07	01:37:03	01:37:40				
11.	01:37:54	01:37:59	01:37:47	01:38:22	01:37:47	01:37:55		
12.	01:38:28	01:38:37			01:38:17	01:38:31		
13.	01:41:45	01:41:50	01:41:47	01:41:51				
14.	01:45:50	01:45:55	01:45:52	01:45:57				
15.	01:46:22	01:46:31	01:46:25	01:46:31	01:46:21	01:46:33	01:46:22	01:46:31
16.	01:46:48	01:46:55	01:46:47	01:46:50	01:46:50	01:46:55	01:46:47	01:46:54
17.	01:47:10	01:47:15	01:47:10	01:47:14			01:47:11	01:47:24
18.	01:47:44	01:47:51	01:47:41	01:47:47	01:47:39	01:47:47	01:47:42	01:47:47
19.	01:57:42	01:57:50	01:57:41	01:57:51	01:57:39	01:57:47	01:57:43	01:57:50
20.	01:58:43	01:58:50	01:58:42	01:58:52	01:58:37	01:58:47	01:58:41	01:58:53

	MA Scored by Sleep Technologist		ACF Detected MA		GLR Detected MA		NLEO Detected MA	
	Start Time	Stop Time	Start Time	Stop Time	Start Time	Stop Time	Start Time	Stop Time
21.	01:59:08	01:59:14	01:59:07	01:59:11	01:59:05	01:59:15	01:59:10	01:59:16
22.	01:59:57	02:00:02	01:59:58	02:00:03			01:59:52	02:00:04
23.	02:02:09	02:02:16	02:02:08	02:02:11	02:02:07	02:02:15	02:02:09	02:02:15
24.	02:02:35	02:02:43	02:02:34	02:02:39	02:02:31	02:02:39	02:02:27	02:02:39
25.	02:04:40	02:04:46	02:04:37	02:04:43	02:04:39	02:04:47	02:04:40	02:04:47
26.	02:05:10	02:05:17	02:05:05	02:05:17	02:05:06	02:05:13	02:04:58	02:05:13
27.	02:05:49	02:05:54	02:05:47	02:05:53	02:05:50	02:05:55	02:05:47	02:06:00
28.	02:06:52	02:06:59	02:06:50	02:06:57	02:06:50	02:06:55	02:06:47	02:06:57
29.	02:12:43	02:12:50	02:12:43	02:12:47	02:12:39	02:12:47	02:12:34	02:12:43
30.	02:14:15	02:14:21	02:14:18	02:14:22				
31.	02:14:54	02:15:01					02:14:50	02:14:59
32.	02:15:32	02:15:39			02:15:31	02:15:37		
33.	02:19:31	02:19:39			02:19:30	02:19:41	02:19:31	02:19:36
34.	02:20:08	02:20:18	02:20:07	02:20:17	02:20:10	02:20:25	02:20:08	02:20:12
35.	02:20:39	02:20:42	02:20:37	02:20:41				
36.	02:51:21	02:51:38	02:51:21	02:51:34	02:51:22	02:51:33	02:51:27	02:51:33
37.	02:52:07	02:52:18	02:51:59	02:52:11	02:52:11	02:52:17	02:52:06	02:52:12
38.	02:52:49	02:52:52	02:52:48	02:52:52			02:52:47	02:52:51
39.	02:55:05	02:55:13	02:55:04	02:55:15	02:55:08	02:55:15	02:55:05	02:55:13
40.	02:57:24	02:57:35			02:57:25	02:57:37	02:57:15	02:57:28
41.	02:57:55	02:58:02	02:57:53	02:57:59	02:57:52	02:57:59	02:57:54	02:57:58
42.	02:58:18	02:58:37	02:58:18	02:58:26	02:58:17	02:58:27	02:58:09	02:58:22
43.	03:03:27	03:03:37			03:03:21	03:03:31	03:03:21	03:03:28
44.	03:05:25	03:05:36	03:05:26	03:05:30	03:05:21	03:05:31	03:05:08	03:05:34
45.	03:09:40	03:09:54	03:09:40	03:09:50	03:09:39	03:09:47	03:09:42	03:09:50
46.	03:11:20	03:11:35	03:11:20	03:11:31	03:11:15	03:11:27	03:11:21	03:11:26
47.	03:13:01	03:13:15	03:13:00	03:13:12	03:13:04	03:13:15	03:13:04	03:13:11
48.	03:13:39	03:13:53	03:13:37	03:13:51	03:13:39	03:13:47	03:13:41	03:13:50
49.	03:14:59	03:15:13	03:14:59	03:15:06	03:14:56	03:15:01	03:14:57	03:15:09
50.	03:15:41	03:15:49						
51.	03:16:26	03:16:39	03:16:27	03:16:36	03:16:23	03:16:31	03:16:18	03:16:35
52.	03:17:03	03:17:09						

	MA Scored by Sleep Technologist		ACF Detected MA		GLR Detected MA		NLEO Detected MA	
	Start Time	Stop Time	Start Time	Stop Time	Start Time	Stop Time	Start Time	Stop Time
53.	03:17:35	03:17:41	03:17:34	03:17:47	03:17:31	03:17:43		
54.	03:18:23	03:18:29	03:18:23	03:18:29	03:18:22	03:18:31	03:18:17	03:18:27
55.	04:11:30	04:11:40	04:11:29	04:11:43	04:11:28	04:11:35	04:11:21	04:11:35
56.	04:13:05	04:13:11			04:13:10	04:13:23		
57.	04:14:05	04:14:11						
58.	04:14:23	04:14:35			04:14:17	04:14:27	04:14:12	04:14:28
59.	04:16:17	04:16:32			04:16:11	04:16:21	04:16:16	04:16:22
60.	04:16:59	04:17:06					04:17:01	04:17:07
61.	04:52:20	04:52:26			04:52:21	04:52:37	04:52:21	04:52:31
62.	04:52:32	04:52:35						
63.	04:52:45	04:52:52	04:52:47	04:53:09	04:52:47	04:52:55	04:52:43	04:53:00
64.	04:53:14	04:53:20			04:53:06	04:53:19		
65.	04:54:07	04:54:13	04:54:07	04:54:16	04:53:58	04:54:07	04:54:01	04:54:13
66.	04:56:11	04:56:19	04:56:09	04:56:15	04:56:09	04:56:19	04:56:01	04:56:18
67.	04:57:02	04:57:08	04:56:47	04:57:06	04:57:07	04:57:31	04:57:05	04:57:10
68.	05:00:39	05:00:56	05:00:42	05:00:47	05:00:43	05:00:47	05:00:43	05:00:47
69.	05:02:58	05:03:12	05:03:01	05:03:11	05:02:58	05:03:09	05:03:02	05:03:11
70.	05:05:12	05:05:17	05:05:12	05:05:17	05:05:09	05:05:23	05:05:12	05:05:16
71.	05:05:27	05:05:36						
72.	05:08:18	05:08:23	05:08:17	05:08:21			05:08:17	05:08:21
73.	05:12:28	05:12:39	05:12:31	05:12:36	05:12:31	05:12:39	05:12:27	05:12:35
74.	05:13:30	05:13:36						
75.	05:14:46	05:14:52						
76.	05:19:53	05:20:00						
77.	05:20:33	05:20:41	05:20:33	05:20:37			05:20:33	05:20:40
78.	05:22:15	05:22:29						
79.	05:25:08	05:25:15	05:25:06	05:25:14	05:25:10	05:25:19	05:25:11	05:25:16
80.	05:25:44	05:25:50						
81.	05:27:11	05:27:17	05:27:10	05:27:16	05:27:07	05:27:15		
82.	05:29:07	05:29:12			05:29:09	05:29:19		
83.	05:29:55	05:30:02	05:29:55	05:29:59	05:29:56	05:30:03	05:29:54	05:29:59
84.	05:43:05	05:43:11						

	MA Scored by Sleep Technologist		ACF Detected MA		GLR Detected MA		NLEO Detected MA	
	Start Time	Stop Time	Start Time	Stop Time	Start Time	Stop Time	Start Time	Stop Time
85.	05:44:08	05:44:17	05:44:00	05:44:09	05:44:03	05:44:13	05:44:02	05:44:09
86.	05:44:37	05:44:44						
87.	05:46:30	05:46:41	05:46:31	05:46:36				
88.	05:46:51	05:47:02	05:46:52	05:47:00	05:46:50	05:46:57	05:46:47	05:47:00
89.	05:48:28	05:48:35	05:48:29	05:48:33	05:48:27	05:48:33	05:48:30	05:48:38
90.	05:48:47	05:48:58	05:48:48	05:48:57	05:48:50	05:48:55	05:48:50	05:48:56
91.	05:49:47	05:49:57	05:49:49	05:49:54	05:49:50	05:49:55	05:49:47	05:49:54
92.	05:51:53	05:52:00						
93.	05:52:18	05:52:24	05:52:18	05:52:26	05:52:15	05:52:21	05:52:21	05:52:26
94.	05:53:04	05:53:13	05:52:59	05:53:04	05:53:00	05:53:07	05:52:54	05:53:10
95.	05:54:01	05:54:13	05:54:01	05:54:07	05:54:03	05:54:09	05:54:04	05:54:10
96.	05:55:11	05:55:20						
97.	05:55:54	05:55:59					05:55:51	05:55:58
98.	05:57:52	05:58:02	05:57:52	05:57:58	05:57:50	05:57:57	05:57:50	05:58:04
99.	05:58:17	05:58:21	05:58:16	05:58:21			05:58:16	05:58:21
100.	05:58:43	05:58:49						
101.	05:59:02	05:59:09						
102.	05:59:21	05:59:26	05:59:19	05:59:25				
103.	05:59:54	05:59:59						
104.	06:00:11	06:00:16						
105.	06:00:27	06:00:33	06:00:26	06:00:36			06:00:28	06:00:35
106.	06:02:12	06:02:16	06:02:09	06:02:13			06:02:13	06:02:31
107.	06:02:36	06:02:39						
108.	06:02:59	06:03:06	06:02:57	06:03:05	06:03:06	06:03:13	06:02:56	06:03:03
109.	06:04:01	06:04:11	06:04:01	06:04:15	06:04:01	06:04:15	06:04:02	06:04:07
110.	06:05:06	06:05:17	06:05:06	06:05:16			06:04:58	06:05:15
111.	06:05:27	06:05:32						
112.	06:07:39	06:07:51	06:07:37	06:07:40				
113.	06:10:39	06:10:45	06:10:39	06:10:43				
114.	06:12:01	06:12:07	06:12:00	06:12:06				
115.	06:13:00	06:13:05	06:12:57	06:13:04	06:12:58	06:13:07	06:12:59	06:13:04
116.	06:13:14	06:13:22	06:13:14	06:13:21				

	MA Scored by Sleep Technologist		ACF Detected MA		GLR Detected MA		NLEO Detected MA	
	Start Time	Stop Time	Start Time	Stop Time	Start Time	Stop Time	Start Time	Stop Time
117.	06:13:39	06:13:44						
118.	06:15:15	06:15:24			06:15:15	06:15:23		
119.	06:17:00	06:17:07	06:16:54	06:17:00			06:16:59	06:17:05
120.	06:22:59	06:23:04	06:22:59	06:23:05	06:22:56	06:23:03	06:22:59	06:23:04
121.	06:24:48	06:24:55	06:24:47	06:24:52	06:24:47	06:24:54	06:24:47	06:24:55
122.	06:29:14	06:29:19	06:29:13	06:29:17	06:29:09	06:29:19		
123.	06:30:07	06:30:11			06:33:00	06:33:07		
124.	06:30:57	06:31:06	06:30:59	06:31:06				
125.	06:33:03	06:33:13	06:33:02	06:33:06			06:32:57	06:33:12
126.	06:34:24	06:34:29						
127.	06:35:37	06:35:45						
128.	06:36:05	06:36:10						
129.	06:36:59	06:37:17	06:36:57	06:37:01	06:36:56	06:37:01	06:37:02	06:37:05
130.	06:37:30	06:37:37						
131.	06:42:55	06:43:04	06:42:54	06:42:58	06:42:58	06:43:13	06:42:59	06:43:06
132.	06:44:36	06:44:41						
133.	06:46:22	06:46:30						
134.	06:49:23	06:49:31	06:49:23	06:49:26	06:49:23	06:49:35	06:49:23	06:49:27
135.	06:51:31	06:51:37						
136.	07:02:59	07:03:14	07:03:05	07:03:08	07:03:04	07:03:11	07:03:07	07:03:14